Benchmark of quantum and classical heuristics on the TSP

BOMBARDELLI Martin, LACOMME Philippe & VULPESCU Bogdan

Université Clermont Auvergne (LIMOS-LPCA) / CIFRE (CGI)

Ecole doctorale Sciences Pour l'Ingénieur

Laboratoire de Physique de Clermont

Context and goal

- Quantum computing (QC) is a highly promising field that does not yet seem to have reached maturity.
- The use of quantum computers could lead to advances in numerous domains such as cybersecurity, material research, molecular discovery for medicine, and operational research.
- The aim of this paper is to assess the current capabilities of quantum computing in the field of operational research for combinatorial optimization.
- Here, we focus on a Travelling Salesman Problem (TSP)

Problem description

- The Travelling Salesperson Problem (TSP) is a well studied problem.
- A salesperson needs to travel to N different cities, find the shortest path visiting each city exactly once and coming back to the start. Given a complete weighted graph:

  G = (V, E, w)
- Find the decision variables which minimize:

$$\text{Cost} = \sum_{k=0}^{n-1} \sum_{i=0}^{n-1} \sum_{j=0}^{n-1} d_{i,j}\, x_{i,k} x_{j,(k+1) \bmod n}$$

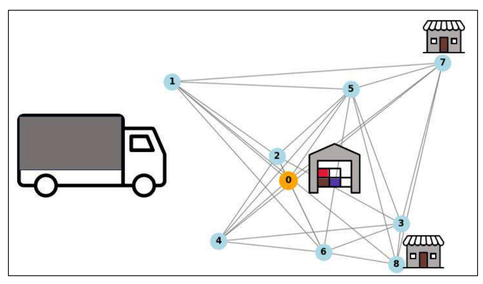

Problem examples

- This Problem has many self-explanatory business relevant applications
- The most obvious being transport companies for goods and supply chain approvisation and robustness.
- Finding a good solution to this problem can be an important factor contributing to reducing the transportation costs of any company.
- Sometimes the number of different possibilities can become unbearable for a conventional computer as the number of cities increases.
- Here we have two solutions of the trip minimizing the distances of France's 600 most populated cities. First one is the optimal solution and second one is a greedy solution.
- This problem also has many relevance in the context of IT hardware optimization to shorten the distances between two components on a chip.

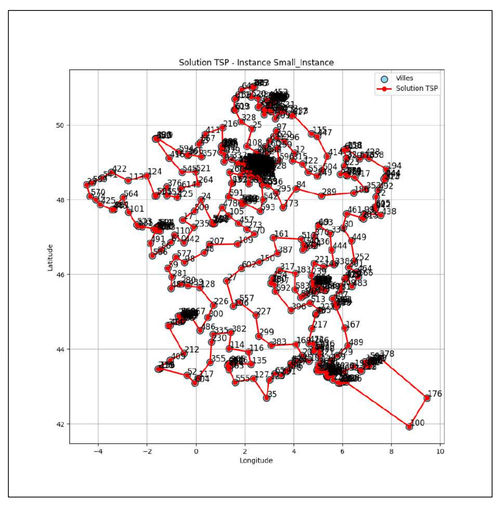

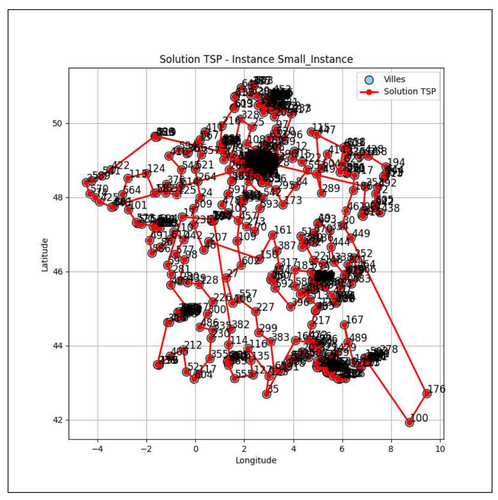

Results

- To test this problem on a quantum computer we had to tweak the model to get a Quadratic Unconstrained Binary Minimization Problem.
- This is the only type of function we could minimize on all quantum computers at our disposal.
- We then proceed to compare the results in terms of quality and time complexity of the quantum solver versus some classical heuristics we implemented.
- We also use a state-of-the-art solver to get a grasp at the current capabilities of the quantum solvers in the realm of combinatorial optimization
- As of now, the results do not seem to meet the expectation neither in terms of quality nor in terms of speed, but we might get improved results later.

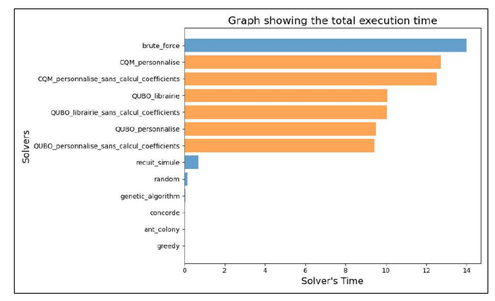

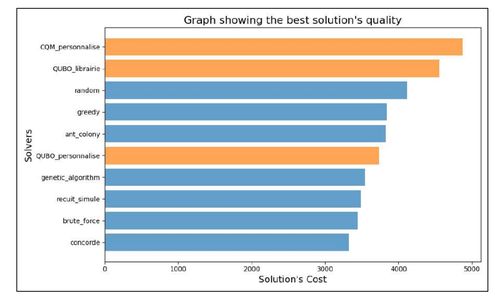

Future Publications

Conferences

Martin Bombardelli, Gérard Fleury, Philippe Lacomme, Bogdan Vulpescu. Introduction to photonic quantum gates. 22nd EU/ME meeting x Quantum School. Kaiserslautern 2nd - 5th September 2025

ArXiv

Martin Bombardelli, Philippe Lacomme, Bogdan Vulpescu. Comparison Benchmark of quantum and classical heuristics on the TSP.

Conclusions

Our goal is to study various technologies of quantum hardware and its applications in the operational research field. Find the potential gains and hopefully improve the quality of the algorithms currently used.

Bibliography

1. **Eric Bourreau, Gérard Fleury et Philippe Lacomme. IQAOA for Two Routing Problems: A Methodological Contribution with Application to TSP and VRP. In : Journal of Quantum Computing6.1 (2024), p. 25-51.**
2. **Gerhard Reinelt. TSPLIB A traveling salesman problem library. In : ORSA journal on computing 3.4 (1991), p. 376-384.**
3. **Jehn-Ruey Jiang et Chun-Wei Chu. Classifying and benchmarking quantum annealing algorithms based on quadratic unconstrained binary optimization for solving NP-hard problems. In : IEEE access11 (2023), p. 104165-104178.**

A 0.95fJ Analog MAC Operation in Standard CMOS for Neural Network Inference

M. Bouchakour, E. Bergeret, G. Sicard, K. Abdelouahab, F. Berry

Objectives

- Develop a fully analog Multiply–Accumulate (MAC) circuit for neural network (NN) inference in standard CMOS.
- Support two-quadrant multiplication (positive and negative weights) without dedicated negative-weight storage.
- Achieve ultra-low energy operation and compact area, enabling efficient on-chip inference for edge AI.

Introduction: Analog Computing for AI

- MAC operations constitute over 99% of NN workloads, making their efficiency critical for AI hardware [1].
- Digital MACs are power- and area-hungry, especially for large-scale inference.
- **Analog computing** leverages device physics for computation, offering orders-of-magnitude energy savings [5].
- Neural networks tolerate analog non-idealities (noise, mismatch), enabling robust inference even with low-precision or approximate analog hardware [1].

Proposed Analog MAC Cell

- Utilizes bulk-modulated PMOS transistors in sub-threshold operation for exponential current control.
- Achieves two-quadrant multiplication through a novel circuit: one branch for the weighted input, another for bias cancellation.
- Compatible with standard CMOS; no special process or negative weight storage required.
- The circuit output is given by $I_{out} = I_{out1} - I_{out2} = a \cdot I_{in} \cdot w'$, where w' is function of V_{BS}.

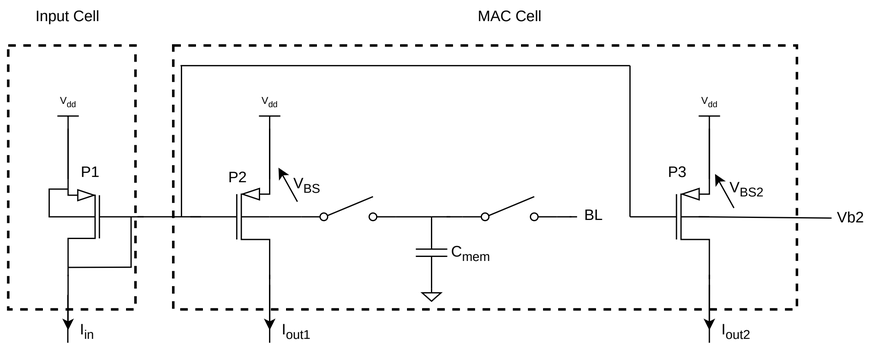

Figure: Schematic of the proposed analog MAC cell.

Methods: Circuit Operation

- Multiple cells are connected on the same output line for vector-vector multiplication.

$$I_{out} = \sum_{i=1}^{N} I_{in}(i) \cdot a \cdot w'(i)$$

- Input and output lines are respectively pre-charged and discharged before computing cycles, allowing for faster operation.
- The cell is turned on for a limited duration, and left idle the rest of the time, enhancing efficiency.
- Energy per operation is directly proportional to the computing cycle duration.
- Computing time is limited by the settling time of the output currents.

Results: MNIST Benchmark

- Evaluated on MNIST digit classification with a 784×10 MAC array.
- Achieved 91% accuracy (matching software baseline) with analog hardware simulation.
- Energy per MAC: **0.95 fJ** (65 nm CMOS, 1.5 ns compute time).
- Efficiency: 2105 TOPS/W.
- Energy per inference: **0.92 pJ** (average over 10,000 test images).

Metric	**This Work**	[3]	[2]	[4]
Tech. (nm)	65	22	16	180
TOPS/W	2105	2989	121	47.6

Table: Comparison with recent analog MAC implementations.

Advantages and Limitations

- **Advantages:**
  - No need for separate negative weight storage.
  - Standard CMOS compatibility.
  - Ultra-low energy, scalable to large arrays.
- **Limitations:**
  - Analog weight retention time $\sim 10\mu s$ (periodic refresh needed).
  - Sensitive to device mismatch; chip-specific training or calibration may be required.
  - Output subtraction circuit and refresh energy not included in baseline MAC energy.

Conclusion

- Demonstrated a fully analog, low-power MAC cell in standard CMOS for NN inference.
- Achieves state-of-the-art energy efficiency and competitive accuracy for MNIST.
- Future work: full system integration, chip measurements, and robust training against mismatch and drift.

References

[1] B. Murmann, "Mixed-Signal Computing for Deep Neural Network Inference," *IEEE Trans. VLSI Syst.*, vol. 29, no. 1, pp. 3–13, Jan. 2021.

[2] H. Jia *et al.*, "Scalable and Programmable Neural Network Inference Accelerator Based on In-Memory Computing," *IEEE J. Solid-State Circuits*, vol. 57, no. 1, pp. 198–211, Jan. 2022.

[3] R. Nägele *et al.*, "Analog Multiply-Accumulate Cell With Multi-Bit Resolution for All-Analog AI Inference Accelerators," *IEEE Trans. Circuits Syst. I*, vol. 70, no. 9, pp. 3509–3522, Sep. 2023.

[4] F. Kenarangi *et al.*, "A Single-MOSFET Analog High Resolution-Targeted (SMART) Multiplier for Machine Learning Classification," *IEEE J. Emerg. Sel. Top. Circuits Syst.*, vol. 11, no. 4, pp. 816–828, Dec. 2021.

[5] A. Sebastian, M. Le Gallo, R. Khaddam-Aljameh, and E. Eleftheriou, "Memory Devices and Applications for In-Memory Computing," *Nat. Nanotechnol.*, vol. 15, no. 7, pp. 529–544, Jul. 2020.

Contact

- Email: mohamed.bouchakour@uca.fr

Active learning of excursion set confidence regions for simulators with functional outputs

Lucas Brunel, encadré par Rodolphe Le Riche (LIMOS), Bruno Sudret (ETH Zurich), Mathieu Balesdent (ONERA) & Loïc Brevault (ONERA)

ONERA, Université Paris Saclay & LIMOS (CNRS, EMSE, Université Clermont Auvergne)

Context

- Design of complex systems using **computationally expensive simulators with functional outputs**
- A single run of the simulator returns the field value over the entire mesh, whose node have coordinates $\boldsymbol{x} \in \mathcal{X}$
- **Uncertainties on the simulator input**, a random vector $\boldsymbol{U}$, making the outputs a **random field**

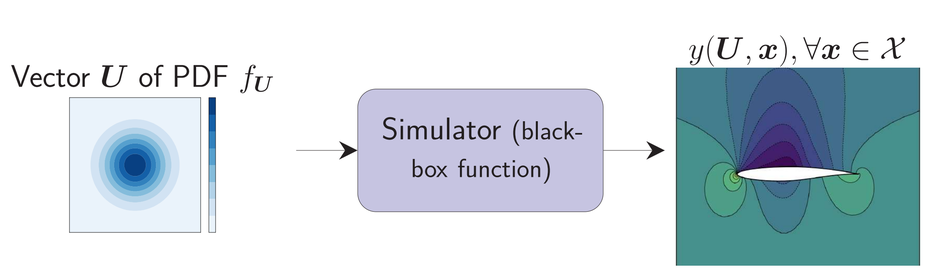

Illustrative example

- Glide-back trajectory of a reusable space launcher first stage
- $\boldsymbol{U} \in \mathbb{R}^{14}$: aerodynamic coefficients, wind perturbations (represented by 10 random variables), thrust vector angle, and time of boost-back cut off
- $\boldsymbol{x} \in \mathbb{R}$: the distance to landing site
- Simulator $y(\boldsymbol{U}, \boldsymbol{x})$: numerical solution of the equations of motion
- The vehicle leaving the flight corridor (hatched area) is considered excursion

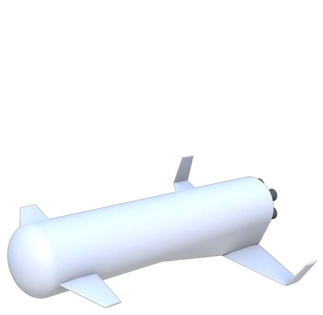

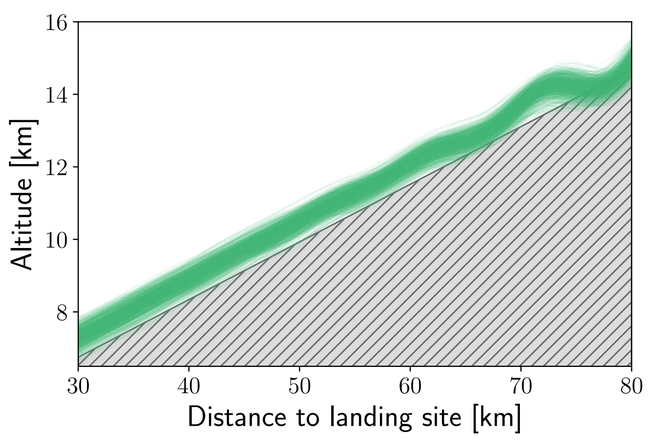

- For a trajectory, the set of all mesh locations where the launcher is outside the flight corridor is called the **excursion set** [1]:

$$\mathcal{E}(\boldsymbol{U}) = \{\boldsymbol{x} \in \mathcal{X} : y(\boldsymbol{U}, \boldsymbol{x}) \notin \text{flight corridor}\}$$

Research problem

- Accurately estimate a **confidence region** for the excursion set [2], that is, a region $\mathcal{C}_\alpha$ which has a probability greater than or equal to α of containing the excursion set:

$$\Pr_{\boldsymbol{U}}(\mathcal{E}(\boldsymbol{U}) \subset \mathcal{C}_\alpha)$$

Surrogate-based estimation

- Monte Carlo estimate of the statistics $\Rightarrow$ need for a **surrogate model**
- A combination of **principal component analysis** [3] and **Gaussian process regression** [4]
- This enables the **prediction** $\hat{\mathcal{C}}_\alpha$ of the confidence region $\mathcal{C}_\alpha$

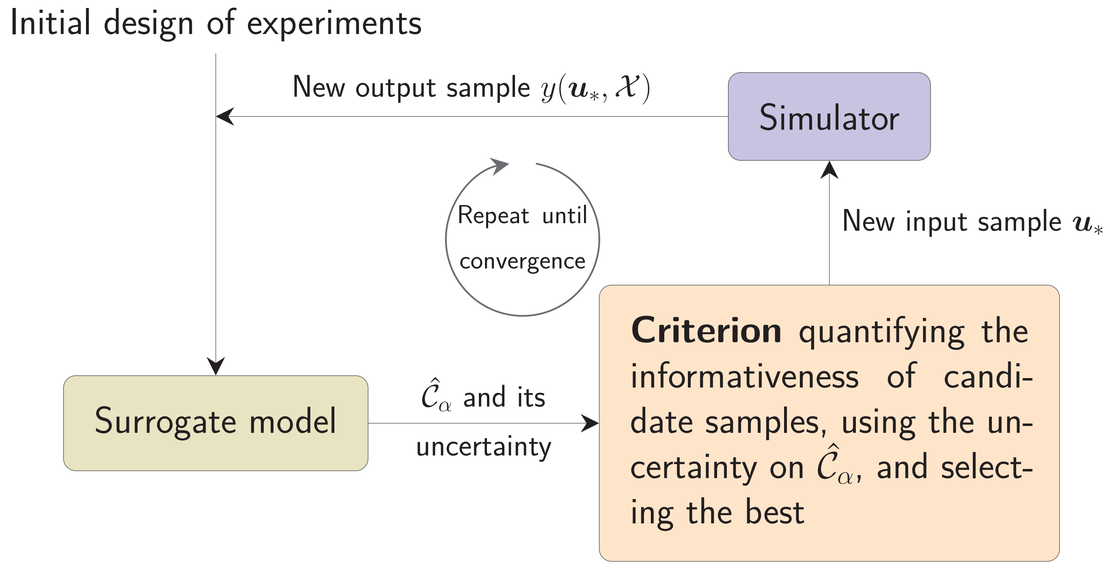

Results

- Computing the confidence region with a confidence level $\alpha = 95\%$
- **Performance metrics:**
  - Probability that the estimated confidence region contains the excursion set: $\hat{\alpha} = \Pr_{\boldsymbol{U}}(\mathcal{E}(\boldsymbol{U}) \subset \hat{\mathcal{C}}_\alpha)$
  - Volume of the mismatch between the true confidence region and its estimate: $\mathrm{Vol}(\mathcal{C}_\alpha \triangle \hat{\mathcal{C}}_\alpha) = \mathrm{Vol}\left((\mathcal{C}_\alpha \backslash \hat{\mathcal{C}}_\alpha) \cup (\hat{\mathcal{C}}_\alpha \backslash \mathcal{C}_\alpha)\right)$
- Proposed method (red dash-dotted line) compared to a surrogate trained with an LHS design [5] of equal computational budget (blue dashed line)
- Despite the small difference in $\hat{\alpha}$ (left), the difference in the mesh space (right) is large, with 1 km vs. 10 km

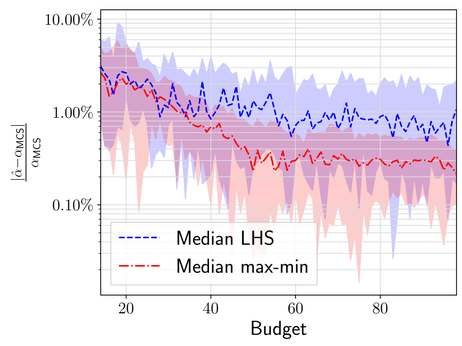

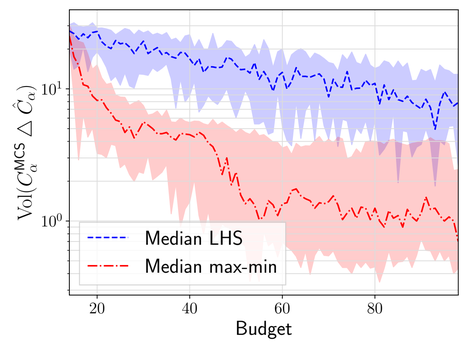

- 20 repetitions of $\hat{\mathcal{C}}_\alpha$ for the LHS (blue) and active learning (red) strategies
- Variability caused by the choice of the initial design is significantly reduced

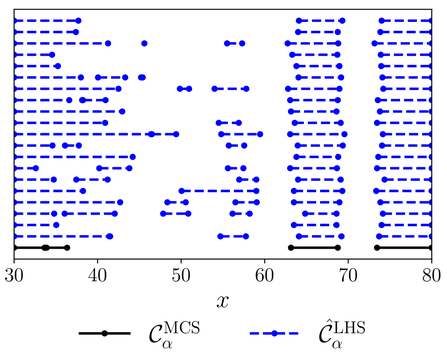

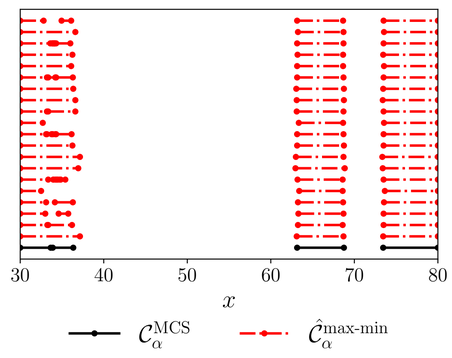

Conclusion and outlook

Summary:

- **Accurate and robust estimation of the confidence region** for an excursion set of a **simulator with functional output** at reduced computational cost
- Application to as **aerospace case study** with relevant performance metrics

Perspectives:

- Study the sources of **epistemic uncertainty**: the Gaussian processes and the choice of initial design of experiments
- Investigation of **more efficient sampling techniques** than standard Monte Carlo to estimate the various statistics

Publications and communications

- **Journal:**
  - Lucas Brunel, Mathieu Balesdent, Loïc Brevault, Rodolphe Le Riche and Bruno Sudret. A survey on multi-fidelity surrogates for simulators with functional outputs: Unified framework and benchmark. *Computer Methods in Applied Mechanics and Engineering*, 435:117577, 2025.
- **Conferences:**
  - UNCECOMP, June 2025, Rhodes, Greece (oral presentation).
  - ECCOMAS, June 2024, Lisbon, Portugal (oral presentation).
  - MORTech, November 2023, Paris-Saclay, France (poster presentation).

References

[1] Ilya Molchanov. *Theory of Random Sets*. Probability and Its Applications. Springer-Verlag, London, 2005.

[2] Joshua P. French and Stephan R. Sain. Spatio-temporal exceedance locations and confidence regions. *The Annals of Applied Statistics*, 7(3):1421–1449, September 2013.

[3] I. T. Jolliffe. *Principal Component Analysis*. Springer Series in Statistics. Springer-Verlag, New York, 2002.

[4] Carl Edward Rasmussen and Christopher K. I. Williams. *Gaussian Processes for Machine Learning*. The MIT Press, November 2005.

[5] Thomas J. Santner, Brian J. Williams, and William I. Notz. Space-filling designs for computer experiments. In *The Design and Analysis of Computer Experiments*, Springer Series in Statistics, pages 145–200. Springer, New York, NY, 2018.

Approches mathématiques pour l'aide à la gestion des lacs eutrophes

Ioana CHIRU[1,2], Eloïse COMTE[2], Catherine CHOQUET[3], Guillaume DEFFUANT[2], Delphine LATOUR[1]

1. Université Clermont Auvergne
2. INRAE UR LISC
3. La Rochelle Université

Ecole doctorale Sciences Pour l'Ingénieur

Objectif

Développer des outils numériques d'aide à la gestion de lacs eutrophes.

Contexte biologique

Phénomène eutrophisation

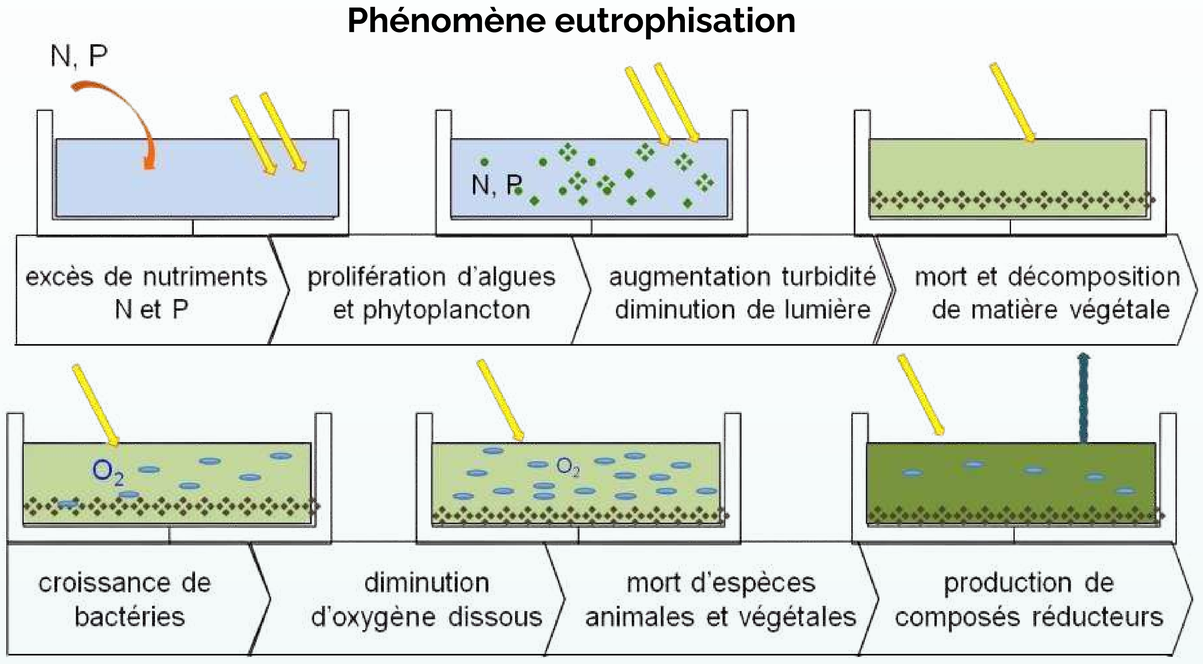

Université de Lorraine
https://rpn.univ-lorraine.fr/UVED/impacts-environnementaux-acv/eutrophisation-des-eaux/co/processus.html

Pigmentation des cyanobactéries

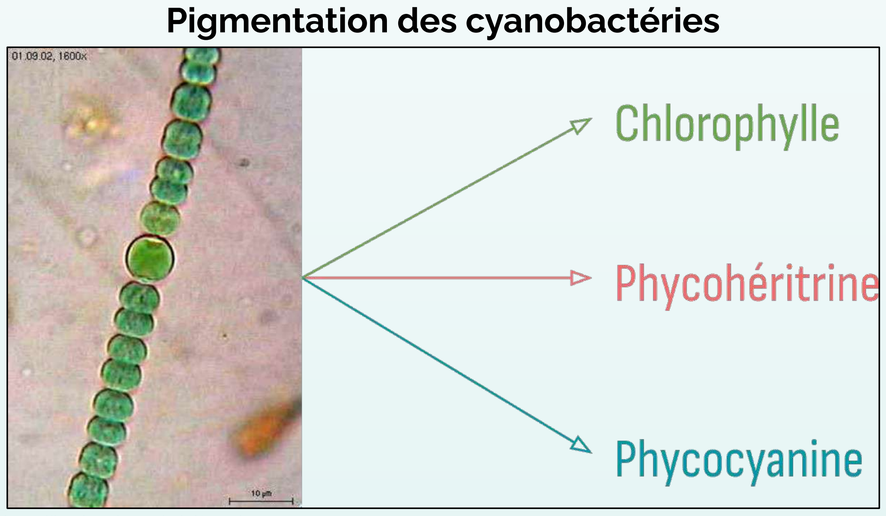

https://fr.wikipedia.org/wiki/Cyanobacteriota

Modélisation mathématique

Problème de Contrôle Optimal [Choquet & Comte, 2023]

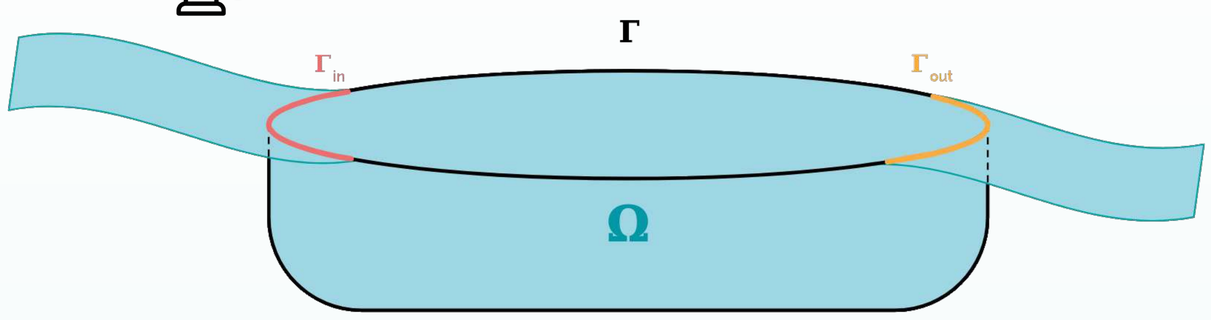

Fonction Objectif

$$\max_{P(t,x)} \int_0^T \Big(\int_{\Gamma_{in}} \underbrace{B(t,\sigma,P(t,\sigma))}_{\text{bénéfices}} e^{-\rho t} d\sigma - \int_\Omega \underbrace{D(t,x,c(t,x))}_{\text{dommages}} e^{-\rho t} dx \Big) dt$$

Modèle d'état, stock de phosphore S, concentration en cyanobactéries c, phosphore entrant P, vitesse du fluide v

$$\partial_t S = -\underbrace{\mathrm{div}(vS)}_{\text{convection}} - \overbrace{b(S)S}^{\text{dégradation}} + \underbrace{h(S)}_{\text{relargage}} + \overbrace{d_S \Delta S}^{\text{diffusion}} - \underbrace{f(S,c)c}_{\text{Monod}} \quad \text{dans } \Omega_T$$

$$\partial_t c = -\underbrace{\mathrm{div}(vc)}_{\text{convection}} - \overbrace{m(c)c}^{\text{dégradation}} + \underbrace{d_c \Delta c}_{\text{diffusion}} + \underbrace{f(S,c)c}_{\text{Monod}} \quad \text{dans } \Omega_T$$

Conditions initiales et au bord

$$S_{|t=0} = S_0,\ c_{|t=0} = c_0 \quad \text{dans } \boldsymbol{\Omega}$$
$$S = P\ ;\ (cv - d_c \nabla c)\cdot \mathbf{n} = 0 \quad \text{sur }]0,T[\times \boldsymbol{\Gamma}_{in}$$
$$(Sv - d_S \nabla S)\cdot \mathbf{n} = (cv - d_c \nabla c)\cdot \mathbf{n} = 0 \quad \text{sur }]0,T[\times \boldsymbol{\Gamma}$$
$$r_S S + (Sv - d_S \nabla S)\cdot \mathbf{n} = R_S(S) \quad \text{avec } r_s \leqslant 0,\ \text{sur }]0,T[\times \boldsymbol{\Gamma}_{out}$$
$$r_c c + (cv - d_c \nabla c)\cdot \mathbf{n} = R_c(c) \quad \text{avec } r_c \leqslant 0,\ \text{sur }]0,T[\times \boldsymbol{\Gamma}_{out}$$

Outils

Réflectance et satellites

Réflectance des pigments

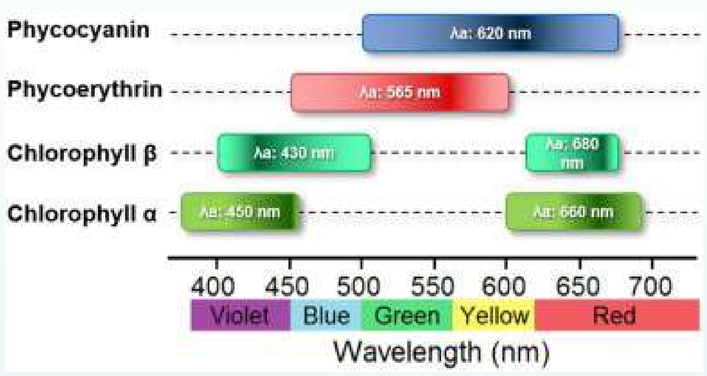

[Hsieh-Lo et al., 2019]

Algorithme de calcul de concentration

$$MPH = R(\lambda_{max}) - R(664) - \frac{R(885) - R(664) \times (\lambda_{max} - 664)}{885 - 664}$$

avec R(λ) la réflectance pour la longueur d'onde λ et λ_{max} la position du pic le plus haut entre les bandes de 681, 709 et 753nm.

[Matthews et al., 2012]

$$[chl - a] = 2.72 + 6903.13 \times MPH$$

Satellites

sentinel-2

Venus

Exemple de résultat issu de la littérature

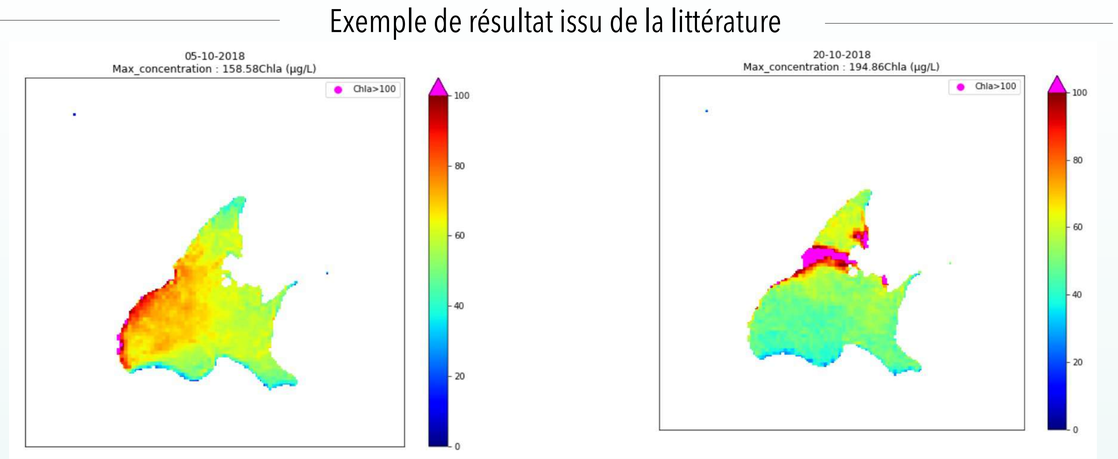

[Diene, 2023]

Bibliographie

(1) Choquet, C., & Comte, E. (2023). Optimal control of lake eutrophication. *Journal of Mathematical Analysis and Applications*, *528*(2), 127528. https://doi.org/10.1016/j.jmaa.2023.127528

(2) Diene, D. (2023). Analyse par images satellite de la dynamique d'eutrophisation des lacs : application au lac d'Aydat (Rapport de stage non publié). INRAE

(3) Hsieh-Lo, M., Castillo, G., Ochoa-Becerra, M. A., & Mojica, L. (2019). Phycocyanin and phycoerythrin : Strategies to improve production yield and chemical stability. *Algal Research*, *42*, 101600. https://doi.org/10.1016/j.algal.2019.101600

(4) Matthews, M. W., Bernard, S., & Robertson, L. (2012). An algorithm for detecting trophic status (chlorophyll-*a*), cyanobacterial-dominance, surface scums and floating vegetation in inland and coastal waters. *Remote Sensing of Environment*, *124*, 637-652. https://doi.org/10.1016/j.rse.2012.05.032

Jewelry workshop scheduling by reinforcement learning

Thomas Combettes, Violaine Antoine, Farouk Toumani

Université Clermont Auvergne, LIMOS, CNRS, Clermont-Ferrand, France

Objectives

1. Create a scheduler that is fast and proposes robust scheduling solutions
2. Optimize the coordination of various artisanal stages in jewelry manufacturing
3. Implement reinforcement learning techniques to manage complex scheduling constraints

Introduction

- NEO-FUGU® is a company with 50 employees based in Clermont-Ferrand and specialized in developing management software for the jewelry industry, but their software offering does not include a planning and scheduling module.
- Workshop scheduling in fine jewelry consists of organizing and sequencing jewelry manufacturing. This process coordinates various artisanal stages (jewelry-making, setting, polishing) while managing constraints associated with precious materials and specific techniques. The goal is to reconcile craftsmanship excellence with deadline requirements.

Methods

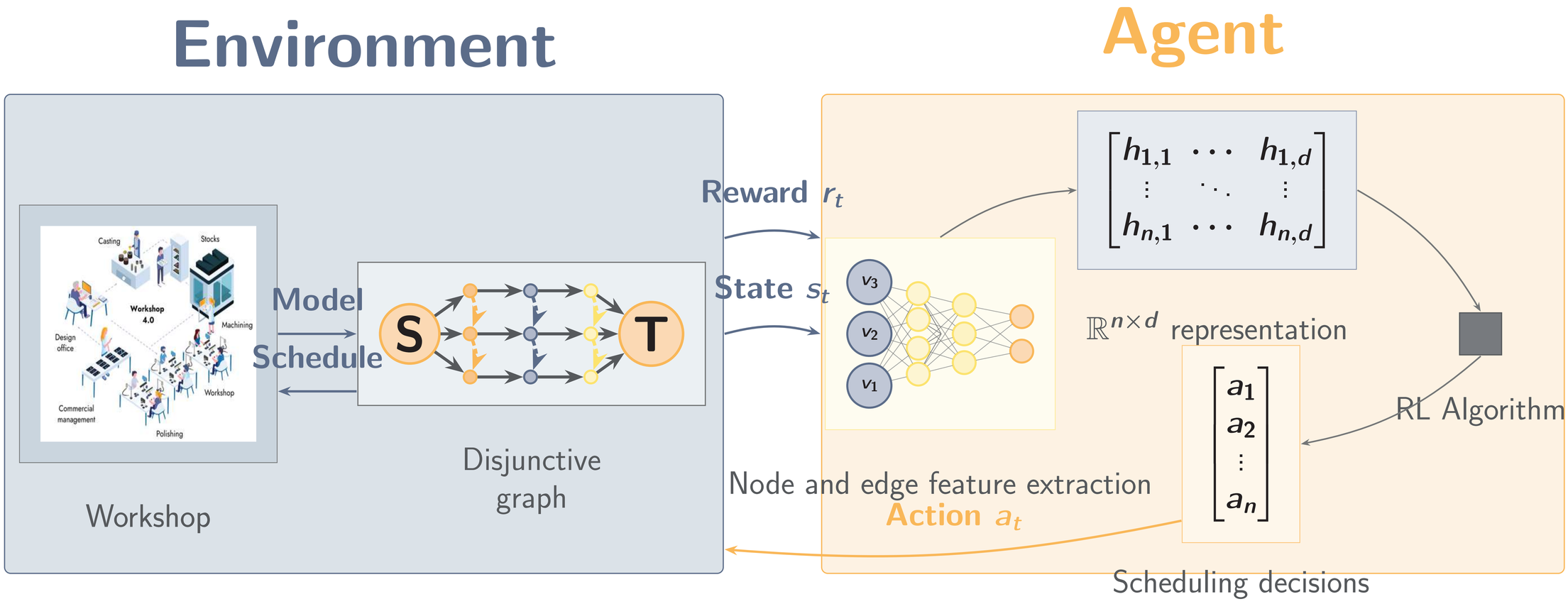

Specials constraints

- **Multi-skilled operators**: Each artisan has specific competencies (jeweler, polisher, crimper).
- **Batch operations**: Electroplating and melting processes handle multiple orders simultaneously, requiring capacity-aware scheduling.
- **Material dependencies**: Operations cannot start until precious materials are received and available in stock.
- **Stochastic durations**: Processing times have $\pm 30\%$ uncertainty, requiring robust scheduling approaches.
- **Component interdependencies**: Some manufacturing orders produce components required for other orders, creating precedence constraints.
- **Subcontracting flexibility**: Certain operations can be outsourced based on workload and competency criteria.

References

1 Infantes, G., Roussel, S., Pereira, P., Jacquet, A., & Benazera, E. (2024). Learning to solve job shop scheduling under uncertainty. *Integration of Constraint Programming, Artificial Intelligence, and Operations Research (CPAIOR 2024). Lecture Notes in Computer Science*, 14742, 329-345.

2 Bengio, Y., et al. (2021). Machine learning for combinatorial optimization: A methodological tour d'horizon. *European Journal of Operational Research*, 290(2), 405-421.

Contact Information

- Email: thomas.combettes@neo-logix.fr thomas.combettes@limos.fr
- Laboratory: LIMOS, Université Clermont Auvergne
- Company: NEO-FUGU®, Clermont-Ferrand

Apprentissage et transfert de compétences pour des applications robotiques

Doctorant : Antonio Claudio DE SOUSA DOS SANTOS FILHO

Encadrants : Sébastien LENGAGNE, Benoit THUILOT

Ecole Doctorale Sciences Pour l'Ingénieur

Contexte

- L'apprentissage en robotique :

- Efficace dans les tâches dynamiques. 👍
- Efficace dans les tâches non structurés. 👍
- Apprendre pour chaque nouveau robot. 👎
- Temps de calcul, énergie... 👎

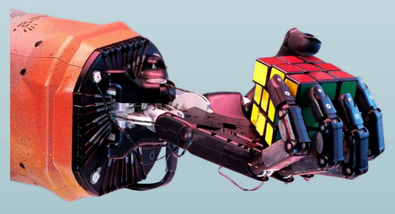

Fig 1 : Apprentissage pour les tâches complexes.[1]

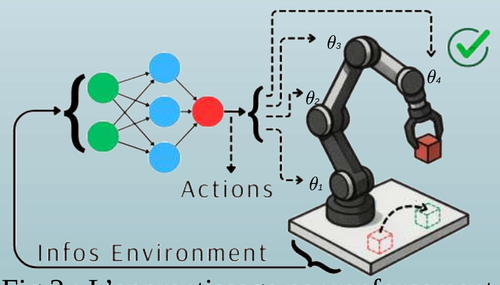

Fig 2 : L'apprentissage par renforcement en robotique.

- Le transfert de compétences :

- Réduire le coût d'énergie. 👍
- Réduire le temps de calcul. 👍
- Différents morphologies. 👎
- Différents contraintes physiques. 👎

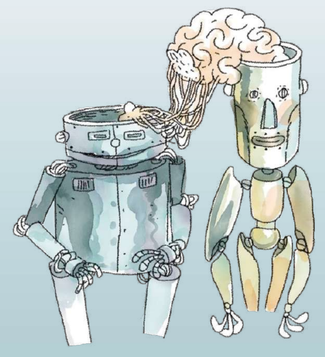

Fig 3 : Transfert de compétences entre robots.[2]

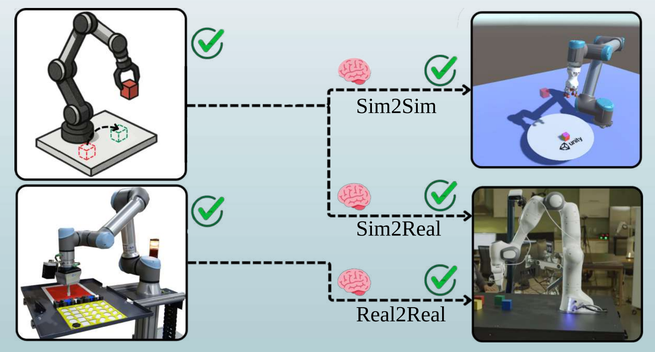

Fig 4 : Transfert de compétences Sim2Sim, Sim2Real et Real2Real.

Objectifs

I. Proposer un **framework** pour **l'évaluation** de différentes méthodes de transfert de compétences entre robots.

II. Effectuer le transfert de compétences entre les différents **robots physiques réels** en **boucle fermée**.

I. Framework de Comparaison

- Objectif : évaluer des méthodes de transfert de compétences entre robots sur plusieurs tâches robotiques, en simulation et sur des robots réels.

Méthodes à évaluer

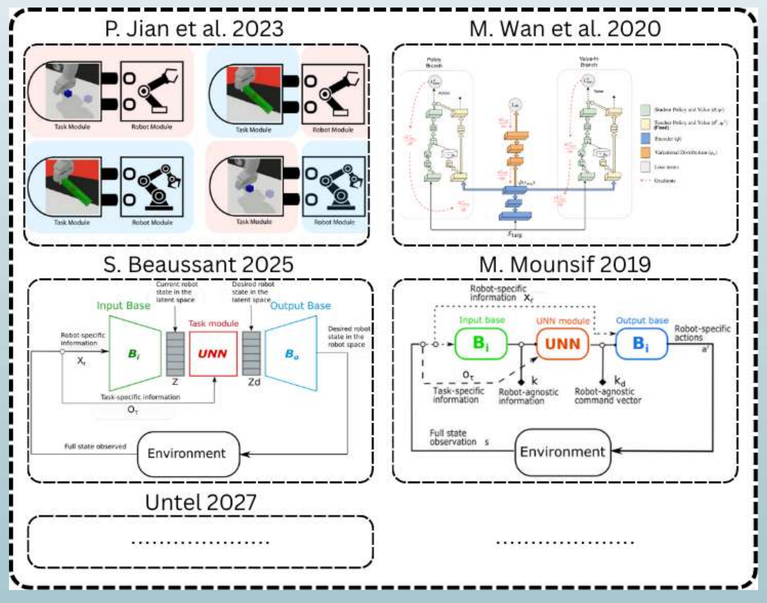

TL Framework

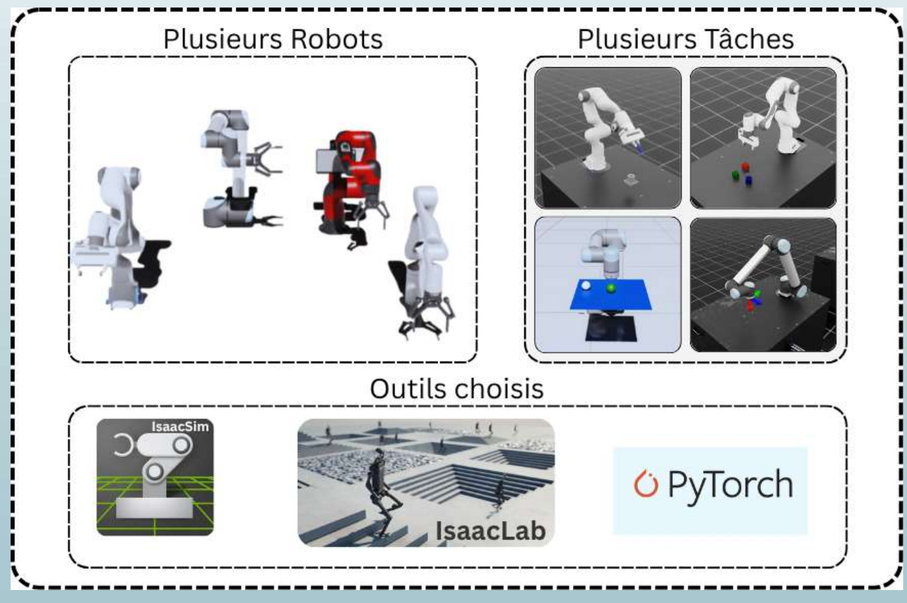

Métriques

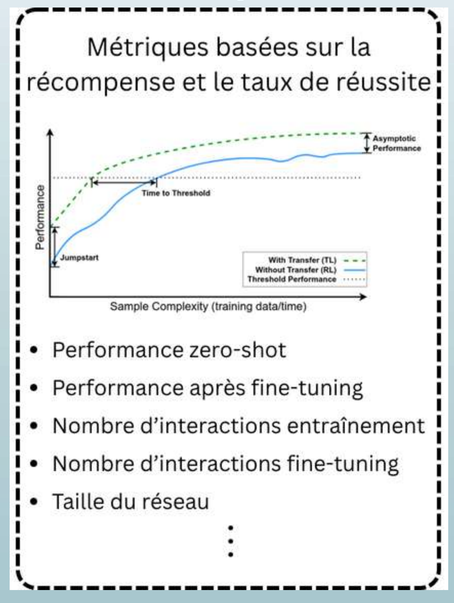

- Performance zero-shot
- Performance après fine-tuning
- Nombre d'interactions entraînement
- Nombre d'interactions fine-tuning
- Taille du réseau

⋮

- Travaux en cours :

- Implémentation et comparaison de différentes méthodes de transfert de compétences.
- Ajout de nouveaux robots et de différents algorithmes d'apprentissage dans le framework.

II. Transfert en Boucle Fermée

- Transfert de compétences en boucle fermée avec :

- Différents robots réels.
- Différents capteurs.
- Différents retards.

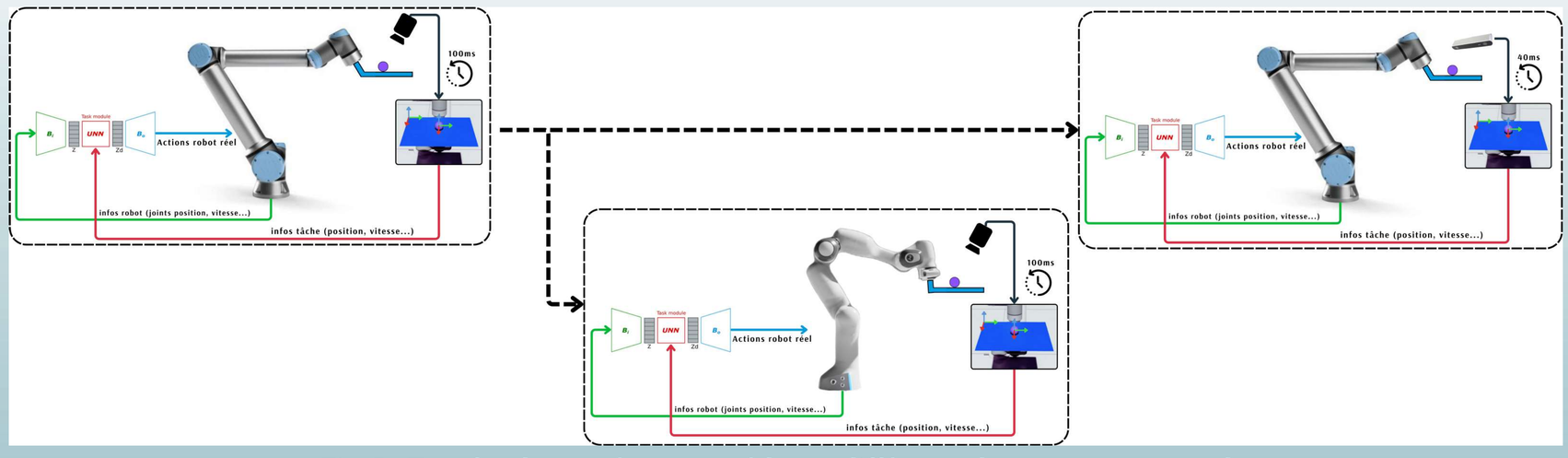

Fig. 5 : Transfert de compétences en réel entre différents robots, capteurs et retards.

[1] OpenAI, "Solving Rubik's Cube with a Robot Hand," OpenAI, Oct. 15, 2019. [Online]. Disponible: https://openai.com/index/solving-rubiks-cube.
[2] The Data Frog, "Image from: Image Recognition with Transfer Learning," The Data Frog, Sep. 25, 2022. [Online]. Disponible: https://thedatafrog.com/en/articles/image-recognition-transfer-learning.
[3] M. Wan et al. "Mutual information based knowledge transfer under state-action dimension mismatch," arXiv preprint arXiv:2006.07041, 2020.
[4] P. Jian et al. "Policy stitching: Learning transferable robot policies," arXiv preprint arXiv:2309.13753, 2023.
[5] M. Mounsif et al., "Universal notice network: Transferable knowledge among agents," in Proc. 6th Int. Conf. Control, Decision and Information Technologies (CoDIT), IEEE, 2019.
[6] S. Beaussant et al. "Towards zero-shot cross-agent transfer learning via latent-space universal notice network," Robotics and Autonomous Systems, 2025.

Modélisation et de la simulation du brouillard dans les images en contexte polarimétrique

Koundioun Dembélé[1], Frédéric Bernardin[1], Jean−François Cornet[2], Amine Ben Daoued[1], Frédéric Szczap[3], Jean−Philippe Tarel[4]

1 CEREMA, 2 Institut Pascal, 3 UCA/LaMP 4 COSYS/Pics-L

Introduction

La polarisation étudie le comportement des champs électriques associés à la propagation de la lumière. Une lumière est dite polarisée si les champs électriques associés à cette propagation sont orientés de manière particulière (linéaire, circulaire ou elliptique) sinon elle est non polarisée. L'imagerie polarimétrique pourrait être utilisée dans plusieurs domaines scientifiques. **En télédétection** pour la surveillance et la détection des changements dans la végétation et dans les champs agricoles. **En industrie**, elle est utilisée pour contrôler la qualité des surfaces et des matériaux pour la détection d'éventuels défauts ou variations de texture invisible à l'œil nu ou par l'imagerie classique. **En défense et sécurité**, l'imagerie polarimétrique est utilisée pour détecter les objets camouflés et la surveillance et détection des zones sensibles et complexes à accéder. **En médecine,** elle est utilisée comme outil d'aide au diagnostic médical. Elle offre la possibilité de bien caractériser les tissus biologiques (détection d'anomalies précoces dans les tissus, augmentation du contraste). **En réalité augmentée et interfaces intelligentes**, l'imagerie polarimétrique est en phase exploratoire pour améliorer la reconnaissance faciale et le suivi oculaire. Pour **le transport**, elle pourrait être utilisée pour améliorer la **visibilité aérienne**, **maritime** et la **navigation automobile** dans les **conditions météorologiques dégradées où la visibilité est faible**. Ma thèse vise à explorer les potentialités offertes par l'imagerie polarimétrique pour améliorer la visibilité météorologique des véhicules autonomes dans le brouillard. Pour cela, on se basera sur les études similaires réalisées comme [1], [2], [3], [4] pour proposer notre approche d'estimation de la distance de visibilité météorologique. Toutes ces études ont prouvé que l'imagerie polarimétrique est la mieux adaptée pour détecter et estimer la distance de visibilité dans le brouillard par rapport à l'imagerie classique.

Objectifs

Développement des modèles et des méthodes pour caractériser les conditions de visibilité dégradée dans l'imagerie polarimétrique.

Première partie:

Exploration/développement de modèles simples basés sur la physique prenant en compte la polarimétrie dans des conditions météo dégradées. (SWEET modifié)

SWEET: **S**imulating **WE**ather for int**E**lligent **T**ransportation

Deuxième partie:

Comparaison simulation physique et numérique (Différents niveaux de raffinement de modèles)

Méthodes

Dans notre méthodologie, on fera à la fois de l'expérimentation et de la simulation pour estimer les propriétés optiques du brouillard qui aboutiront à la distance de visibilité météorologique.

Prototype expérimental

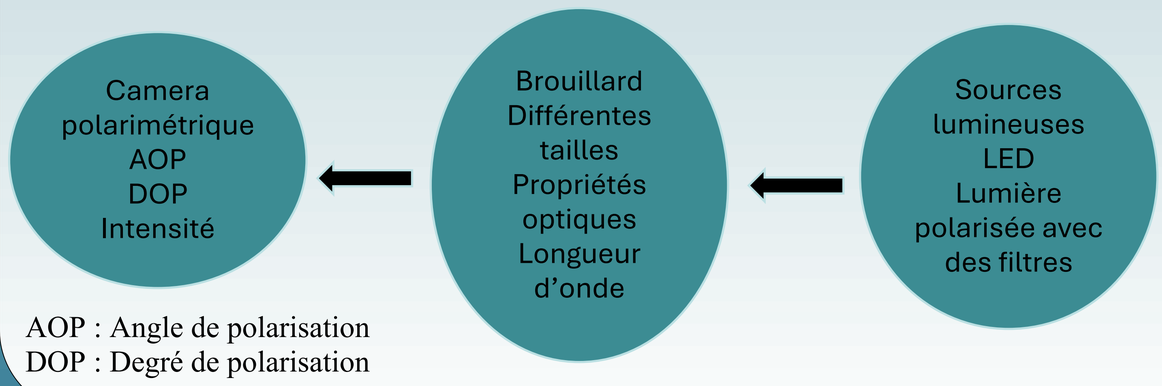

AOP : Angle de polarisation
DOP : Degré de polarisation

Moyens expérimentaux

Figure 1: Caméra polarimétrique

La plateforme PAVIN météo extrême du CEREMA Clermont-Ferrand a servi de local pour les premières acquisitions de données de ma thèse en début juin 2025. Lors de cette campagne de mesure, plusieurs caméras RGB et polarimétriques comme celle que j'utilise dans ma thèse (Figure 1) ont été utilisées pour déterminer les propriétés optiques du brouillard en présence des sources lumineuses différentes (LED, lumière polarisée avec des filtres et la lumière du jour).

La plateforme PAVIN (Figure 2) offre la possibilité de fournir des conditions de mesures proches de la chaussée urbaine (brouillard avec différentes tailles, la pluie, lumière LED/ jour, marquage au sol, etc.)

Plateforme **PAVIN** avec les caméras classiques et polarimétriques pour les mesures dans le cadre du projet scientifique **ANR-INARI** dont ma thèse en fait partie.

Figure 2: Plateforme PAVIN météo extrême (brouillard et pluie) située à Clermont Ferrand, elle a 50 m de long et 7 m de large.

INARI: vIsion multimodale pour une NAvigation et une commande Robuste de véhIcule autonome

Simulation numérique

Dans cette partie, on cherchera à développer le modèle SWEET du CEREMA en intégrant la polarisation et cela en traitant l'équation du transfert radiatif (ETR) du vecteur de Stokes (Forme vectorielle).

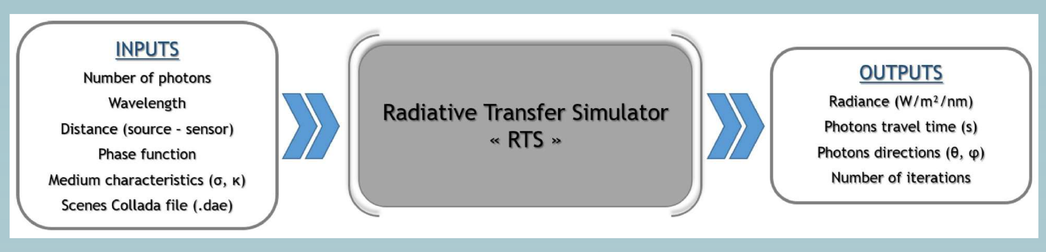

Figure 3 : Les entrées et les sorties du modèle SWEET du CEREMA.
Source : **Amine Ben-Daoued, Pierre Duthon et Frédéric Bernardin, SWEET: A Realistic Multiwavelength 3D Simulator for Automotive Perceptive Sensors in Foggy Conditions, J. Imaging 2023.**

Résultats

Les premières mesures sont en cours d'acquisition ce début juin 2025 dans le cadre du projet **ANR-INARI**. Ces mesurent permettront d'évaluer comment se comporte les différentes polarisations (linéaire, circulaire etc.) dans le brouillard.

Bibliographie

1- Ballesta-Garcia, M et al Experimental charactérization of polarized light backscattering in fog environments, Sensors 2023
2- Ballesta-Garcia, M et al Polarimetric imaging vs conventional imaging; Evaluation of image contrast in fog, Atmosphere 2021.
3- Fu, Q. et al, Study of sea fog environment polarisation transmission characteristics.
Appl. Sci. 2022
4-Tianwei, H. et al, Broad-Band Transmission Characteristics of Polarizations in Foggy Environments. Atmosphere. 2019
5- Amine Ben-Daoued, Pierre Duthon et Frédéric Bernardin, SWEET: A Realistic Multiwavelength 3D Simulator for Automotive Perceptive Sensors in Foggy Conditions, J. Imaging 2023.

Planning multi-functional forest management at the landscape scale

UNIVERSITÉ Clermont Auvergne
Ecole doctorale Sciences Pour l'Ingénieur

INRAE
Laboratoire d'ingénierie pour les systèmes complexes

Clémentine de Montgolfier

Jean-Denis Mathias (LISC), Jean-Baptiste Pichancourt (LISC), Marion Jourdan (SILVA)

Introduction

Managing multi-functional forests— for timber, carbon storage, and biodiversity—requires planning at both the stand and landscape scales. While stand-level management can enhance local biodiversity, it may lead to homogenization across the landscape, reducing habitat diversity and increasing vulnerability to disturbances [1]. Landscape-scale approaches are better suited to address these broader ecological dynamics and support more resilient forest systems [2].

However, implementing effective landscape-scale planning is complex. It involves not only deciding what management actions to take but also where to apply them across heterogeneous forested areas.
To address these challenges, innovative tools from complex systems dynamics and control theory are needed. These methods can help explore a broad set of planning strategies that account for spatial structure, trade-offs, and the need for multi-functionality in forest landscapes..

Spatial functions

Wood production

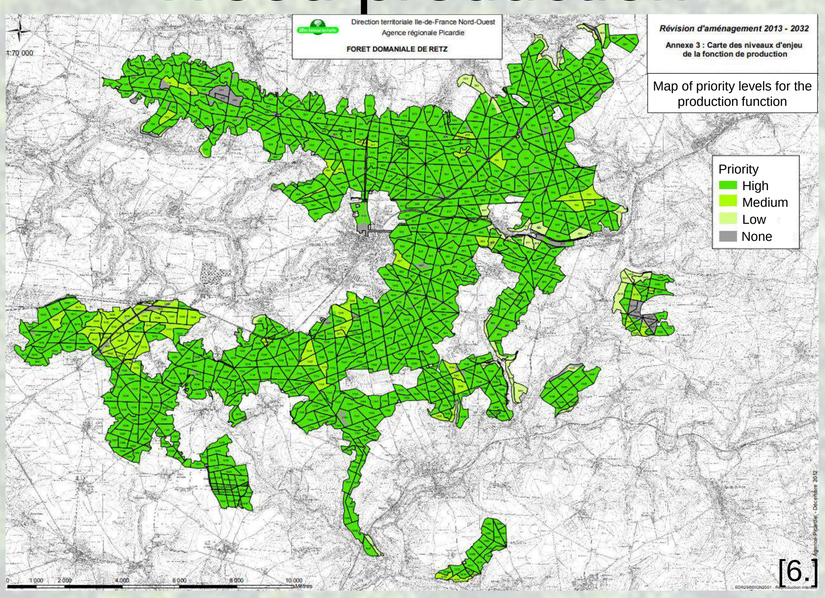

[6.]

Biodiversity and habitat

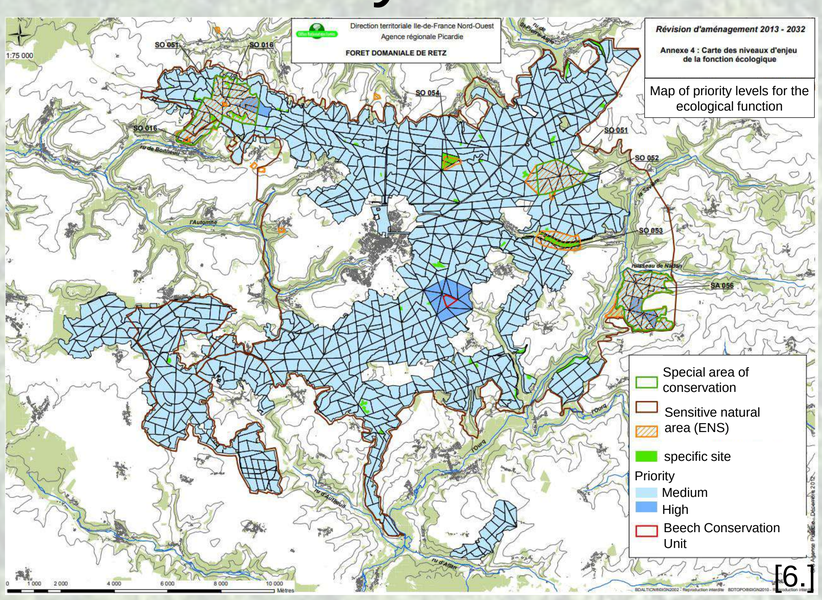

[6.]

Social utility

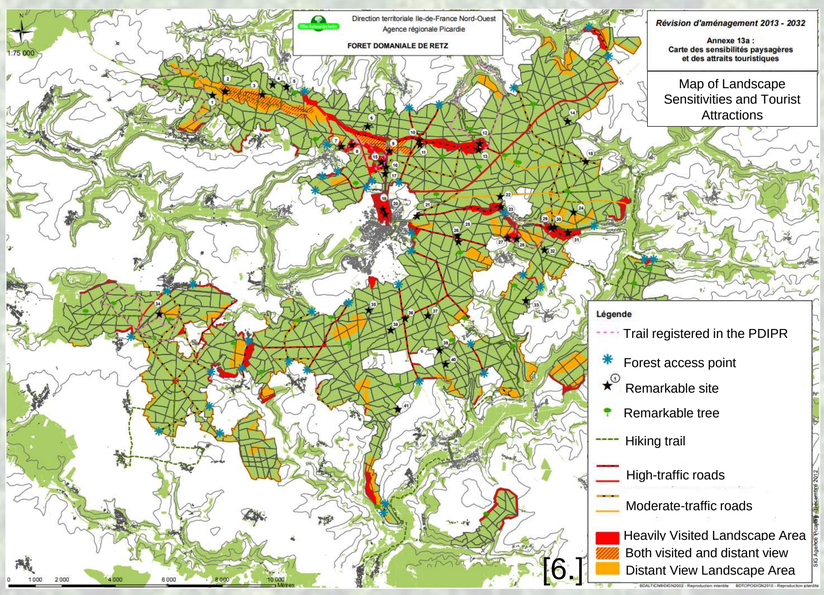

[6.]

The maps reveal the spatial complexity of forest management challenges.

- Diverse functions and goals to address
- Uneven spatial scales: some very local, others global
- Overlapping zones, potential hotspots for conflict

Method development

Challenges

The complexity of terrain and ecosystems across large landscapes presents significant challenges for management methods, including:

- Modeling ecosystems accurately at broad spatial scales
- Managing the computational complexity due to a large number of possible management actions
- Meeting multiple, often conflicting constraints simultaneously
- Adaptability of tools for different use (limit of optimality)

Goals

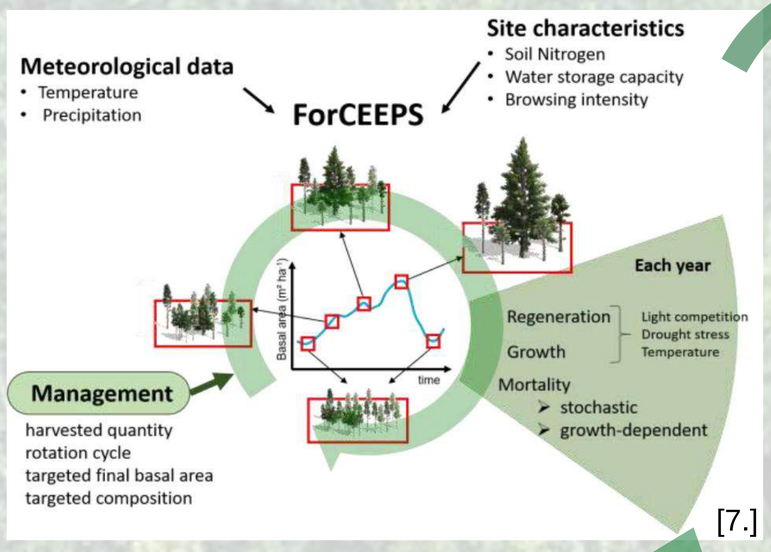

[7.]

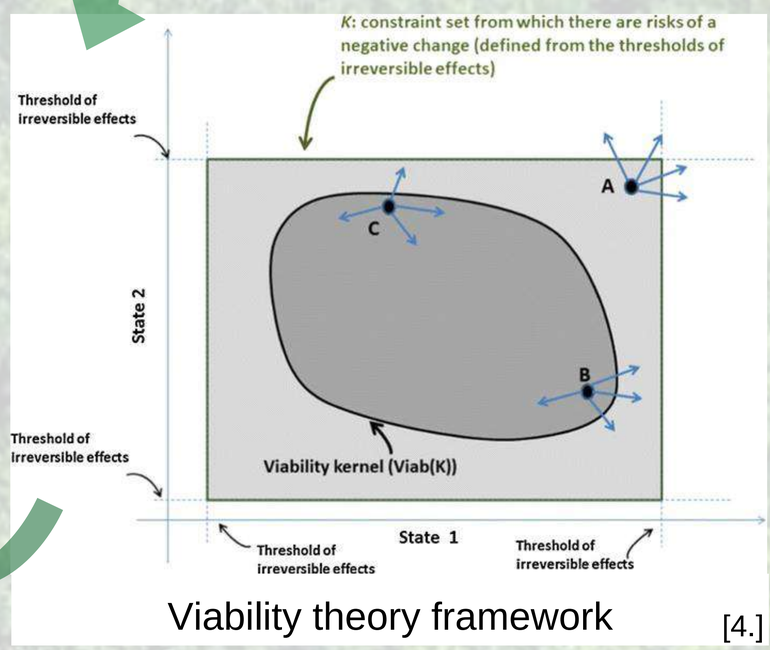

Viability theory framework [4.]

- Extend the mechanistic forest model ForCEEPS to predict dynamics at the forest scale
- Apply viability theory to formulate forest management as a control problem under multiple constraints

Conclusion

Managing forests at the landscape scale is challenging due to the complexity of ecosystems, the diversity of services they provide, and the need to balance production, biodiversity, social demands, and climate adaptation.
New tools like control theory can help by revealing system dynamics and offering flexible pathways, allowing managers to adapt strategies to their local context [4].

To make this possible, new governance structures will be needed—ones that support collaboration and long-term planning across scales [5].

Bibliography

1. **Heinrichs, S., et al. (2019). *Landscape-scale tree mixtures benefit plant and lichen biodiversity*. Forests, 10(1), 73.**
2. **Duflot, R., Fahrig, L., Mönkkönen, M. (2022). *Management diversity promotes biodiversity in production forests*. Biol. Conserv., 268, 109514.**
3. **Morin, X., Bugmann, H., de Coligny, F., et al. (2021). *A gap model for ecosystem function and tree composition under climate change*. Funct. Ecol., 35(4), 955–975.**
4. **Mathias, J.-D., Bonté, B., et al. (2015). *Viability theory and forest management flexibility*. Environ. Manage., 56(5), 1170–1183.**
5. **Pichancourt, J.-B., Brias, A., Bonis, A. (2025). *Integrating adaptation pathways and Ostrom's framework for sustainable governance of social-ecological systems in a changing world.***
6. **ONF (Office National des Forêts). Plan d'aménagement forestier de la forêt domaniale de Retz 2013–2032.**
7. **Jourdan, M. (2018). *Le rôle de la diversité sur la stabilité des processus des écosystèmes forestiers en contexte de changement climatique*. Thèse de doctorat, AgroParisTech. ffNNT : 2018AGPT0009ff.**

Set Reconfiguration and First Order Logic

Jona Dirks, Mamadou Kanté, Alexandre Vigny
LIMOS / Université Clermont Auvergne

Imagine overlooking trams industriously moving through a rush-hour city, when suddenly an accident is blocking one of the core intersections. Is it possible to reroute while keeping a safe distance between the trams and only driving on the right side of the road? And if a computer is to hand, how fast can you compute it? The answers can be derived from Set Reconfiguration on graphs.

Graphs

A graph G consists of a set of vertices $V(G)$ and a set of edges $E(G)$ that connect pairs of these vertices. Imagine vertices as points and edges as lines each connecting two of these points. Often it is useful to give edges a direction (imagine edges as arrows), this is called a directed graph.

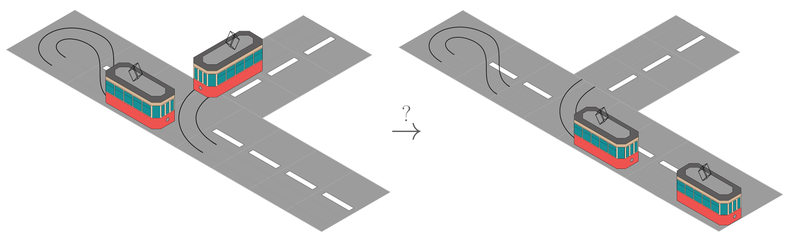

Fig. 1: Stuck and unstuck trams that can be represented using graphs

Graphs are a useful tool to model reality, as they leave out unnecessary information. For example, the essence of the tram network above is formalized by the graphs on the right. Additional information, such as the position of trams, might be represented by a subset of the vertices.

Complexity Theory

Complexity Theory determines how hard a problem is to solve by analyzing how much resources are required so solve it. The analysis is based on the size of the input.
Parameterized Complexity tries to give a more detailed understanding by introducing parameters: numbers that further describe the instance. Some problems that are considered not to be efficiently solvable in the traditional setting can become tractable given the right parameter.

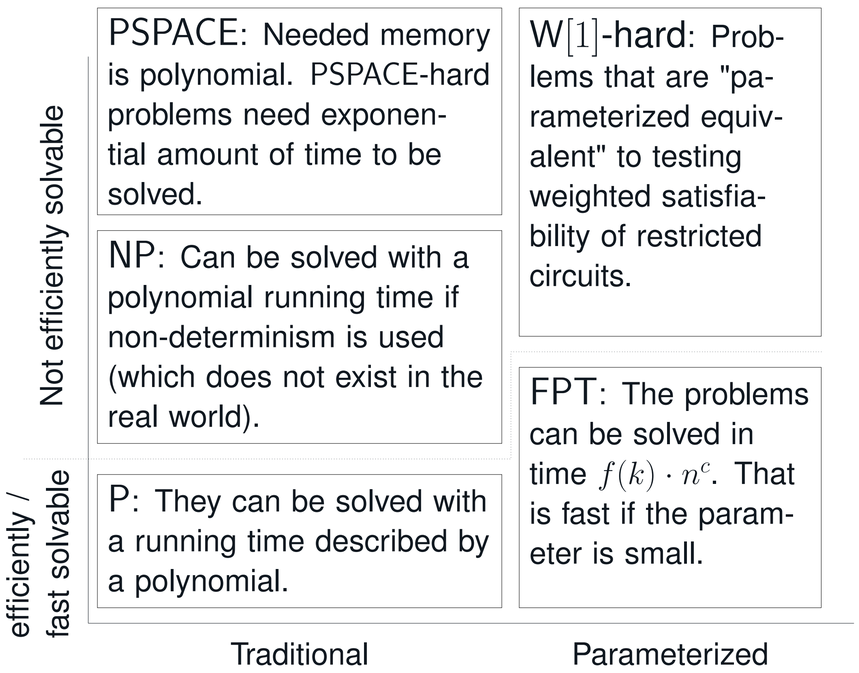

Fig. 2: For us relevant complexity classes

Structural Parameters

Very often the solution size (k) is taken as a parameter. We can also consider parameters that describe the graph.
Many problems become tractable on trees. Thus, one of the classical parameters is treewidth, that measures how similar to a tree a graph is.

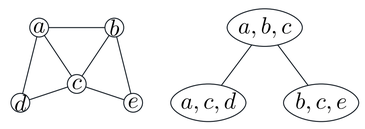

Fig. 4: A graph and a tree-decomposition showing similarity to trees

Example

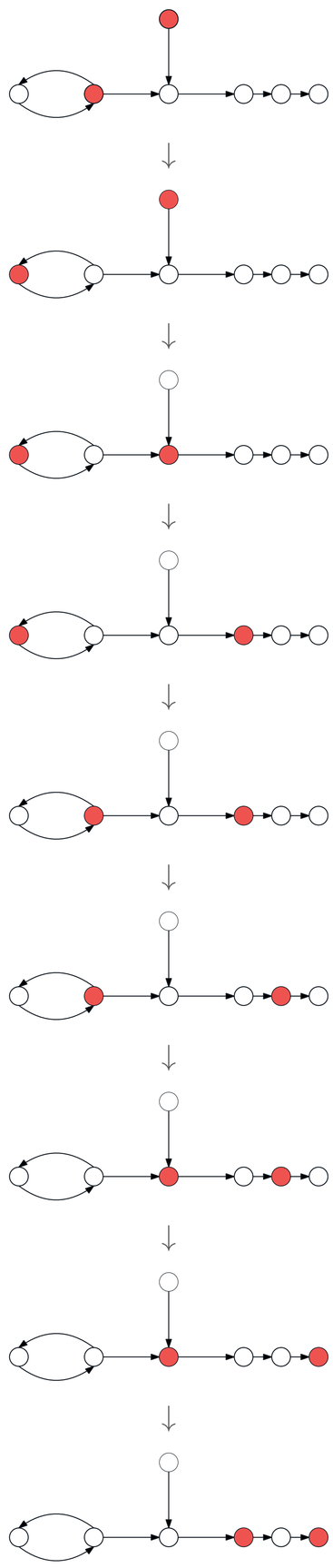

Fig. 3: A Independent Set Reconfiguration Sequence

Problem Definition

Graph Reconfiguration (in general)
Input: A graph G and two solutions S, D for a problem P
Question: Does there exist a sequence $S = S_1, \ldots, S_\ell = D$ of solutions for P in G such that S_i is a neighbor of S_{i+1}.

Problems. One might consider any problem. Here we consider Independent Set.

Independent Set
Input: A graph G, a integer k
Question: Does there exists a subset of k vertices $S \subseteq V(G)$ such that none of them are neighbors.

An example of an independent set of size 2 is marked in red on all graphs to the left.

Neighboring Configurations. We treat the elements of the independent set as tokens that travel over the graph. Two main models studied for undirected graphs:

- **Token Jumping:** In each step one token can jump from any vertex to any other vertex.
- **Token Sliding:** In each step one token can move towards a neighboring vertex.

Only Token Sliding plays out different for directed graphs. We additionally require that token only move along the edge direction. These problems are abbreviated with ISR-TJ, ISR-TS and ISR-DTS.
To come back to the example from the introduction, what we want to solve there is ISR-DTS. With trams being considered tokens, moving through the graph along the possible travel directions. The independent set assures the necessary safety distance. As the reconfiguration in Fig. 3 shows, the desired state of Fig. 1 is obtainable from the initial state.

What is known

The undirected setting of ISR-TS and ISR-TJ is quiet well understood, even though open questions remain. However, the complexity of the directed setting remains largely unknown. Only recently ISR-DTS has been studied in the literature [3].

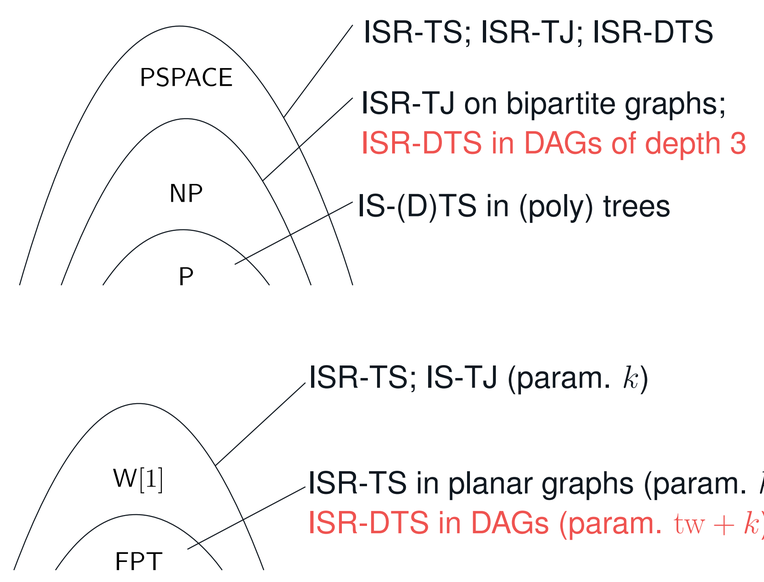

Fig. 5: Overview on Complexity of ISR

What is the idea for moving forward?

In the real world, we often encounter problems that are variations of the pure problems studied in the literature. Proving that individual problems are tractable is tedious work.
To cover many of these cases we have argumentative tools called Meta-Theorems. Meta-Theorems use that many problems can be expressed within certain logics, like First Order Logic. The Idea is to show that every problem expressible in a certain logic is solvable on certain graph classes.

References

All figures are own illustrations; Fig 5 is based on [1], the highlighted parts from [2], the non heightened directed result from [3].

[1] Nicolas Bousquet et al. “A survey on the parameterized complexity of reconfiguration problems”. In: *Comput. Sci. Rev.* 53 (2024), p. 100663.
[2] Jona Dirks and Alexandre Vigny. *Token Sliding Reconfiguration on DAGs*. 2025.
[3] Takehiro Ito et al. “Independent Set Reconfiguration on Directed Graphs”. In: *Intl. Symp. on Mathematical Foundations of Computer Science (MFCS)*. Vol. 241. LIPIcs. Schloss Dagstuhl - Leibniz-Zentrum für Informatik, 2022, 58:1–58:15.

Modèles d'ordonnancement stochastique avec prise en compte de contraintes prescriptives de la maintenance.

Durrieu Maëlys[1,2]
Dalla Torre Alex[3], Gayon Jean-Philippe[1], Massonnet Guillaume[2]

[1]Université Clermont-Auvergne, [2]IMT Atlantique, [3]Université Catholique de l'Ouest

Ecole doctorale Sciences Pour l'Ingénieur

Introduction

Le contexte

L'efficacité de la production est un sujet important dans l'industrie, et les travaux d'optimisation sur ce sujet permettent de réduire le gaspillage de matières premières, la consommation énergétique, ainsi que les coûts de production.

Définitions

Recherche opérationnelle : approche quantitative permettant de produire de meilleures décisions. Elle fournit des outils pour rationaliser, simuler et optimiser l'architecture et le fonctionnement des systèmes industriels et économiques.

Ordonnancement : détermination de l'ordre dans lequel les tâches et les opérations de production seront réalisées pour optimiser l'utilisation des ressources et atteindre les objectifs fixés.

Maintenance : ensemble des opérations permettant de maintenir ou de rétablir un matériel, un appareil, un véhicule, etc., dans un état donné, ou de lui restituer des caractéristiques de fonctionnement spécifiée.

Le projet POMPIER

Dans le projet POMPIER, on cherche à faire converger les objectifs d'optimisation des processus de production et ceux en lien avec la maintenance des équipements ; en effet, l'usure des équipements de production influence directement les performances de la production :
- Risque de panne grave : remplacement d'un équipement, danger…
- Diminution de l'efficacité : production moins fiable (produits non-conformes), utilisation de plus d'énergie pour un même travail…
- Arrêt de la production.

Afin d'éviter ces inconvénients, il est possible de procéder à diverses opérations de maintenance dites préventives, c'est-à-dire intervenant avant la panne. Celles-ci peuvent être de différents types :
- Périodique : maintenance tous les X semaines
- Utilisation : maintenance tous les X produits créés
- Conditionnelle : basée sur l'état du système, maintenance déclenchée par le dépassement d'un seuil
- Prédictive : basée sur l'analyse des données
- Prescriptive : basée sur l'analyse des données, plus d'explicabilité quant aux causes de l'usure.

Ma thèse

On s'intéresse dans le cadre de ma thèse plus spécifiquement à l'optimisation de l'ordonnancement et de la maintenance de façon conjointe. Le but est donc d'intégrer des décisions de maintenance dans l'ordonnancement, et ainsi d'optimiser la production à court ou moyen terme, en prenant en compte les effets des décisions de production et de maintenance sur l'état des équipements et sur l'efficacité des solutions proposées.

Bibliographie

[1] Collin Drent et al. Manufacturing & Service Operations Management (2024) *Condition-Based Production for Stochastically Deteriorating Systems: Optimal Policies and Learning.*
[2] Michiel A. J. Uit Het Broek et al. Manufacturing & Service Operations Management (2020) *Condition-Based Production Planning: Adjusting Production Rates to Balance Output and Failure Risk.*
[3] Michiel A. J. Uit Het Broek et al. Reliability Engineering & System Safety (2021) *Joint condition-based maintenance and condition-based production optimization.*

Méthodes

Dans un premier temps, nous nous sommes intéressés à une version simple du problème : nous avons considéré un seul équipement de production, un seul produit créé par cet équipement uniquement. Dans ce cadre, le but est de maximiser le revenu par unité de temps, en horizon infini, c'est-à-dire d'optimiser en moyenne les gains liés à la création de produits moins les coûts liés à la production (coûts énergétiques, matières premières, main d'œuvre, rebuts…) et ceux liés aux opérations de maintenance et de panne.

Décisions à prendre

Les décisions à prendre à tout instant, influençant l'objectif sont les suivantes :
- Est-ce que l'on démarre une opération de maintenance ?
- Si oui, de quel type ?
- Si non, à quelle vitesse produit-on ?

Hypothèses

Nous avons considéré que la vitesse (ou cadence) de production influence la détérioration de l'état de l'équipement, et que cette détérioration est caractérisée par une fonction de dégradation. Par exemple, plus la vitesse de rotation d'une foreuse est élevée, plus l'équipement s'usera rapidement (de façon proportionnelle au carré de la vitesse de rotation).

La vitesse de production influence également les gains liés à la création de produits, et les coûts énergétiques : par exemple, plus la vitesse est élevée plus le nombre de produits créés sera important, mais plus le risque de rebut (produits « ratés ») sera élevé, et plus la consommation énergétique sera importante.

Ainsi, la prise de décision consiste en un compromis entre produire vite et conserver l'équipement dans un état correct.

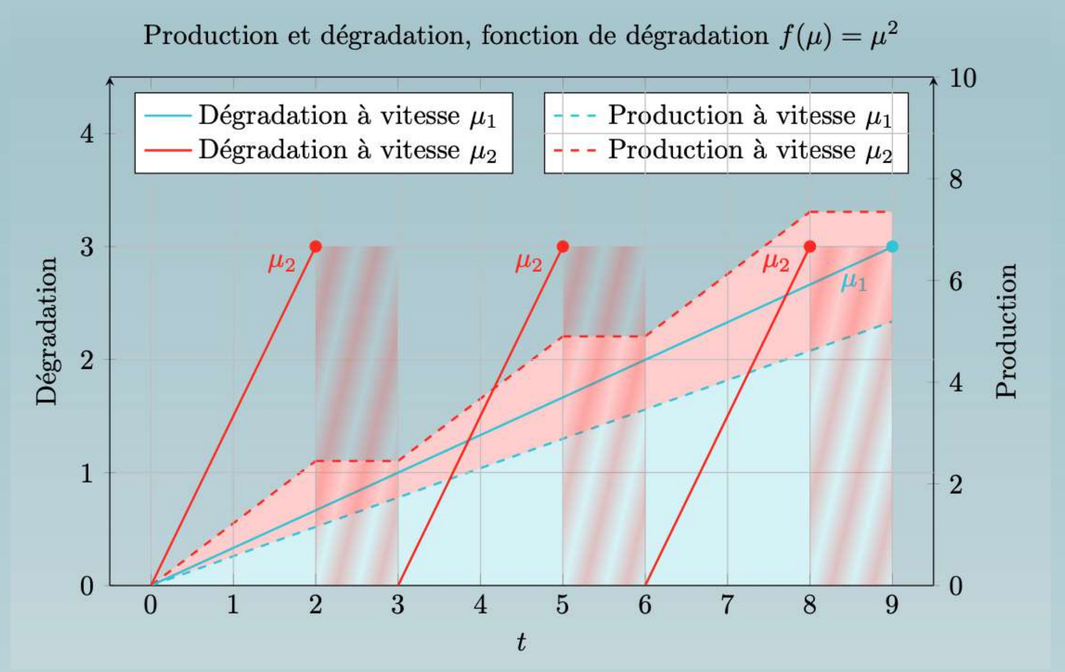

Modélisation et premiers résultats

Nous avons modélisé le problème sous la forme d'une chaîne de Markov.
Dans le cas déterministe, c'est-à-dire où l'on suppose que la dégradation du système n'est pas aléatoire mais parfaitement connue, on montre que la meilleure solution est de *produire à une seule vitesse optimale, puis d'effectuer une opération de maintenance préventive juste avant le seuil de dégradation maximal autorisé* (dont la date est connue), et de répéter ce cycle à l'infini.
Dans le cas où la dégradation suit une loi de probabilité aléatoire dont les paramètres sont influencés par la vitesse (selon une fonction de dégradation connue), on montre un résultat similaire.

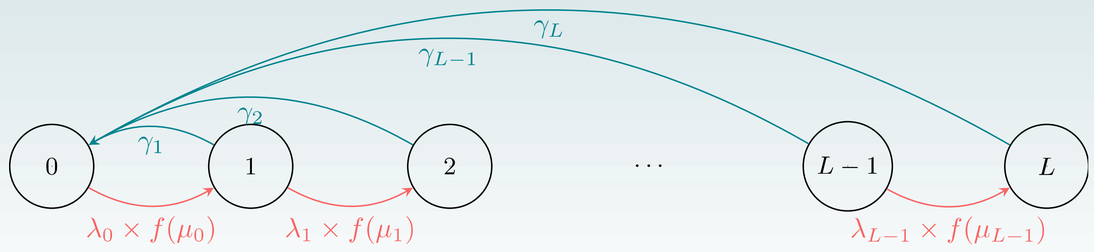

Contact : maelys.durrieu@doctorant.uca.fr

OPTIMISATION DE LA PRODUCTION DE BIOHYDROGÈNE À PARTIR DE SOUS-PRODUITS ORGANIQUES INDUSTRIELS

Sara El Abyad, Samir Taha, Jean-Sébastien Guez et Christophe Vial

UMR CNRS 6602, Institut Pascal, axe GePEB

INTRODUCTION

La dépendance aux combustibles fossiles accentue la pollution et le changement climatique, rendant urgente la transition énergétique.

Le bio-hydrogène (bio-H_2), vecteur propre issu de sources renouvelables, se présente comme une solution durable et respectueuse de l'environnement. Avec une combustion qui ne produit que de l'eau et une densité énergétique élevée, il offre un fort potentiel comme carburant alternatif.

Bio-H_2 est largement utilisé dans l'industrie (synthèse d'ammoniac, raffinage, métallurgie, électronique) et suscite un intérêt croissant dans le secteur de la mobilité durable (transports terrestres, aériens et maritimes).

La production de H_2 peut être réalisée par plusieurs voies, notamment la gazéification et la pyrolyse de la biomasse, l'électrolyse de l'eau, la thermolyse à haute température, ainsi que des procédés biologiques tels que la photofermentation et la **fermentation sombre**.

La fermentation sombre est un procédé biologique, indépendant de la lumière, dans lequel des bactéries anaérobies strictes ou facultatives dégradent des substrats organiques pour produire du bio-H_2, du dioxyde de carbone, ainsi que des acides gras volatils (AGV).

La fermentation sombre se déroule en trois étapes clés : l'hydrolyse des macromolécules complexes, l'acidogénèse produisant des acides organiques, alcools, CO_2 et bio-H_2, puis la phase de production d'hydrogène proprement dite, où des voies métaboliques spécifiques convertissent les intermédiaires en bio-H_2 et AGV.

Avantages	Inconvénients
1. Production continue du H_2 sans lumière 2. Substrat : Diverses sources de carbone 3. Produits : H_2 + CO_2 + métabolites à valeur ajoutée (AGV) 4. Mise en œuvre facile 5. Application simple	1. Rendement faible en bio-H_2 2. Le mélange de gaz produit contient du CO_2 qui doit être séparé 3. Sensibilité à la concentration d'hydrogène pouvant inhiber la production

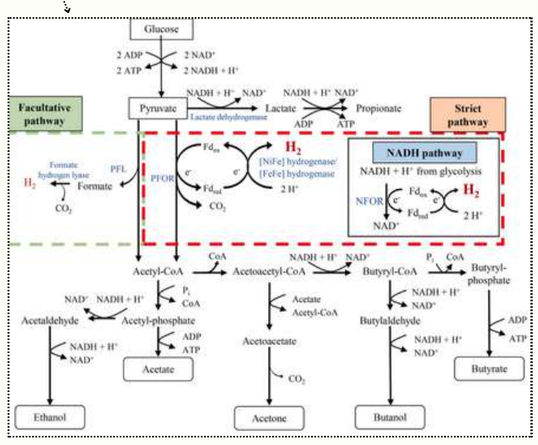

FACTEURS INFLUENÇANT LA FERMENTATION SOMBRE

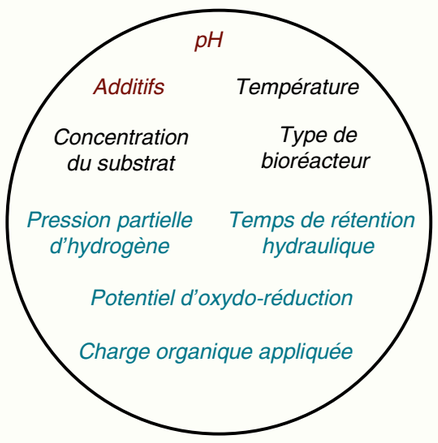

--- Diminue la production du bio-H_2

--- Augmente la production du bio-H_2

Le lactosérum, sous-produit liquide de la fabrication du fromage, représente 85-95 % du lait initial et contient 55 % de ses nutriments, dont une forte teneur en lactose responsable de sa charge organique élevée. Souvent considéré comme un déchet en raison de son fort impact environnemental (demande chimique en oxygène (DCO) importante), il peut néanmoins être valorisé par fermentation sombre pour produire des composés à valeur ajoutée, comme des acides organiques.

MATÉRIELS ET MÉTHODES

FERMENTATION SOMBRE EN BOUTEILLE

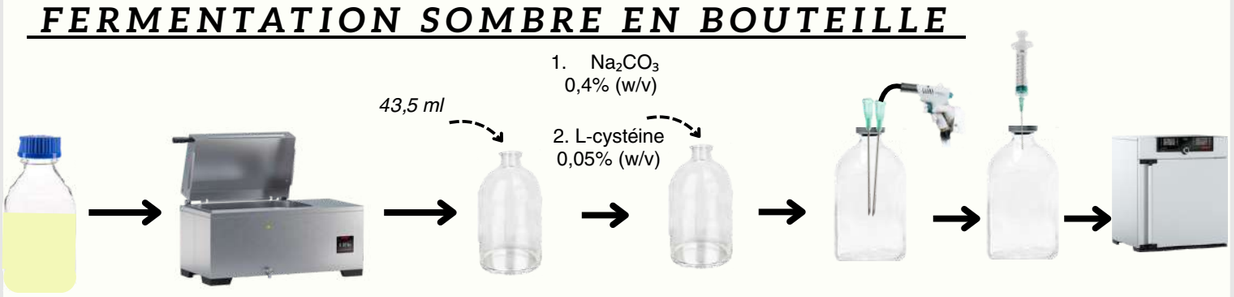

Chauffage du lactosérum 15 min à 60°C — *Transvasement du lactosérum* — *Ajout des additifs* — *Fermeture de la bouteille puis bullage de CO_2 pendant 15 s* — *Ajout d'inoculum 10% (v/v)* — *Incubation à 37°C*

FERMENTATION SOMBRE EN BIORÉACTEUR

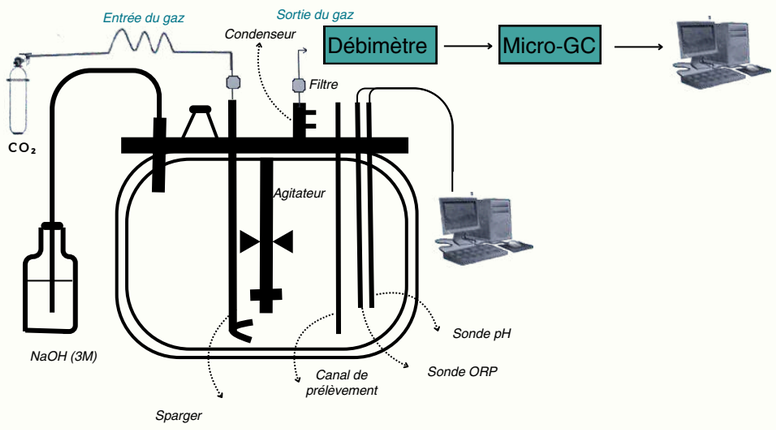

MODÉLISATION DE LA PRODUCTION D'HYDROGÈNE

Modèle cinétique de Gompertz

$$H(t) = P \cdot exp\left\{-exp\left[\frac{R_m \cdot e}{P}(\lambda - t) + 1\right]\right\}$$

H(t) (mL) : volume total d'hydrogène produit au temps de culture t (h)

P (mL) : volume maximal d'hydrogène produit

R_m (mL/h) : vitesse maximale de production d'hydrogène

λ (h) : phase de latence

RÉSULTATS

1- CARACTÉRISTIQUES PHYSICO-CHIMIQUES

Paramètres	Sérum moyen Lot 1 (SM)	Sérum effluent (SE)	Sérum p.pressé (SPR)	Sérum p.persillé (SPE)
pH	6,54 ± 0,06	5,72 ± 0,02	5,97 ± 0,02	5,13 ± 0,03
NO_3-N (mg/L)	2,25 ± 0,29	2,48 ± 0,06	2,64 ± 0,09	4,54 ± 0,38
Sulfate (mg/L)	341,5 ± 8,2	264,1 ± 2,8	437,3 ± 12,2	994,7 ± 16,7
Sulfite (mg/L)	8,29 ± 0,09	3,29 ± 0,01	13,47 ± 0,06	43,83 ± 0,47
NH_4 (mg/L)	65,7 ± 0,9	131,8 ± 2,0	33,6 ± 0,5	134,8 ± 2,0
Phosphate (mg/L)	0,78 ± 0,01	0,93 ± 0,01	1,36 ± 0,02	1,10 ± 0,02
Lactose (g/L)	36,6	34,7	33,4	38,8
Protéines (g/L)	6,6 ± 0,3	8,6 ± 0,1	6,6 ± 0,2	8,2 ± 0,1
Azote total (g/L)	0,830 ± 0,002	0,850 ± 0,002	0,850 ± 0,002	0,910 ± 0,002
DCO totale (g/L)	51,8 ± 0,1	52,9 ± 0,6	44,8 ± 0,4	55,4 ± 0,2
DCO soluble (g/L)	48,5 ± 0,1	50,7 ± 0,3	41,6 ± 0,8	46,7 ± 0,3
Matière sèche (%)	4,637 ± 0,004	4,673 ± 0,013	4,189 ± 0,011	4,852 ± 0,037

Les différents sérums sont riches en matières organiques

2- FERMENTATION SOMBRE EN BOUTEILLE

Sérum	SM (Lot 1)	SE	SPE	SPR
pH_i	**7,51**	**7,61**	**7,59**	**7,47**
mol H_2/mol lactose	1,67	0,96	0,44	1,78
Productivité (mmol/L.h)	2,3	1,2	0,6	2,1

Bouteilles agitées incubées à 37°C pendant 64 h en discontinu

Le SM et SPR présentent la productivité et le rendement en hydrogène les plus élevés

3- FERMENTATION SOMBRE EN BIORÉACTEUR

Substrat : Sérum moyen (Lot 2)

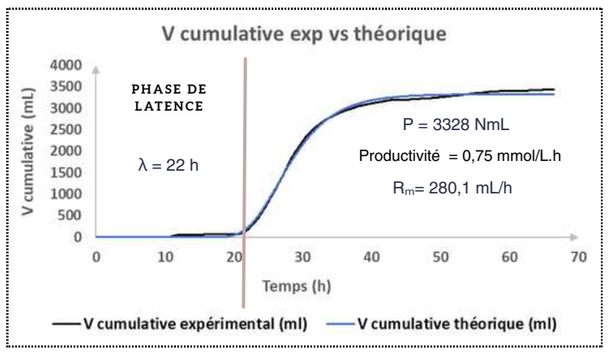

Figure 1 : Volume cumulatif d'hydrogène produit en fonction du temps

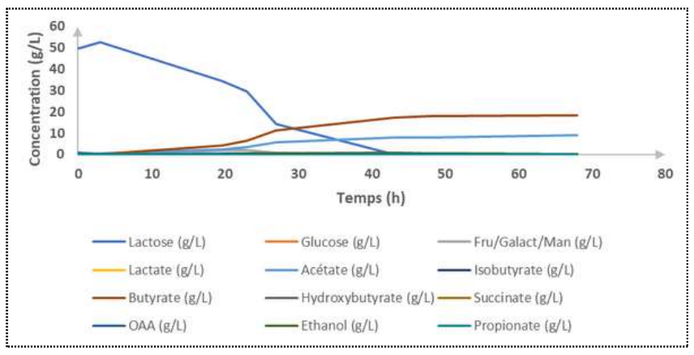

Figure 2 : Concentration des AGV produits en fonction du temps

Culture réalisée à 37°C , pH=6,5, à 200 rpm en discontinu

Le lactosérum moyen a permis d'atteindre une productivité en bio-H_2 de 0,75 mmol/L.h, avec une conversion majoritaire du lactose en acétate et butyrate, indiquant la prédominance de ces voies métaboliques

CONCLUSION

Différents types de sérums, aux compositions variées, ont démontré leur capacité à produire du bio-H_2 en discontinu, avec des rendements variables. Le rendement maximal, de 1,78 mol H_2/mol lactose a été obtenu avec le lactosérum pressé, et une productivité de 0,75 mmol/L·h a été atteinte en bioréacteur utilisant le lactosérum moyen lot 2.

REFERENCES

1- Ahmad, Ashfaq, et al., 2024
2- Imbeault, Nathalie, 1997
3- Jain, Rupal, et al., 2024
4- León-López, A., et al., 2022
5- Mahfouf, Esma, and Kerroum Derbal., 2023
6- Sim, Xue Yan, et al., 2023
7- Vera-Bravo, Ricardo, et al., 2022
8- Vishakha, S. S., S. W. Kulkarni, and W. Minal, 2013

ETUDE, MODELISATION ET COMMANDE D'UN PHOTOBIOREACTEUR PILOTE A DILUTION DU FLUX SOLAIRE

Anne **FISCHBACH**[a], Jean-François **CORNET**[a], Jérémi **DAUCHET**[a], Fabrice **GROS**[a], Thomas **VOURC'H**[a]
[a]Université Clermont Auvergne, Clermont Auvergne INP, CNRS, Institut Pascal, F-63000 Clermont-Ferrand, France
Contact: ***anne.fischbach@uca.fr***

CONTEXTE

Les microalgues et cyanobactéries présentent un vaste potentiel d'applications, des protéines pour l'alimentation aux pigments industriels, en passant par des polysaccharides pour la médecine, ainsi que des biocarburants. Leur polyvalence suscite un intérêt croissant, rendant crucial l'optimisation de leur production. Plusieurs types d'optimisations sont possibles : l'optimisation cinétique en volume menant à la conception de réacteurs plans, et, dans le cas de cette thèse, **l'optimisation énergétique ayant abouti à la conception du réacteur DiCoFluV (Dilution Contrôlée du Flux solaire en Volume).**

FONCTIONNEMENT DU PHOTOBIORÉACTEUR DICOFLUV

Deux optimisations possibles

Optimisation cinétique en volume

$$< r_X >_{\max} \propto a_{light} \times \ln\left(1+\frac{\overline{q}_0}{K}\right)$$

Equation générale : pour augmenter la vitesse de croissance $\langle r_x \rangle$, il faut augmenter la surface spécifique et la densité de flux q_0

Réacteurs plans

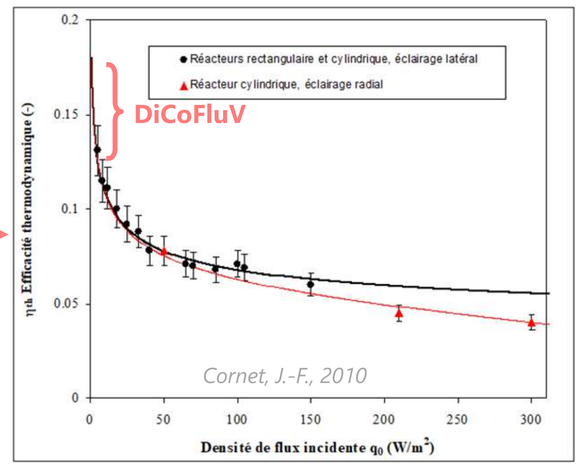

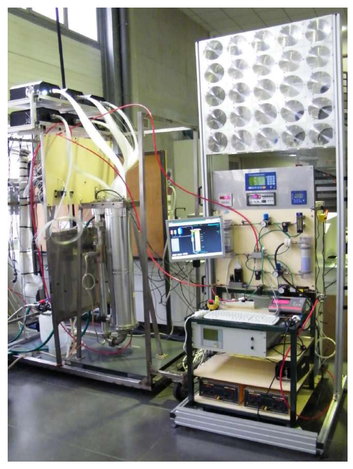

Le DiCoFluV, pilote à TRL 5, où **la dilution est assurée par une captation solaire** grâce à 25 lentilles de Fresnel (0,45 m^2) avant sa **redistribution en volume par 977 fibres optiques** à éclairage latéral (8 m^2). Elles plongent dans le volume réactionnel et permettent l'éclairage de la biomasse microalgale dont l'agitation est fournie par un système air-lift externe.

Optimisation énergétique

$$< s_X >_{\max} \cong \eta(\overline{q}) \frac{\overline{q}}{\Delta g'_X} M_X$$

Dans le PBR DiCoFluV : on cherche une productivité en surface maximale $\langle s_x \rangle$
→ pour augmenter $\langle s_x \rangle$, il faut augmenter l'efficacité thermodynamique

Réacteur DiCoFluV

Le concept DiCoFluV fonctionne sur le principe de la dilution solaire. Le but est de s'approcher le plus possible du rendement maximum naturel qui est de 20% pour les microalgues et de 15% pour les cyanobactéries. Calculé sur le PAR (Photosynthetically Active Radiations) qui correspond à 40% du spectre solaire, ce rendement est divisé par deux lorsqu'il est calculé sur la totalité du spectre solaire. Ce rendement et la vitesse moyenne de production de la biomasse $\langle r_x \rangle$ sont calculés par un **modèle de connaissance prédictif.**

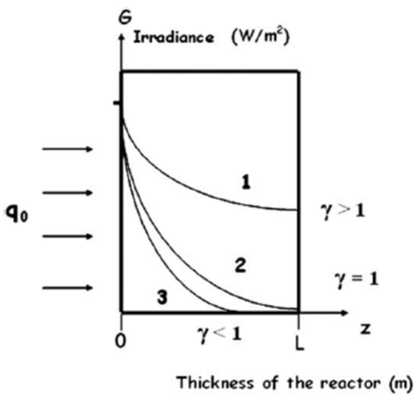

L'optimum de fonctionnement du PBR dépend de deux paramètres :

1. La densité de flux incidente
2. L'épaisseur optique de culture, composée de :
   i. La géométrie du réacteur
   ii. Le coefficient d'absorption des photons
   iii. **La concentration en biomasse**

Les zones sombres (zones sans lumière) génèrent de la respiration (sauf pour les cyanobactéries), et l'apport excessif de photons détériore significativement le rendement.

MODÈLE DE CONNAISSANCE

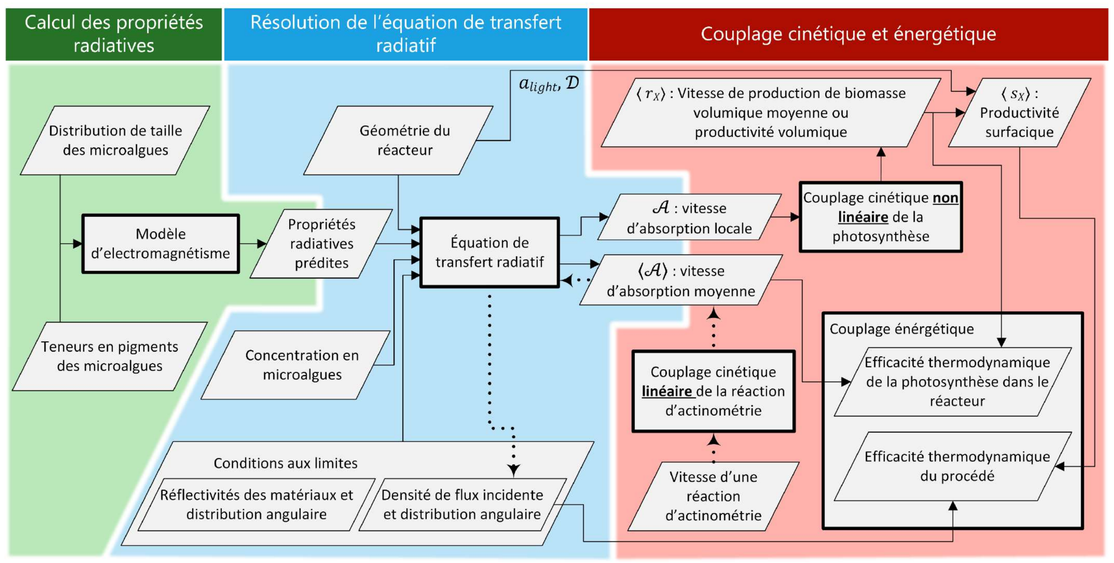

Rochatte, V, 2016

A partir des **propriétés optiques de la teneur en pigments** et **de la distribution de taille des microalgues**, on utilise un modèle d'électromagnétisme (théorie de Mie ou approximation de Schiff) afin de prédire leurs propriétés radiatives. Ces dernières servent à résoudre l'équation de transfert radiatif (ETR) conduisant au champ de vitesse d'absorption du rayonnement en volume à partir duquel on peut **déduire le champ des vitesses de réaction** en formulant le couplage thermocinétique. *(Dauchet, J. et al., 2015.)*

Dans le réacteur DiCoFluV, la densité de flux lumineuse est entre 0 et 10 W/m^2 à la surface des fibres. L'hypothèse est que la variation pigmentaire devrait être faible comparé aux réacteurs plans, où la variation de flux est comprise entre 0 et 450 W/m^2 (PAR).

Aujourd'hui, les modèles sont basés sur des teneurs en pigments constantes. Un des travaux de cette thèse vise à définir une nouvelle formulation de la loi de couplage à pigments variables.

MODÈLE DE REPRÉSENTATION

vitesse moyenne de production $\langle rx \rangle$ = **photosynthèse** + **respiration**

$$\langle rx \rangle = Cx * \left\{ ln\left(\left(\frac{K + A_{max}}{K + A_{min}}\right)^{\frac{\alpha * K}{\tau a}}\right) + ln\left(\left(\frac{Kr + A_{max}}{Kr + A_{min}}\right)^{\frac{\beta}{\tau a}}\right) - \beta_{nuit} \right\}$$

Pour simplifier la commande du réacteur, la vitesse moyenne de production est exprimée avec une équation de couplage thermocinétique (ETR + cinétique photosynthèse/respiration) en 1D dans un milieu uniquement absorbant, où A correspond à une vitesse d'absorption des photons et α, β, τa sont des paramètres agrégés.

Cette vitesse de production de la biomasse varie en fonction de :

1. **La météo : on subit le cycle jour/nuit et le cycle saisonnier**
2. **La teneur en pigments dans la biomasse**

Ce modèle de représentation servira à appréhender la production en fonction de la densité de flux du jour N+1 et de la concentration Cx du jour N, au moment de la récolte en fin de journée.

Le réacteur fonctionnera en mode semi-continu. Le soir, une quantité V.Cx de biomasse sera prélevée en fonction des conditions météorologiques du lendemain, selon les prévisions de MétéoFrance. Les expériences seront faites sur une cyanobactérie (Spiruline) et une microalgue (Chlorelle). β_{nuit} (h^{-1}) correspond à la valeur de respiration la nuit spécifique à l'organisme étudié.

Le but est de prouver que la technologie DiCoFluV est bien à l'optimum thermodynamique en solaire réel.

REFÉRENCES

Cornet, J.-F. Chemical Engineering Science 65, 2 (2010): 985-998.
Rochatte, V. Thèse (2016), Université Blaise Pascal - Clermont-Ferrand II, n° d'ordre 2705.
Dauchet, J.; Blanco, S.; Cornet, J.-F.; Fournier, R. Journal of Quantitative Spectroscopy and Radiative Transfer 161 (2015): 60-84.

Foundation models for industrial visual defect detection

Mehdi Gharbage[1,2], Céline Teuliere[1], Pierre Bouges[2] and Thierry Chateau[1]

[1] Université Clermont Auvergne, CNRS, SIGMA Clermont, Institut Pascal, F-63000 Clermont-Ferrand,France
[2] Manufacture Française des Pneumatiques Michelin

A visual representation of some image embeddings

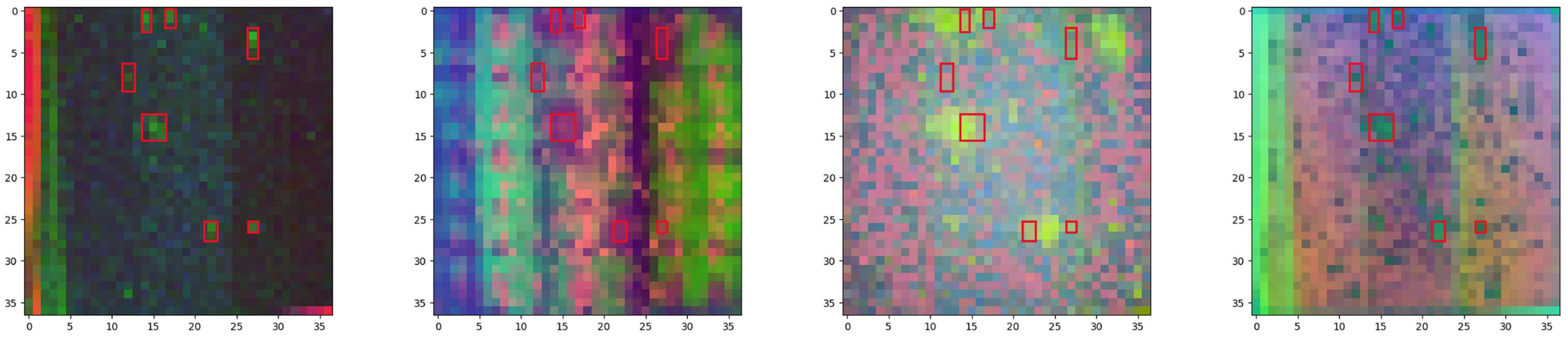

(a) Supervised training (b) DinoV2 [1] (c) AdaCLIP [2] (d) SAM [3]

Figure: Visualization of the 3D PCA on some image embeddings of the surface of a tire with defects (red boxes)

Abstract

Recent **foundation models** have brought valuable visual and textual semantic prior knowledge and have proven high zero-shot and few-shot performance in various domains. Meanwhile, the **industrial domain** suffers highly from the lack of labeled data for supervised learning scenarios in **defect detection** and classification. In this perspective, we investigate the use of **foundation models** by leveraging their high generalization ability.

Context & Motivation

- **Context**:
  - Fine-grained and complex industrial defect detection and classification
  - Most efficient and accurate methods rely on supervised learning
  - Supervised pretraining limits the "one-model, multi-datasets" scenario
- **Motivations**:
  - Few-shot learning ability

Objectives

- Achieve **Data efficiency** and **Supervision efficiency**
- Mutualize defect detection models (mono-task models ⇒ **multi-task model**)
- Objective of this preliminary study: Do current foundation models have the ability to address the challenges of industrial defect detection?

Comparative evaluation of anomaly detection methods

Method	F1	AP
DSR (SOTA, full-shot)	-	85.5
PatchCore (1-shot)	54.6	52.7
PatchCore (5-shots)	53.6	54.3
AnomalyDino† [4] (1-shot)	61.7	62.0
AnomalyDino† [4] (2-shots)	67.5	63.8
AnomalyDino† [4] (5-shots)	65.9	64.2
AdaCLIP† [2] (0-shot)	61.4	64.2
AdaCLIPS† (full-shot)	**81.3**	**88.7**

Table: Pixel level metrics on the KSDD2 dataset. Foundation model based methods†.

Method	$mAP^{IoU=.50}$	Precision	Recall
Best method (fully supervised)	**0.71**	**0.59**	**0.94**
AnomalyDino [4] (5-shots)	0.004	0.14	0.22
AdaCLIP [2] (0-shot)	0.06	0.38	0.25
AdaCLIPS (full-shot)	0.09	0.58	0.71

Table: Detection metrics of defect on tires (private dataset). Precision and Recall are computed for $IoU = 0.2$.

Are current Foundation models already data efficient?

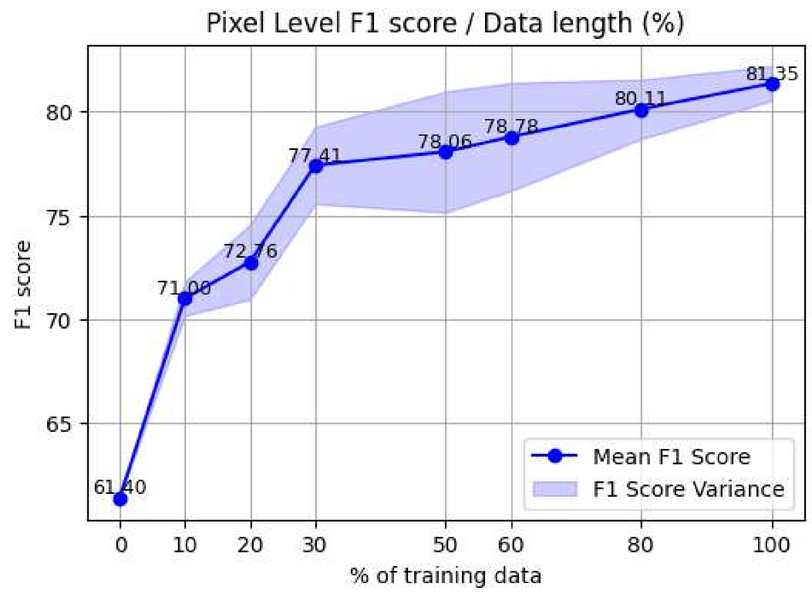

Figure: Influence of training data quantity (AdaCLIP fine-tuned on KSDD2 training set)

Are current foundation models sufficiently discriminating?

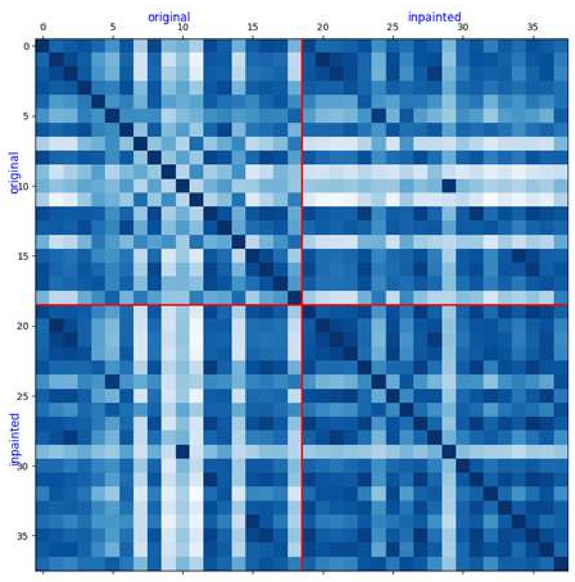

Figure: Similarity matrix on the CLS token of CLIP's ViT encoder on some tire images with defects and their corresponding inpainted images.

(a) Original

(b) Inpainted

Conclusion and Future work

- **Conclusion**:
  - Current foundation models semantic prior knowledge is not aligned enough with industrial domain semantics
- **Future work**:
  - Embed industrial knowledge to current foundation models
  - Adapt current foundation models to different input modalities

Acknowledgments

This work made in FACTOLAB (commun laboratory UCA, CNRS, Michelin) and International Research Center "Innovation Transportation and Production Systems" of the I-SITE CAP 20-25 frameworks was supported by Michelin Tyres Manufacturer.

References

[1] Maxime Oquab et al. *DINOv2: Learning Robust Visual Features without Supervision*. 2024.
[2] Yunkang Cao et al. *AdaCLIP: Adapting CLIP with Hybrid Learnable Prompts for Zero-Shot Anomaly Detection*. 2024.
[3] Alexander Kirillov et al. *Segment Anything*. 2023.
[4] Simon Damm et al. *AnomalyDINO: Boosting Patch-based Few-shot Anomaly Detection with DINOv2*. 2024.

Foundation models for industrial visual defect detection

Mehdi Gharbage[1,2], Céline Teuliere[1], Pierre Bouges[2] and Thierry Chateau[1]

[1] Université Clermont Auvergne, CNRS, SIGMA Clermont, Institut Pascal, F-63000 Clermont-Ferrand,France
[2] Manufacture Française des Pneumatiques Michelin

A visual representation of some image embeddings

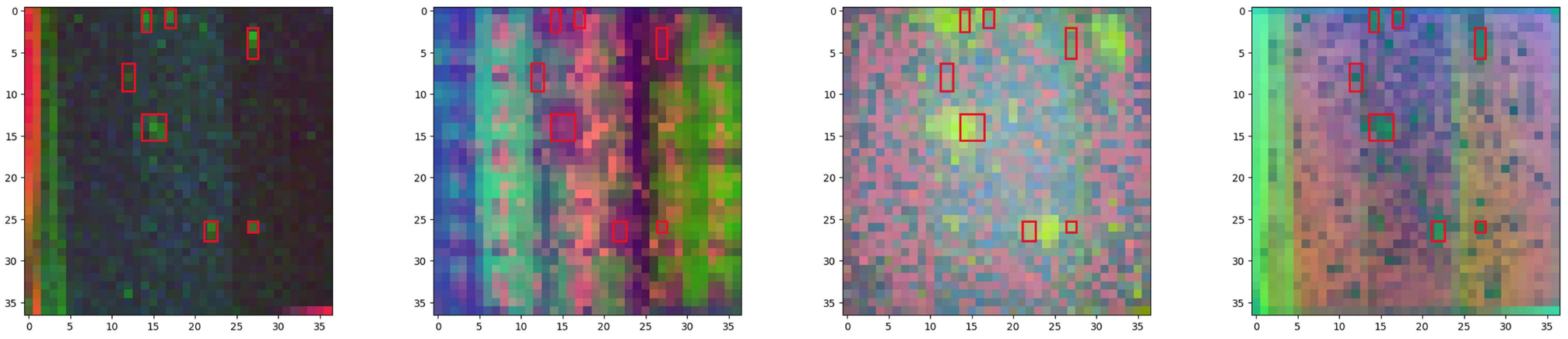

(a) Supervised training (b) DinoV2 [1] (c) AdaCLIP [2] (d) SAM [3]

Figure: Visualization of the 3D PCA on some image embeddings of the surface of a tire with defects (red boxes)

Abstract

Recent **foundation models** have brought valuable visual and textual semantic prior knowledge and have proven high zero-shot and few-shot performance in various domains. Meanwhile, the **industrial domain** suffers highly from the lack of labeled data for supervised learning scenarios in **defect detection** and classification. In this perspective, we investigate the use of **foundation models** by leveraging their high generalization ability.

Context & Motivation

- **Context**:
  - Fine-grained and complex industrial defect detection and classification
  - Most efficient and accurate methods rely on supervised learning
  - Supervised pretraining limits the "one-model, multi-datasets" scenario
- **Motivations**:
  - Few-shot learning ability

Objectives

- Achieve **Data efficiency** and **Supervision efficiency**
- Mutualize defect detection models (mono-task models ⇒ **multi-task model**)
- Objective of this preliminary study: Do current foundation models have the ability to address the challenges of industrial defect detection?

Comparative evaluation of anomaly detection methods

Method	F1	AP
DSR (SOTA, full-shot)	-	85.5
PatchCore (1-shot)	54.6	52.7
PatchCore (5-shots)	53.6	54.3
AnomalyDino† [4] (1-shot)	61.7	62.0
AnomalyDino† [4] (2-shots)	67.5	63.8
AnomalyDino† [4] (5-shots)	65.9	64.2
AdaCLIP† [2] (0-shot)	61.4	64.2
AdaCLIPS† (full-shot)	**81.3**	**88.7**

Table: Pixel level metrics on the KSDD2 dataset. Foundation model based methods†.

Method	$mAP^{IoU=.50}$	Precision	Recall
Best method (fully supervised)	**0.71**	**0.59**	**0.94**
AnomalyDino [4] (5-shots)	0.004	0.14	0.22
AdaCLIP [2] (0-shot)	0.06	0.38	0.25
AdaCLIPS (full-shot)	0.09	0.58	0.71

Table: Detection metrics of defect on tires (private dataset). Precision and Recall are computed for $IoU = 0.2$.

Are current Foundation models already data efficient?

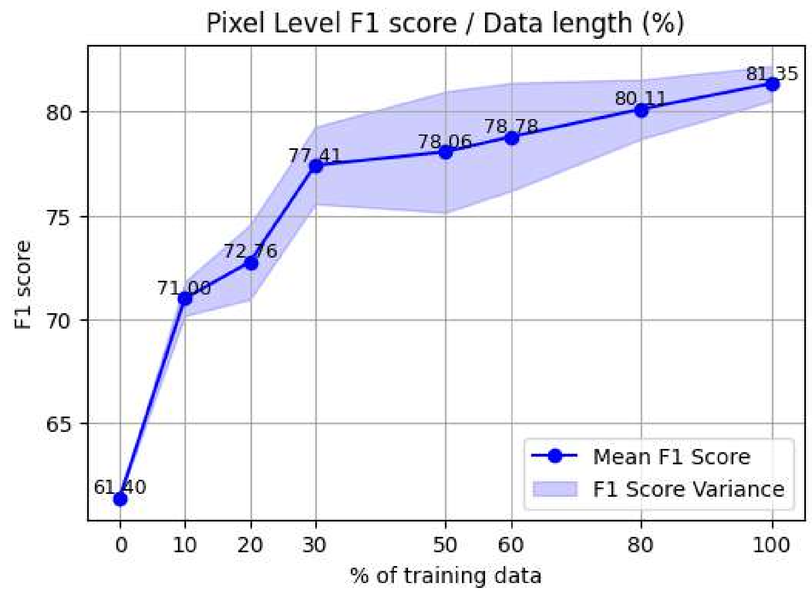

Figure: Influence of training data quantity (AdaCLIP fine-tuned on KSDD2 training set)

Are current foundation models sufficiently discriminating?

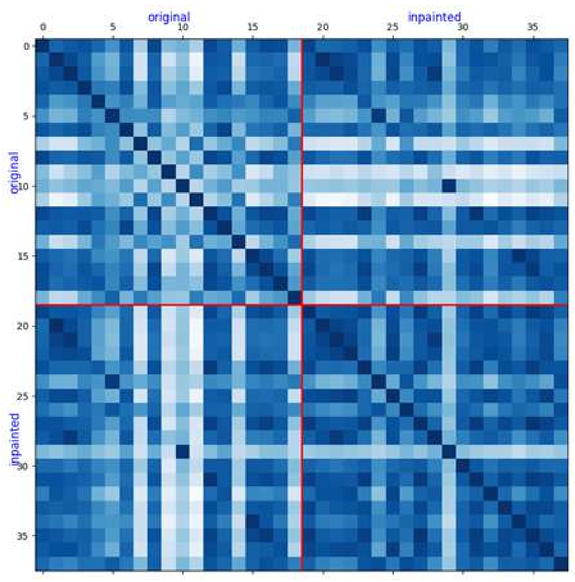

Figure: Similarity matrix on the CLS token of CLIP's ViT encoder on some tire images with defects and their corresponding inpainted images.

(a) Original

(b) Inpainted

Conclusion and Future work

- **Conclusion**:
  - Current foundation models semantic prior knowledge is not aligned enough with industrial domain semantics
- **Future work**:
  - Embed industrial knowledge to current foundation models
  - Adapt current foundation models to different input modalities

Acknowledgments

This work made in FACTOLAB (commun laboratory UCA, CNRS, Michelin) and International Research Center "Innovation Transportation and Production Systems" of the I-SITE CAP 20-25 frameworks was supported by Michelin Tyres Manufacturer.

References

[1] Maxime Oquab et al. *DINOv2: Learning Robust Visual Features without Supervision*. 2024.
[2] Yunkang Cao et al. *AdaCLIP: Adapting CLIP with Hybrid Learnable Prompts for Zero-Shot Anomaly Detection*. 2024.
[3] Alexander Kirillov et al. *Segment Anything*. 2023.
[4] Simon Damm et al. *AnomalyDINO: Boosting Patch-based Few-shot Anomaly Detection with DINOv2*. 2024.

Advanced hybridization of metaheuristics and constraint programming techniques for the integration of energy constraints in assembly line balancing problems.

Thiago Giachetto de Araujo, Matthieu Py, Laurent Deroussi and Nathalie Grangeon

Université Clermont Auvergne, CNRS, Clermont Auvergne INP, Mines Saint-Étienne, LIMOS, 63000 Clermont-Ferrand, France

Context & Motivations

- This thesis focuses on robotic **assembly line balancing problems**.
- Traditionally, assembly line balancing problems aim to minimize the number of workstations or the cycle time.
- Otherwise, this work incorporates energy constraints, specifically aiming to **minimize the energy consumption peak**.

Objectives

1. Propose **metaheuristics**
2. Investigate the applicability of **constraint programming** to this domain
3. Explore a less usual form of **hybridization** between **metaheuristics** and **constraint programming**, particularly Boolean satisfiability and constraint satisfaction problem.

Simple Assembly Line Balancing Problem with Power Peak Minimization (SALB3PM)

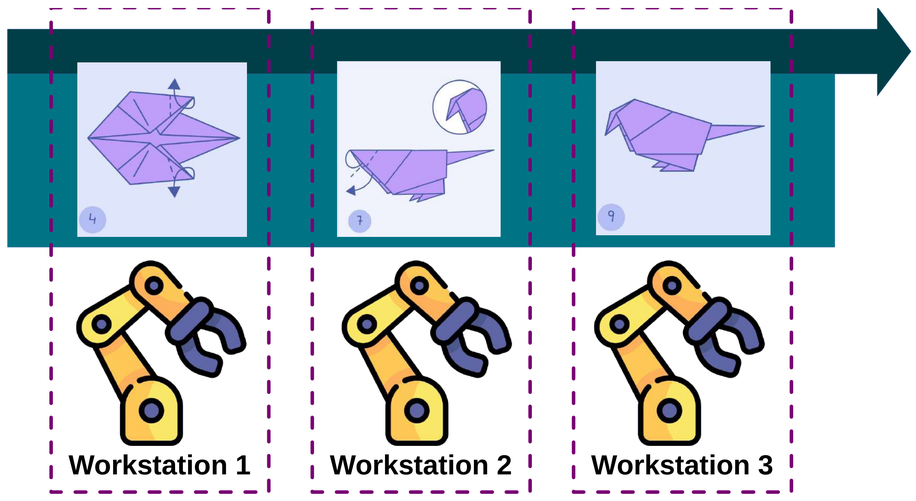

The **SALB3PM** (Gianessi et al., 2019) is an extension of the SALBP feasibility problem (SALBP-F) with additional energy constraints, where:

- The **number of workstations** m and **cycle time** c are given parameters. **Cycle time** is the time each unit of the product remains at each workstation.
- Each task $j \in O = \{1, ..., n\}$ has a **fixed power consumption** w_j and a **fixed processing time** t_j (independent of workstation assignment).
- Instantaneous power consumption at time t is the sum of the power consumption of all tasks executed at time t.
- It is necessary to **assign** each task to **exactly one workstation**.
- If task i precedes task j, (1) task i must be assigned to a workstation *earlier* in the production line than task j, or (2) if assigned to the same workstation, task i must **complete execution** before task j begins.

Task (j)	1	2	3	4	5	6	7
t_j	2	3	2	2	3	2	2
w_j	10	20	10	20	20	20	10

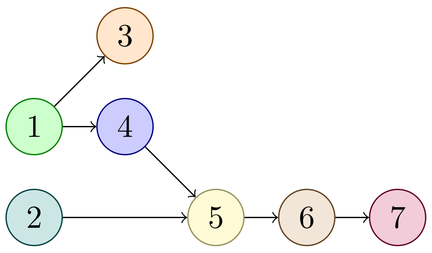

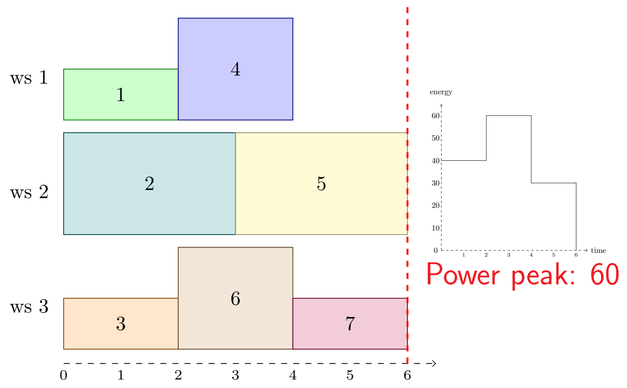

Figure: Feasible solution for the SALB3PM

- It is necessary to schedule tasks and obey the cycle time. Therefore, **all tasks assigned to a workstation should end until the cycle time**. Tasks overlapping is not permitted.
- The objective is to find a feasible task assignment and schedule that **minimizes peak power consumption**.

First approach: A Multi-start algorithm

- A multi-start framework with local search

Figure: Multi-start framework

- A **three vector-based representation** (Tasks order (V), Assignment (A), and Delay vectors (D))

V	2	1	4	5	3	6	7
A	1	1	3	2	2	3	3
D	1	0	0	0	1	0	0

Figure: Solution representation

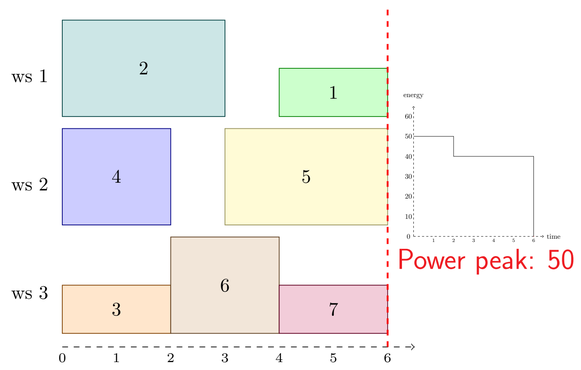

- **Priority-based solution generation** with semi-random prioritization
- Neighborhood moves: **Task insertion**, **Tasks swap**, and **Delay increment**
- An evaluation function that penalizes the cycle time infeasibility
  - Dynamic penalty for cycle-time violations, randomly adjusted at each iteration.

First results

- We conducted computational experiments on a benchmark with 130 instances. Four algorithm variants were compared.

Variant	Description
V1	Baseline variant
V2	**Without the swap move** to assess its impact
V3	**Fixed penalty factor** (set to the maximum energy consumption)
V4	**Single-iteration** variant to evaluate the benefit of restarts

Table 1 shows aggregate results for all instances, grouped by variant:

- Maximum and average relative gaps
- Count of instances where each variant achieved:
  - The best solution in at least one run (#best), in all runs (#best10)
  - At least one feasible solution (#feasible), in all runs (#feasible10)

Table: Comparison considering all instances

Metrics	Variant			
	V1	V2	V3	V4
gap.max(%)	**24.07**	**24.07**	**24.07**	88.46
gap.avg(%)	2.04	**1.98**	2.25	13.48
#best	66	**69**	58	24
#best10	40	**43**	38	14
#feasible	**124**	**124**	**124**	102
#feasible10	**123**	**123**	**123**	78

References

Thiago G. Araujo, Matthieu Py, Laurent Deroussi, and Nathalie Grangeon. Study about a multi-start metaheuristic approach for the salb3pm. In *CoDIT*, 2025. (in press).

Paolo Gianessi, Xavier Delorme, and Oussama Masmoudi. Simple Assembly Line Balancing Problem with Power Peak Minimization. In Farhad Ameri, Kathryn E. Stecke, Gregor von Cieminski, and Dimitris Kiritsis, editors, *Advances in Production Management Systems. Production Management for the Factory of the Future*, volume 566, pages 239–247. Springer International Publishing, September 2019.

Acknowledgments

This study was supported in part by the International Research Center "Innovative Transportation and Production Systems".

thiago.giachetto_de_araujo@uca.fr

Impacts Of Bio-Based Materials On Urban Heat Island

HIJAZI Zeina[1], OULDBOUKHITINE Salah-Eddine[1], BAKKOUR Amer[1] , BIWOLE Pascal[2], SAILOR David[3] , AMZIANE Sofiane[1]

1 Université Clermont Auvergne, Clermont Auvergne INP, CNRS, Institut Pascal, F-63000 Clermont–Ferrand, France
2 California State Polytechnic University, Humboldt, School of Engineering, Arcata, CA 95521, USA
3 School of Geographical Sciences and Urban Planning, Arizona State University, Tempe, AZ, USA

Introduction

❑ **Context:**

- Modeling of hygrothermal transfer in bio-based envelopes across a street canyon, considering the physical phenomena occurring within the street canyon environment.

❑ **Problematic:**

- There is a lack of knowledge regarding the behavior of bio-based materials, particularly at the micro scale, influenced by their hygrothermal properties.

❑ **Objective:**

- A simulation tool is proposed to enable a comprehensive analysis of the hygrothermal behavior of bio-based materials at the microscale, relative to a conventional reference model.

Methodology

❖ *1.Street canyon model*

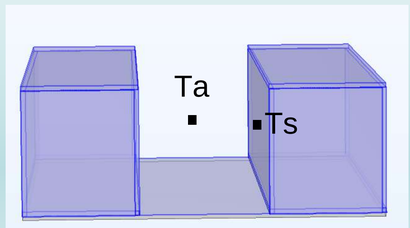

Comparison between

1.Concrete material
2.Wood material

❖ *2.Three main model*

1.Radiation Model
2.CFD Model
3.Heat and moisture transfer

Comparison Criteria

1.Surface temperature Ts
2.Air temperature Ta

Impacts on urban heat island

Validation

❖ *Modeling at the Micro scale: Reference concrete model*

1 3D street canyon built

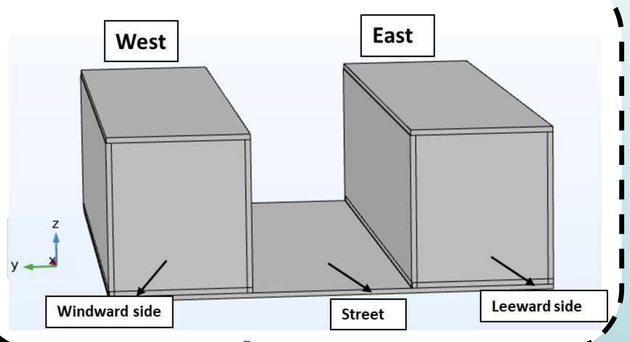

2 Experimental Monitoring

Monitoring

From 2012-07-23 12:30:00
Until 2012-07-23 19:40:00

In situ measurements of:

- Short wave radiation
- Wind speed and direction
- Surface **T**
- Outdoor **T** and **RH**

The Climbat Project is located in La Rochelle France

3 Model implementation

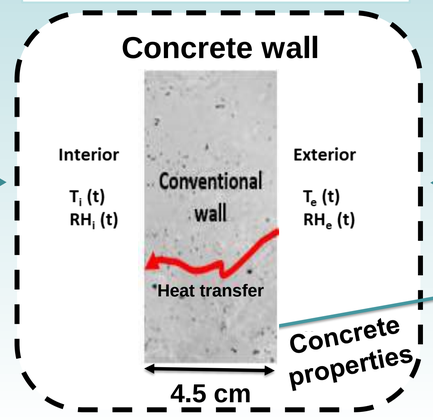

Thermal conductivity ($W \cdot m^{-1} \cdot K^{-1}$)	2.36
Density ($Kg.m^{-3}$)	2150
Specific Heat Capacity ($J.Kg^{-1}.K$)	915

❖ *First Results*

Validation at Wall Scale

Stream lines of airflow

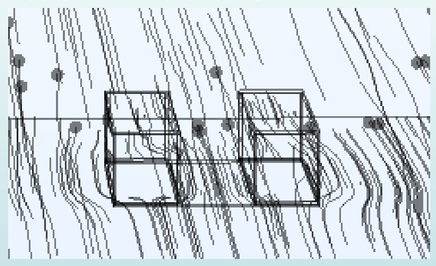

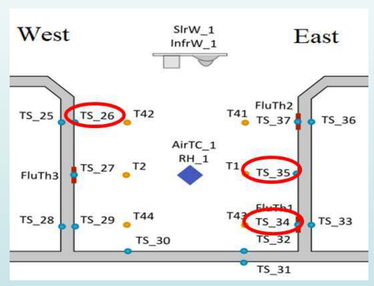

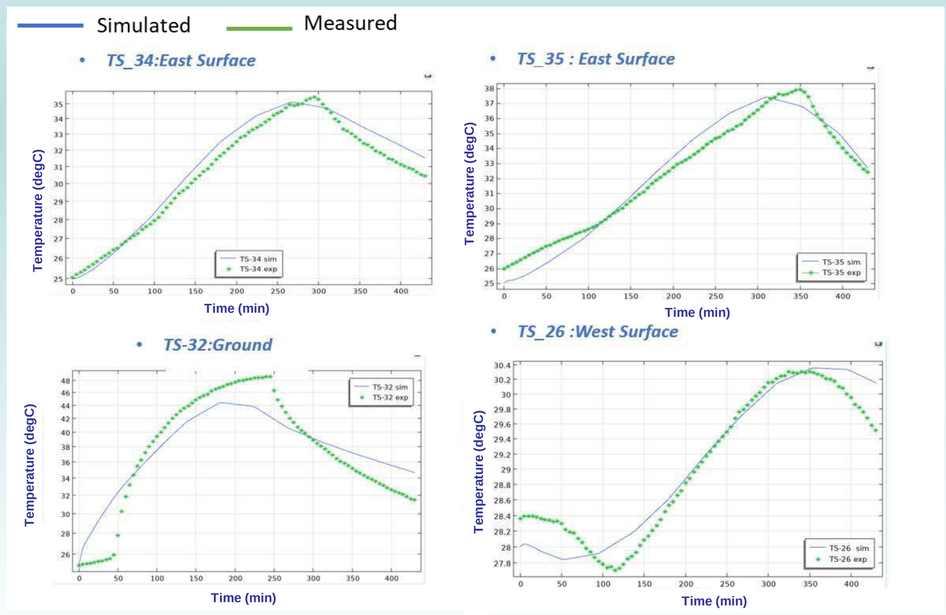

Application

➢ **Concrete vs Wood**

➢ ***Modeling at the wall scale***

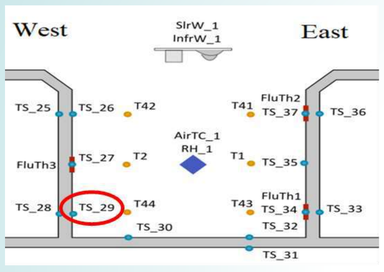

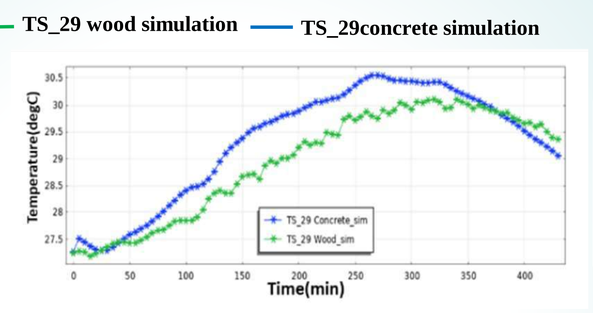

The **temperature difference** between concrete and wood ranges from **~0.5°C to 1.5°C**, depending on the time and location

➢ ***Modeling at the Exteroir Air domain***

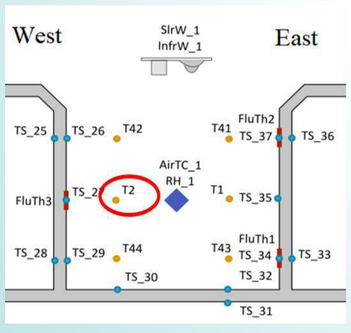

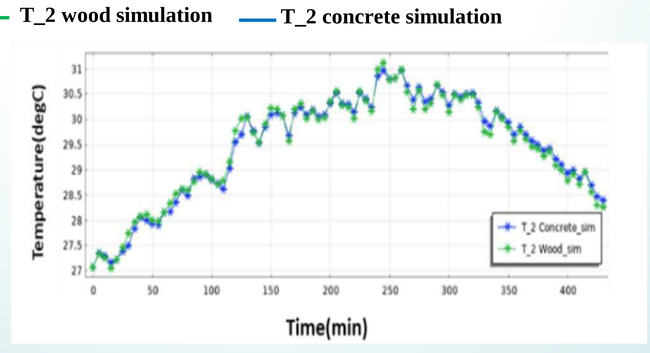

General Observations: Concrete and wood have almost identical outdoor air temperature profiles at T_2

Perspective

➢ **Evaluate human comfort at pedestrain level:**

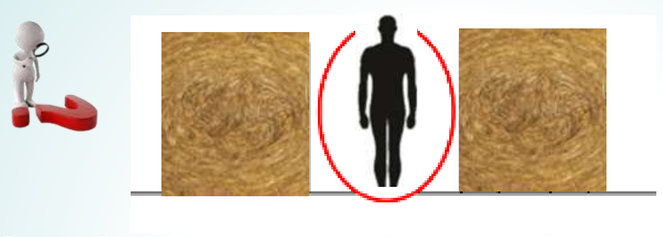

➢ **Simulate the effect of wall material properties (type, thermal conductivity, albedo, thickness)**

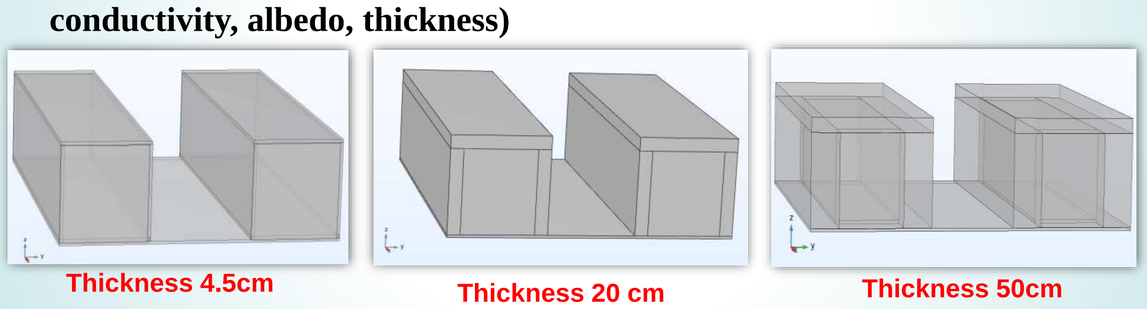

Thickness 4.5cm | Thickness 20 cm | Thickness 50cm

➢ **Analyze key parameters (radiative heat flux, surface & air temperature, UHI intensity)**

➢ **Behavoir of bio based materials on UHI at micro scale in compared to reference model**

Zeina.HIJAZI@doctorant.uca.fr

A mixed-integer linear programming model for data collection from buried sensors with a drone

FATIHA BENDALI[1], CHRISTOPHE CARIOU[2], YUANKANG HU[1], JEAN MAILFERT[1] and LAURE MOIROUX-ARVIS[2]

1. Laboratoire, LIMOS, UMR CNRS 6158, Université Clermont Auvergne
2. Laboratoire, TSCF, UR INRAE

Goals

- Finding a simple and efficient model for path planning for UAVs in agriculture.
- Testing the model in a real-world use case.
- We propose a mixed-integer linear model that combines obstacle avoidance and path planning algorithms.

Introduction

Nowadays, communicating sensors are widely used in agricultural plots to measure physical characteristics of the topsoil. For the sake of protection, the devices are often buried. In consequence, their radio waves are attenuated and communication distances are shorter. A communication range of a sensor is modeled by a truncated hemisphere which defines its neighborhood, as illustrated in Figure 1.

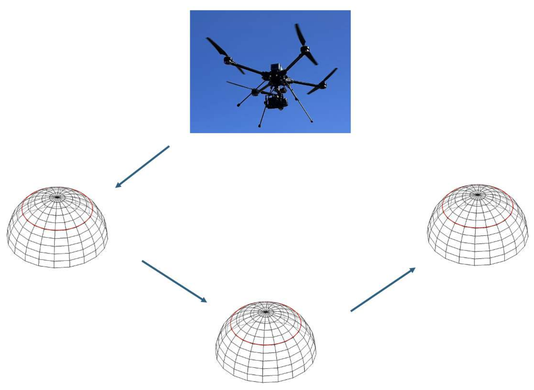

Figure 1:Communication range model of sensors[1]

In our study, a Unmanned Aerial Vehicle(UAV) collects sensor data by flying between the sensor communication areas, at different altitudes to avoid obstacles. We propose a mixed integer linear model that integrates both obstacle avoidance and path planning to achieve global optimization of the target path. Presently we use a solver for the real used instances.

Methods

We describe a three-dimensional mixed integer linear model handling the CETSP[2][3] with obstacles. In order to obtain a totally linear model, we assume that any domain i is a squared box $\mathcal{C}_i$ centered a point c_i of length side l_i. The take-off (resp. landing) area of the drone is numbered by 0 (resp. $|V|+1$). The distance between two points p and q is the Manhattan distance $d_1(p,q)$.

Mathematical Section

- $\mathcal{V}$: Set of domains (sensor areas), $\mathcal{V} = [0, n+1]$, $n = |V|$,
- $\mathcal{H}(0, n+1)$: the set of Hamiltonian paths from the vertex 0 to vertex $n+1$,
- $\mathcal{X}$: the set of incidence vectors x^μ, where $\mu \in \mathcal{H}(0, n+1)$,
- $x_{ij} \in \{0, 1\}$: Binary variable equal to 1 if the UAV travels directly from domain i to domain j,
- $\mathcal{E}$: Set of directed edges (i, j) between domains,
- $s_i = (s_{ix}, s_{iy}, s_{iz})$: hitting point coordinates in domain i,
- α_{ij}: Manhattan distance between the point s_i and the point s_j, if $x_{ij} = 1$.
- D_M: A large constant (big-M) used to linearize constraints.

The objective is to minimize the total trajectory length of the UAV by summing inter-domain distances, while ensuring each domain is visited once and obstacles are avoided.

$$
\begin{aligned}
\min \quad & \sum_{(i,j)\in\mathcal{E}} \alpha_{ij} \\
\text{s.t.} \quad & \alpha_{ij} \geq d_1(s_i, s_j) - D_M(1 - x_{ij}) \ \forall (i,j) \in \mathcal{E} \\
& x = (x_{ij}) \in \mathcal{X} \\
& s_i \in \mathcal{C}_i \qquad \forall i \in \mathcal{V} \\
& \alpha_{ij} \geq 0
\end{aligned}
$$

Avoiding obstacles

By using a Digital Surface model, we have obtained a description of the ground surface of the INRAE experimental farm. We are then able to check the presence of obstacles in a cubic shaped area between every pair of sensors (i, j) as shown in Fig. 3. We also determine the highest point Zmax in the set of obstacles O, so that the drone is guaranteed to fly over them between i and j.

Results

In all experiments, we will fix the location of the start and end points of the UAV flight (based on the real agricultural data), and then we randomly extract the coordinates of 15 sensor points from these data as experimental data. There are three possible radii in each test, 40, 80, and 120.

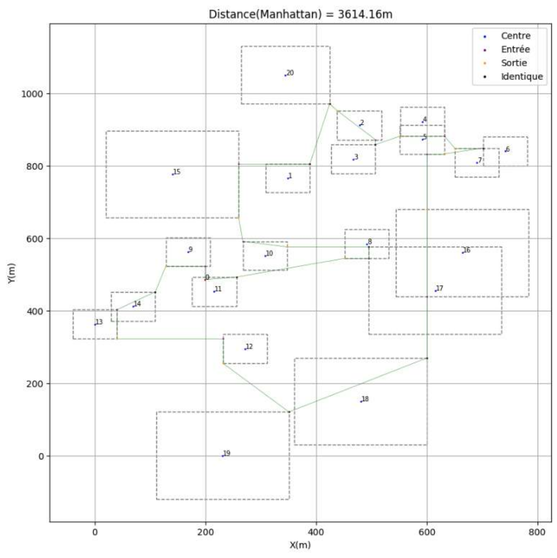

Figure 2:2D map of drone trajectory

Contact Information

- Email: Yuankang.HU@doctorant.uca.fr
- Phone: 07 66 86 07 79

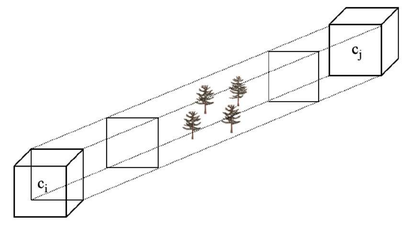

Figure 3:Obstacles within sensor range

Conclusion

We propose a fully linear model that integrates obstacle avoidance with path planning, and solve the CETSP in cluttered environments using CPLEX as a standard MILP solver. The approach will be compared to experimental results in [4] and will be applied to real-world agricultural use cases.

This work was supported by the International Research Center "Innovation Transportation and Production Systems" of the I-SITE CAP 20-25".

References

[1] Cariou, C., Moiroux-Arvis, L., Bendali, F., & Mailfert, J. (2024, May). Optimal route planning of an Unmanned Aerial Vehicle for data collection of agricultural sensors. In IEEE INFOCOM 2024-IEEE Conference on Computer Communications Workshops (INFOCOM WKSHPS) (pp. 1-6). IEEE.

[2] Fischetti, M., Salazar-Gonzalez, J. J., & Toth, P. (2007). The generalized traveling salesman and orienteering problems. In The traveling salesman problem and its variations (pp. 609-662). Boston, MA: Springer US.

[3] Behdani, B., & Smith, J. C. (2014). An integer-programming-based approach to the close-enough traveling salesman problem. INFORMS Journal on Computing, 26(3), 415-432.

[4] Coutinho et al. (2016). A branch-and-bound algorithm for the close-enough traveling salesman problem. INFORMS Journal on Computing, 28(4), 752-765.

Étude des couplages non linéaires dus aux fréquences de collisions dans les formulations en intégrale de chemin résolues par la méthode de Monte Carlo

Introduction

La méthode de Monte Carlo (MMC) est une **approche statistique de résolution d'intégrales**, applicable à de nombreux domaines dès lors qu'il est possible de reformuler l'observable comme l'**espérance mathématique** d'une variable aléatoire:

$$A = \int_{D_x} f(x)\, dx = \int_{D_x} p_X(x)\, \frac{f(x)}{p_X(x)} dx = \mathbb{E}\left[\frac{f(x)}{p_X(x)}\right]$$

Avec A une observable, x une variable comprise dans le domaine D_x, f une fonction continue et dérivable sur D_x, X une variable aléatoire définie sur D_x et sa pdf $p_X(x)$.

Dans ces cas, la MMC offre une alternative directe et efficace aux méthodes dites déterministes (souffrant plus de la complexité géométrique des sujets d'étude), à condition de tirer parti de certains principes avancés en statistique et en informatique, tels que :

- les **lois statistiques fondamentales** : loi des grands nombres, théorème central limite ; la double randomisation
- les **techniques de réduction de variance** : échantillonnage par importance, méthodes à variance nulle, reformulation des intégrales ;
- l'**analyse de sensibilité**
- les avancées en **informatique graphique**.

Origines des Non-linéarités

- le phénomène étudié est régi par une équation non linéaire,
- plusieurs phénomènes interagissent de façon couplée non linéaire,
- l'observable dépend de manière non linéaire des paramètres (ex. température, densité).

Méthode des collisions nulles [6]

Le principe consiste à majorer la fréquence de collision $k(x)$ par un coefficient fictif constant $\hat{k} = k(x) + k_n(x)$, où $k_n(x)$ correspond au taux de collisions nulles. L'équation de transport devient:

$$\frac{df(x)}{dx} = -\hat{k} f(x) + \hat{k}\left[\frac{k(x)}{\hat{k}(x)} S(x) + \frac{k_n(x)}{\hat{k}(x)} f(x)\right]$$

Ce qui mène à une formulation intégrale adaptée à une résolution par Monte Carlo :

$$f(x) = \mathbb{E}\left[\frac{\frac{k(x)}{\hat{k}} S(x) + \frac{k_n(x)}{\hat{k}} f(x)}{\hat{p}_X(x)}\right]$$

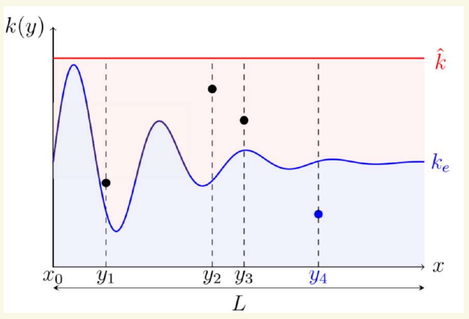

Cette figure montre une trajectoire simulée par un algorithme à collisions nulles (ACN). Les points noirs indiquent des collisions fictives (rejets), et le point bleu une collision réelle, où l'information est retenue. L'objectif est d'homogénéiser une extinction variable k(t) en une valeur constante $\hat{k}$, en introduisant des collisions fictives selon une loi de Bernoulli de paramètre $B(x) = \frac{k(x)}{\hat{k}}$.

Les algorithmes à collisions nulles (ACN) offrent un cadre pour le couplage entre un transport stochastique et une autre physique agissant sur la fréquence de collision.

Interprétations :

- **Physique** : les collisions nulles sont vues comme des diffuseurs avant, rendant le milieu virtuellement homogène.
- **Probabiliste** : elles correspondent à des échantillons rejetés d'un processus d'acceptation-rejet basé sur $\hat{k}(x)$.
- **Mathématique** : la non-linéarité est éliminée via un développement en série de l'exponentielle, ramenant le problème à une somme d'intégrales linéaires.

Typologie des Couplages [4]

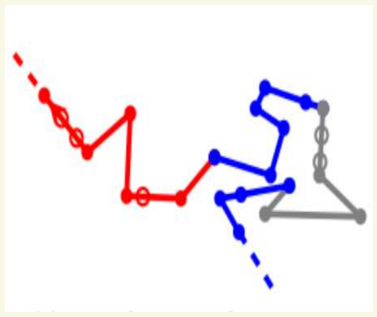

Couplage par les sources :
Un chemin Monte Carlo (ex. : rayonnement, en rouge) est échantillonné pour estimer une source dépendante d'une autre physique (ex. : conduction). Un second chemin (en bleu) est alors lancé pour évaluer cette grandeur. Le processus peut être récursif si la dépendance se propage.

Couplage par la fréquence de collision :
Lorsque la fréquence de collision n'est pas connue a priori, un chemin secondaire (noir) est lancé à chaque collision du chemin principal (rouge) pour l'estimer. La collision est acceptée avec une probabilité égale au rapport entre le poids Monte Carlo et le majorant de la fréquence de collision.

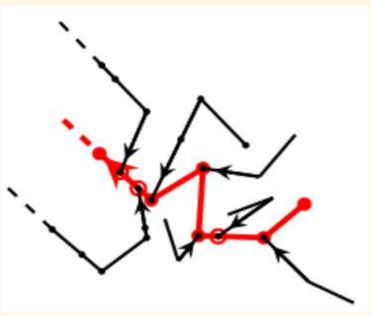

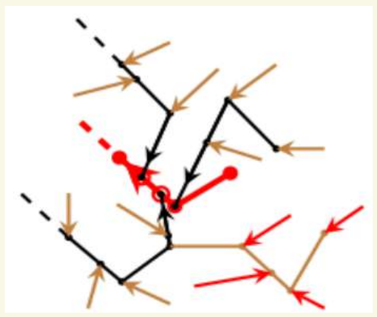

Couplage non-linéaire emboîté :
La fréquence de collision peut dépendre d'autres constantes elles-mêmes inconnues, nécessitant des chemins emboîtés (ex. : rouge → noir → marron). Ce schéma permet de modéliser des cinétiques non-linéaires

Etat de l'art

Thèse de Jean-Marc Tregan [1] :
Implémentation dans un logiciel de calcul de transfert thermique (Stardis) d'un couplage non linéaire avec un rayonnement de surface σT^4.

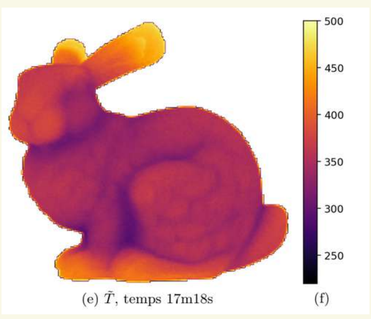

(e) $\tilde{T}$, temps 17m18s (f)

Thèse de Abderrahim SAHIM [5] :
Exemple de couplage par la constante des vitesses $k(t)$ dans un champ de température non-prescrit :

$$k(t) = A \exp\left(\frac{-E_a}{RT(t)}\right) = A \exp\left(-(RT(t))^{-1} E_a\right)$$

On a deux sources de non-linéarité de la dépendance en température T par la constante des vitesses : de part l'exponentielle et de part en puissance -1 de la température.

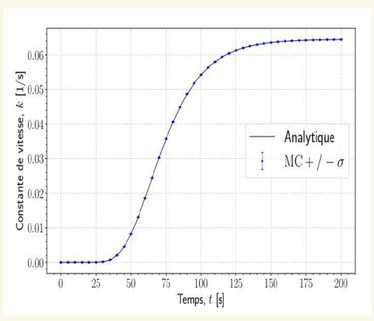

Évolution de la constante de vitesse, $k(t)$. Le résultat obtenu par la méthode de Monte Carlo est accompagné de barres d'erreur (symbole), pour $N = 10^5$ réalisations. La ligne continue représente la solution analytique.

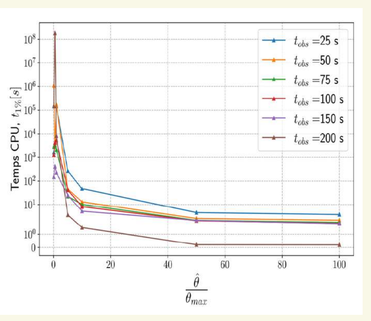

Évolution des temps de calcul CPU, $t_{1\%}$, en fonction de $\hat{\theta}/\theta_{\max}$, et pour différents temps d'observation, afin d'estimer la constante de vitesse, $k_1(t)$ obtenue avec la méthode de Monte Carlo, pour $N = 10^5$ réalisations.

Bibliographie

1. Tregan, J.-M. (2020). Thermique non-linéaire et Monte-Carlo. *Thèse, UT3 Paul Sabatier.*
2. Galtier, M. (2014). Statistique du rayonnement hétérogène. *Thèse, Mines Albi.*
3. Nyffenegger-Pere, Y. (2023). Couplage rayonnement/spectroscopie. *Thèse, UT3.*
4. Bati, M. et al. (2023). Couplage Conduction/Convection/Rayonnement.
5. Sahim, A. (2025). MC pour systèmes réactifs. *Thèse, Toulouse INP.*
6. El Hafi, M. et al. (2020). Null-collision MC. *JQSRT*, 260, 107402.

Doctorant : Adrien Jasselaire[1]
Direction : Pr. Jean-François Cornet[2]
Co-direction : Pr. Mouna El Hafi[3]

[1]Institut Pascal , [2]Université SIGMA Clermont , [3]École des Mines d'Albi – Laboratoire RAPSODEE

Dynamic Analysis of Internally Damped Rotating Laminated Shafts

N. JLASSI[1], V.GAGNOL [2], P. JOYOT[3], B. Chedli BOUZGARROU[2]

[1]Univ. Clermont Auvergne, ESTIA-Institute of Technology, EstiaR, F-64210 Bidart, France,[2]Univ. Clermont Auvergne, Sigma Clermont, Institut Pascal, 63000 Clermont-Ferrand, France, [3]Univ. Bordeaux, EstiaR, F-64210 Bidart, France

Objectives

1. Analyze the mechanical properties of rotating laminated composite shafts
2. Study the influence of internal damping in composites with viscoelastic behavior.
3. Evaluate the effects of stacking sequence and fiber orientation on critical speeds, instability thresholds, and natural frequency response.

Introduction

- Composite and hybrid rotating shafts provide a superior strength-to-weight ratio and stiffness compared to metallic shafts, making them essential for applications in aerospace and automotive industries. Their laminate properties allow optimization of stiffness and strength for specific applications. However, their anisotropy complicates dynamic analysis, particularly in predicting natural frequencies and internal damping behavior. Beam theories are often used to model rotating composite shafts, This study uses a finite shell element model based on the Classical Lamination Theory (SH-CLT) to predict the dynamic behavior while accounting for internal damping in laminated composites.

Numerical setup

- Fully Metallic Shaft
  - A 5mm thick single-layer steel shaft [Metal] with a central steel disk.
- Fully Composite Shaft
  - 5 mm thick carbon- fiber epoxy shaft with fiber orientations of [0°], [45°] and [90°].
- Hybrid Metallic-Composite Shaft (HCS)
  - 5 mm thick shaft with a 2.5 mm metallic inner layer and two 1.25 mm composite layers [Metal,0°,90°].

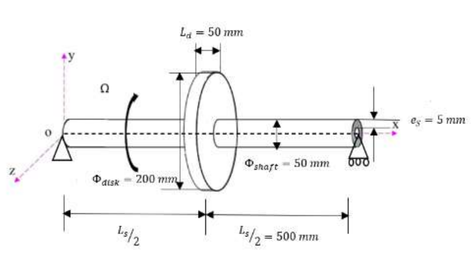

Figure 1:Academic rotor under study

Methods

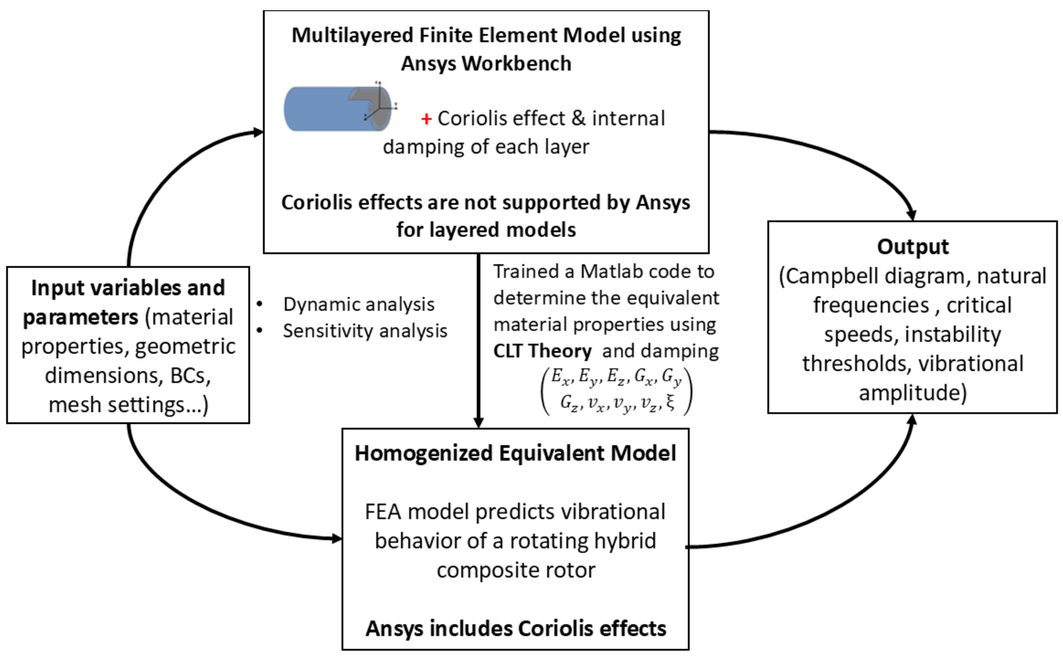

Model Formulation

- Classical Lamination Theory (CLT):
  - CLT calculates shaft strength, simplifying multilayered shafts into one layer.
- Rotordynamics Equation of Motion:

$$[M]\{\ddot{d}\} + [C_i + C(\Omega)]\{\dot{d}\} + [K + K_i(\Omega)]\{d\} = \{F(t)\}$$

- Rayleigh Damping:

$$C = \alpha M + \beta K; \xi = \frac{\eta_{xx} + \eta_{yy} + \eta_{xy}}{6}$$

where $[M]$ is the mass matrix, $[C(\Omega)]$ is the global gyroscopic matrix, Ω is the rotational speed, $[K]$ is the stiffness matrix, $\{F(t)\}$ is the generalized force vector, $\{d\}$, $\{\dot{d}\}$, and $\{\ddot{d}\}$ are respectively the nodal displacement,velocity, and acceleration vectors, η_{xx} is the loss factor in the x-direction, η_{yy} is the loss factor in the y-direction, η_{xy} is the loss factor for in plane shear, α and β are Rayleigh damping coefficients, ξ is the global damping ratio.

Results

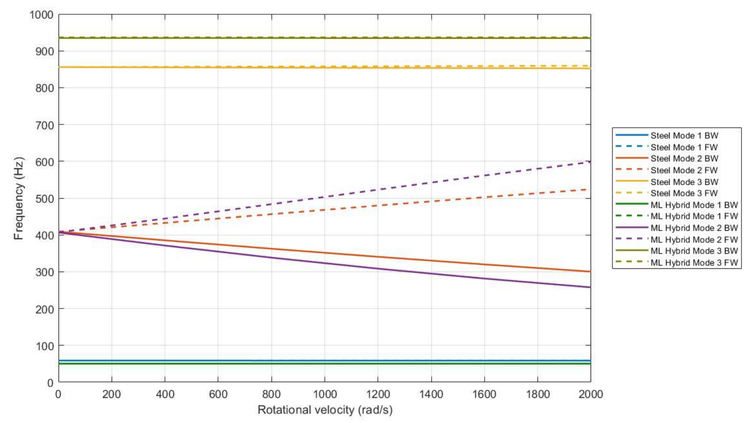

Figure 2:Campbell Diagram Comparing Homogenized HCS and Metallic Model

- First three bending natural frequencies for both multilayer and homogenized models at rest 0 rad/s:

Configurations	1B (Hz)	1F (Hz)	2B (Hz)	2F (Hz)	3B(Hz)	3F(Hz)
Multilayer HCS	50,47	50,59	406,49	407,13	934,74	936,29
Homogenized layer	49,37	49,46	389,07	389,49	907,6	909,23
Single- layer metallic shaft	57,46	57,47	398,98	399,03	835,26	835,28
Relative Error (%) (Layered vs smeared HCS)	2,18	2,23	4,29	4,33	2,9	2,89
Relative Difference (%) (HCS vs Metallic Shaft)	12,16	11,97	1,88	2,03	11,91	12,09

- First three bending natural frequencies: Homogenized HCS vs. Metallic model at 2000 rad/s:

Configurations	1B (Hz)	1F (Hz)	2B (Hz)	2F (Hz)	3B(Hz)	3F(Hz)
Homogenized layer HCS	49,31	49,52	246,27	572,19	904,83	912,01
Single- layer metallic shaft	57,56	57,87	292,26	514,45	833,56	840,64
Relative Difference (%) (HCS vs Metallic Shaft)	14,33	14,42	15,73	11,22	8,55	8,49

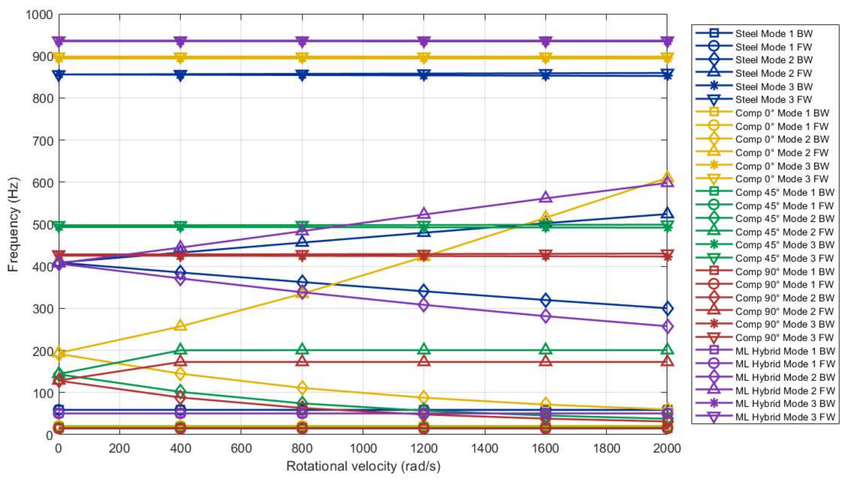

Figure 3:Campbell diagram showing stacking sequence effects on natural frequencies for different configurations

Conclusion

- The homogenization method, based on Classical Laminate Theory (CLT) closely matches the multilayered model's natural frequencies at rest for the hybrid metallic-composite shaft, with errors increasing at higher frequencies yet remaining acceptable **($< 4.5\%$)**.
- HCS has higher frequencies than the metallic shaft from the 3rd mode, showing greater stiffness, while the metallic shaft surpasses HCS in the 1st and 2nd modes with a 8–16% relative difference at 0 and 2000 rad/s.
- Material and fiber orientation affect frequencies **[*Metal*]** shaft has highest stiffness; **[90]** lowest. Hybrid shaft (HCS) yields frequencies close to metal's with 23.5% less weight. Gyroscopic effects amplify frequency splits.
- Future studies should focus on the experimental evaluation of rotors to verify simulation results.

Contact Information

- Email: naoures.jlassi@estia.fr

Combinatorics Behind the Routing and Spectrum Assignment Problem

Victoria KAIAL, Prof. Annegret K. WAGLER

LIMOS, Université Clermont Auvergne

Motivation

The Routing and Spectrum Assignment Problem can be interpreted in combinatorial terms and relying on such properties can substantially improve the solution methods [3, 7].

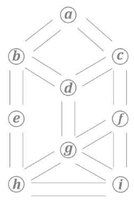

An optical network can be represented as a graph.

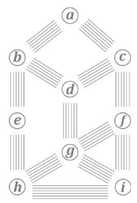

The optical spectrum is divided into slots. Channels are formed by consecutive slots.

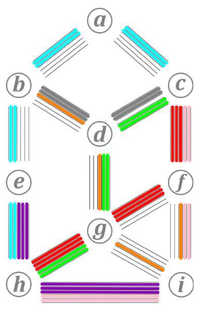

Each data traffic demand needs to be assigned a route and a channel s.t. those whose paths share an edge use disjoint channels.

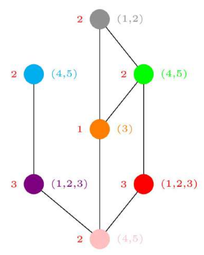

Conflict graph encoding which channels cannot overlap for the chosen routing.

Once a routing has been fixed, the **spectrum assignment is equivalent to interval coloring in the conflict graphs of the routes**.

Our aim: studying multiband scenarios by investigating substructures in the conflict graphs of the routes that cause difficulties for the interval colorings. For that, the study of edge intersection graphs of the routes is indispensable. The first subnetwork equipped to operate a new spectral band will certainly be a spanning tree in the original optical network (to allow connections between all possible origin/destination pairs).

Edge Intersection Graphs of Paths

Formally, the conflict graph of the routes is an edge intersection graph of paths.

Given a set $\mathcal{P} = \{P(v)\}_{v \in V}$ of paths over a host graph H, its edge intersection graph
- has V as vertex set, and
- has the edge $uv \iff P(u)$ and $P(v)$ have at least one edge in common.

Host graph	Class
path	interval
tree	EPT
cycle	circular-arc

The characterization of EPT graphs by minimal forbidden induced subgraphs remains an open problem. We present our first results in that direction.

First results: Minimal non-EPT and non-interval graphs [4]

Interval graphs are EPT. Then, **every non-EPT graph has an induced minimal non-interval subgraph.** Where the complete list of the latter is known [5]:

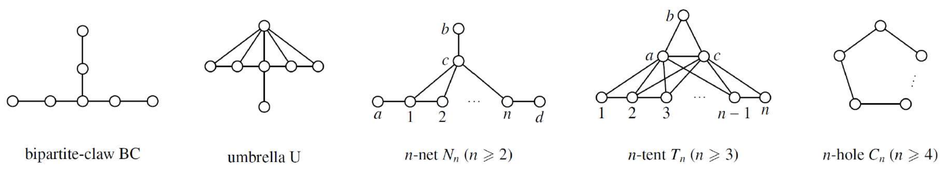

Theorem

The only minimal non-interval minimal non-EPT graphs are n-tents for $n \geqslant 5$.

Golumbic and Jamison (1985) determined all non-EPT graphs obtained by adding one vertex to a hole [2]. We extended this result to all minimal non-interval graphs:

Theorem

The minimal non-EPT graphs $G \oplus v$ obtained by adding one vertex v to a minimal non-interval graph G are exactly the graphs where

- *G is an n-hole and the neighborhood of v is as described in [2], or*
- *G is a bipartite claw, an umbrella, a 3-tent, a 4-tent or an n-net ($n \geqslant 2$) and either*
  - *v is universal, or*
  - *$G \oplus v$ is one of the 15 graphs listed in [4].*

Operations on cliques [1]

We found two operations on cliques that preserve the property of being non-EPT. Both generalize edge-subdivision.

- The **clique-stretching operation.** Given a clique Q of a graph G, delete all edges of $G[Q]$[a], add a vertex v and make it adjacent to exactly the vertices in Q .

- The **clique-edge-stretching operation.** Given u_1, u_2 in a clique Q of a graph G, subdivide the edge u_1u_2 and make the new vertex v adjacent to every vertex in Q.

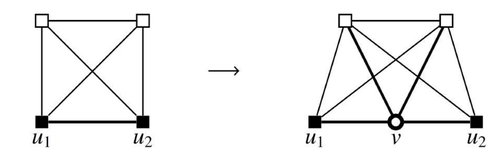

The interest of these operations lies in the fact that they can be used to construct minimal non-EPT graphs.

- Obtaining known families of minimal non-EPT graphs using the operations.
  - Tents

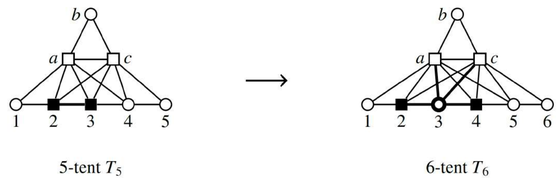

  - Nets with an added universal vertex
  - All non-EPT graphs $C_n \oplus v$ can be obtained by iteratively applying edge subdivisions and clique-edge-stretchings starting from one of the graphs:

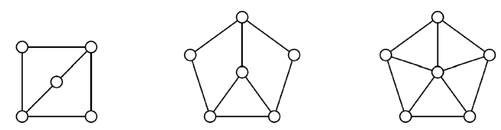

- Two new infinite families of minimal non-EPT graphs were obtained using the operations.

Next steps

- Necessary and sufficient conditions for the operations to preserve minimality of non-EPT graphs.
- Minors for other families of (minimal) non-EPT graphs.
- Other operations?
- Extending results to k-trees.
- Implications on interval colorings and the RSA.

References

[1] Mariana Escalante, Victoria Kaial, and Annegret K Wagler.
Stretching Operations Applied to Cliques of Edge Intersection Graphs of Paths in Trees.
XIII Latin American Algorithms, Graphs, and Optimization Symposium, 2025 (submitted).

[2] Martin Charles Golumbic and Robert E Jamison.
The edge intersection graphs of paths in a tree.
Journal of Combinatorial Theory, Series B, 38(1):8–22, February 1985.

[3] Victoria Kaial, Hervé Kerivin, and Annegret K. Wagler.
On non-superperfection of edge intersection graphs of paths.
Discrete Optimization, 54:100857, 2024.

[4] Victoria Kaial and Annegret K Wagler.
Minimal non-EPT graphs based on minimal non-interval graphs.
European Conference on Combinatorics, Graph Theory and Applications, 2025 (accepted) hal-05007099.

[5] Cornelis Lekkerkerker and Johan Boland.
Representation of a finite graph by a set of intervals on the real line.
Fundamenta Mathematicae, 51(1):45–64, 1962.

[6] Clyde L Monma and Victor K Wei.
Intersection graphs of paths in a tree.
Journal of Combinatorial Theory, Series B, 41(2):141–181, 1986.

[7] J P Nant P H Fernandes da Silva, H Kerivin and A Wagler.
Solving the routing and spectrum assignment problem, driven by combinatorial properties.
Networks, 2023.

[a] If V' is a subset of vertices of a graph G, $G[V']$ denotes the subgraph of G induced by V'

victoria.kaial@doctorant.uca.fr

The Potential of Vegetal Concrete and Rammed Earth for a Hybrid Insulation Solution

Sara KHALIL[1], Omayma HOMORO[1], Salah OULDBOUKHITINE[1], Sofiane AMZIANE[1]

[1] *Université Clermont Auvergne, Clermont Auvergne INP, CNRS, Institut Pascal, F-63000 Clermont–Fd, France*

1 INTRODUCTION

Rammed Earth (RE) is a traditional construction technique that involves compacting moist earth into layers within a framework

- Locally-sourced
- Multi-coupling Medium
- Dual Porosity

Many rammed earth buildings in Auvergne-Rhone-Alpes region

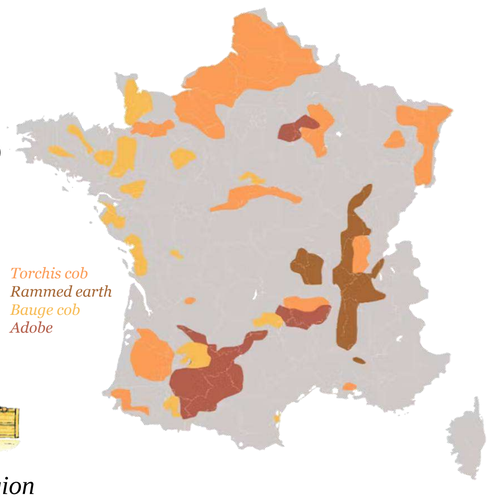

Challenges

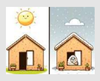

Thermally, comfort summer but cold winter

Hygroscopic, moisture sensitivity

Insulation required !

Mechanically, weak tension and shear

Research gap

- Why to insulate RE walls with vegetal concrete?
- How to implement this insulation effectively?
- What is the optimal solution for combining materials?
- How is the mechanical behaviour affected?

Rammed Earth *Vegetal Concrete*

2 METHODS

Formulation

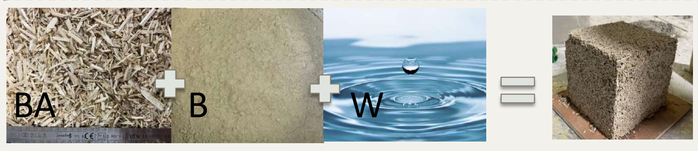

Mixing ratio of 1:1:0.5 (W:B:BA)

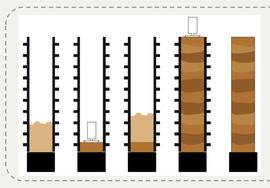

Compaction using pneumatic rammer

Water content ~ 11%

Assembling

Interface designing solution

Adhesion and Bonding Strength

Testing Methods

Compression test setup

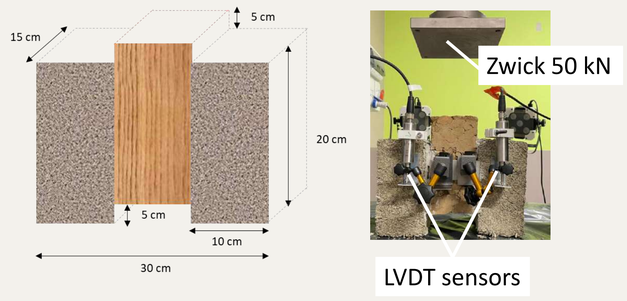

Push-out test configuration and setup

3 RESULTS

Material	Composition
Rammed earth (RE)	Gravel: 45.3%, Sand: 26.9%, Silt: 14.4%, Clay: 13.4%
Hemp-lime concrete (HTrad)	Hemp shives + Commercial lime (Tradical PF 70)
Hemp-cement concrete (HCSA)	Hemp shives + low-alkaline sulfoaluminate (CSA)

Properties		RE		HCSA		HTrad	
		Average	*CV %*	*Average*	*CV %*	*Average*	*CV %*
Physical	ρ_{dry} *[kg/m3]*	1939.42	3.03	365.88	5.1	390.55	1.6
	λ *[W.m^{-1}.K^{-1}]*	1.283	6.3	0.056	-	0.06	1.38
Mechanical	σ_c *(MPa)*	2.088	5.7	0.32	7.9	0.59	8.9
	E *(MPa)*	97.92	24.9	20.94	32.48	28.57	27.6
	ε_p *(mm/mm)*	0.069	4.9	0.097	12.83	0.139	6.8

RE

- Two-phase mechanical response, brittle post-peak.
- Homogenous deformation.
- Initiation of cracks.
- Minor strain concentration.

HTrad & HCSA

- Three-phase mechanical response, ductile post-peak.
- Relatively uniform displacement.
- Strain diffusion is more pronounced for HTrad.
- Higher heterogeneity in deformation for HTrad.

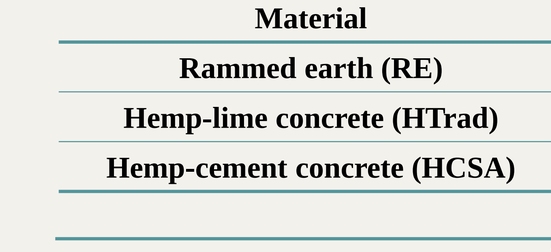

Assembling – issues and challenges

(a) Mould growth at the interphase.
(b) Mould growth on rammed earth.
(c) Detachment of the hemp concrete from the rammed earth.

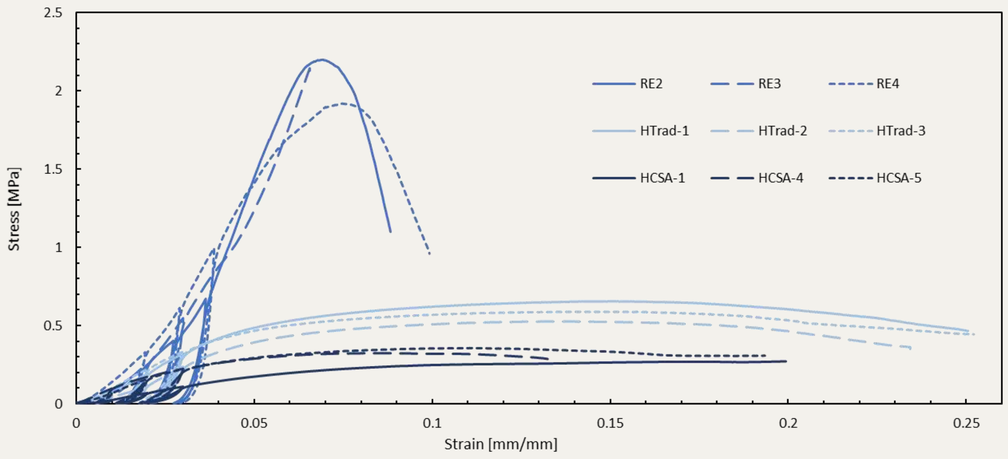

Stress-strain curves for three specimens tested per each material

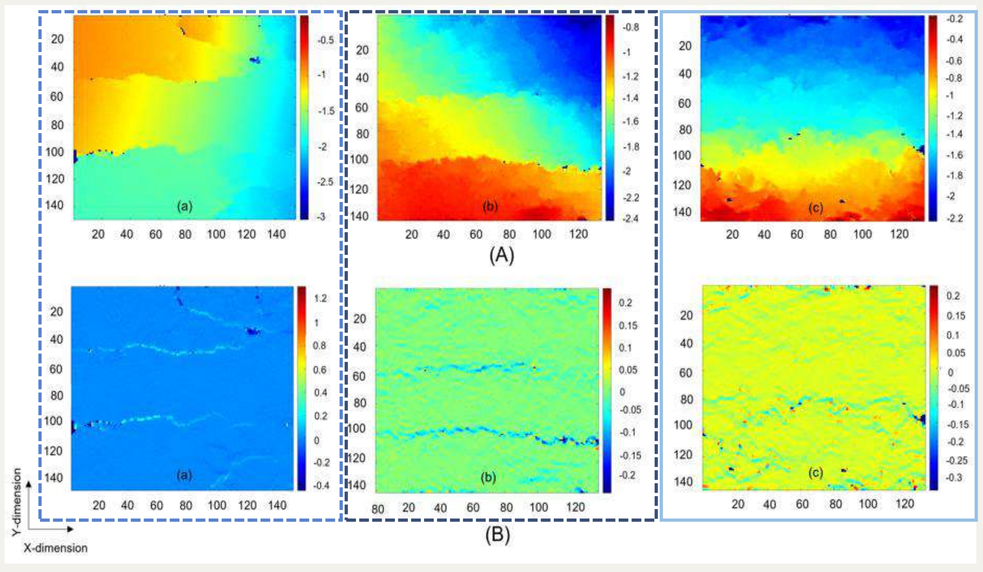

(A) vertical full field displacement ***dy [mm]*** *and (B) vertical strain* ***εyy*** *considering that for (a) RE4 at 5% strain rate, (b) HCSA-5 and (c) HTrad-1 at 1.5% strain rate*

4 CONCLUSION

- RE showed high strength and stiffness but brittle failure, while vegetal concrete exhibited lower mechanical performance with better thermal insulation and ductility.
- HTrad was selected as the optimal insulating layer, offering a balance between mechanical compatibility and thermal efficiency.
- To overcome the assembling challenges, optimized curing protocols, improved interface treatments, and refined mix designs are essential.

REFERENCES

1. *Bardouh, R., Toussaint, E., Amziane, S., Marceau, S., 2024a. Mechanical behavior of bio-based concrete under various loadings and factors affecting its mechanical properties at the composite scale: A state-of-the-art review.*
2. *Ávila, F., Puertas, E., Gallego, R., 2021. Characterization of the mechanical and physical properties of unstabilized rammed earth: A review.*
3. *Giuffrida, G., Ibos, L., Boudenne, A., Allam, H., 2024. Exploring the integration of bio-based thermal insulations in compressed earth blocks walls.*

Development of a Structured MCDM Methodology for Sustainability Evaluation, Selection, and Improvement of Manufacturing Processes

Luna Geo Kitila[12], Emmanuel Duc[1], Severine Duriex[2], Getasew Taddese[3]

[1]Sigma Clermont, Clermont Auvergne INP

[2]IMT Mines Albi, Université Toulouse

[3]Addis Ababa Institute of Technology, Addis Ababa University

Problem Statement and Motivations

- Selecting a sustainable manufacturing process is a complex task.
- It requires balancing economic, environmental, and social factors.
- This complexity increases due to conflicting criteria and uncertain expert preferences.
- The rise of Additive Manufacturing (AM) and new technologies increases the range of options and adds to the decision-making complexity."
- There is a clear need for structured decision-making tools that can:
  - Handle uncertainty, Integrate human judgment, Support sustainability across the product lifecycle

Objectives

1. To develop a structured methodology for evaluating and comparing different manufacturing processes under sustainability considerations.
2. To integrate fuzzy logic into decision-making to handle the imprecision in expert judgments.
3. To assess sustainability in manufacturing process selection by integrating qualitative and quantitative criteria.
4. To validate the methodology through a real world case study comparing different manufacturing processes
5. To conduct sensitivity analysis
6. To analyze ways for improving lower ranked manufacturing alternatives in decision making

Proposed Methodology

- Choosing a suitable MCDM method depends on factors like data type, calculation time, simplicity, and transparency. This study uses FAHP–FTOPSIS method to sustainable manufacturing process selection.
- The methodology consists of Five Phases;
  - **Phase 1:** Definition Phase: choosing the necessary criteria and alternatives
  - **Phase 2:** Data Collection: Use of linguistic and numerical data to account for uncertainty.
  - **Phase 3:** DM Phase: integrated FAHP-FTOPSIS decision methodology for ranking of alternatives. use of CRITIC Method to determine the stability
  - **Phase 4**: Sensitivity Analysis: manipulation of the weights
  - **Phase 5:** Rank Improvement: Spider Chart Analysis and Sensitivity Coefficient analysis

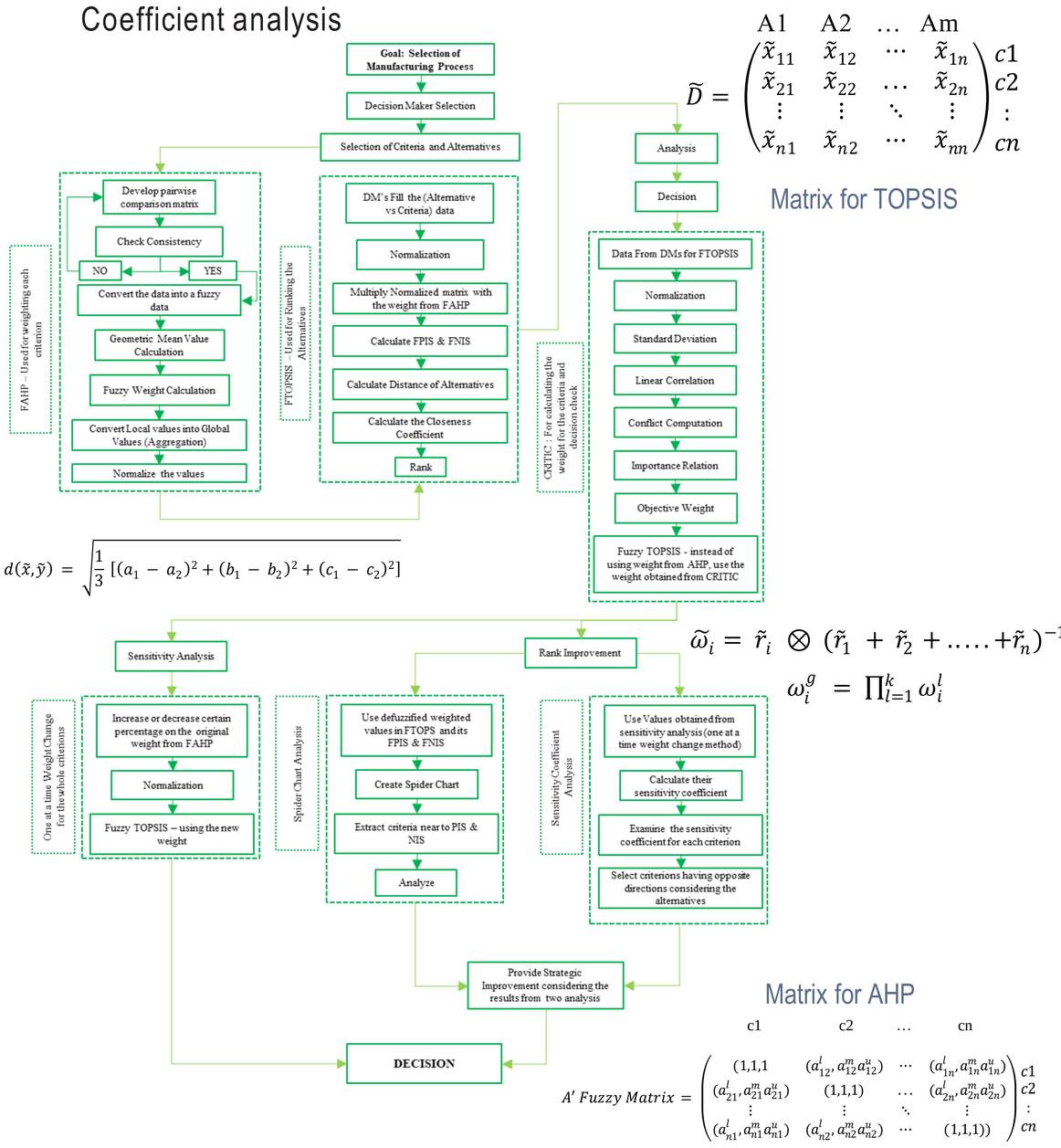

$$\tilde{D} = \begin{array}{c} \begin{matrix} A1 & A2 & \dots & Am \end{matrix} \\ \begin{pmatrix} \tilde{x}_{11} & \tilde{x}_{12} & \cdots & \tilde{x}_{1n} \\ \tilde{x}_{21} & \tilde{x}_{22} & \dots & \tilde{x}_{2n} \\ \vdots & \vdots & \ddots & \vdots \\ \tilde{x}_{n1} & \tilde{x}_{n2} & \cdots & \tilde{x}_{nn} \end{pmatrix} \begin{matrix} c1 \\ c2 \\ : \\ cn \end{matrix} \end{array}$$

Matrix for TOPSIS

$$d(\tilde{x},\tilde{y}) = \sqrt{\frac{1}{3}\left[(a_1 - a_2)^2 + (b_1 - b_2)^2 + (c_1 - c_2)^2\right]}$$

$$\tilde{\omega}_i = \tilde{r}_i \otimes (\tilde{r}_1 + \tilde{r}_2 + \dots . + \tilde{r}_n)^{-1}$$

$$\omega_i^g = \prod_{l=1}^{k} \omega_i^l$$

Matrix for AHP

$$A' \text{ Fuzzy Matrix} = \begin{array}{c} \begin{matrix} c1 & c2 & \dots & cn \end{matrix} \\ \begin{pmatrix} (1,1,1 & (a_{12}^l, a_{12}^m a_{12}^u) & \cdots & (a_{1n}^l, a_{1n}^m a_{1n}^u) \\ (a_{21}^l, a_{21}^m a_{21}^u) & (1,1,1) & \dots & (a_{2n}^l, a_{2n}^m a_{2n}^u) \\ \vdots & \vdots & \ddots & \vdots \\ (a_{n1}^l, a_{n1}^m a_{n1}^u) & (a_{n2}^l, a_{n2}^m a_{n2}^u) & \cdots & (1,1,1)) \end{pmatrix} \begin{matrix} c1 \\ c2 \\ : \\ cn \end{matrix} \end{array}$$

Case Study: Additive and Conventional Manufacturing

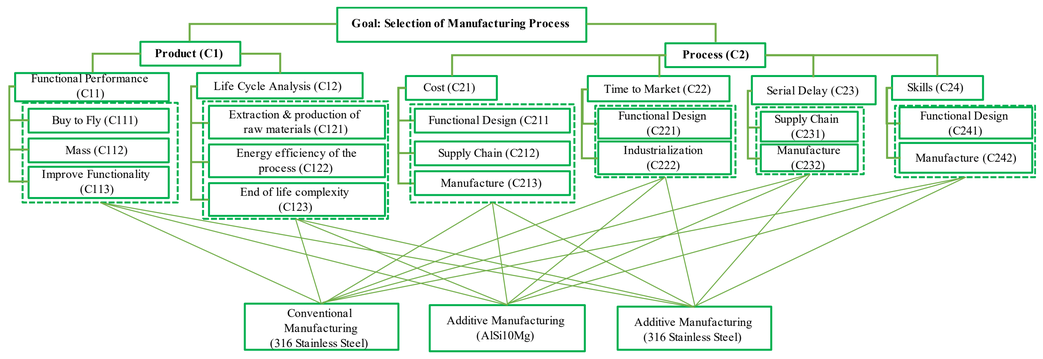

The proposed methodology is illustrated through the study conduct by Diegel et al., on the manufacturing process of hydraulic manifold

Alternatives	Material	Process
Alternative 1	316 Stainless steel	Conventional manufacturing
Alternative 2	AlSi10Mg	Additive Manufacturing
Alternative 3	316 Stainless steel	Additive Manufacturing

Table 1 : Alternatives, material and process in manufacturing of hydraulic manifold

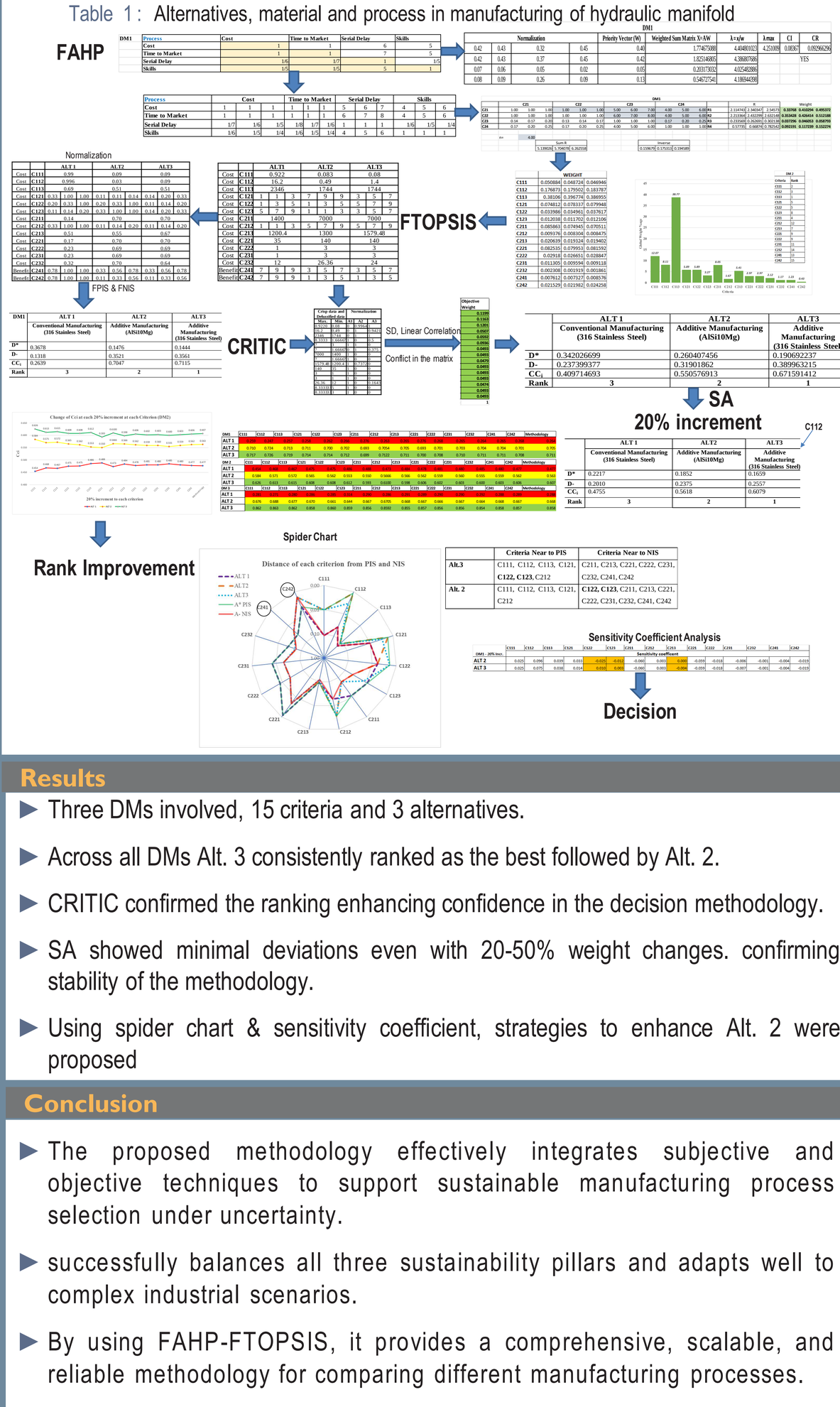

	Criteria Near to PIS	Criteria Near to NIS
Alt.3	C111, C112, C113, C121, **C122, C123**, C212	C211, C213, C221, C222, C231, C232, C241, C242
Alt. 2	C111, C112, C113, C121, C212	**C122, C123**, C211, C213, C221, C222, C231, C232, C241, C242

Results

- Three DMs involved, 15 criteria and 3 alternatives.
- Across all DMs Alt. 3 consistently ranked as the best followed by Alt. 2.
- CRITIC confirmed the ranking enhancing confidence in the decision methodology.
- SA showed minimal deviations even with 20-50% weight changes. confirming stability of the methodology.
- Using spider chart & sensitivity coefficient, strategies to enhance Alt. 2 were proposed

Conclusion

- The proposed methodology effectively integrates subjective and objective techniques to support sustainable manufacturing process selection under uncertainty.
- successfully balances all three sustainability pillars and adapts well to complex industrial scenarios.
- By using FAHP-FTOPSIS, it provides a comprehensive, scalable, and reliable methodology for comparing different manufacturing processes.
- The consistent results across multiple validation techniques highlight the method's reliability and adaptability.
- This methodology can further be utilized in other sectors as material selection, supply chain optimization.

Acknowledgments

- Campus France, the Embassy of France in Addis Ababa, and the Ethiopian Ministry of Education

Contact Information

- Email: luna.kitila@sigma-Clermont.fr

Développement d'un système d'instrumentation du tassement différentiel des structures soumises au retrait-gonflement des argiles

Mathilde LEFEBVRE[1,2], Alaa CHATEAUNEUF[1,2], Mathilde MORVAN[1]

1- Université Clermont Auvergne, Clermont Auvergne INP, CNRS, Institut Pascal, Clermont-Ferrand, France

2- CIDECO, 28 Place Henri Dunant, TSA 50400, F-63001 Clermont-Ferrand Cedex 1, France

Ecole doctorale Sciences Pour l'Ingénieur

Contexte

- Le retrait-gonflement des argiles (RGA) est un phénomène provoqué par les variations de teneur en eau dans les sols argileux. Lors des périodes sèches, le sol se rétracte, et lors des périodes humides, il gonfle. Ces mouvements volumétriques peuvent provoquer des tassements différentiels sous les bâtiments.

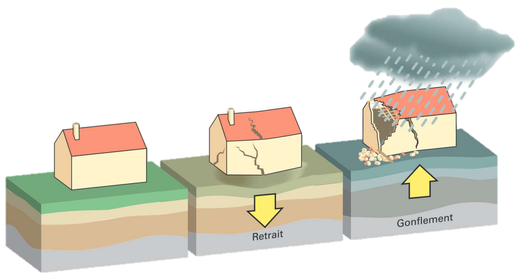

Figure 1 : Illustration du phénomène de retrait-gonflement [1]

- Avec le changement climatique, les épisodes de sécheresse deviennent plus fréquents et plus intenses. En 2022, les dommages liés au RGA ont atteint un niveau record de plus de 3 milliards d'euros. Sur la dernière décennie, la sécheresse est même devenue le premier poste d'indemnisation au titre des catastrophes naturelles, devant les inondations (52 % de la sinistralité Cat Nat) [2].

Problématique

- Malgré l'ampleur des désordres liés au retrait-gonflement des argiles, la modélisation du comportement différentiel des structures reste difficile en raison de la complexité et du caractère multifactoriel du phénomène.
- Les méthodes actuelles reposent sur des essais en laboratoire, mais les projets de recherche nationaux ARGIC-1 et ARGIC-2 ont montré un écart important entre prédictions théoriques et observations sur le terrain [3].
- Les dispositifs de surveillance in situ pour les bâtiments touchés restent rares car ils sont coûteux, difficiles à mettre en œuvre ou fournissent peu d'informations, ce qui les rend peu adaptés aux structures touchées.
- Une question se pose : ***Comment surveiller efficacement les structures soumises au retrait-gonflement des argiles par une instrumentation adaptée, peu coûteuse et exploitable ?***

Démarche

Le système d'instrumentation envisagé

- Le projet vise à instrumenter les structures avec des capteurs optiques pour mesurer les tassements différentiels, ainsi que des sondes de succion pour suivre l'évolution hydrique du sol. Le développement des capteurs optiques est mené par le service recherche et développement de l'entreprise CIDECO. Les tassomètres seront positionnés aux coins de la structure, la précision visée est de l'ordre de 0,1 mm. Des tests sont prévus en laboratoire pour valider la précision des mesures avant leur déploiement sur site.

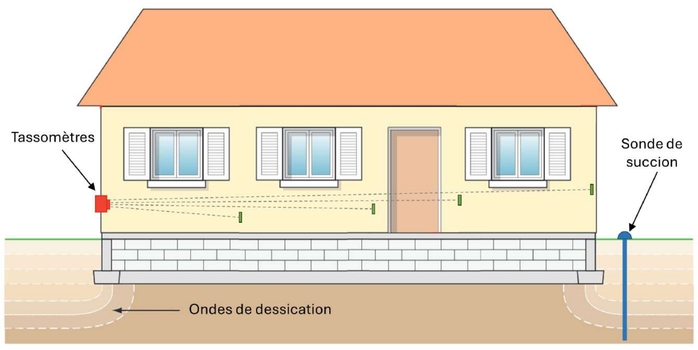

Figure 2 : Illustration du système d'instrumentation envisagé

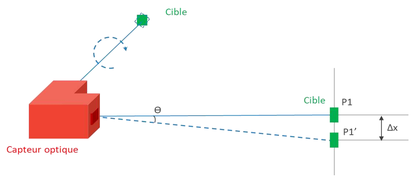

Figure 3 : Principe de la mesure du tassement par les capteurs optiques

Modélisation du comportement du système

- Une revue des approches existantes (empiriques, analytiques, numériques) a permis de sélectionner un modèle analytique couplé hydromécanique, adapté au contexte du RGA.
- Le modèle de retenu permet un compromis entre les modèles empiriques (calculs rapides mais trop simplistes) et les modèles numériques 3D (plus précis mais coûteux en temps de calcul et données).
- Il permet d'intégrer les variations de succion et les chargements mécaniques, tout en étant compatible avec la démarche de suivi in situ.

Expérimentation en laboratoire

- Des essais à échelle réduite sont envisagés pour :
  - valider le fonctionnement du système de capteurs,
  - tester la capacité des différents modèles à estimer les déformations observées,
  - comparer la précision des différentes approches de modélisation.

Figure 4 : Illustration d'un banc d'essai géotechnique à échelle [4]

Vers un modèle prédictif

- En combinant les mesures in situ avec la modélisation, et grâce à une analyse inverse, l'objectif est de permettre au modèle d'estimer les paramètres manquants propres à chaque configuration instrumentée. Une fois calibré, il pourrait être utilisé pour évaluer la vulnérabilité de la structure face à différents scénarios climatiques.

Modélisation de l'interaction sol gonflant - structure

- Modélisation du comportement du sol gonflant par une loi basée sur l'approche de surface d'état [5].
- Modélisation des échange sol-atmosphère pour calculer la diffusion de la succion dans le sol [6].

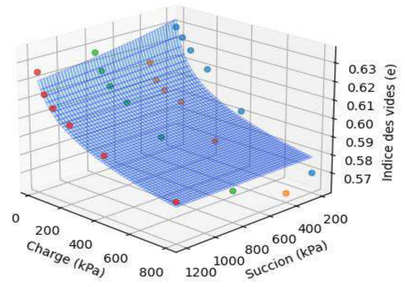

Figure 5 : Surface d'état Unsat-1 pour le sol de Régina

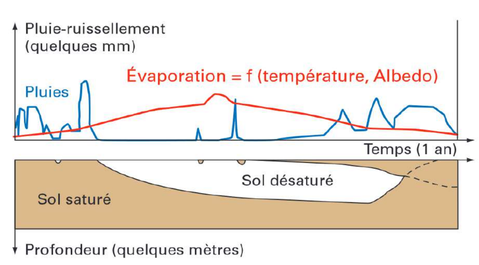

Figure 6 : Diagramme précipitations-évaporation [1]

- Modélisation simplifiée de l'interaction sol-gonflant structure (bâti → poutre). Le modèle de Jahangir [7] est un modèle couplé hydromécanique qui permet un compromis entre pertinence physique et complexité numérique, ce qui le rend particulièrement adapté à une démarche de surveillance in situ.

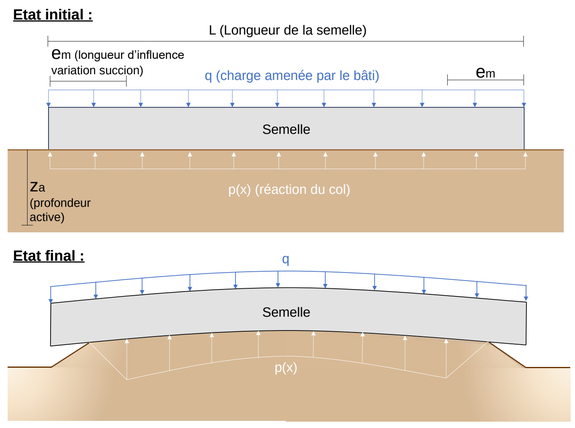

Figure 7 : Illustration du modèle d'interaction sol-structure en contexte de RGA

- Exemple de résultats pour 2 types de bâtiment : calcul de la réaction du sol, des tassements différentiels et des tassements totaux du sol

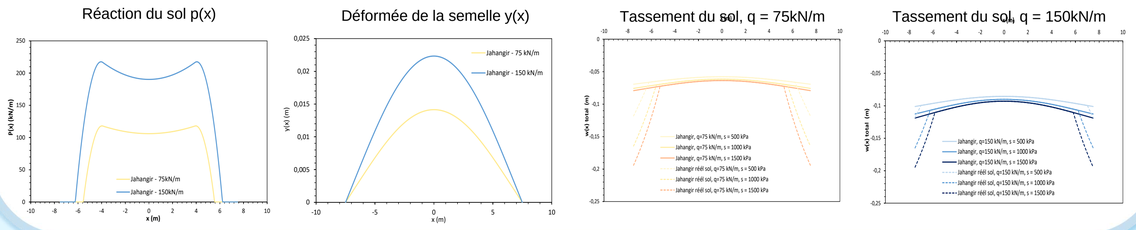

Références

[1] Béchade, A.-F., 2021. La pathologie des fondations superficielles: diagnostic, réparations et prévention, 2e éd. ed, Guide Pathologies des bâtiments. CSTB éditions AQC, Marne-la-Vallée Paris.

[2] Moncoulon, D., Desarthe, J., Naulin, J.P., Onfroy, T., Tinard, P., Wang, Z.X., Hajji, C., Veysseire, M., Dequé, M., Régimbeau, F., 2023. Conséquences du changement climatique sur le coût des catastrophes naturelles en France à l'horizon 2050. Caisse Centrale de Réassurance & Météo France, Paris.

[3] Vincent, M., Cojean, R., Fleureau, J.M., Cui, Y.J., Jacquard, C., Kazmierczak, J.B., Masrouri, F., Tessier, D., Alimi-Ichola, I., Magnan, J.P., 2009. Rapport de synthèse final du projet ARGIC (Analyse du retrait/gonflement et de ses incidences sur les constructions)

[4] Marwan, A., Hassoun, M., Villard, P., Emeriault, F., & Farhat, A. (2020). Subsidence prediction of reinforced soil layer by geosynthetic using large-scale 1g physical model. Proceedings of the International Association of Hydrological Sciences.

[5] Vu, H.Q., Fredlund, D.G., 2003. Uncoupled and coupled solutions of two-dimensional swelling in expansive soils.

[6] El-Garhy, B., Wray, W., 2004. Method for Calculating the Edge Moisture Variation Distance. Journal of Geotechnical and Geoenvironmental Engineering.

[7] Jahangir, E., Deck, O., Masrouri, F., 2013. An analytical model of soil–structure interaction with swelling soils during droughts. Computers and Geotechnics 54, 16–32.

Analyse du comportement mécanique de structures légères bois-acier-textile et leurs assemblages sous sollicitations réelles

Théo LEGRAND[1,2]

Sébastien DURIF[1] ,Nicolas SAUVAT[1], Abdelhamid BOUCHAIR[1]

1 - Université Clermont Auvergne, Clermont Auvergne INP, CNRS, Institut Pascal, F-63000, Clermont-Ferrand, France

2 - Texabri, 38121, Reventin-Vaugris, France

Ecole doctorale Sciences Pour l'Ingénieur

CONTEXTE

Structure métallo-textile de Texabri

Objectifs industriels

- Baisser l'impact carbone de structures métallo-textile de Texabri
- Remplacer les poutres en acier par des poutres en acier formé à froid et en bois
- Développer des vérifications propres aux poutres mixtes dans le logiciel RFEM6

Objectifs scientifiques

- Elaborer un modèle de la solution mixte
- Mesurer l'effet de la toile sur la structure
- Analyser l'impact des conditions climatiques sur la nouvelle solution

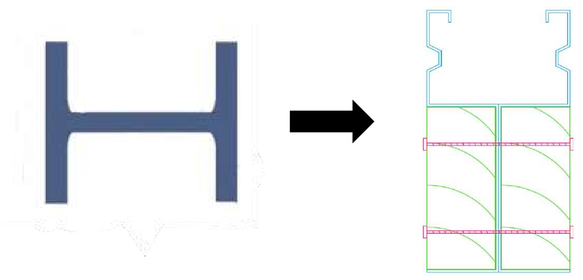

Solution poutre actuelle *Solution poutre visée*

ACIER-BOIS

Problématique

L'acier et le bois se comportent de manière différentes, et peuvent avoir des avantages qui compensent leurs faiblesses respectives :

- L'acier protège le bois de l'eau, et limite le fluage.
- Le bois permet d'éviter les instabilités mécaniques de l'acier [1].

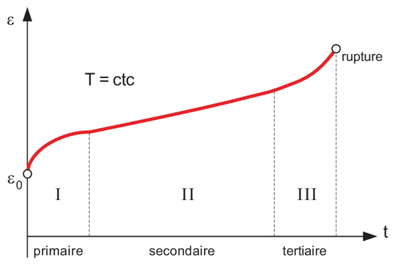

Courbe de fluage

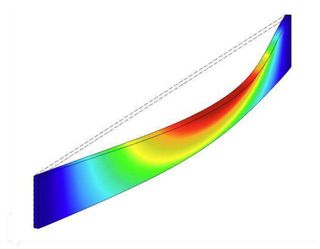

Déversement

Critère	Paramètre	Bois (GL24h)	Acier (S275)
Durabilité		Dégradation biologique	Corrosion
Variation dimensionnelle	Dilatation thermique [µm/m/°C]	4	12
	Hygrométrie *Retrait volumique total* [%]	11	0
Paramètre matériau	Module d'élasticité [MPa]	11000	210000
	Masse volumique [kg/m3]	420	7850
	Module de franchissement (E/ρ) [MJ/kg]	26,2	26,8
Comportement	Fluage	Oui	Non
	Tenue mécanique	Fragile	Ductile
	Propriétés directionnelles	Orthotrope	Isotrope

Différences de comportement entre l'acier et le bois [2],[3],[4]

Résolution

- Valider par l'expérimentation un modèle numérique qui permettra de développer des formules de vérification.
- Intégrer les formules dans un logiciel type ingénieur pour l'entreprise.

Expérimentation [5]

Modélisation numérique [5]

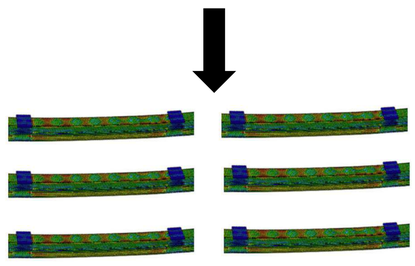

Etude paramétrique [5]

Introduction dans RFEM6

TOILE

Problématique

La toile exerce une tension sur la structure métallique : il est nécessaire de mesurer cet effort.

Elle a un comportement complexe lors de la mise en tension :

- Phénomène d'embuvage [6]. Le tissu ne récupère pas après la première charge dû au frottement entre fibre et matrice.
- Comportement hyperélastique [7] (les logiciels ne prennent pas en compte le comportement réel lors de la recherche de forme).

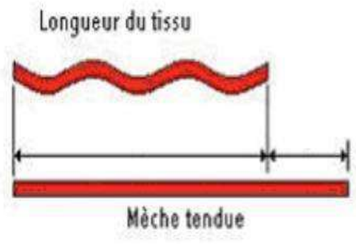

Définition de l'embuvage

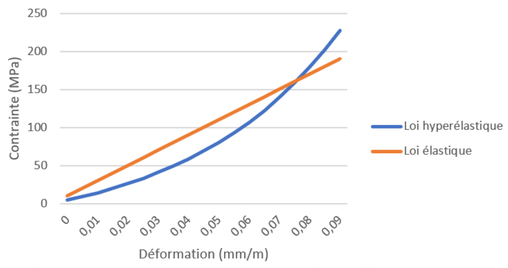

Comparaison entre une loi élastique et hyperélastique

Résolution

- Mesurer les efforts de la toile sur la structure à l'aide de palpeurs.
- Vérifier que le modèle numérique correspond à la réalité.

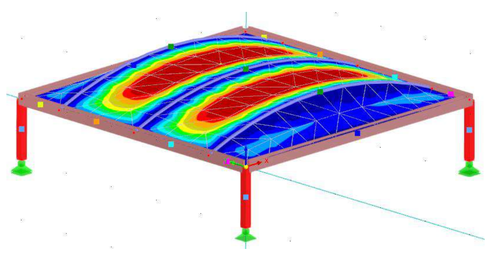

Modélisation numérique (RFEM6)

Expérimentation toile

BIBLIOGRAPHIE

[1] B. Jurkiewiez, S. Durif, A. Bouchair, et C. Grazide, « *Experimental and analytical study of hybrid steel-timber beams in bending* », *Structures*, vol. 39, p. 1231-1248, mai 2022, doi: 10.1016/j.istruc.2022.03.055.

[2] FNB, « *Le retrait du bois* ». mars 2019

[3] Comité Technique CEN/TC 250, *Eurocode 3 - Calcul des structures en acier - Partie 1-1 : règles générales et règles pour les batiments*, Norme francaise homologuée P 22-311-1, octobre 2005.

[4] Comité Technique CEN/TC 250, *Eurocode 5 - Conception et calcul des structures en bois - Partie 1-1 : généralités - règles communes et règles pour les batiments*, Norme francaise homologuée P 21-711-1, novembre 2005.

[5] Di Ma, Kim J.R. Rasmussen et Hao Zhang, « *Numerical investigation of the flexural-torsional behaviour of built-up cold-formed steel beams* », Thin-Walled Structures, Volume 212, July 2025, doi.org/10.1016/j.tws.2025.113183

[6] J. B. Pargana, D. Lloyd-Smith, et B. A. Izzuddin, « *Advanced material model for coated fabrics used in tensioned fabric structures* », *Eng. Struct.*, vol. 29, nº 7, p. 1323-1336, juill. 2007, doi: 10.1016/j.engstruct.2006.09.001.

[7] J. Skelton, « *Mechanical properties of coated fabrics* », *Mech. Flex. Fiber Assem.*, p. 461-469, 1980.

Want a Crack-Free House? Start with the Soil! The Swelling–Shrinkage Phenomenon

Zahraa Lehaf, Mathilde Morvan, Pierre Breul

Université Clermont Auvergne, CNRS, SIGMA Clermont, Institut Pascal, Clermont-Ferrand, France

Ecole doctorale Sciences Pour l'Ingénieur

Introduction



⚠ Swelling shrinkage classified as real hazard
💰 3.3 Billions economic cost in France
🔍 Critical need to indicate the reasons

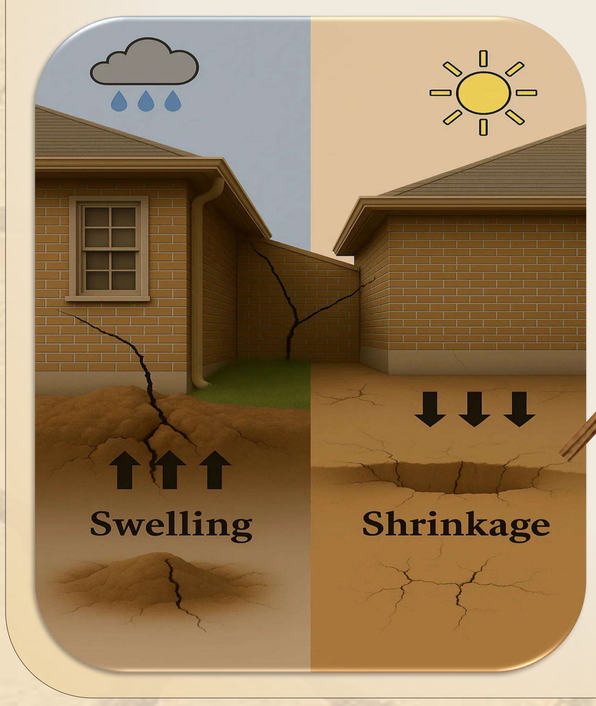

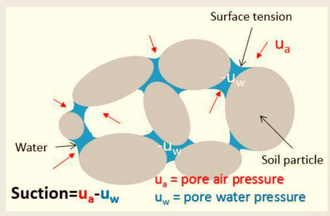

Suction
physicochemical phenomenon

What are the causes?

How to facilitate predicting this problem?

Methodology

Practical equations to facilitate work

Driving parameters at suction level

Relate swelling to suction and microstructure

Relate swelling to geotechnical parametes

Testing stage

- Geotechnical characterization
  - Atterberg limits
  - Methylene blue
  - Particle size
- Swelling
  - Oedometer tests
- Water Retention
  - Suction measurements with filter paper

Bibliographic part: parameters that might affect swelling

Results

Practical equations to facilitate work

Different Mixes to study variability of soils

4 different mixes Natural soil: Argile Aulnat Allier (AA)
95% AA with 5% Artificial Clay (AC)
90% AA with 10% AC
85% AA with 15% AC

Property \ Soil	AA	95/5 AA/AC	90/10 AA/AC	85/15 AA/AC
Plastic Limit	22%	26%	29%	31%
Liquid Limit	43%	52%	62%	85%
Plasticity Index	21%	26%	33%	54%
VBS	3.96	4.49	5.97	8.8
Particles < 2 µm	43.50%	46%	51%	51%
Particles < 80 µm	94.7%	93.6%	92%	92.5%
Specific Gravity	2.63	2.72	2.76	2.8

Swelling Tests

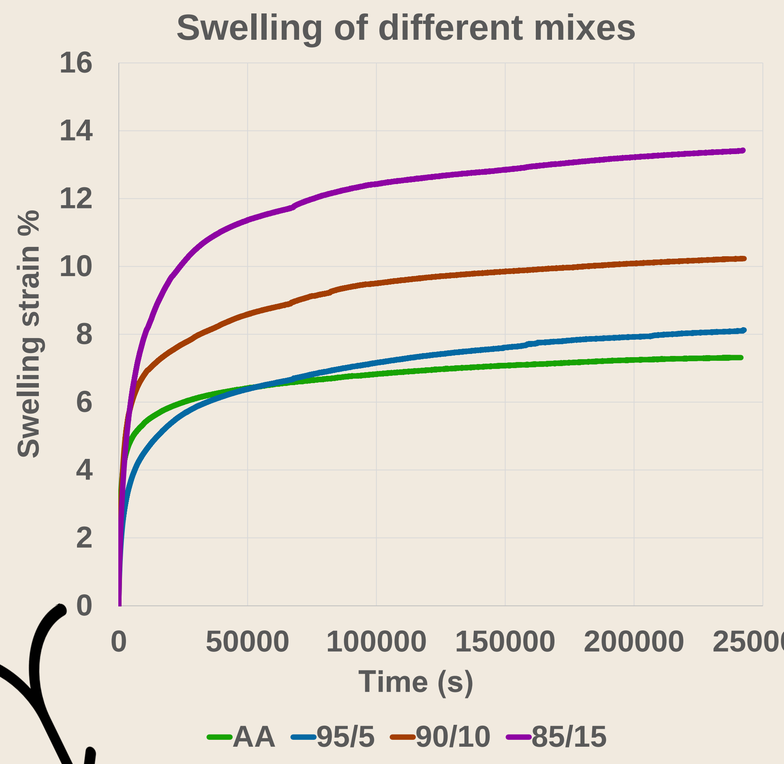

Testing different combination of parameters with different mathematical models for choosing the best relation

Suction Visualization by WRC

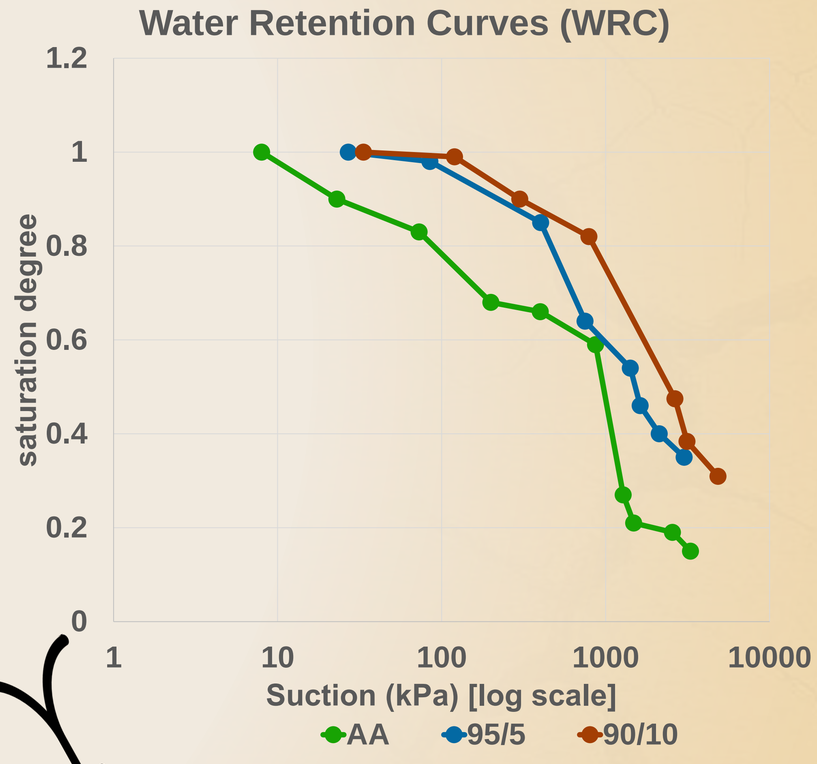

Checking the effect of suction by studying relation of effective stress on swelling: Models of Bishop and Khalili

Conclusions

- The addition of artificial clay (AC) to natural clay (AA) increases swelling potential and water retention capacity.
- Swelling behavior changes with geotechnical parameters of various mixes.
- Suction measurements and water retention curves visualize at microstructure what is causing macrostructure changes.
- Conducting various tests on different soils allows to construct predictive models while identifying the underlying driving forces.

References: *Zemenu, G., Martine, A., & Roger, C. (2009). Analyse du comportement d'un sol argileux sous sollicitations hydriques cycliques.*
CEREMA Web Resource. (2022). Phenomenon of shrinkage and swelling of clayey soils (RGA)
Caisse Centrale de Réassurance. (2021)
Delage, P. (2002). Experimental unsaturated soil mechanics.

For more info please scan

Détection d'anomalies 3D explicable à partir de nuage de points dans un usage industriel

Rémi Lhoste [1,2] Damien Delhay [1] Zakaria Baou[1] Antoine Vacavant [2]

[1]O2game, 60200, Compiègne

[2]Institut Pascal, Université Clermont Auvergne, UMR 6602 UCA/SIGMA/CNRS, 63171 Aubière, France

Anomalie : Élément qui s'écarte des caractéristiques attendues ou de la norme établie.

Contexte et motivations

- Pourquoi la détection d'anomalies 3D?
  - Limites actuelles : Les méthodes 3D existantes manquent de robustesse et consomment trop de ressources pour l'industrie.
  - Utilisation dans des applications critiques (analyse de coque d'avion, de caténaire, agroalimentaire).
  - Les variations de couleur, d'éclairage et de texture ne permettent pas toujours d'analyser les défauts en 2D.

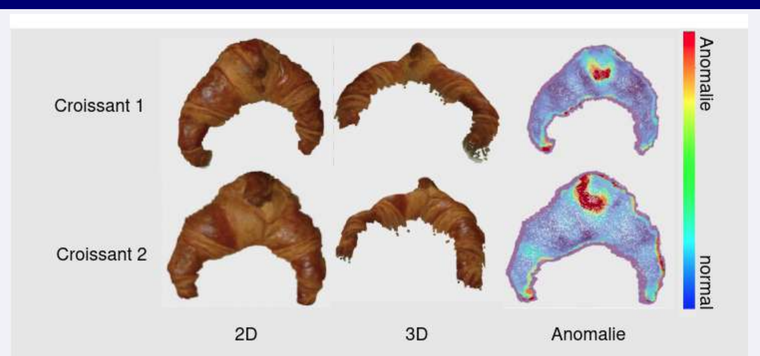

Objectif de la thèse

- Développer des algorithmes 3D plus performants que les approches 2D+3D actuelles.
- Réduire les besoins computationnels pour l'industrialisation.
- Améliorer l'explicabilité pour les secteurs critiques.
- Valider sur des applications industrielles réelles.

Défis techniques

- Les nuages de points sont irréguliers et non-structurés.
- Le paradigme actuel utilise beaucoup de mémoire RAM.
- Manque de données par rapport à la 2D.
- L'acquisition des données est multi-capteurs.

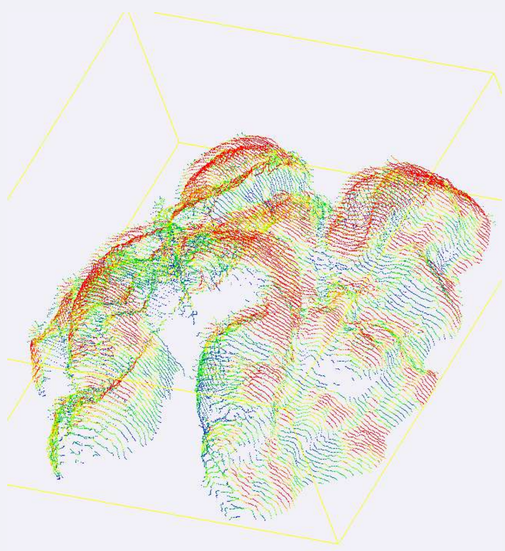

Méthodes developpées

- MAESTRO (Masked Auto Encoder Self-supervised Through Reconstruction Only) [Lhoste, 2025]
  - Approche multi-echelle.
  - Sans banque de mémoire (moins d'utilisation de la ram).
  - Un seul modèle pour plusieurs classes.
- Approche en cours : reconstruction en caractéristiques profondes
  - Plus de robustesse sur des données bruitées.
  - Plus d'expressivité dans la reconstruction.

Méthodes developpées

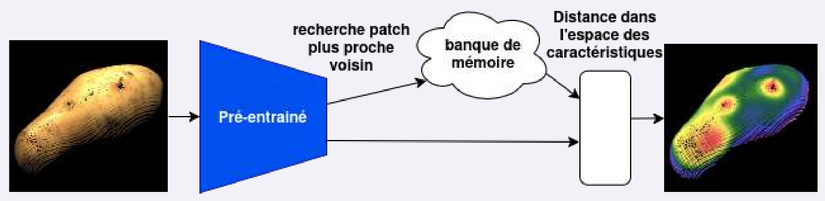

(a) Paradigme par caractéristiques

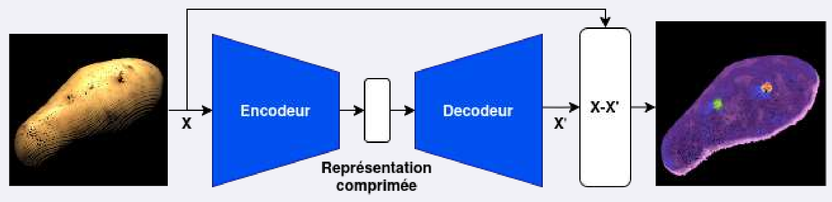

(b) Paradigme par reconstruction (notre approche)

Expérimentations

- Performance sur le jeu de données MVTec 3D-AD [Bergmann, 2022]:
  - Atteinte des résultats état de l'art sur plusieurs catégories agro-alimentaires.

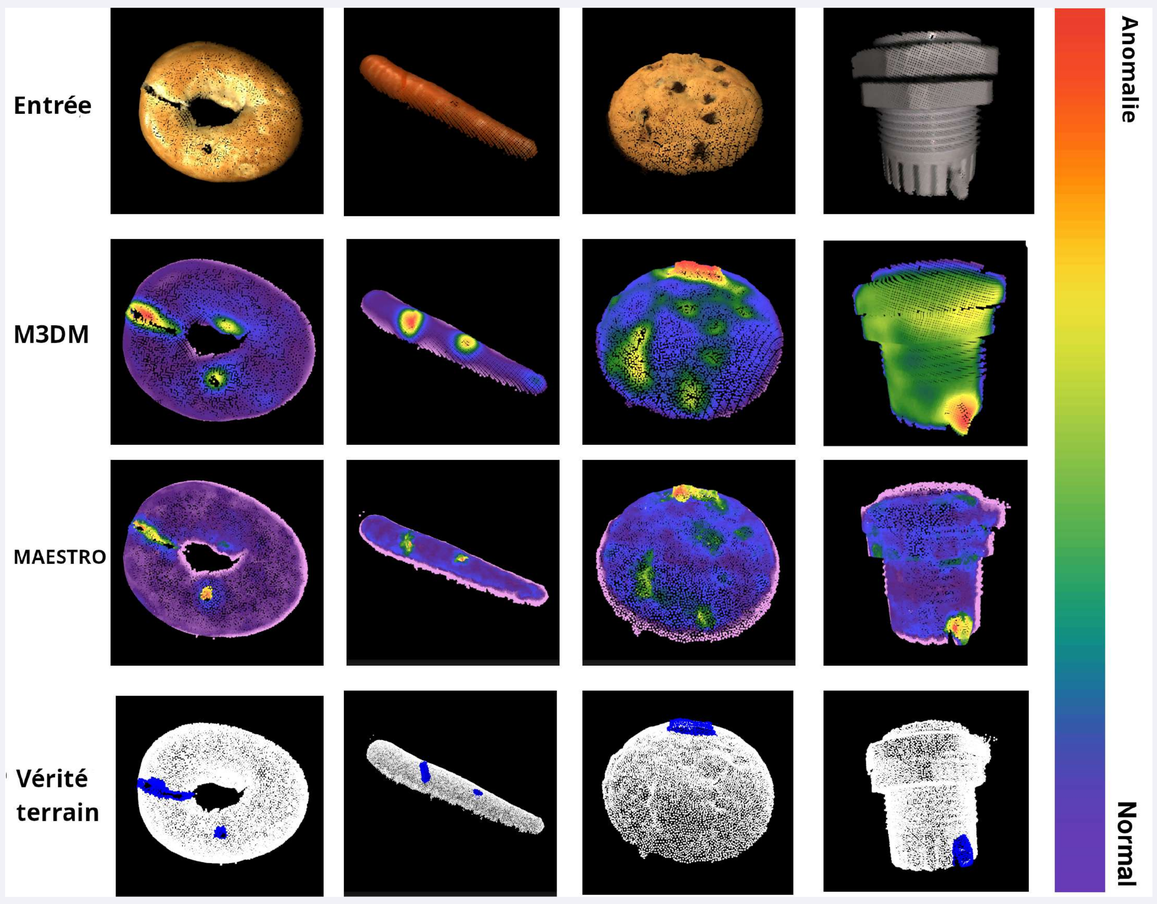

- Efficacité computationnelle et performances:
  - Des patchs plus petits permettent une inférence plus rapide, réduisant les coûts computationnels et surpassant M3DM [Wang, 2023].
  - Notre modèle basé sur la reconstruction réduit la consommation mémoire à 2GB contre 45GB pour M3DM [Wang, 2023].

Conclusion et Perspectives

- Utilisation vers des modèles multi-capteurs.
- Comprendre les limites et biais des modèles developpées.
- Adaptation du modèle à de nouveaux objets industriels et valorisation dans des applications industrielles.

Réferences

[Bergmann et al., 2022] P. Bergmann, X. Jin, D. Sattlegger, C. Steger. The MVTec 3D-AD Dataset for Unsupervised 3D Anomaly Detection and Localization. Proceedings of the 17th International Joint Conference on Computer Vision, Imaging and Computer Graphics Theory and Applications, 2022.

[Wang, 2023] Yue Wang and Jinlong Peng and Jiangning Zhang and Ran Yi and Yabiao Wang and Chengjie Wang. Multimodal Industrial Anomaly Detection via Hybrid Fusion. 2023 IEEE/CVF Conference on Computer Vision and Pattern Recognition (CVPR), 2023.

[Lhoste, 2025] R. Lhoste, A. Vacavant, D. Delhay. MAESTRO: A Full Point Cloud Approach for 3D Anomaly Detection Based on Reconstruction. 20th International Conference on Computer Vision Theory and Applications (VISAPP), 2025.

Covering problems related to graphs: monitoring segments with drones

Lorieau Lucas

Université Clermont-Auvergne, CNRS, Mines de Saint-Étienne, Clermont-Auvergne-INP, LIMOS

Motivation

- Lots of networks and infrastructures require a fine-grained monitoring (*e.g.* energy networks, railway systems, computer networks...).
- This monitoring tends to be automated and thus require algorithms to ensure and overseer the monitoring.
- Furthermore, arising technologies are to be integrated in such environments (*e.g.* drones) and require new inventive solutions to operate them.

Figure 1:A drone used to perform monitoring operations

Covering problems in graph theory

- Networks are represented by *graphs*, objects composed of *vertices* connected together by *edges*.
- One can then define several covering problems, for instance :
  - vertex cover: select a set of covering vertices, each edge must be adjacent to a covering vertex;
  - geodetic set: select a set of terminals, each vertex must lie on a shortest path between two terminals.

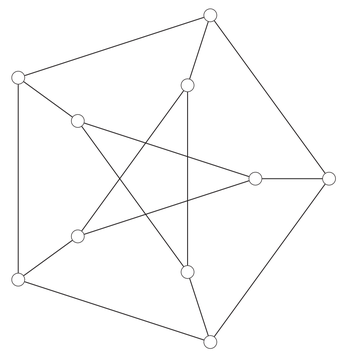

Figure 2: An example of a graph

- We will focus on a special case of *dominating set*. In dominating set, one selects a set of dominating vertices, each vertex must have one dominating vertex as a neighbor.
- In general, all problems cited above are NP-hard, *i.e.* difficult to solve.

Multidepot Drone Segment Covering

- In this problem, we want to cover with drones a set of segments $\mathcal{S} = \{S_1, \ldots, S_n\}$ on a common line.
- These drones depart from a set of depots $\mathcal{D} = \{D_1, \ldots, D_k\}$, and have a limited autonomy. They cannot fly for more than a distance L before joining back their origin depot.
- The goal is to compute a valid set of tours $\mathcal{T} = \{T_1, \ldots, T_m\}$ for the drones so that they cover the set $\mathcal{S}$ of segments with the minimal number of tours / the minimal distance flown in an efficient way (*i.e.* in polynomial computing time regarding values n, m and k).

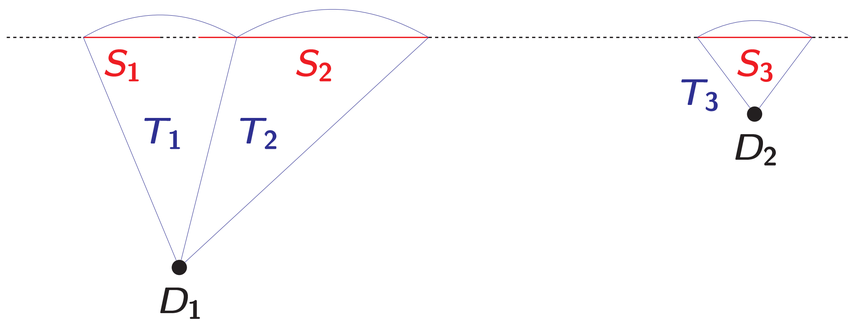

Figure 3: An example of solution with two depots, three segments and three tours

One depot : dynamic programming

- In [1], two algorithms are presented for instances that have only a single depot. For optimizing the number of tours, a simple greedy algorithm is described.
- Key ideas for length optimization: computing a small set of tours containing the optimal solution and use test feasible solutions in a clever way (dynamic programming).

Two depots : challenges and solutions

- Impossible to reuse the same techniques with two depots.
- Still possible to compute a set of possible tours by decomposing the instances into smaller, managable ones:
  - A core instance where both depots are used $\longrightarrow$ need of a new algorithm for this part;
  - Two exernal ones where only one depot is used $\longrightarrow$ reuse of the algorithms of [1].
- We obtain a polytime optimal algorithm for optimizing the number of tours, and an algorithm with arbitrary precision for optimizing the total length.

More depots : reduction to a dominating set problem

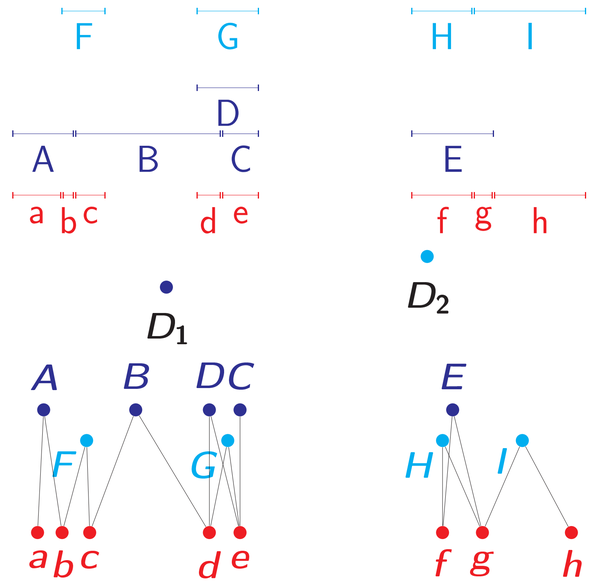

Figure 4:The reduction to Red-Blue Dominatig Set

Conclusion

- We design new algorithms generalizing the previous known results on tractability in the double depot setting and general setting.
- Further developpements can be imagined: covering segments on a grid instead of a line, allowing drones to depart from one depot and arrive in another one ...

Acknowledgments

- This work has been conducted under the supervision of Laurent Beaudou, Florent Foucaud and Pranabendu Misra.

References

[1] Sergey Bereg, José-Miguel Díaz-Báñez, Alina Kasiuk, Miguel-Angel Pérez-Cutiño, and Fabio Rodríguez.
Covering segments on a line with drones.
Information Processing Letters, 188:106540, February 2025.

[2] Laurent Beaudou, Florent Foucaud, Lucas Lorieau, and Pranabendu Misra.
An efficient algorithm for a drone bidepot segment covering problem.
International Symposium on Mathematical Foundations of Computer Science, submitted (2025).

Contact Information

- Web: https://perso.limos.fr/ lulorieau/
- Email: lucas.lorieau@limos.fr

Scenes understanding by multimodal imaging

Edoardo Malaspina
SMA-RTY SAS / UCA

Introduction

Different modalities ⟶ Different features highlighted

***Fig. 1**: Visible image.*

***Fig. 2**: NIR image.*

***Fig. 3**: SWIR image.*

***Fig. 4**: LWIR image.*

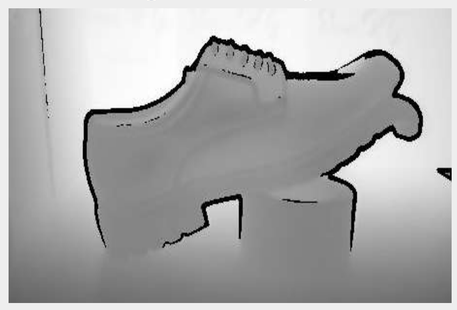

***Fig. 5**: ToF image.*

Image/Video Registration

CuDi Descriptor for keypoint matching

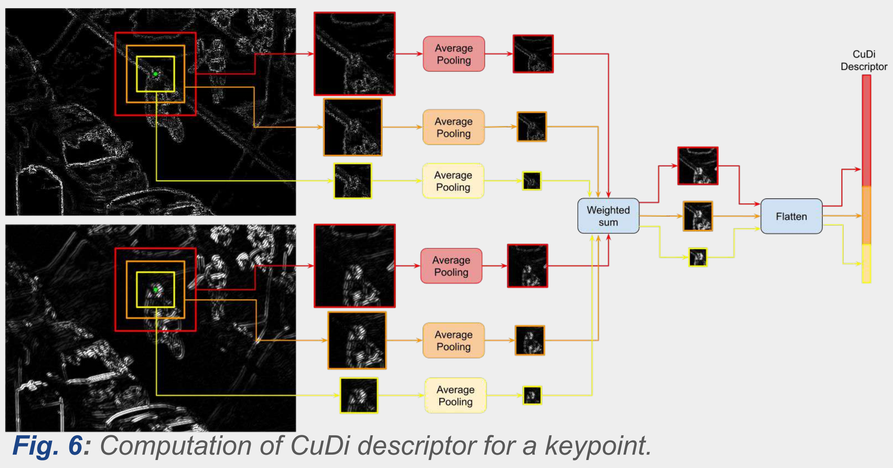

***Fig. 6:** Computation of CuDi descriptor for a keypoint.*

***Fig. 7:** Matched keypoints between thermal and visible.*

PlugAndFilter: refining previous matches

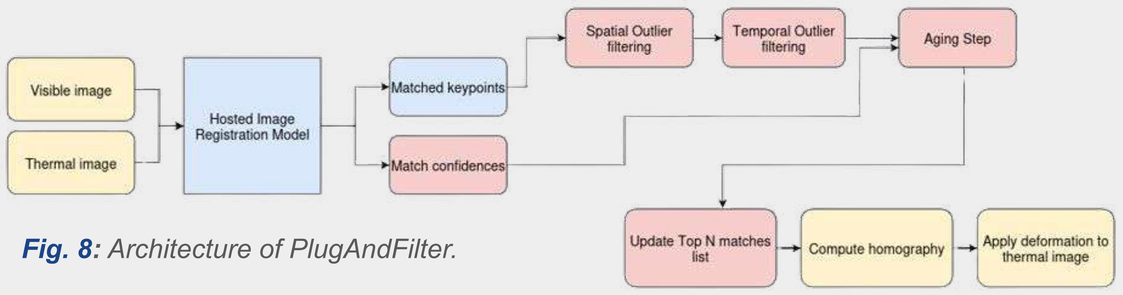

***Fig. 8:** Architecture of PlugAndFilter.*

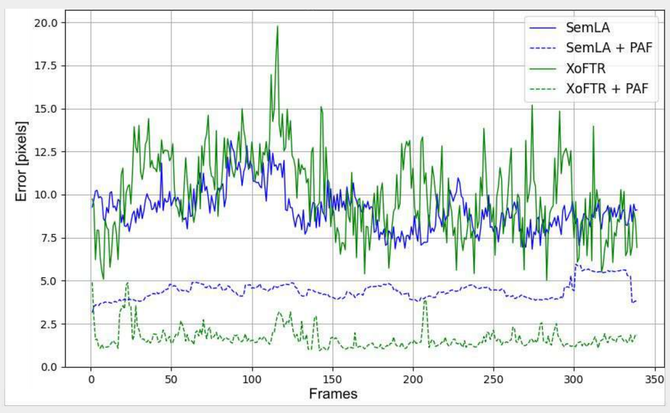

***Fig. 9:** Matching Error (in pixel) of two different Deep Learning architecture (SemLA[1] e XoFTR[2]) with and without PlugAndFilter across frames of a video.*

[1] XIE, Housheng, et al. Semantics lead all: Towards unified image registration and fusion from a semantic perspective. *Information Fusion*, 2023
[2] TUZCUOĞLU, Önder, et al. Xoftr: Cross-modal feature matching transformer. In: *Proceedings of the IEEE/CVF Conference on Computer Vision and Pattern Recognition*. 2024

Image/Video Fusion

Combine the information from the different modalities to obtain new features

***Fig. 10**: Thermal-Visible overlay.*

***Fig. 11**: Thermal-Visible fusion using AutoEncoders.*

***Fig. 12**: ToF-Visible overlay.*

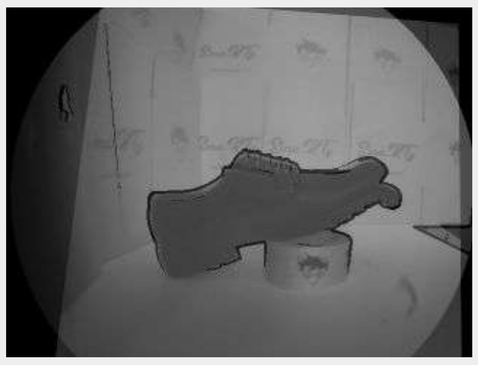

***Fig. 13**: ToF-Visible 3D reconstruction.*

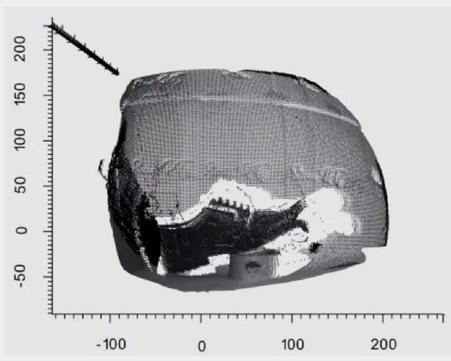

Multimodal Segmentation

***Fig. 14**: Visible image and segmentation.*

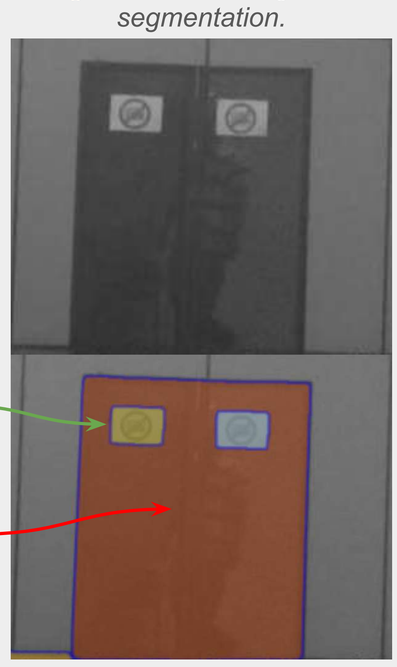

***Fig. 15**: Thermal-image and segmentation.*

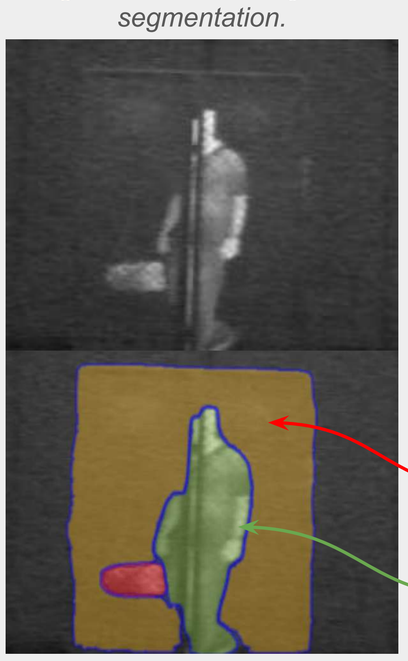

Improving segmentation quality using information from both Visible and LWIR

Signs detected

No person detected

No Signs detected

Person detected

Both Signs and Person detected

***Fig. 16**: Thermal-Visible overlay and segmentation.*

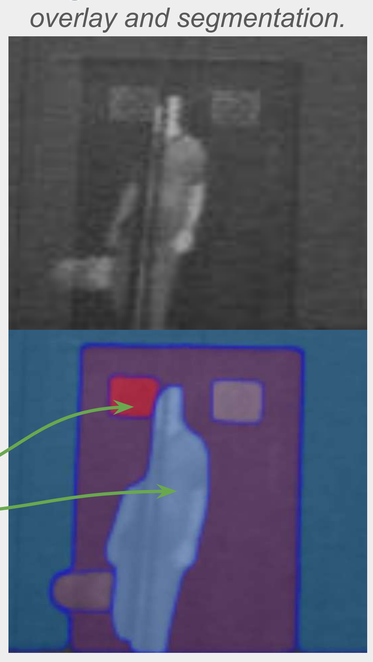

REMAIN | Interreg Sudoe | Co-funded by the European Union
Université Clermont Auvergne | Institut Pascal sciences de l'ingénierie et des systèmes | SMARTY Connecting Intelligence

URBAN HEAT STRESS
TOOLS FOR PREDICTION, EVALUATION, AND MITIGATION

"Designing Cooler Cities through Data-Driven Planning"

Context

- Cities are getting hotter due to Urban Heat Islands (UHI) and climate change.
  - It is worth to mention that **5,000 death in 2023 heatwave in France**

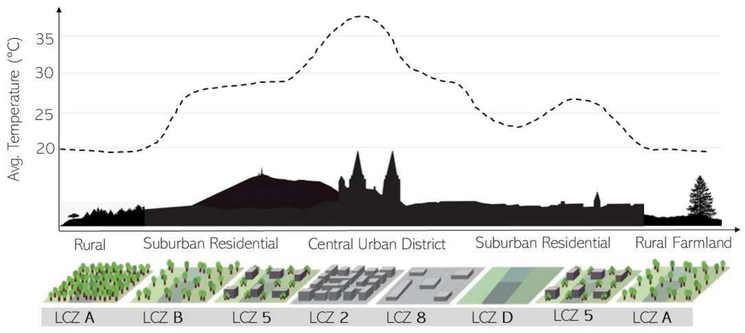

Horizontal Profiling of Urban Heat Island (UHI) in Clermont Métropole

OBJECTIVES

- Provide practical tools that help stakeholders predict, evaluate, and mitigate urban heat stress. Three tools were created, targeting temperature prediction, vulnerability assessment, and urban morphology analysis.

Data Collection

106,000
Cells 1- ha resolution

4 Millions
values collected

Spatial Data

Meteorological Data

Socio-demographic Data

Land Surface Temperature (LST)

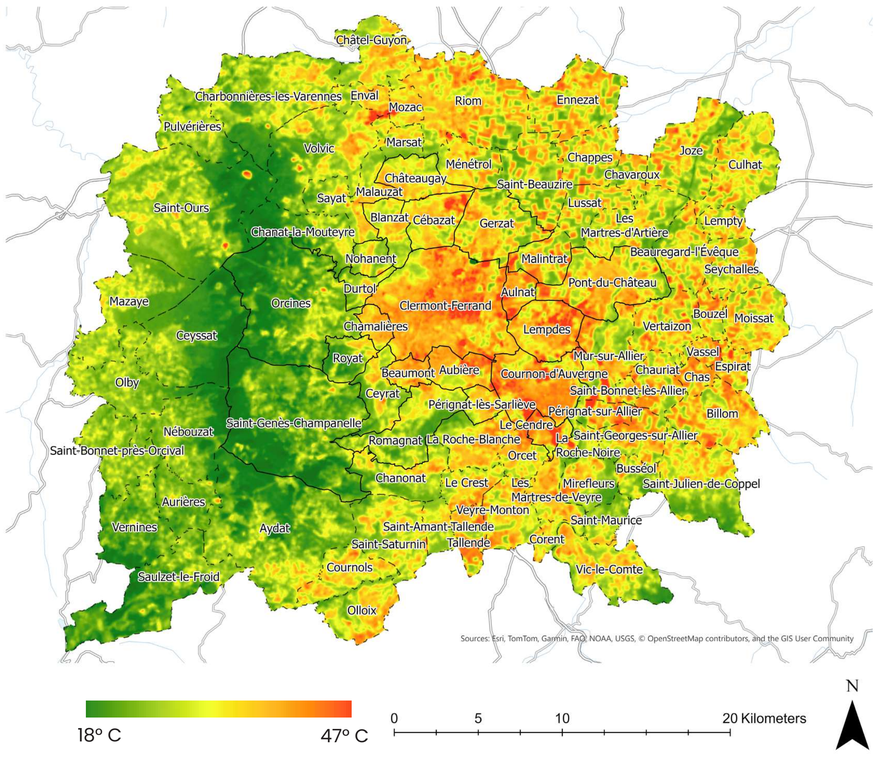

TOOL 1: LST Prediction from Urban Features

- Built a regression model using 8,000 grid cells (1 ha each)
- Extracted layers: Collected data covered terrain, vegetation, infrastructure, and urban form.
- Identified strongest predictors: Topography, green cover (NDVI), road area, building height, and gross floor area (GFA)

Developed a model:
$LST = 30.62 + 4.69 \cdot Topo + 2.97 \cdot RoadArea - 23.12 \cdot NDVI + 0.89 \cdot \ln(1+GFA) - 0.14 \cdot (NDVI \cdot GFA) - 0.29 \cdot (Topo \cdot GFA)$

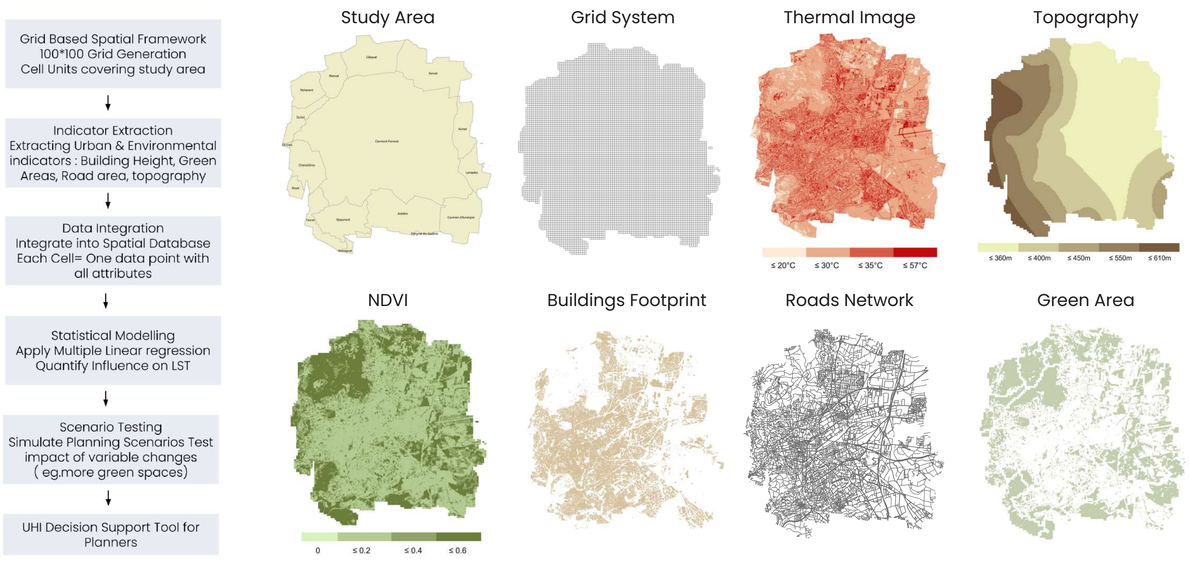

TOOL 2: UHI VULNERABILITY INDEX

- Focus on age-based vulnerable populations, particularly children (<14) and older adults (>65).
- 10 indicators across 3 categories: exposure , sensitivity and adaptive capacity
- Utilized a spatial multi-criteria analysis (SMCA) framework, combining empirically derived and expert-elicited weighting approaches
- Calculated and produced spatially explicit UHI Vulnerability Index maps.

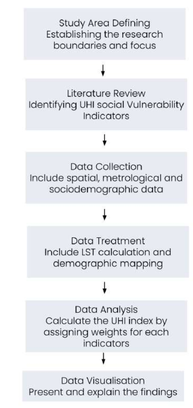

	Indicator	First scenario Assigned weight	Second scenario Assigned weight	Third Scenario Assigned weight
Exposure	LST	10%	20%	10,6%
	UHI Intensity	10%	20%	11,1%
	Population Density	6%	5%	9,5%
	Topography	4%	5%	11,2%
Sensitivity	Vulnerable Group Density	30%	15%	10,5%
	NDBI	12%	8%	10,6%
	Building Height	8%	7%	7,8%
Adaptive Capacity	NDVI	7%	7%	11,1%
	Proximity to Natural Areas	5%	7%	9,5%
	Proximity to Capacity Facilities	8%	6%	8,1%

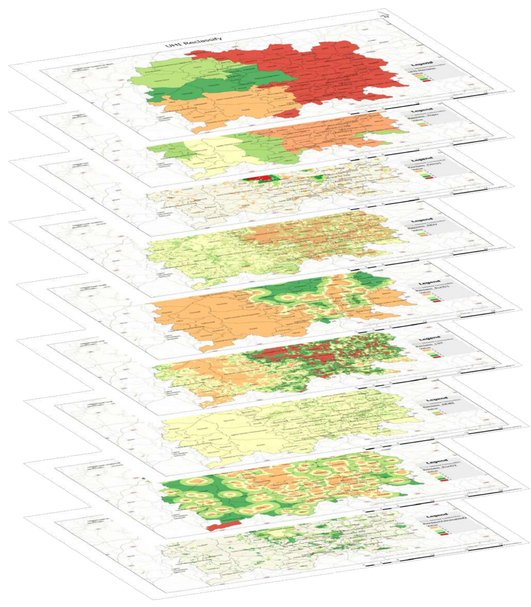

=

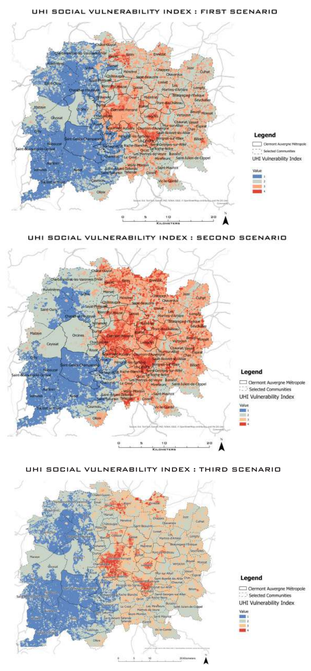

TOOL 3: School Heat Exposure and Urban Morphology

- Applied Local Climate Zones (LCZ) classification to assess urban morphology
- Conducted buffer analysis (250m) around 78 elementary schools
- Investigated LST variations across different morphology types
- Demonstrated the impact of urban form on school heat exposure.

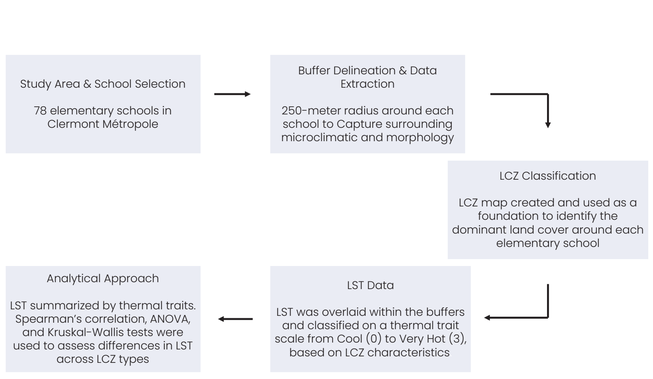

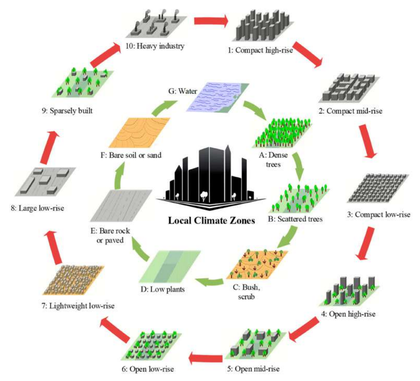

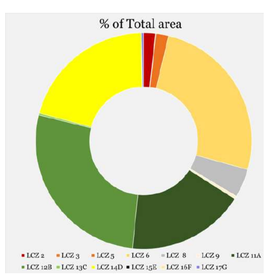

LCZ Code	LCZ Type	Area (m²)	% of Total area
LCZ 2	Compact mid-rise	5,320,000	1.76%
LCZ 3	Compact low-rise	300,000	0.10%
LCZ 5	Open mid-rise	5,670,000	1.87%
LCZ 6	Open low-rise	77,380,000	25.54%
LCZ 8	Large low-rise	12,980,000	4.28%
LCZ 9	Sparsely built	1380000	0.46%
LCZ 11A	Dense trees	53,460,000	17.64%
LCZ 12B	Scattered trees	82,440,000	27.21%
LCZ 13C	Bush, scrub	850,000	0.28%
LCZ 14D	Low plants	620,300,00	20.47%
LCZ 15E	Bare rock or paved	260,000	0.09%
LCZ 16F	Bare soil or sand	20,000	0.01%
LCZ 17G	Water	890,000	0.29%
	Sum	302,980,000	100.00%

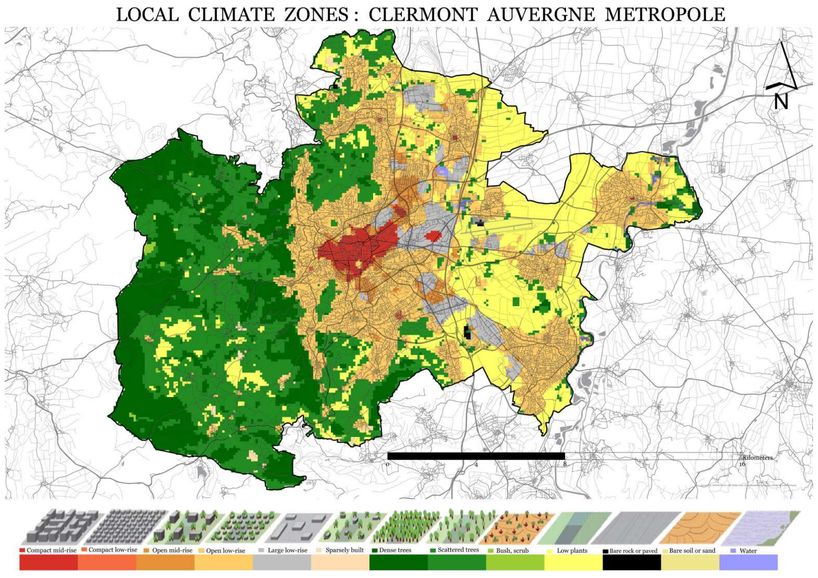

Conclusion: Implications for Urban Planning

The developed tools support evidence-based urban design and climate adaptation strategies to mitigate heat stress, especially for socially and thermally vulnerable populations.

Future Work

- Integrate predictive models for heat wave scenarios.
- Develop a digital twin framework to analyze indoor and outdoor thermal comfort.

Saffa Mansour, Aurélie Talon, Pierre Breul

Université Clermont Auvergne, Clermont Auvergne INP, CNRS, Institut Pascal, Clermont-Ferrand, France

Algorithm q-Acceptant Convex Geometry

Anthony Meunier, Lhouari Nourine, Simon Vilmin

Limos

Objectives

1. Characterizing the class of convex geometries associated with q-acceptant choice function.

Introduction

- A choice function over a set A is defined in [1] as a mapping S that associates each subset B of A to a subset $S(B)$ of B.
  - $S(B)$ is the *choosed outcome*, B is a subset of outcomes of A.
- About choice function?
  - Concept of social choice theory which as impact in many field such as game theory, decision strategie or microeconomics
  - There exists different type of choice function satisfying or not a restrained pull of axioms

Definition

- A **closure operator** on a set X is an application $\phi : 2^X \to 2^X$ for all $F \subseteq X$ s.t.:
  - extensivity: $F \subseteq \phi(F)$.
  - monotonicity: $F' \subseteq F \Rightarrow \phi(F') \subseteq \phi(F)$.
  - idempotence: $\phi(\phi(F)) = \phi(F)$.
- A **closed set** F is a set such that $F = \phi(F)$.
- ϕ is **antiexchange** if for each closed set F, and all distinct $x, y \notin F$, if $x \in \phi(F \cup y)$ then $y \notin \phi(F \cup x)$.
- We call $\mathcal{C} = \{\phi(F) \mid F \in 2^X\}$ a **closure system**.
- $\mathcal{C}$ is a **convex geometry** if and only if the associated closure operator ϕ is antiexchange.
- An element x of a closed set F is an **extreme point** if $\phi(F) \setminus x \in \mathcal{C}$.
- In a convex geometry, a closed set M is **irreducible** if there exists a unique x such that $M \cup \{x\} \in \mathcal{C}$.
- We note $\mathcal{C}_x = \{C \mid C \in 2^X, x \in C\}$ and $\mathcal{C}_{\bar{x}} = \{C \mid C \in 2^X, x \notin C\}$
- In the context of convex geometry the extreme point function is our choice function.

Representation of an acceptant

- $\mathcal{C}$ is q-acceptant if for all $F \in \mathcal{C}$ we have $|F| = \min(q, |F|)$

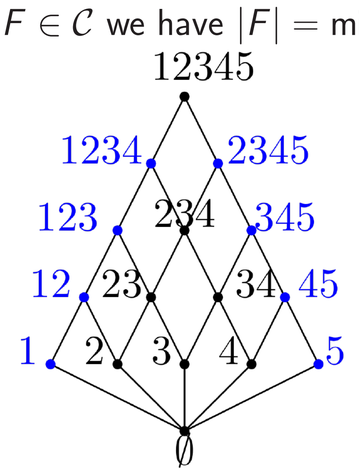

Figure: Example of a 2-acceptant convex geometry with $\mathcal{M}$ in blue

- In a set Σ, called implication bases, we associate the choosed outcome, $ex(F)$, and the outcome, F.
  - $\Sigma = \{15 \to 234, 14 \to 23, 25 \to 34, 13 \to 2, 24 \to 3, 35 \to 4\}$
- An Antichain, noted $\mathcal{A}$, is the set of choosed outcome of size q with their outcome greater than q
  - $\mathcal{A} = \{15, 14, 25, 13, 24, 35\}$
- The set of irreducible closed set, noted $\mathcal{M}$
  - $\mathcal{M} = \{1234, 2345, 123, 345, 12, 45, 1, 5\}$

Problem: Given representation, verify that it represent a q-acceptant convex geometry?

Well known property

- Let $\mathcal{A}$ be a q-acceptant antichain on X. Then $|\mathcal{A}| = \binom{n-1}{q}$ [2]
- In a q-acceptant convex geometry every $F \in 2^X$, $\phi(F)$ has q predecessor.
- Let $|M| \geq q$ and $M \in \mathcal{M}$. Then there exists a unique $x \in X$ such that $M \setminus x \in \mathcal{M}$. [3]

Results - Implication bases

- Let $\Sigma = \{ex(F) \to F \setminus ex(F) | F \in \mathcal{C}, |F| > q\}$ the implication base associated to $(X, \mathcal{C})$. Then, $(X, \mathcal{C})$ is a q-acceptant convex geometry if and only if the following conditions hold:
  1. for each choosed outcome F of Σ, $|F| = q$ and their does not exists a choosed outcome F', $F \neq F'$, such that $\phi(F) = \phi(F')$
  2. the set $\{\phi(F) \mid F$ is a premise of $\Sigma\}$ is exactly the set of closed sets with more than q elements of $(X, \mathcal{C})$
  3. for each subset Y of X of size $q+1$ there exists $F \to \phi(F) \setminus F \in \Sigma$ such that $F \subseteq Y$
- We deduce a polynomial algorithm recognizing the acceptance in 3 part such that for any $F \in 2^X, |F| \geq q$:
  - Verifying that the mapping between $ex(F)$ and $\phi(F)$ is unique.
  - Verifying that there is no closed set $\phi(F)$ with $|ex(F)| > q$
  - Verifying that for all $\phi(F)$ such that $|\phi(F)| = q+1$, we have $|ex(F)| = q$.

Results - Antichain

- Let $(X, \mathcal{C})$ be a non-trivial q-acceptant convex geometry and let $x \in ex(X)$. Then $(X \setminus x, \mathcal{C}_x)$ is $(q-1)$-acceptant and $(X \setminus x, \mathcal{C}_{\bar{x}})$ is q-acceptant.
- Partition of a q-acceptant

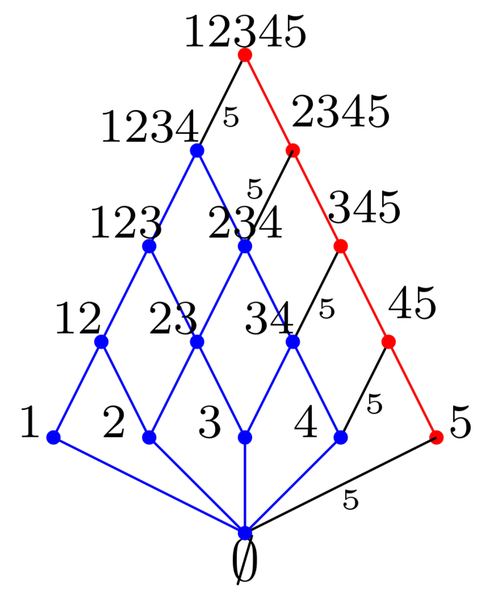

Figure: Example of partition of a 2-acceptant convex geometry on $X = \{1, 2, 3, 4, 5\}$, with in blue the 2-acceptant convex geometry and the 1-acceptant in red.

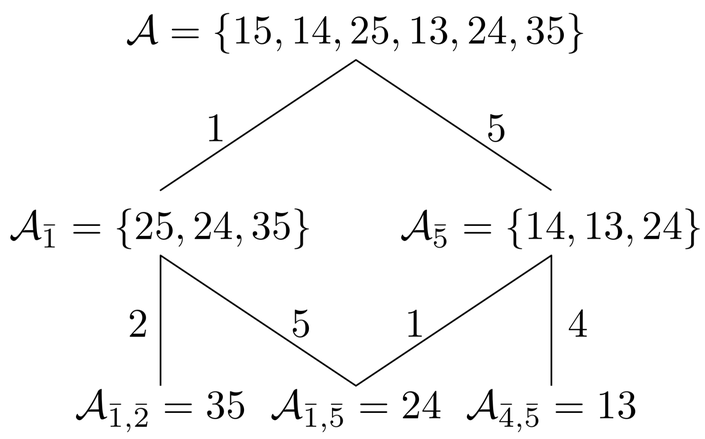

Figure: Recognition of the acceptance of the previous example with the algorithm

- From this property, we propose an algorithm which build the upper part of the lattice from the top.

Coming work

- Is the algorithm proposed for the antichain correct and polynomial?
- Exploiting the structure of the irreducible closed set, we want to leverage what is called *colored poset* to design an algorithm recognizing the acceptance of $\mathcal{M}$.

References

[1] Hervé Moulin.
Choice functions over a finite set: a summary.
Social Choice and Welfare, 2(2):147–160, 1985.

[2] Battal Dogan, Serhat Doğan, and Kemal Yildiz.
On acceptant and substitutable choice rules.
SSRN Electronic Journal, 01 2017.

[3] Serhat Doğan.
Explorations to Refine Aizerman Malishevski's Representation for Path Independent Choice Rules.
PhD thesis, Bilkent Universitesi (Turkey), 2020.

anthony.meunier@doctorant.uca.fr

Modélisation d'un écosystème hydrogène associé aux énergies renouvelables intermittentes

Ecole doctorale Sciences Pour l'Ingénieur

Yosra Mezghani[1,2], Gilles Dussap[1], *Lucie Poulet*[1] *Philippe FIani*[2], Fab*rice Gros*[1]

1 : Université Clermont Auvergne, Institut Pascal, UMR 6602, Clermont-Ferrand, France
2 : Sherpa Engineering, Nanterre, France

Auteur correspondant : y.mezghani@sherpa-eng.com

Introduction

L'hydrogène est une solution prometteuse pour le stockage de l'énergie renouvelable.

Limites de l'hydrogène : Légèreté, faible densité volumique et inflammabilité :
⟶ Défis majeurs en matière de sécurité
⟶ Stockage coûteux et techniquement complexe

Une alternative : les e-fuels:
- ✅ Stabilité
- ✅ Facilité de stockage
- ✅ Adaptés au transport

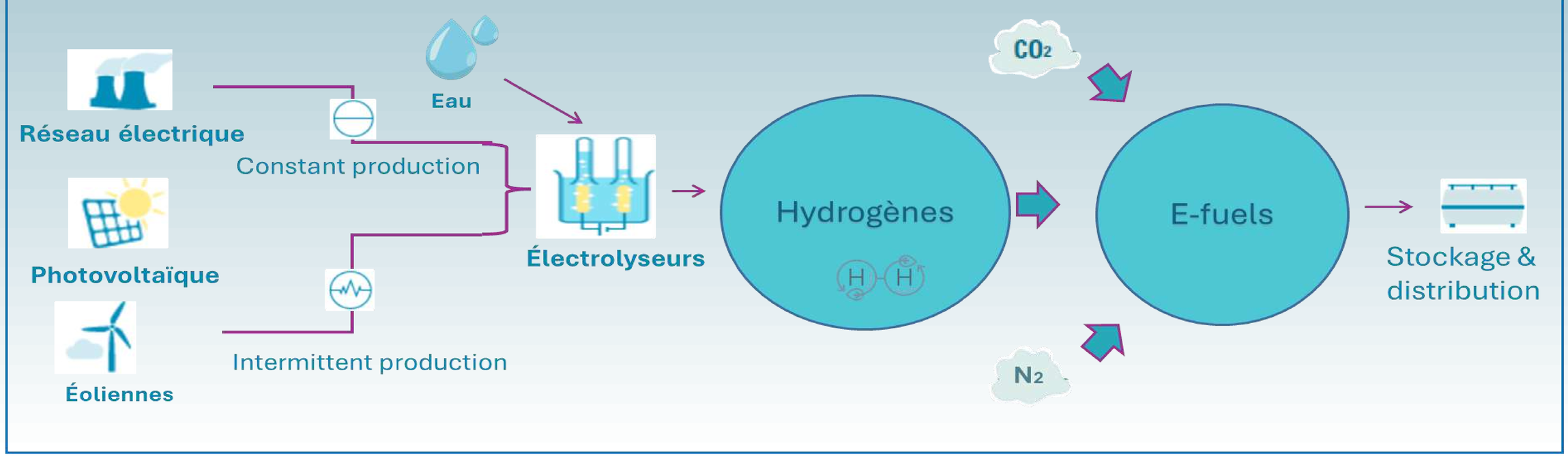

Objectifs

1. Concevoir un modèle intégré représentant un écosystème hydrogène complet.
2. Optimiser la production et la conversion de l'hydrogène en des e-fuels selon des critères technico-économiques et environnementaux.
3. Évaluer différents scénarios d'exploitation pour guider le dimensionnement et le pilotage optimal du système

Méthodes

1. Modélisation multi-facette [1]:
- Flux d'énergie
- Bilans de matière
- Impacts environnementaux
- Aspects économiques (CAPEX / OPEX)

2. Modélisation multi-niveau [1] :
- Les flux globaux de l'écosystème
- Des modèles mécanistiques détaillés

3. Digital Twin :
- Une réplique virtuelle du système énergétique en temps réel
- Tester et optimiser les scénarios d'exploitation

Outils de modélisation:
- ProSim [2]
- MATLAB Simulink

Optimisation multi-objectif:
- À l'aide de la plateforme Osmose (développée par l'IPESE – EPFL [3])

Résultats

Premiers résultats obtenus pour le développement de l'électrolyseur

Espèce	À l'anode	À la cathode	Total
Quantité d'hydrogène (Nm^3/h)	0,02	1,97	1,99
Quantité d'oxygène (Nm^3/h)	0,99	0	0,99

Composant	Flux H2-OUT	Flux O2-OUT
Eau	3,2 %	3,2 %
Hydrogène	96,8 %	1,5 %
Oxygène	0 %	95,3 %

Conclusion

Ce projet vise à maximiser les performances globales d'un écosystème d'hydrogène en intégrant les dimensions techniques, économiques et environnementales

Bibliographie

[1] Fauvel C., Claveau F., and Chevrel P., "Energy Management in multi-consumers multi-sources System: A Practical Framework," Proceedings in IFAC WC, 2014.
[2] Mónica Sánchez, Ernesto Amores, Lourdes Rodríguez, and CarmenClemente-Jul. Semi-empirical model and experimental validation forthe performance evaluation of a 15 kw alkaline water electrolyzer. In-ternational Journal of Hydrogen Energy, 43(45):20332–20345, 2018.
[3] Meire Ellen Gorete Ribeiro Domingos, Daniel Flórez-Orrego, Moisés Teles dos Santos,Silvio de Oliveira Junior, and François Maréchal. Process modeling and integrationof hydrogen and synthetic natural gas production in a kraft pulp mill via black liquorgasification. Renewable Energy, 219:119396, 2023.

Luminous robots coordination in more adversarial environments

Oussama Nahnah (**Oussama.nahnah@uca.fr**) - LIMOS - UCA

Dr. Anaïs Durand, Pr. Pascal Lafourcade

Contexte

- We use **luminous robots (1)**, which operate in **observe – compute – move cycles (2).**
- These robots function **without memory, without communication, without a compass,** and have **limited visibility (3)**.
- They move in a **discrete grid**, making decisions based only on their local perception.

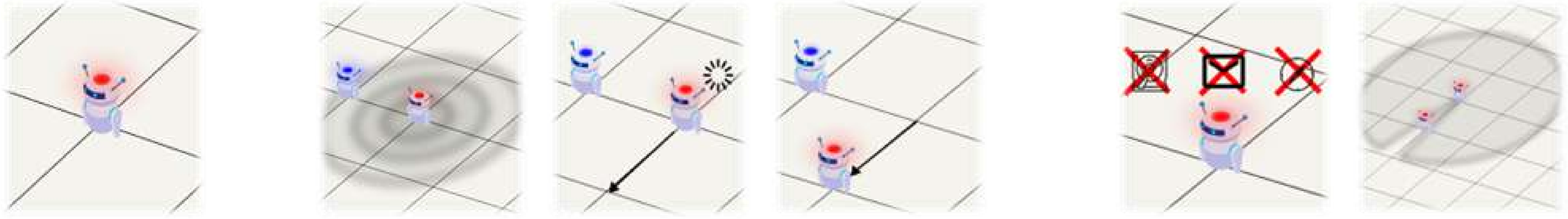

(1) **(2)** **(3)**

- **An algorithm** is a set of **rules**.
- **A rule** is a local instruction applied by a robot. It contains:
  - **A view (4):** what the robot sees around it (other robots + their colors).
  - **A direction (5):** where it should go (up, down, left, right, or stay still).
  - **A color change (6)**: if necessary.

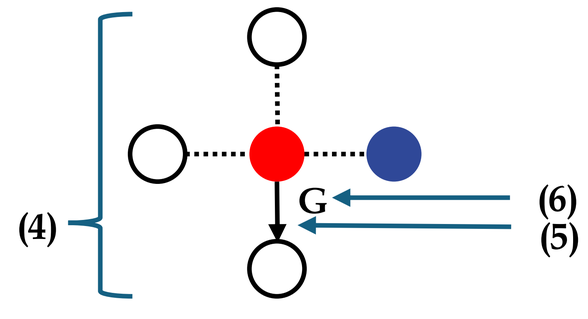

Problem Statement

- Visit every position in a discrete (grid) environment infinitely often.

Objective of the Thesis

- Create a tool for automatic algorithm generation for robots by computer.

Structure of the Algorithm Generator

- Generate all possible valid **views**
- Generate all possible valid **rules**
- Generate all possible valid **sub-solutions** for new situations
- **Inject** into an existing valid **algorithm**
- Test and validate

Case Study

- A grid containing an obstacle at the center.
- **New Sub-Algorithms (7) + Existing Algorithm (ref1) (8) = New Valid Algorithms (9)**

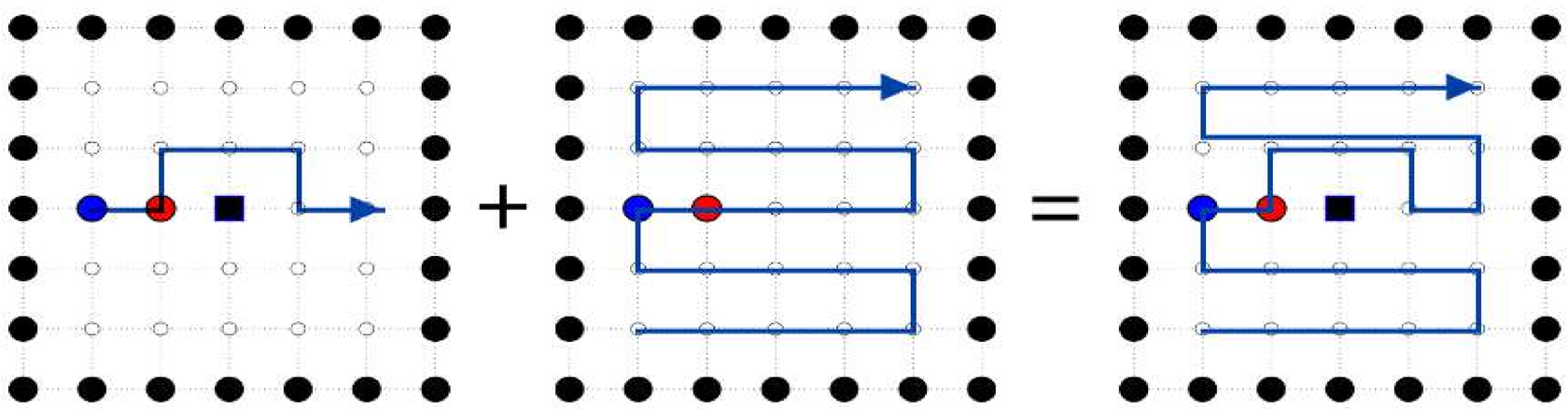

(7) **(8)** **(9)**

Résultats

Results & Validation

- Over **120 new algorithms** generated
- Validation: simulations (ref2) and mathematical proofs

Open Question

- Generate solutions without relying on existing algorithms
- Explore complex cases (obstacle next to a wall, obstacle indistinguishable from the wall, etc.)

References

(ref1) Optimal Exclusive Perpetual Grid Exploration by Luminous Myopic Opaque Robots with Common Chirality

(ref2) https://bramas.pages.unistra.fr/robot-grid-exploration-simulator/

Enhancing wireless communications using Machine Learning

Guy Anthony NAMA NYAM

Sup. Oussama HABACHI Gérard CHALHOUB

Université de Clermont Auvergne, Clermont Auvergne INP, LIMOS

Objectives

1. Improve network performance to guarantee Quality of Experience (QoE)

Context

- Smart cities increasingly use ICT to better manage urban infrastructure and services.
- Wireless connectivity is at the heart of this transformation.
- Proliferation of connected devices (IoT sensors, smartphones, surveillance drones, autonomous vehicles, ...)
- Rapid growth of multimedia services requiring real-time exchange

The network configuration must continuously adapt to ensure QoE

Figure 1:Connectivity at the heart of futuristic city

Source : https://www.researchgate.net/publication/330269517

Problem Statement

- Several factors influence the performance of wireless communication networks
  - Environmental factors: physical obstacles, electromagnetic interference, weather conditions
  - Factors related to network characteristics: bandwidth and frequency, Type of technology (wifi 5/6/7, 4G, 5G, ...)
  - Factors related to usage: number of connected devices, type of traffic (real-time applications, massive data transfers, ...) , user mobility.
  - and much more

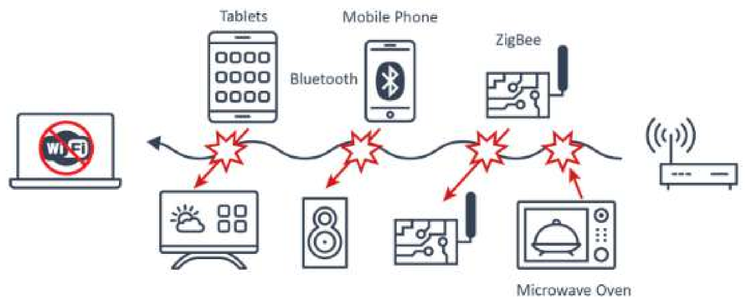

Figure 2:Example of wifi-interference

Human control is no longer feasible for managing (flexibility, robustness, etc.) next-generation networks (NGNs).

Objective of the Thesis

Propose intelligent self-adaptive models to real-time changes in order to maintain optimal throughput performance in dense wireless communication networks.

Approach and results

- ns-3 as a simulation tool for wireless communication networks
- Observe the state S_t of the environment (wireless networks)
  - SINR, Transmit delay, RTT, BER, ...
- From the state, the model or agent adapts the network configuration (called action) A_t
  - MCS, Contention window, Backoff, ...
- The agent receives a reward R_t for the action
- The process repeats with the new state S_{t+1}

The agent's objective is to maximize its cumulative reward

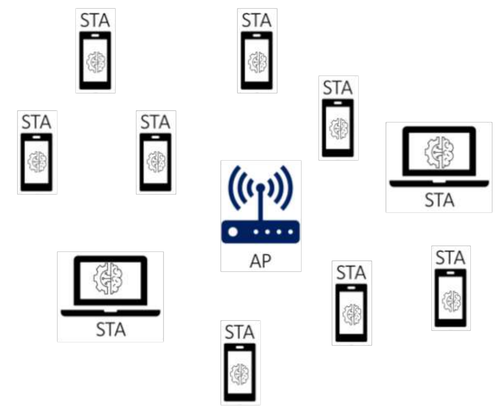

Figure 3:Deployment phase: decentralized and autonomous DRL model

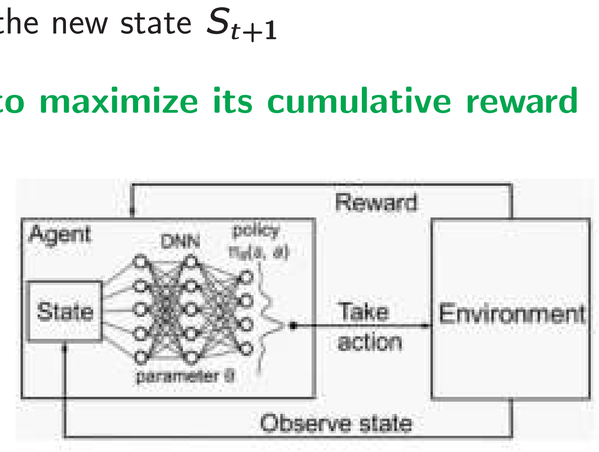

Figure 4:Deep Reinforcement Learning approach

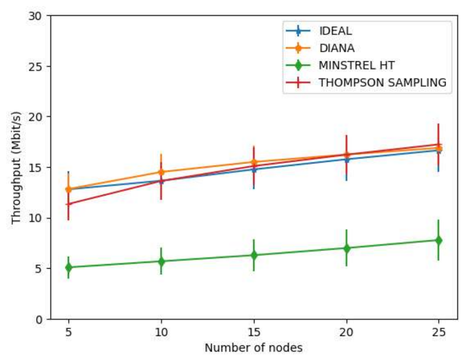

Figure 5:Goodput comparaison

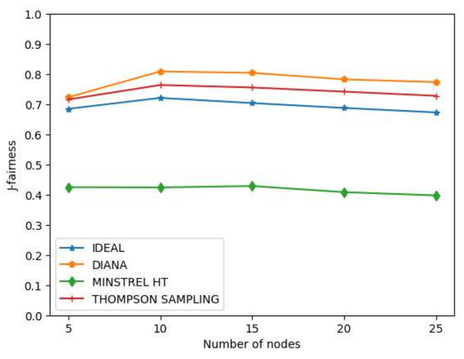

Figure 6:Fairness comparaison

References

[1] Ibrahim Sammour, Gerard Chalhoub.
Application-level data rate adaptation in wi-fi networks using deep reinforcement learning.
2022 IEEE 96th Vehicular Technology Conference (VTC2022-Fall), 2022.

[2] Rúben Queirós et al.
Wi-Fi Rate Adaptation using a Simple Deep Reinforcement Learning Approach
2022 IEEE ISCC, 2022.

Zero-shot cooperative annotation by two pretrained models in hydrogen bubble flow study

Trong Nghia Ngo[1], Christophe Vial[1], Adib Essid[1], Jean-Sébastien Guez[1] and Thierry Chateau[1]

[1] Université Clermont Auvergne, Clermont Auvergne INP, CNRS, Institut Pascal, 63000 Clermont-Ferrand, France

Abstract

An automatic annotation pipeline is proposed for bubble flow detection, exploiting pre-trained models to significantly speed up the annotation process.

Objectives

1. This study addresses exploring the hydrogen bubble flow images captured by the hight speed Chronos camera. The ultimate objective is to extract a size distribution of hydrogen bubbles.
2. In general, the annotation step usually takes a long time to finish. Therefore, finding a way to speed up the process is the core of this work.

Context & Motivation

- In the hydrogen-liquid transfer coefficient researches [1], the behavior comprehension of bubble flow in the bioreactors plays a vital role. Various coefficients, such as the volumetric-mass transfer coefficient, the interfacial surface, and the average Sauter diameter [2], are directly related to the detection and measurement of hydrogen bubble flow.
- The first step in this study consists of creating and annotating a dataset for the different detectors. However, the annotation procedure presents new challenges, such as tininess, overpopulation of the bubbles, and occlusion among them. In fact, each image might contain 600 to 1900 bubbles, and their size varies from 1x2 pixels to 54x29 pixels. All of these cause tiredness during the annotation.

Pipeline overview

- In this work, an automatic annotation two-step pipeline combining FastSAM [3] (localization) and OpenCLIP [4] (assignment) was introduced; we called it FSOC. In our case, two categories are proposed : a "single bubble" and "several bubbles". For now, the size estimation of each bubble in a group is still not done. The different categories are assigned to exclude bubble groups during bubble size distribution computing.

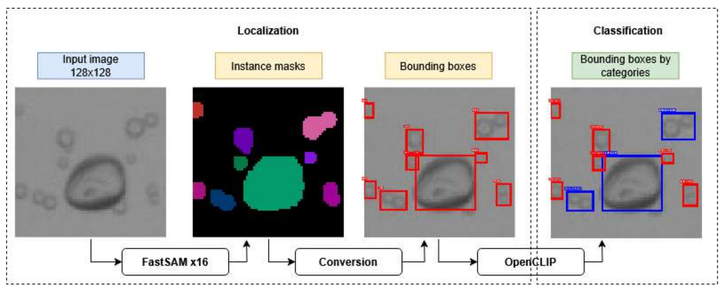

Figure 1: Proposed FSOC annotating pipeline—the illustration is zoomed in to be more visible.

Acquisition settings and data

- In the data acquisition step, a transparent PVC column plays as a reaction medium. The distilled water is injected from the top of the column, while a hydrogen flow (air or hydrogen) is pumped in the opposite direction.

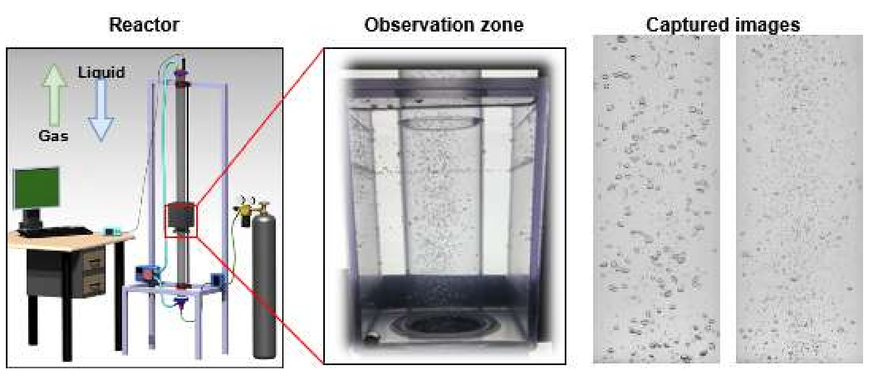

Figure 2: Reactor, observation zone and data examples.

Table 1: Dataset overview

Dataset	Image size	Train qty	Val qty	Train instances	Val instances
Original manual data	470x1216	7	5	7617	4686
FSOC data	128x128	455	–	15068	–
Manual data	128x128	455	325	15913	9558

Results

- Experiments employed the FasterRCNN [5] model and AITOD [6] metrics.

Table 2: Comparison of annotation time per image each approach in minutes

Dataset	Time (min)	Time (max)	Time (average)
Manual	180 min	300 min	240 min
FSOC	1 min 30 s	5 min	3 min

- A significant gain in annotation time by the FSOC annotation pipeline is shown in Table 2.

Table 3: Comparison of training results on validation set (manual data)

Dataset	Category	mAP@50	mAP@vt	mAP@t	mAP@s	mAP@m
Manual	**General**	0.852	0.366	0.590	0.667	0.729
	Single bubble	0.874	0.367	0.63	0.728	0.85
	Several bubbles	0.83	0.366	0.549	0.606	0.607
FSOC	**General**	0.414	0.062	0.16	0.265	0.374
	Single bubble	0.53	0.11	0.24	0.362	0.55
	Several bubbles	0.297	0.014	0.08	0.169	0.198

- In Table 3, the results of the model using the FSOC data are still limited compared to the results of the model using the manual data.

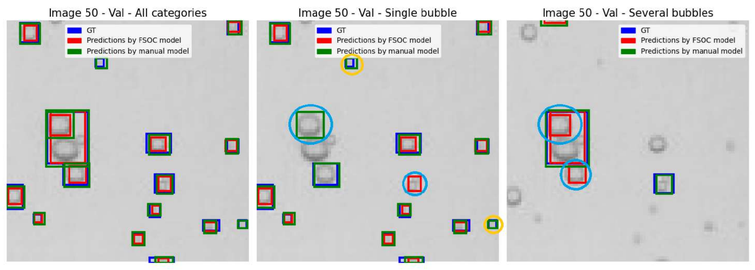

Figure 3: Predictions on a validation image for three scenarios (Both categories, only the single bubble, and several bubbles)

- Overall, the model that uses the FSOC data localizes the bubbles well but not that well in the assignment phase, as shown in Figure 3.

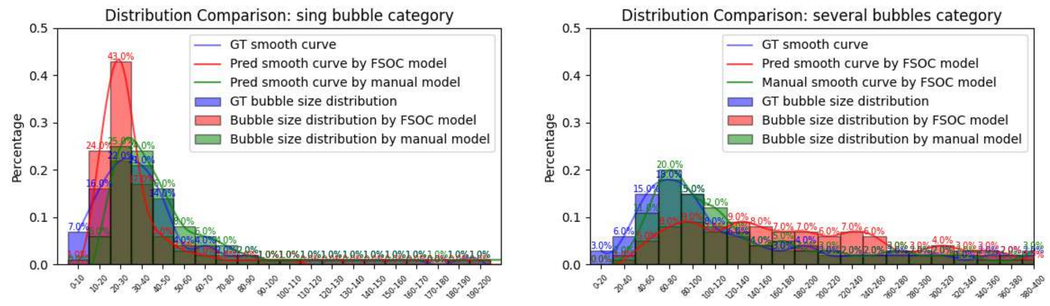

Figure 4: Prediction / GT size distribution by category

- In Figure 4, the FSOC model predictions exhibit a high bias toward the very tiny bubbles in the "single bubble" category (left). A slight bias is presented toward the large bubbles in the "several bubbles" category (right).

Conclusion and Future work

- In the first experiments, our results show that the FSOC pipeline worked with significantly reduced annotation time. The performance of FSOC is still limited due to the inadequate FastSAM output process, and OpenCLIP did not perform as expected. However, these drawbacks can be improved by going further with post-process FastSAM masks and fine-tuning the OpenCLIP with little manual data. In addition, we aim to use this pipeline as a pre-annotation tool in combining corrections at the human level. Based on the previous strategies, we can boost both the annotation speed and the quality of the created datasets. Currently, we are applying it in our work.

Acknowledgments

- This work has been sponsored by te Graduate Track for Intelligent and Innovative Mobility (GT IIM) of the SFRI CAP GS project (French National Research Agency: ANR Grant 20-SFRI-0003)

References

[1] M. Keramati et al. "Intensification of ex-situ biomethanation in a bubble column bioreactor by addition of colonized biochips". In: *Bioresource Technology Reports* 27 (2024), p. 101938.

[2] B. Sanogo et al. "Exploring the impact of proteins and surfactant on oxygen mass transfer in gas-liquid bioreactors: an experimental investigation". In: *Chemical Engineering Science* (Dec. 2024), p. 121146.

[3] X. Zhao et al. *Fast Segment Anything*. arXiv:2306.12156. 2023.

[4] I. Gabriel et al. *OpenCLIP*. Version 0.1. Version 0.1. July 2021.

[5] S. Ren et al. "Faster R-CNN: Towards Real-Time Object Detection with Region Proposal Networks". In: *IEEE Transactions on Pattern Analysis and Machine Intelligence* 39.6 (2017), pp. 1137–1149.

[6] J. Wang. *COCO API for AI-TOD Dataset*. https://github.com/jwwangchn/cocoapi-aitod. 2021.

Design of a Variable Stiffness Overtube with Self-sensing for Robotic Colonoscopy

Alice Nyaga, Frédéric Chapelle, Youcef Mezouar, and Yuri Lapusta

Université Clermont Auvergne, Clermont Auvergne INP, CNRS, Institut Pascal
F-63000 Clermont-Ferrand, France

Background and context

- Colorectal cancer (CRC) prevention relies on screening for the identification and removal of preneoplastic colonic polyps.
- In an overtube-assisted colonoscopy, an overtube is placed over the colonoscope to facilitate insertion and maneuvering.

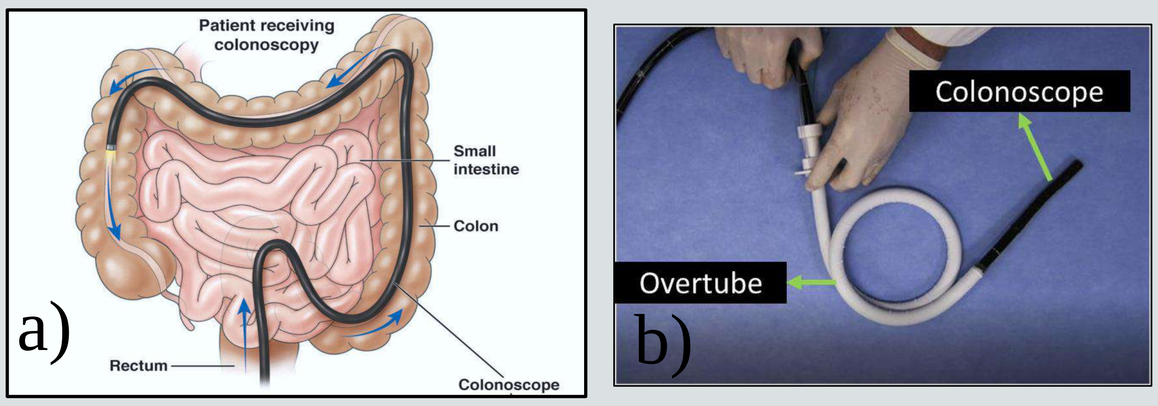

Figure 1: a) Colonoscopy procedure [1]. b) Overtube over colonoscope [2].

- Loop formation by the colonoscope is one of the major causes of incomplete colonoscopies, hence missed colorectal cancers.
- The loss of mobility and precision in positioning the colonoscope makes it difficult to perform other therapeutic operations.

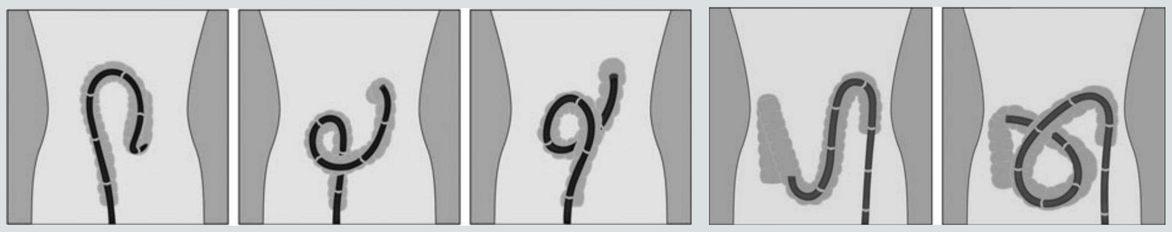

Figure 2: Types of loops formed during colonoscopy [3].

Objectives

- Development of an overtube with a higher stiffness range based on variable stiffness technology.
- Develop a self-sensing strategy allowing for a functional control system for the overtube system.

Operational scenario

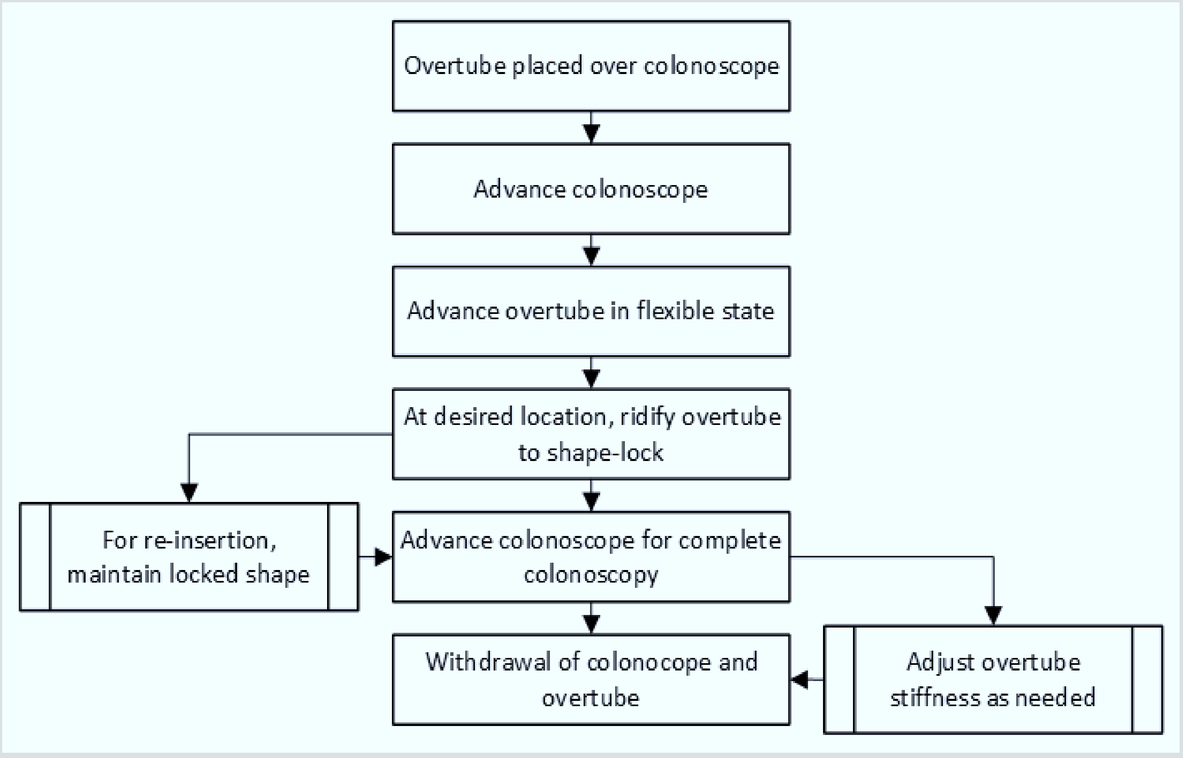

Colonoscope + Overtube insertion

- Addition of an overtube to colonoscope results in a greater displacement of scope.

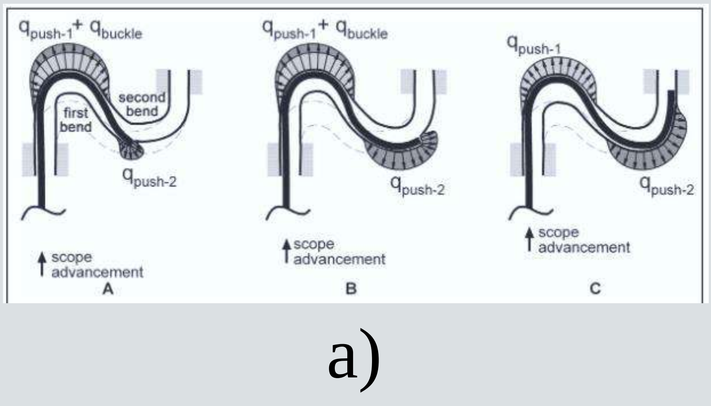

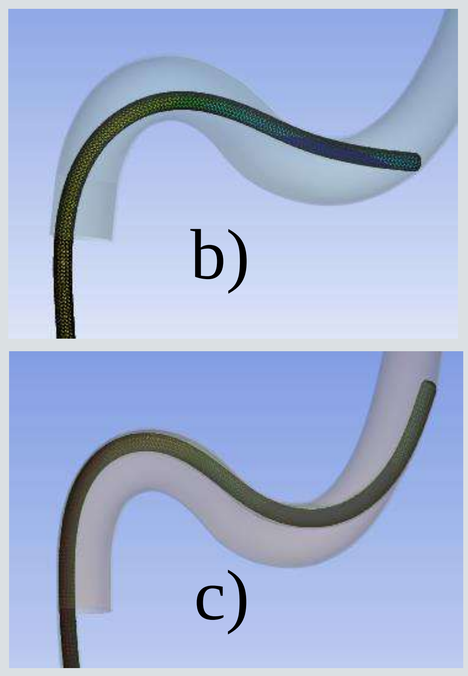

Figure 3: a) Stages of scope advancement through the second sigmoid colon bend [4]. b) FEM simulation of scope insertion without overtube. c) FEM simulation of scope insertion with overtube.

Stiffness (Rigid state)	Stiffness (Flexible state)	Ultimate force	Activation time	External diameter	Device temperature
$\geq 330 Ncm^2$	$\leq 165 Ncm^2$	$\geq 16N$	as small as possible	$\leq 15\ mm$	$\leq 41\ °C$

Figure 4: System requirements for the overtube [5].

References

1. American Gastroenterological Association, https://patient.gastro.org/colonoscopy/
2. Park, N., Abadir, A., Chahine, A., Eng, D., Ji, S., Nguyen, P., ... & Samarasena, J. B. (2022). A Novel Dynamic Rigidizing Overtube Significantly Eases Difficult Colonoscopy. *Techniques and Innovations in Gastrointestinal Endoscopy*, 24(2), 116-120.
3. Roberts-Thomson, I. C., & Teo, E. (2009). Colonoscopy: Art or science?. *Journal of gastroenterology and hepatology*, 24(2), 180-184.
4. Loeve, A. J., Fockens, P., & Breedveld, P. (2013). Mechanical Analysis of Insertion Problems and Pain During Colonoscopy: Why Highly Skill-Dependent Colonoscopy Routines are Necessary in the First Place… and How They May be Avoided. *Canadian Journal of Gastroenterology and Hepatology*, 27(5), 293-302.
5. Blanc, L., Delchambre, A., & Lambert, P. (2017, July). Flexible medical devices: Review of controllable stiffness solutions. In *Actuators* (Vol. 6, No. 3, p. 23).
6. Moreels, T. G., Macken, E. J., & Pelckmans, P. A. (2013). Renewed attention for overtube-assisted colonoscopy to prevent incomplete endoscopic examination of the colon. *Diseases of the colon & rectum*, 56(8), 1013-1018.

Acknowledgement

This work made in the FACTOLAB (commun laboratory CNRS, UCA, Michelin) and International Research Center "Innovation Transportation and Production Systems"(CIR ITPS) of the I-SITE CAP 20-25 framework, is supported by the CIR ITPS.

This thesis is co-funded by the association of doctors of Saint-Joseph Hospital, we thank them for teaching, clinical, and fundamental research.

Email: alice.nyaga@sigma-clermont.com

Autonomous Vehicles Navigation under 3D Traversability Constraints

OROU MOUSSE Charifou[1,2], Dieumet DENIS[2], François MARMOITON[1], Roland CHAPUIS[1]

[1] Université Clermont Auvergne, Institut Pascal, Clermont-Ferrand - France, firstname.last_name@uca.fr

[2] Sherpa Engineering, 55 avenue des Champs Pierreux, 92000 Nanterre - France, f.lastname@sherpa-eng.com

Context

MOBITER (Mobilité autonome en milieux tout Terrain)

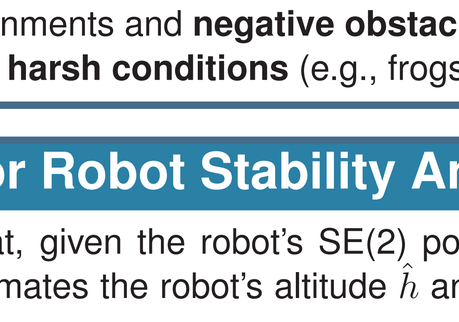

Main Points

- Accurate **3D modeling of the environment**
- **Traversability analysis** in rough terrain
- Global and local **trajectory planning**
- Robustness to **localization uncertainties** and **GPS-denied zones**
- Handling **incomplete and noisy perception**
- Consideration of dynamic environments and **negative obstacles**
- Non-conventional obstacles and **harsh conditions** (e.g., frogs, rain)

Attidue Estimation for Robot Stability Analysis

Determine a mapping $\mathcal{F}$ such that, given the robot's SE(2) position $\mathbf{p}$ and an environmental model M, it estimates the robot's altitude $\hat{h}$ and attitude $\hat{\theta}$, resulting in a full SE(3) pose:

$$\mathcal{F}(\mathbf{p}, M) = (\hat{h}, \hat{\theta})$$

Assumptions :

- Wheels remain in constant contact with the ground (rigid body)
- Roll and pitch only depend on terrain topology

Wheel-Ground contact models: circle-based or rounded-rectangle.

Results :

Attitude Estimation during a Speed Bump Traversal.

Off-Road Navigation Framework

The proposed attitude estimation method is lightweight (runtime $\approx 0.15\,\mu s$ per pose), direct, and precise (maximum errors $\leq 5°$ with both models) for 3D rollout prediction. The criterion used for stability analysis is the **Zero Moment Point (ZMP)**, whose y-position is computed as follows:

$$y_{\text{ZMP}} = -\frac{I_{xx}}{mg}\ddot{\phi} + h_{\text{cg}}\phi - \frac{h_{\text{cg}}}{g}a_{y,\text{CG}}$$

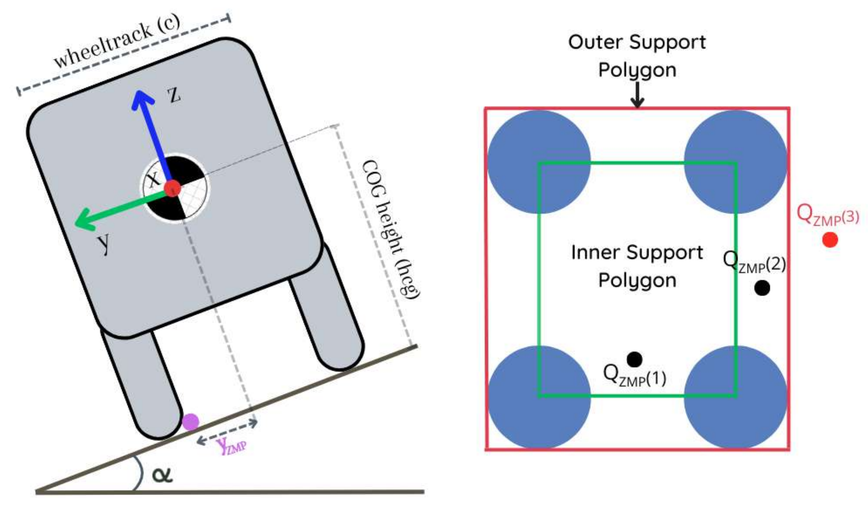

Comparison of the ZMP y-position with the vehicle wheeltrack.

The rollover probability is given by:

$$\mathbb{P}(\text{rollover}|\mathcal{P}) = 1 - \exp\left(-\frac{y_{\text{ZMP}}}{\tau}\right), \quad \tau = \frac{c}{6}$$

A RMS acceleration constraints is used to regulate risk-taking tendencies. These accelerations encode the vehicle **Mechanical Vibrations** and are used as a control variable to adjust the level of aggressiveness during navigation.

$$\bar{a}_m = \sqrt{\frac{1}{N}\sum_{i=1}^{N}\left(a_{mx}^2 + a_{my}^2 + a_{mz}^2\right)}$$

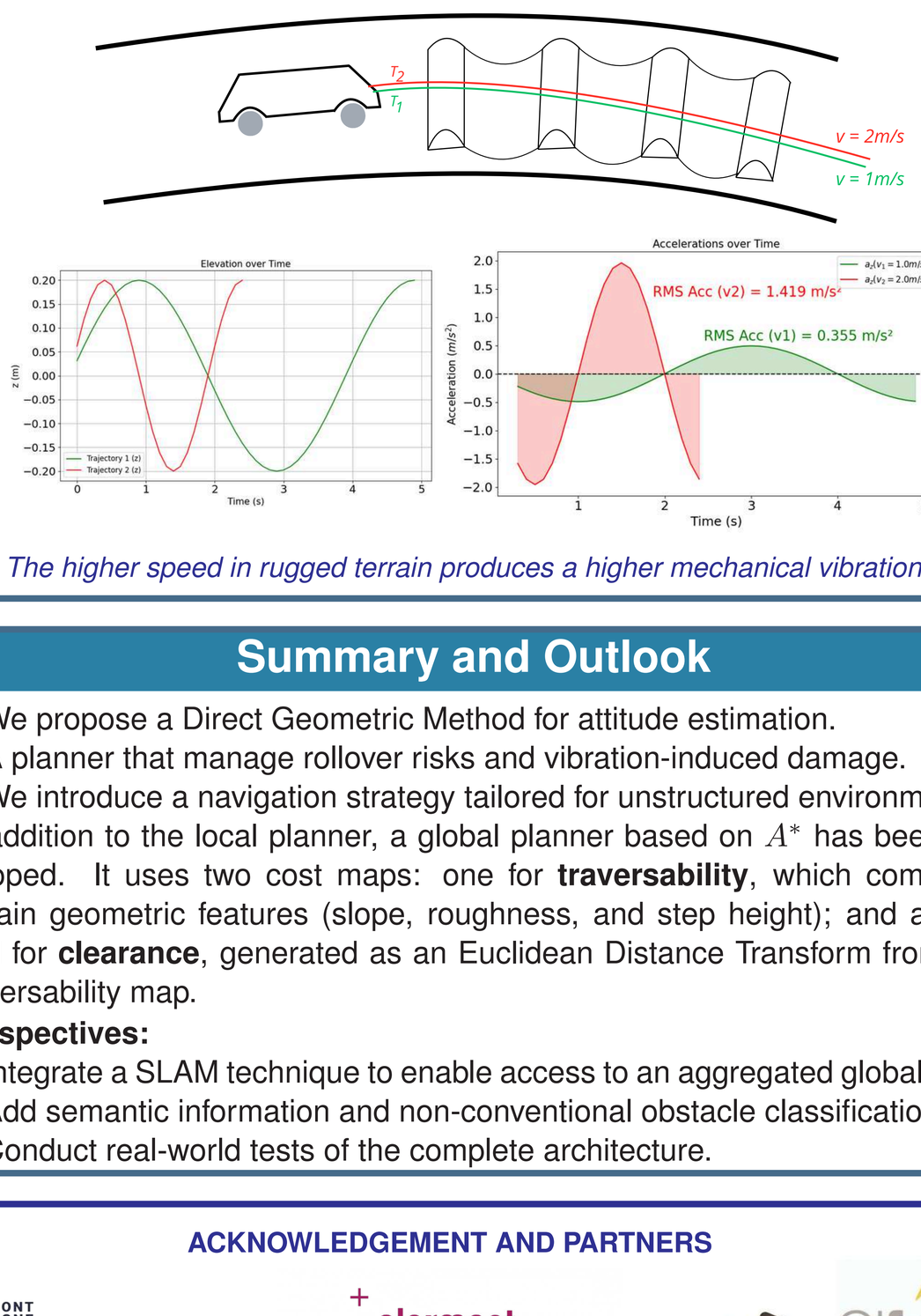

The higher speed in rugged terrain produces a higher mechanical vibrations.

Summary and Outlook

- We propose a Direct Geometric Method for attitude estimation.
- A planner that manage rollover risks and vibration-induced damage.
- We introduce a navigation strategy tailored for unstructured environments.

In addition to the local planner, a global planner based on A^* has been developed. It uses two cost maps: one for **traversability**, which combines terrain geometric features (slope, roughness, and step height); and a second for **clearance**, generated as an Euclidean Distance Transform from the traversability map.

Perspectives:

- Integrate a SLAM technique to enable access to an aggregated global map.
- Add semantic information and non-conventional obstacle classifications.
- Conduct real-world tests of the complete architecture.

KEY REFERENCES

[1] Charifou Orou Mousse, Mohamed Benrabah, Dieumet Denis, François Marmoiton, Roland Chapuis. ***"Efficient Attitude Estimation for Mobile Wheeled Robots Using Elevation Maps"***. 12th IFAC Symposium on Intelligent Autonomous Vehicles, May 2025, Phoenix Arizona, USA, United States

[2] Orou Mousse, Charifou, et al. ***"A Framework for Optimal Navigation in Situations of Localization Uncertainty."*** Sensors 23.16 (2023): 7237

ACKNOWLEDGEMENT AND PARTNERS

Understanding Exact Powers of Graphs

Anirudh Rachuri, Dr. Laurent Beaudou

LIMOS, UCA

Objectives

1. Understanding exact cube operation.
2. Recognize exact cubes of graph classes such as trees, bipartite graphs, e.t.c.

Introduction

- Graph $G = (V, E)$, where V is a collection of n vertices and E is a collection of m edges joining pairs of vertices.
- Extremely useful in modelling scenarios where pairwise relations are important.
- Numerous questions on existence and size of certain interesting structures (e.g.: cliques).
- Can be classified based on properties such as structure.

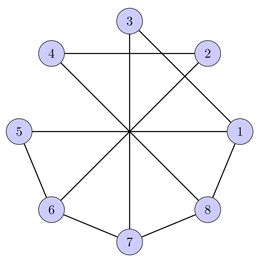

Figure: Graph G

Algorithms

- Graph problems involve finding paths, connections, or structures in networks.
- Algorithms explore, traverse, or optimize over graph structures.
- Efficiency is measured by time and space complexity in terms of input size.
- **Big-O** notation describes how runtime scales with input size (e.g.: no. of vertices n).

An Example

Breadth-First Search (BFS)

- **Objective:** To find shortest paths (by edge count) in unweighted graphs.
- **Idea:** Explore nodes level-by-level using a queue.
- **Time Complexity:** $\mathcal{O}(n + m)$
- Start: $1 \rightarrow$ visits: $3, 5, 8$
- Vertex $3 \rightarrow$ visits: 7
- Vertex $5 \rightarrow$ visits: 6 and so on...
- Thus, shortest path $1 \rightarrow 6$: $1 \rightarrow 5 \rightarrow 6$ (2 edges).

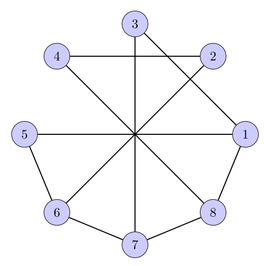

Powers and Exact Powers

- k-th power of graph: join vertices of G at distance $\leq k$.
- k-th **exact** power $G^{\#k}$ of a graph G: join vertices that are at distance exactly k in G.
- Each $G^{\#k}$ is a subgraph/layer of G^k, and the sets of edges in $G^{\#i}$ are disjoint for all i.

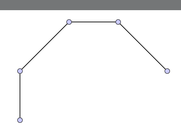

Figure: Graph G

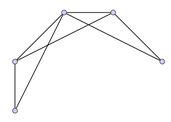

Figure: Square G^2

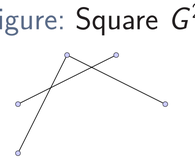

Figure: Exact Square $G^{\#2}$

Applications

- **Wireless Networks:** k-th power models multi-hop communication for routing and broadcasting.
- **Transport Planning:** Models reachability within k stops — useful in transit and logistics networks.
- **Social Networks:** Captures indirect influence and "friend-of-a-friend" proximity.
- **Bioinformatics:** Exact powers reveal structural motifs in protein or gene interaction networks.

Recognition Problem

- If $H^{\#k} = G$, H is the exact $k-$th root of G.
- Given G, can we find the "exact $k-$th root" of G?
- Called the **Recognition Problem**.
- Helps understand the operation and how it changes the structure of the graph.
- Refinement: Given G, can we find trees/bipartite graphs H such that $H^{\#k} = G$?

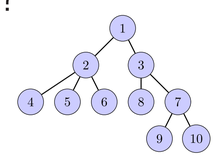

Figure: Tree Graph

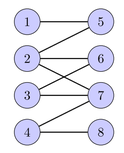

Figure: Bipartite Graph

Other Problems

- **Uniqueness:** Studying the uniqueness of exact power roots, and enumerating all unique exact power roots of a graph.
- **Parameters:** Studying how graph parameters (such as clique, vertex cover) are affected by this operation.
- **"Inverse" Recognition:** Given a graph G with some property, can we find some graph H such that $H^{\#k} = G$?

Some Results

- We built two algorithms for recognition of exact cubes of graphs.
- These algorithms recognize exact cubes of trees and bipartite graphs.
- Both algorithms are constructive, i.e., if the answer is "YES", the algorithm also returns such a graph.
- The tree algorithm relies on the observation that the adjacency of a few fixed vertices help in figuring out almost the entire tree structure.
- The bipartite graph algorithm relies on the observation that exact cubes of bipartite graphs are bipartite, and that the bipartite complement preserves "odd" distances.

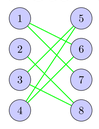

Figure: Graph G

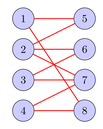

Figure: Bip. Comp. $\overline{G}$

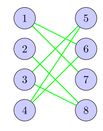

Figure: $\overline{G}^{\#3}$

Conclusion

- In this work, we built algorithms to recognize exact cubes of trees and bipartite graphs.
- We aim to generalize these results to higher exact powers.
- We also plan to examine some graph parameters (such as colouring number, clique number) and their behaviour under the exact power operation.

References

Bai, Y. et al. "Characterizing and recognizing exact-distance squares of graphs". *Discrete Mathematics* (2024).

Brešar, B. et al. "Exact Distance Graphs of Product Graphs". *Graphs and Combinatorics* (2019).

Chang, M.-S. et al. "Linear-Time Algorithms for Tree Root Problems". *Algorithmica* (2015).

Contact Information

- Email: anirudh.rachuri@doctorant.uca.fr

Dynamic Wireless Power Transfer

A. Ramadan, K. El Khamlichi Drissi, K. Tehrani and C. Pasquier
Institute Pascal – Clermont Auvergne University

Objectives

- Consolidate foundational studies on resonant inductive power transfer to establish a comprehensive theoretical framework.
- Analyze efficiency variations caused by environmental factors affecting inductors.
- Ensure continuous power transfer under dynamic operating conditions, such as movement or load changes.
- Develop a robust control strategy to regulate and adapt the wirelessly transferred power in real time.
- Validate system performance through experiments at a real-world scale to ensure practical applicability.

Introduction

- Although the range of electric vehicles (EVs) continues to improve, battery charging remains a critical bottleneck for widespread adoption. Dynamic Wireless Power Transfer (DWPT) presents a promising alternative by allowing EVs to charge wirelessly while in motion over electrified road segments. This approach reduces the need for large onboard batteries and frequent charging stops, improving both convenience and efficiency. At the core of DWPT is magnetic resonance technology, which enables reliable, contactless energy transfer between the road infrastructure and moving vehicles, even under dynamic conditions.

Mathematical Section

- Design Initialization

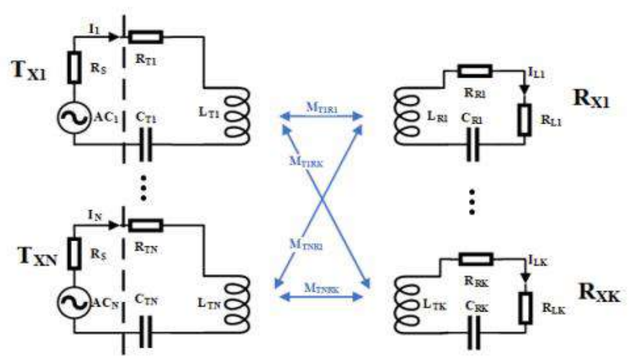

  - Transmitter (Tx_i)
  - Receiver (Rx_j)

- General Equation for Transmitter i :

$$v_{T_i}(t) = v_{C_i}(t) + L_i \cdot \frac{di_i(t)}{dt} + \sum_{j=1}^{m} M_{i,R_j} \cdot \frac{di_{R_j}(t)}{dt} + R_i \cdot i_i(t)$$

- General Equation for Receiver j :

$$v_{S_j}(t) = v_{C_{R_j}}(t) + L_{R_j} \cdot \frac{di_{R_j}(t)}{dt} + \sum_{i=1}^{n} M_{R_j,i} \cdot \frac{di_i(t)}{dt} + R_{R_j} \cdot i_{R_j}(t)$$

- Notes: $R_{R_j} = R_j + R_{load}$

System Design

- Two transmitter configurations are used in DWPT:
  - Simultaneous Contribution:

    Both transmitters are active together, combining their magnetic fields to power the receiver. This provides stable and efficient transfer, especially when the vehicle is centered between them.
  - Sequential Activation:

    Transmitters activate based on the vehicle's position. When the vehicle is between them, both can briefly contribute, creating a power boost—potentially doubling the output with proper spacing and timing.

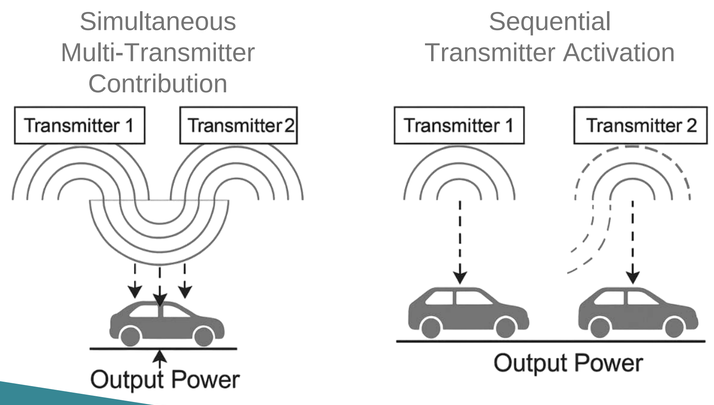

Results

Static 1 by 1 System

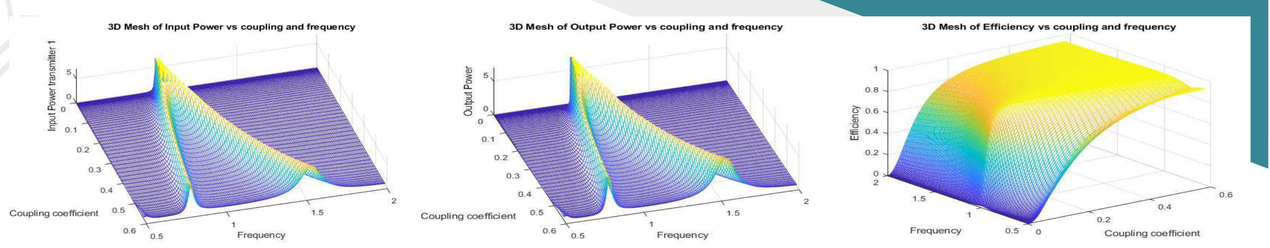

Single transmitter → single receiver

Baseline for efficiency analysis

Sequential Transmitter

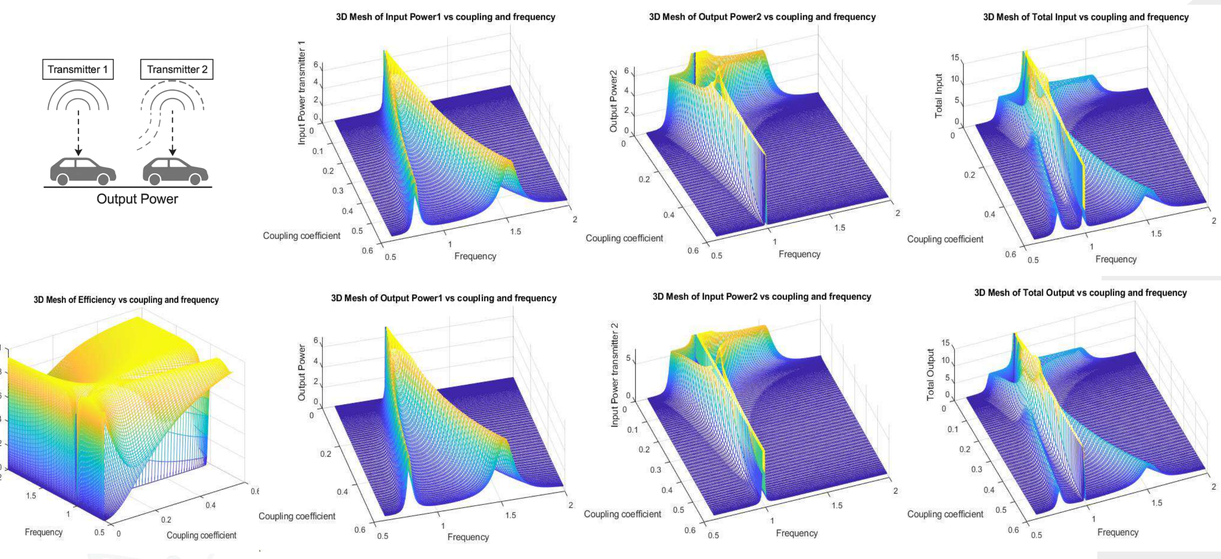

Follows vehicle movement

Risk of power gaps at switchovers

Simultaneous Multi-Transmitter Contribution

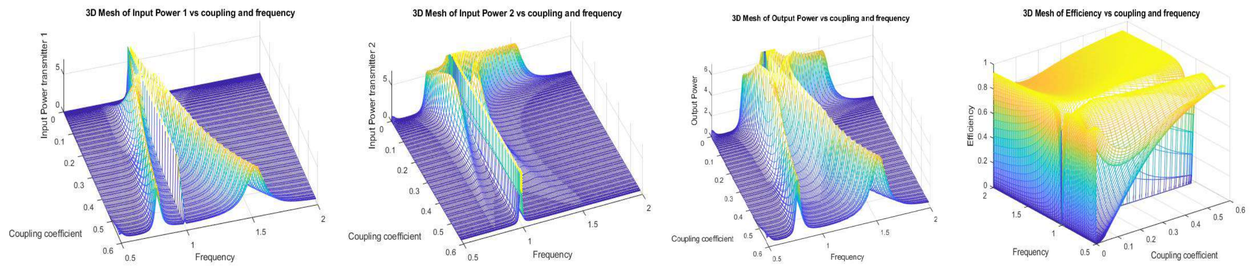

Ensures continuous power

For smooth, high-speed transfer

- Notes: Optimal power transfer occurs along a narrow ridge, making it challenging to maintain this power during dynamic operation.

Conclusions and future work

- To summarize:
  - Investigated Dynamic Wireless Power Transfer (DWPT) using both numerical and model-based simulations.
  - Analyzed system behavior under various conditions, focusing on control strategies involving power radius and operating frequency.
  - Demonstrated the effect of these parameters on power transfer efficiency and system stability during vehicle motion.
- Future Work:
  - Optimize control strategies to maximize power uptake dynamically along the vehicle's path.

References

[1] M. Liang, K. E. Khamlichi Drissi and C. Pasquier, "Optimal frequency for Dynamic Wireless Power Transfer," 2022 24th European Conference on Power Electronics and Applications (EPE'22 ECCE Europe), Hanover, Germany, 2022, pp. 1-10.

[2] Lu, Z.; Zhao, Y.; Liu, D. Adaptive Impedance Matching Scheme for Magnetic MIMO Wireless Power Transfer System. Electronics 2021, 10, 2788. https://doi.org/10.3390/electronics10222788

ahmad.ramadan@doctorant.uca.fr
(+33) 7 63 15 71 86

Using Artificial Intelligence to better understand the development of the Musculoskeletal System

Sami Safarbati (1)(2), Charlène Guillot (1), Fréderic Chausse (2), Christophe Tatout (1)

*1. **iGReD**, UFR de Médecine et des Professions paramédicales, Clermont-Ferrand, France*
*2. Université Clermont Auvergne, Clermont Auvergne INP, CNRS, **Institut Pascal**, Clermont-Ferrand, France*

Objective

The objective is to develop a FAIR solution using tracking by detection paradigm to track NMPs using Ligh sheet microscopy to elucidate how folate deficiency alters the dynamics, fate decisions, and lineage trajectories of neuro-mesodermal progenitors during posterior axis formation

Context

In humans, folate deficiency alters early embryogenesis by disrupting posterior body-axis elongation, thereby impairing the proper formation of the spinal cord and trunk musculature. This pathology has been associated with alterations in a group of cells known as Neuro-Mesodermal Progenitors (NMPs), which remain poorly characterized [4]. To better understand the role of NMPs, we have established a multidisciplinary research project involving biologists developing an in vivo model system (the chicken embryo) to track NMPs during early embryonic development using light-sheet fluorescence microscopy (LSFM), and computer scientists creating solutions for 3D image analysis. To this end, we will integrate an imaging-AI pipeline that combines a previously developed deep-learning network, biom3D, for image segmentation, now implemented with new tracking functions to monitor NMP division, migration in space and time, and their survival under normal versus folate-deficient conditions.

Biom3d : Deep Learning Tool

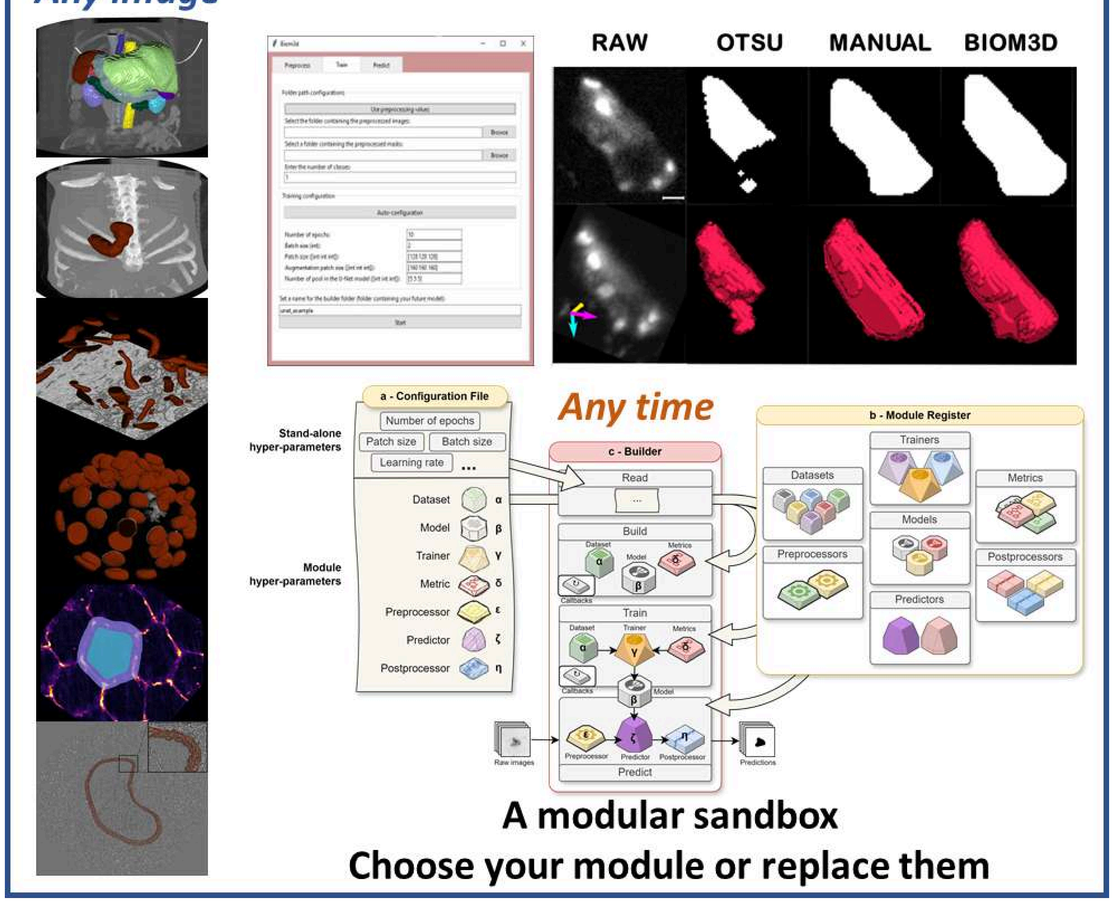

Principle of Light Sheet Microscopy

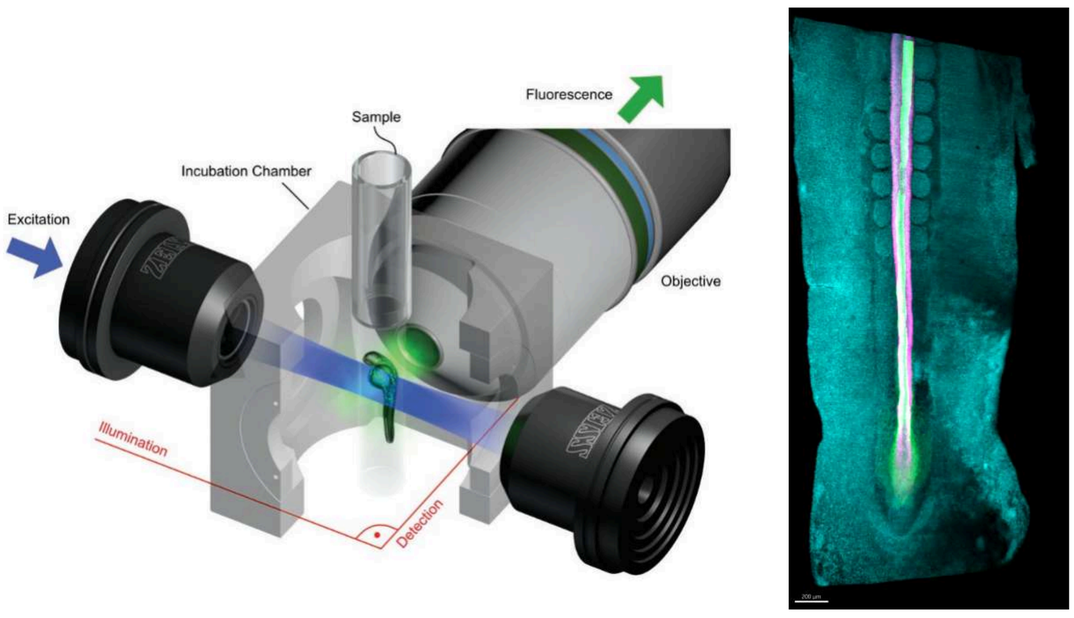

Posterior axis acquisition of chicken embryos using a light sheet microscope

Methodology

First, our 3D analysis follows the tracking-by-detection paradigm combining the two following steps :

3D Segmentation – Raw volumes will be segmented with Biom3D [1] , a deep-learning model trained on manually/semi-automatic annotated NMP nuclei .

Linking & Lineage Reconstruction – Segmented centroids are handed to the current best-ranking tracker from the Cell Tracking Challenge based on multi-hypothesis Kalman and graph optimization [2] to generate time-resolved links; mitoses are identified from branch points, yielding complete lineage trees.

Second, custom Python scripts will extract NMP cell divisions as proliferation rates, differentiation timing, migration vectors, and survival curves.

All steps will be wrapped in a FAIR workflow compatible with an image storage solution called OMERO [3], associating for each image Bio-formats and user metadata and allowing the production of OME-Next Generation File Format (NGFF) outputs like OME-Zarr [3] compatible with large size image format (1TB/embryo).

Finally, the end-user tool will be available as GUI and CLI solutions made available in a public GitHub repository, enabling one-click reproduction and community extensions.

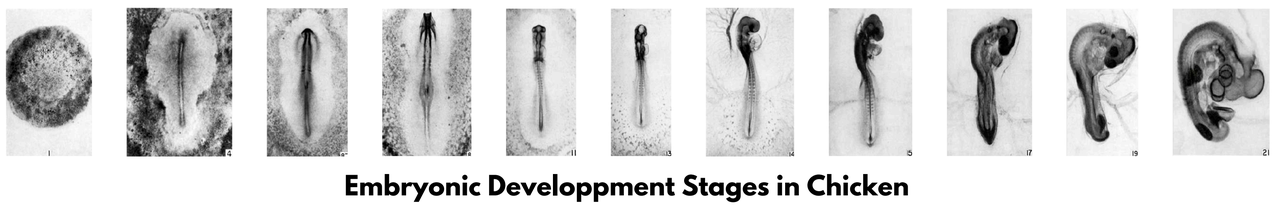

Embryonic Developpment Stages in Chicken

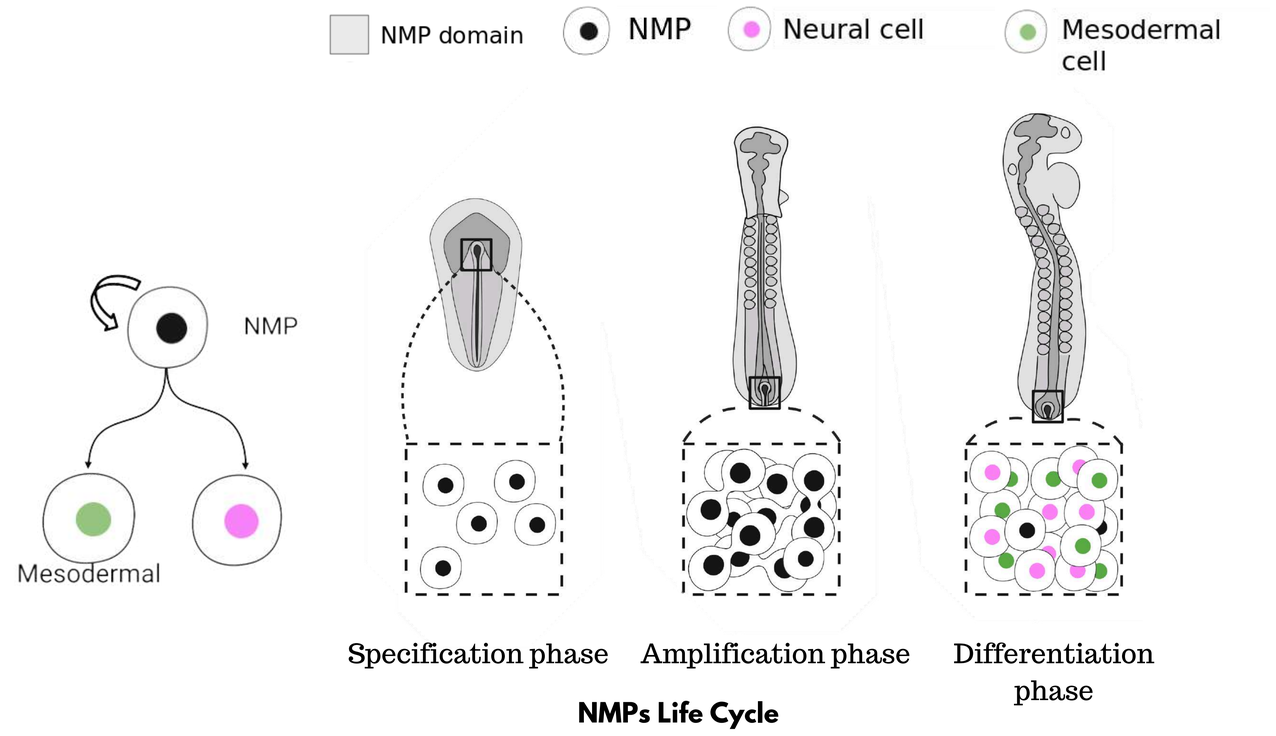

NMPs Life Cycle

Tracking Workflow

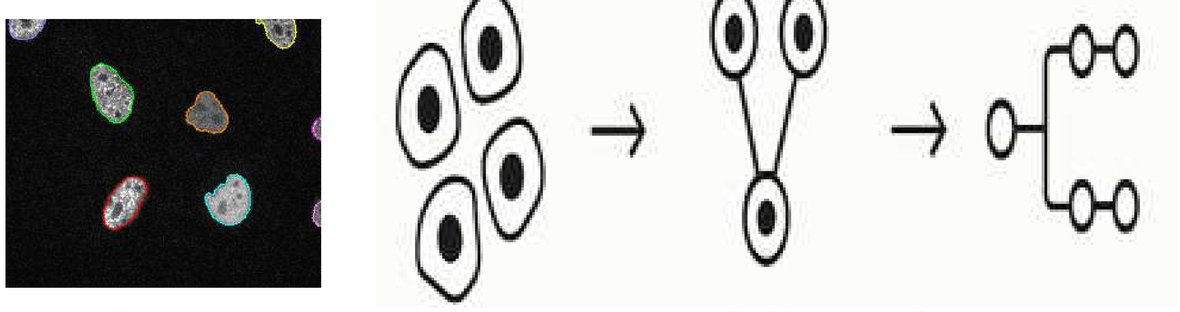

Figure 1

References

[1] Guillaume Mougeot, Sami Safarbati, Hervé Alégot, Pierre Pouchin, Nadine Field, Sébastien Almagro, Émilie Pery, Aline Probst, Christophe Tatout, David E. Evans, Katja Graumann, Frédéric Chausse, and Sophie Desset. Biom3d, a modular framework to host and develop 3d segmentation methods. bioRxiv, 2024.
[2]Maška, M., Ulman, V., Delgado-Rodriguez, P. et al. The Cell Tracking Challenge: 10 years of objective benchmarking. Nat Methods 20, 1010–1020 (2023). https://doi.org/10.1038/s41592-023-01879-y
[3]Allan, Chris et al. “OMERO: flexible, model-driven data management for experimental biology.” Nature methods vol. 9,3 245-53. 28 Feb. 2012, doi:10.1038/nmeth.1896
[4]Henrique D, Abranches E, Verrier L, Storey KG. Neuromesodermal progenitors and the making of the spinal cord. Development. 2015 Sep 1;142(17):2864-75. doi: 10.1242/dev.119768. PMID: 26329597; PMCID: PMC4958456.

- https://github.com/GReD-Clermont/biom3d
- https://github.com/SafarbatiSami

contact : sami.safarbati@uca.fr

Propagation des incertitudes pour la mesure d'impulsions électromagnétiques d'origine nucléaire

J. SERIEN, P. BONNET, C. CHAUVIERE, D. GAPILLOUT

Université Clermont-Auvergne,Institut Pascal,CEA Gramat

Ecole doctorale Sciences Pour l'Ingénieur

Contexte

L'IEMN-HA :

Lors d'une explosion nucléaire à haute altitude, les rayons gamma générés traversent l'atmosphère, ce qui provoque une impulsion électromagnétique de haute amplitude. Ce phénomène est appelé Impulsion électromagnétique nucléaire haute altitude (IEMN-HA), et peut gravement endommager les équipements électroniques à l'échelle nationale, voire continentale.

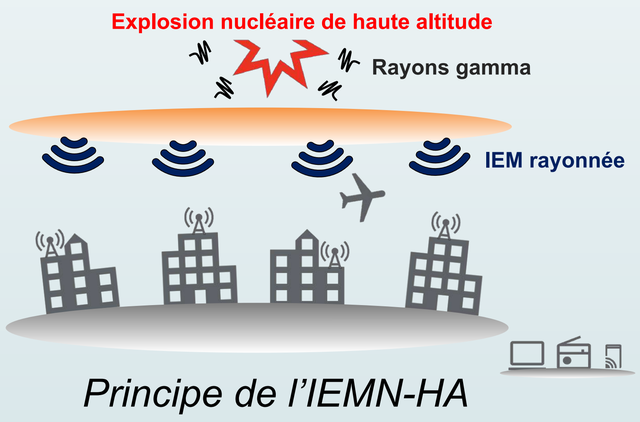

Principe de l'IEMN-HA

Les simulateurs expérimentaux du CEA

Afin de mener des études de vulnérabilité et de durcissement, le CEA dispose de simulateurs expérimentaux permettant de reproduire l'impulsion à l'échelle 1:1, grâce à des générateurs impulsionnels de grandes dimensions. Ainsi, il est possible de soumettre des équipements divers aux effets de l'IEM.

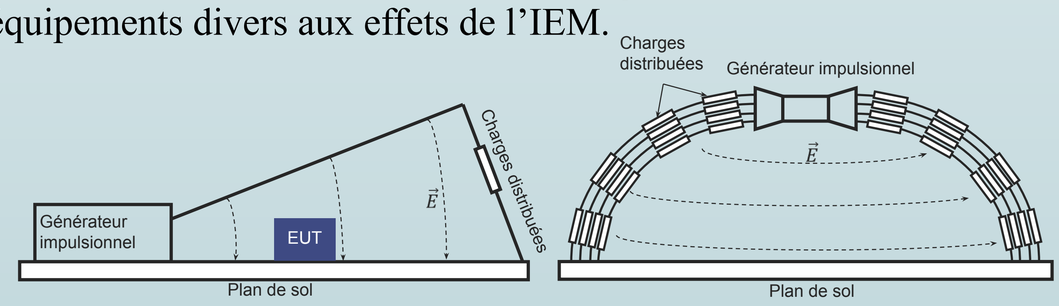

Schémas des simulateurs expérimentaux

Les chaînes de mesure

Pour mener à bien ces études, divers capteurs sont placés au niveau des équipements testés. Toutefois, les appareils de mesure (oscilloscope,VNA, …) nécessaires pour l'utilisation des capteurs doivent être éloignés et protégés de l'impulsion. Il faut donc mettre en place des chaînes de mesure complexes, sources de pertes et d'incertitudes, pour relier les capteurs aux instruments de mesure.

Objectifs

Afin de pallier à ces incertitudes, des marges importantes sont appliquées sur l'amplitude des signaux émis par les générateurs impulsionnels. Une meilleure compréhension (estimation,impact,...) de ces incertitudes permettrait de réduire ces marges.

Les objectifs de ces travaux de thèse sont donc :

-Identifier, modéliser et quantifier les sources et la propagation des incertitudes dans les chaînes de mesure

-retrouver les signaux émis par les générateurs impulsionnels à partir des signaux mesurés et de leurs incertitudes associées

Travaux en cours

La modélisation comportementale :

La modélisation comportementale est très utilisée pour l'étude des amplificateurs de puissance, afin de caractériser des systèmes "boîte noire". Cette méthode nécessite un signal d'entrée et le signal de sortie associé obtenu en sortie du système à étudier. Il est crucial que le signal d'entrée soit le plus représentatif possible de l'ensemble des signaux utilisables en entrée du système. Ensuite, par la méthode des moindres carrés, une modélisation du système est obtenue.

Premiers résultats :

Une méthode de modélisation comportementale dite GMP (Generalized Memory Polynomial)[1], [2], [3] a été implémenté en python, et utilisée pour modéliser un système amplificateur-filtre simulé en python. Le problème direct consiste à prédire le signal de sortie en connaissant l'entrée, et le problème inverse vise à retrouver le signal d'entrée en connaissant la sortie. Le critère NMSE correspond à l'erreur quadratique normalisée entre la prédiction et le signal cible, et permet d'évaluer la précision du modèle.

Le système étudié est composé d'un filtre passe-bande en cascade avec un amplificateur.

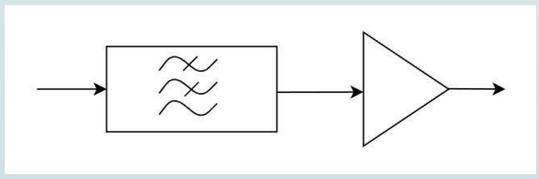

Schéma du système étudié

Pour le problème direct :

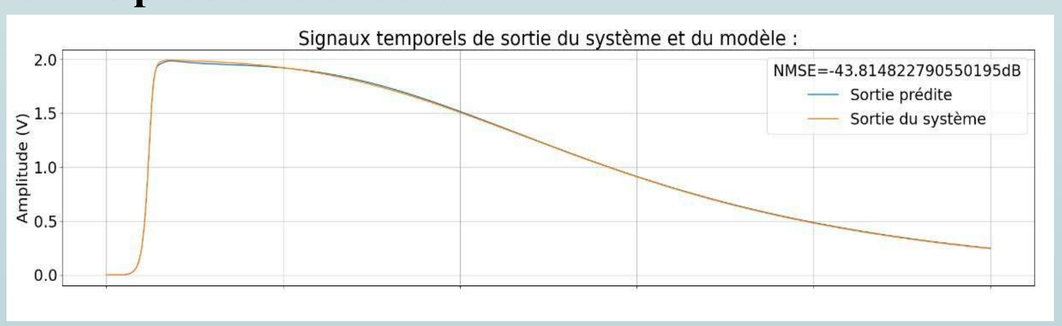

Signal prédit par modélisation comportementale et signal de sortie du système

Pour le problème inverse :

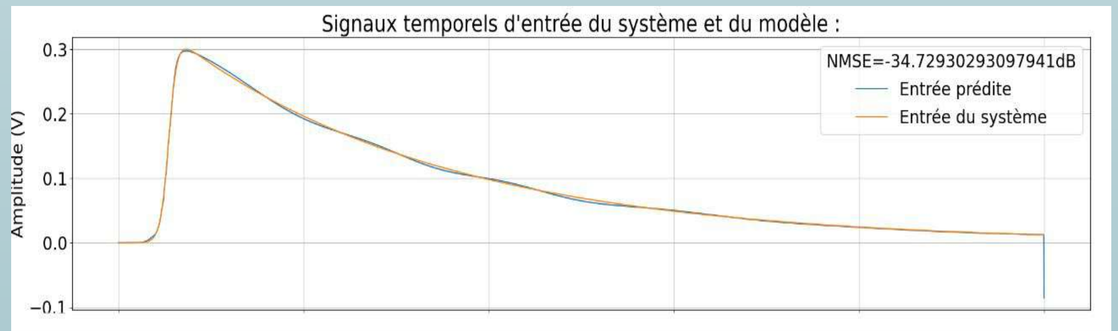

Signal prédit par modélisation comportementale et signal d'entrée du système

Perspectives

-Proposer une modélisation par réseaux de neurones et la comparer avec la modélisation comportementale

-Valider les résultats actuels de manière expérimentale

Bibliographie

1. **D.R Morgan, Z.Ma, J.Kim, M.G.Zierdt, J.Pastalan, "A generalized memory polynomial model for predistorsion of RF power amplifier",IEEE transactions on signal processing, vol.54 NO.10, Octobre 2006**
2. **M.Schetzen, "Nonlinear system modeling based on the wiener theory", proceedings of the IEEE, vol.49, NO.12, December 1981**
3. **A.Zhu, T.J.Brazil, "Behavioral modeling of RF power amplifiers based on pruned Volterra series",IEEE Microwave and wireless components letters, vol. 14, NO. 12, December 2004**

Dynamic First-Order Tree-Decomposition

Javad Taheri, PhD student
Supervised by Mamadou Kanté and Bruno Guillon
LIMOS, UCA

What is it about?

Efficiently updating algorithm outputs as the input data evolves—without starting from scratch.

Introduction

In many situations, we work with evolving data—tables or graphs that change over time—and we need to repeatedly answer a question as the data changes. A familiar example is navigation apps: as your location (or others' locations) changes, the app updates the estimated time to your destination.

- **Static approach:** Recomputes the answer from scratch after each change, ignoring previous work.
- **Dynamic approach:** Reuses previous computations to update the answer efficiently after each change.

In this project, we follow the dynamic approach for data structured as graphs. The question we repeatedly ask is how to compute a *tree-decomposition* of the graph—a fundamental structure that enables efficient solutions for many other problems.

What are we talking about?

A *graph* is a collection of vertices, where some pairs of vertices are connected by edges. A *tree* is a special kind of graph with a simple structure: it has no cycles.
A *dynamic graph* is a graph that evolves over time, with vertices or edges being added or removed.

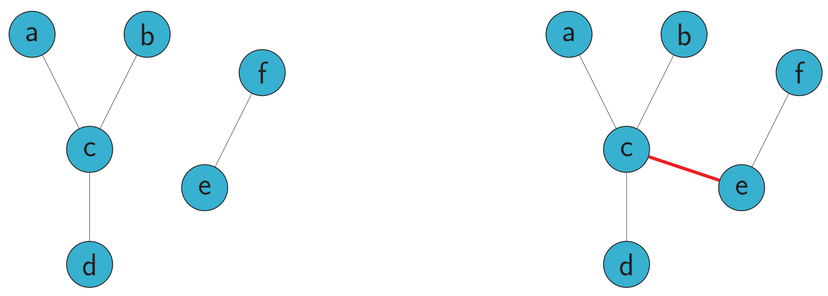

Figure 1:A dynamic graph. The initial graph in the left and the result of adding an edge to it in the right.

Many algorithmic problems are easier to solve on trees than on general graphs. Therefore, it's helpful to approximate complex graphs by simpler tree-like structures.
This is where *tree-decompositions* come in: given a graph G, a tree-decomposition provides a way to represent G as a tree that approximates its structure.

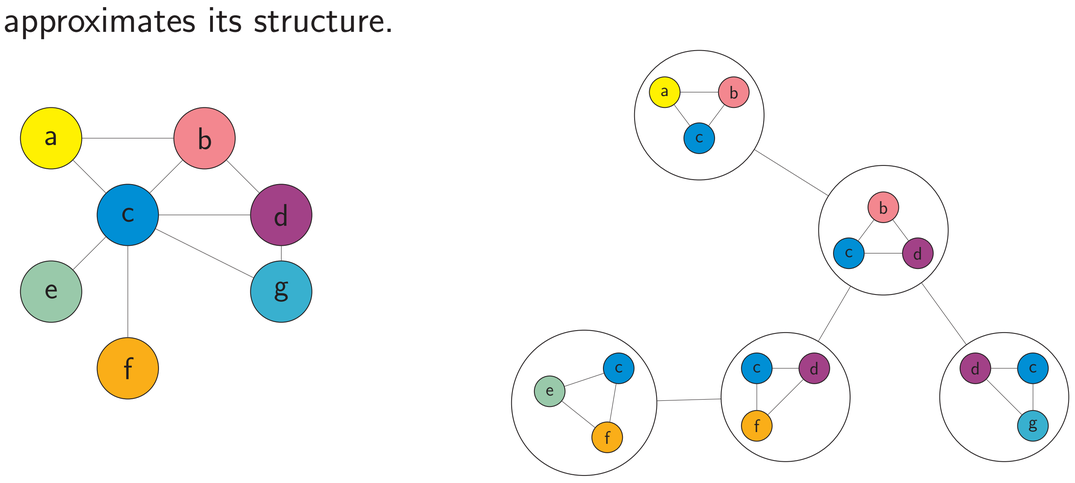

Figure 2:Graph G in left and a tree decomposition of it in right.

Easy and hard? What does it mean?

In mathematics and computer science, we often use formal languages or logical systems to describe abstract objects and their properties—these are called *structures*.
Some structures can be described using simple languages, while others require more complex and expressive ones. This leads to a natural classification: the more complex the language needed to describe a structure, the harder it is to understand or work with.

What do we want?

A tree-decomposition is a complex structure—it's not easy to describe or compute.
Now, imagine we have a *dynamic graph*, one that evolves over time. Can we start with a tree-decomposition (even if it's hard to compute initially), and then efficiently update this description as the graph changes—without starting over each time?

Mathematical logic

Logical symbols help us describe mathematical structures and their properties. Different symbols give rise to logics with different expressive power:

- **First-order logic (FO):** Uses symbols like $\wedge$, $\vee$, $\neg$, and quantifiers like $\exists x$, $\forall x$.
- **Monadic second-order logic (MSO):** Extends FO by adding quantification over sets, like $\exists \boldsymbol{X}$ (for set variables $\boldsymbol{X}$).

MSO is more expressive—and therefore considered "harder"—than FO, because it can describe more complex structures. For example, a *tree-decomposition* can be described in MSO, but not in FO.

Strategy

For a specific class of graphs—called *forests* (collections of trees)—there exists an algorithm to update tree-decompositions.
This algorithm was originally described in *monadic second-order logic* (MSO), as it relies on an unbounded sequence of operations performed step by step.
By applying techniques from *automata theory*, we discovered a way to perform these operations *in parallel*. This breakthrough allows us to express the algorithm in *first-order logic* (FO)—a much simpler framework.

Results

We developed a dynamic tree-decomposition algorithm for specific classes of graphs:

- Forests
- Cactus graphs with bounded degree

Key properties:

- Updates are efficient: the process is expressible in *first-order logic (FO)*.
- After small changes in the graph, the tree-decomposition requires only minor adjustments.

Conclusion

- We introduced a dynamic tree-decomposition algorithm expressible in first-order logic, targeting forests and bounded-degree cactus graphs.
- The tree-decomposition can be updated efficiently, which is crucial for speeding up dynamic programming and other algorithms that rely on it.

References

[1] Neil Immerman.
Dyn-FO: A Parallel, Dynamic Complexity Class.
ACM Press, 1994.

[2] Hans L Bodlaender.
Dynamic algorithms for graphs with treewidth 2.
Springer, 1994.

Contact Information

- Email: javad.taheri369@gmail.com
- Phone: +33 758 00 50 43

Propriétés interfaciales et transfert de masse de l'hydrogène

TAULEIGNE Blandine[a]*, MARCATI Alain[a] et VIAL Christophe[a]

[a] Université Clermont Auvergne, Clermont Auvergne INP, CNRS, Institut Pascal, F-63000 Clermont-Ferrand, France

*blandine.tauleigne@doctorant.uca.fr

Contexte

Dans le cadre de la transition énergétique, un fort intérêt se développe autour de l'hydrogène et de son utilisation. De nouveaux procédés plus verts se développent dans lesquels le **transfert de l'hydrogène** est souvent montré comme une **étape limitante**. C'est pourquoi il apparait essentiel d'examiner cette limitation en étudiant ses **interfaces gaz/liquide** afin de comprendre l'effet de certains paramètres influents (température, pression, présence d'agents de surface…), et ce, d'autant plus que l'hydrogène est moins étudié que d'autres gaz tels que l'air, l'oxygène ou le dioxyde de carbone.

La tension de surface, influencée par la présence d'**agents tensioactifs**, constitue un paramètre central de cette étude. Parmi les applications en développement, on retrouve la bio-méthanation, un sujet de recherche majeur au sein de l'axe GePEB de l'Institut Pascal. Ce procédé met en œuvre du transfert d'hydrogène en milieux biologiques complexes, où des bactéries méthanogènes jouent un rôle central. Or, ces micro-organismes libèrent aussi des biosurfactants, des substances tensioactives qui modifient la tension de surface et les interactions aux interfaces.

Objectifs

- **Comparer le comportement de l'hydrogène aux interfaces gaz-liquide avec l'air sur lequel il existe une littérature abondante.**
- **Étudier le transfert de matière gaz-liquide dans des milieux complexes : présence de tensioactifs (systèmes chimiques) ou de protéines (milieux biologiques).**
- **Relier les résultats à des phénomènes observés en bio-méthanation (moussage) pour intensifier la production de méthane.**

Méthodes

Les méthodes de mesure interfaciales utilisées sont la tensiométrie statique et dynamique, ainsi que la rhéologie interfaciale, à travers un **tensiomètre** présenté ci-dessous. Sa méthode est basée sur une analyse d'image, ainsi une mesure de transfert de matière peut être aussi réalisée avec un suivi de décroissance de taille de bulle.

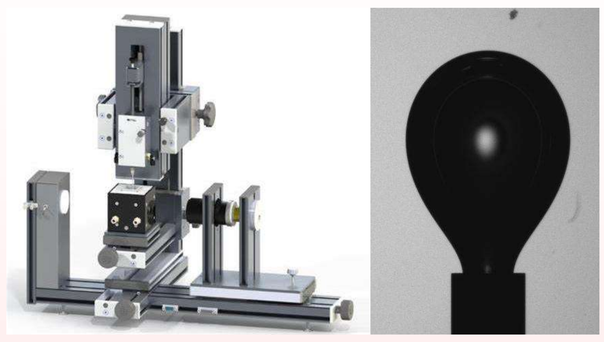

Illustration du tensiomètre Teclis, et une photographie d'une bulle étudiée.

Également, pour analyser ainsi que **visualiser le transfert** de matière d'hydrogène, une méthode colorimétrique, en cours de développement, sera utilisée. La méthode sera ensuite appliquée autour d'une bulle afin de comprendre les phénomènes mis en jeux.

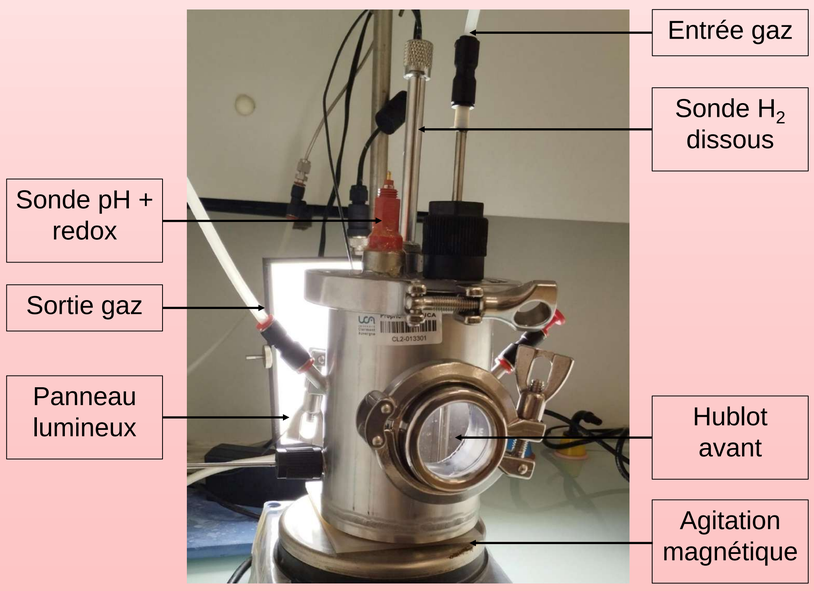

Photographie légendée du matériel expérimental utilisé pour le développement de la méthode colorimétrique.

Résultats

A. Tension de surface

La présence de tensioactifs modifie certaines propriétés dont la formation et le détachement des bulles. On présente ci-dessous **l'influence de la concentration de Tween 20** (T20), et du **débit d'air injecté** sur la formation d'une bulle (d'un volume initial de 1µL) :

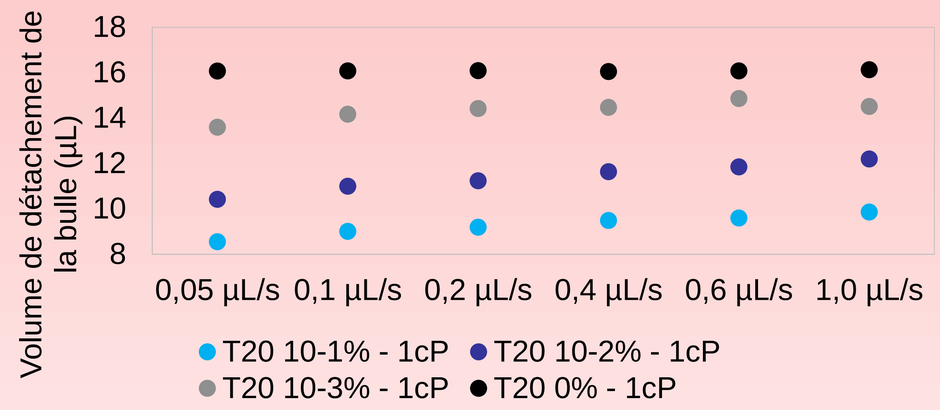

- Plus la concentration est élevée, plus le volume au détachement diminue du fait d'une tension de surface plus faible.
- Plus le débit est élevé, plus le volume au détachement est grand, du fait d'une tension de surface dynamique plus grande.

En effet, les tensioactifs doivent **diffuser** et s'**adsorber** pour réduire la tension de surface. Un débit élevé limite ce temps, entraînant une tension superficielle plus forte lors du détachement.

B. Visualisation du transfert de matière gaz-liquide

Une réaction d'oxydoréduction avec l'**anthraquinone-2-sulfonate de sodium (AQ2S)** semble être adaptée à la visualisation du transfert d'hydrogène, avec une forme oxydée incolore et une forme réduite colorée rouge.

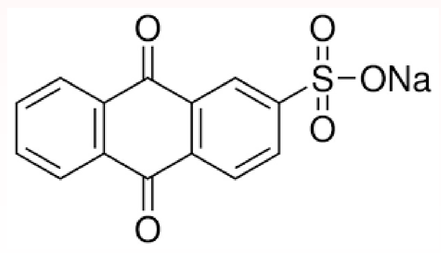

Formule topologique de l'AQ2S.

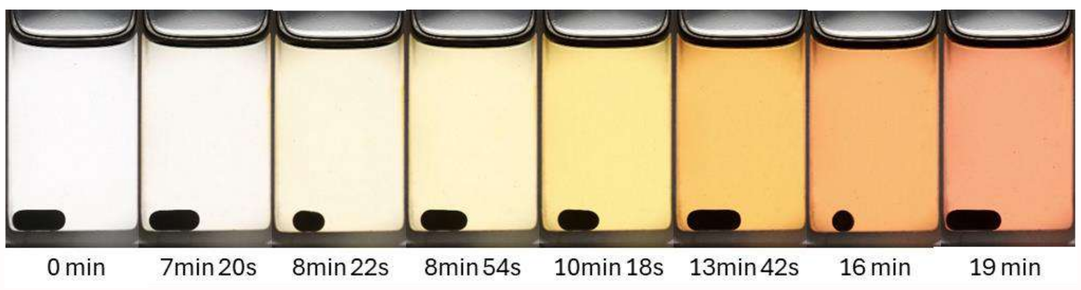

Evolution de la coloration de l'AQ2S en fonction du temps durant une phase d'hydrogénation (C_{AQ2S} = 187 µmol/L + épaisseur liquide = 1 cm).

L'AQ2S, déjà utilisée pour de la détection d'hydrogène[1], semble également offrir la possibilité d'une **quantification du transfert d'hydrogène** avec :

- Une variation de l'intensité de la couleur en fonction de l'épaisseur de liquide traversée,
- Une évolution de l'intensité de coloration linéaire en fonction de la concentration en AQ2S, reflétant la quantité d'hydrogène ayant réagi ou théoriquement dissoute, pour une épaisseur donnée.

Perspectives

- Les travaux sur le détachement des bulles doivent être poursuivis et comparés avec notre gaz d'intérêt, **l'hydrogène**.
- Le lien entre l'intensité de coloration et l'épaisseur de liquide sera approfondi pour remonter à une **concentration en géométrie variable** (échelle de la bulle).

Visualisation d'oxygène dissous autour d'une bulle dans une solution de résazurine[2].

Références

1. ***Silverman, L., & Bradshaw, W. (1956), Analytica Chimica Acta, 15, 31-42.***
2. ***Dietrich, N., & Hebrard, G. (2018), Heat and Mass Transfer, 54(7), 2163-2171.***

Remerciements

Programme AMI CMA Académie des Mobilités Durables pour le financement de la thèse.

MMW Radar and Optical Camera Fusion Architecture for Mobile Robot Perception in Poorly Structured Environments and Adverse Weather Conditions

Alexandre Tête-Neuvy [1], Mathieu Labussière [1], François Marmoiton [1], Pierre Duthon [2] and Omar Ait Aider [1]

[1]Université Clermont Auergne, Clermont Avergne INP, CNRS, Institut Pascal, F-63000 Clermont Ferrand, France,

[2]Cerema, Research Team "Intelligent Transport Systems", 8-10 Rue Bernard Palissy, CEDEX 2, F-63017 Clermont-Ferrand, France

Background & Motivations

- Widespread use of ADAS could reduce the number of accidents in Europe by 15% by 2030.
- Autonomous driving is a promising market, estimated at between $300 and $400 billion over the next decade.
- Perception systems for autonomous navigation are affected by the **structure** and **weather conditions** of the environment.

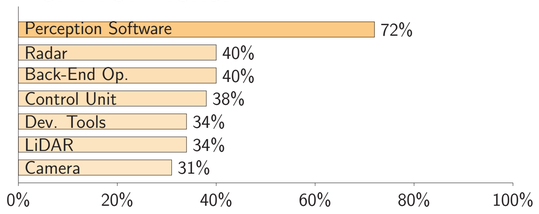

Figure 2: Share of the most critical technologies for autonomous vehicles [2]

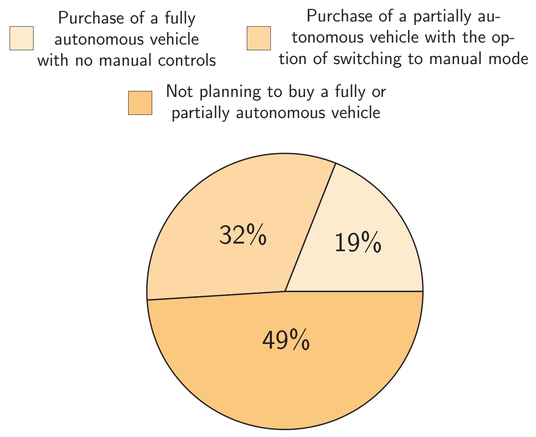

Figure 1: Consumer trends in autonomous vehicle purchases [1]

- Software is the main differential factor in the development of autonomous driving.
- Radar is gaining in popularity thanks to its **robustness** in the face of weather disturbances.

Objectives

- Construction of a consistent database on road environments with different **structures** and **weather conditions**.
- Implementation of a neural network capable of **segmenting** a road scene into semantic instances from the **radar view** with the help of the **RGB camera**.
- Evaluation and characterization of network performance based on criterias to prove its effectiveness.

Why Fuse?

- Camera and radar are **complementary** sensors, and combining them can produce a better sensor.

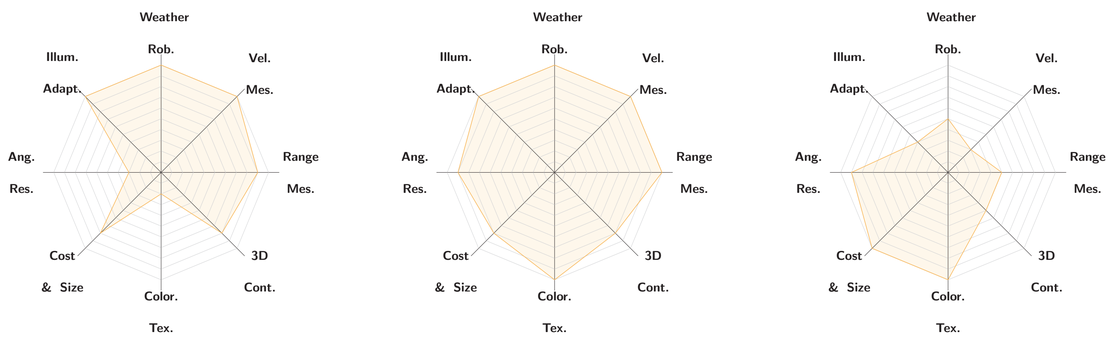

(a) Radar (b) Radar + Camera (c) Camera

Figure 3: Sensor characteristics of radar and camera [3]

- A better sensor means better **object detection** and **tracking**.

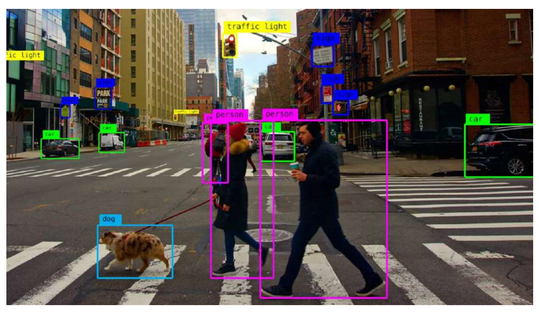

Figure 4: 2D Object Detection Output

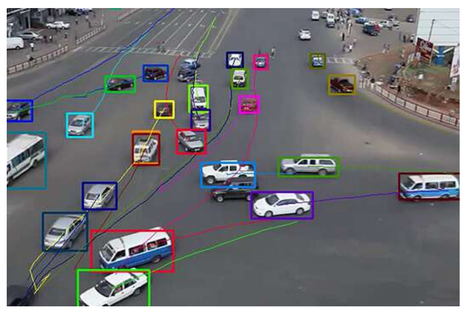

Figure 5: 2D Object Tracking Output

- A better sensor means better **image segmentation**.

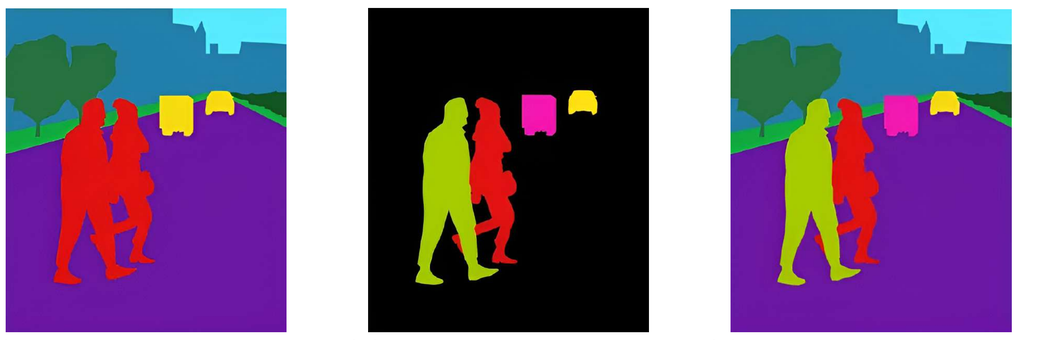

(a) Semantic Segmentation (b) Instance Segmentation (c) Panoptic Segmentation

Figure 6: Image Segmentation Categories

What Fuse?, Where Fuse?

- The camera image is a **front view** of the road scene, while the radar scan is an **bird's eye view** of the road scene.

Figure 7: Camera's Front View

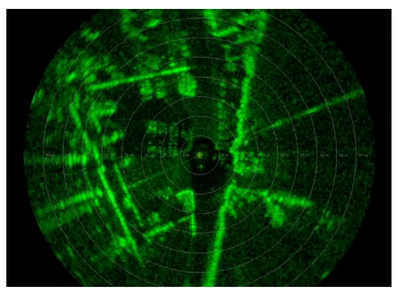

Figure 8: Radar's Bird's Eye View

- The **bird's eye view** of the road scene is a more **complete** and **robust** representation for autonomous navigation.

Experimental Setup

- To implement this radar-camera fusion applied to autonomous navigation, it was decided to use a **mechanical rotation radar** and an **RGB camera**.

Figure 9: Navtech RAS3 Radar

Figure 10: Genie Nano C1630 RGB Camera

- **Real-life testing** of the multimodal fusion model will be carried out on a vehicle modified for autonomous navigation. **Extreme condition tests** will be carried out on *Cerema's Pavin Brouillard et Pluie platform*.

Figure 11: Renault Zoé modified for autonomous driving

Figure 12: Cerema's Pavin Brouillard et Pluie platform

Conclusion

- Current perception systems for autonomous driving are not very robust in **poorly structured environments** and **adverse weather conditions**.
- Radar and camera are **complementary** sensors: the camera captures rich **geometric** and **semantic** information, while radar capture is **robust** to **adverse weather conditions**.

References

[1] Eike Ebel, Martin Kellner, Timo Möller, Felix Rupalla, and Dasha Zuyeva. Hands off: Consumer perceptions of advanced driver assistance systems. *McKinsey's Automotive & Assembly Practice*, 2023.

[2] Derek Chiao, Kersten Heineke, Ani Kelkar, Martin Kellner, Eelizabeth Scarinci, Dmitry Tolstinev, and Johannes Deichmann. Autonomous vehicles moving forward: Perspectives from industry leaders. *McKinsey's Automotive & Assembly Practice and McKinsey Center for Future Mobility*, 2024.

[3] Kun Shi, Shibo He, Zhenyu Shi, Anjun Chen, Zehui Xiong, Jiming Chen, and Jun Luo. Radar and camera fusion for object detection and tracking: A comprehensive survey. *arXiv preprint arXiv:2410.19872*, 2024.

[4] Shanliang Yao, Runwei Guan, Xiaoyu Huang, Zhuoxiao Li, Xiangyu Sha, Yong Yue, Eng Gee Lim, Hyungjoon Seo, Ka Lok Man, Xiaohui Zhu, et al. Radar-camera fusion for object detection and semantic segmentation in autonomous driving: A comprehensive review. *IEEE Transactions on Intelligent Vehicles*, 9(1):2094–2128, 2023.

Acknowledgements

- This work is supported by the *International Research Centre "Inovative Transport and Production Systems"* of the *CAP 20-25 I-SITE*.

Ultra Flexible Factory Layout Optimisation

Mourad BAIOU, Rafael COLARES, David DROULAULT, Hector GATT, TRAN An

LIMOS,UCA - Michelin

Context

1. This thesis focuses on defining the layout for the Ultra Flexible Factory (UFF), a future **Michelin** factory.
2. The **goal** is to optimise the workshop production.

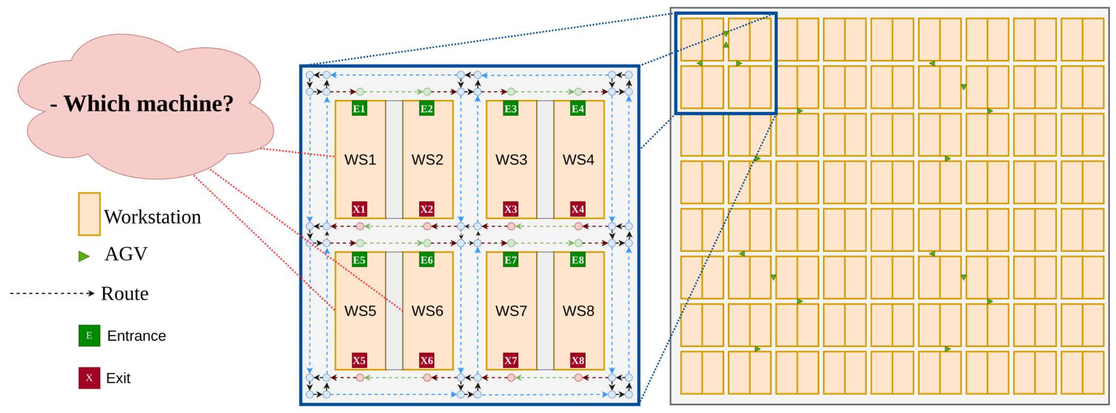

Problem definition

Given

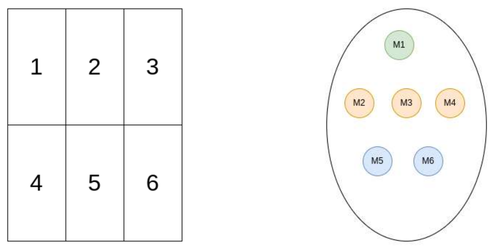

A set of **workstations** and a set of **machines**.

Output

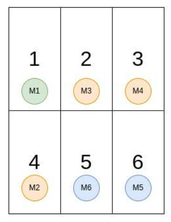

A **layout**: a one-to-one assignment of machines to workstations.

➢ **Goal**: Minimise the material transfer cost

* If the number of machines is less than the number of locations, we can add "empty machines".

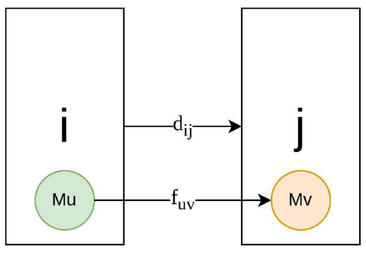

$c(M_u, M_v) = d(i,j) \cdot f(u,v)$

where $d(i,j)$ *is the distance from workstation* i *to workstation* j.

Group flow

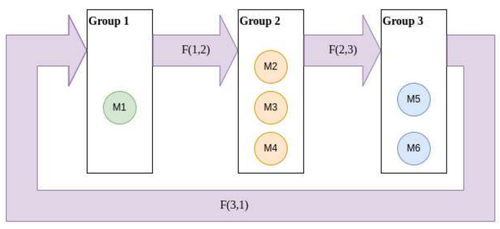

- Machines can be grouped into replica groups.
- The group flow is given.

- The material transfer cost is calculated as the product of the **specific flow** and the **distance**, which are both varied.

Specific flow

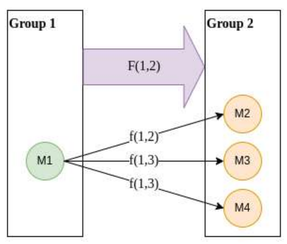

$f(1,2)+f(1,3)+f(1,4) = F(1,2)$

- The total specific flow from machines in one group to another group must match the corresponding group flow.

Workstation orientation and the distance

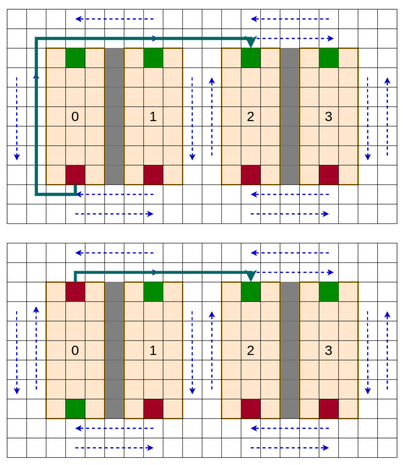

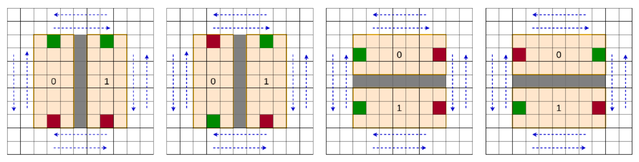

- The distance depends on the orientation of workstations.
- The orientations of the two workstations in one square must be compatible.

Mathematical formulations

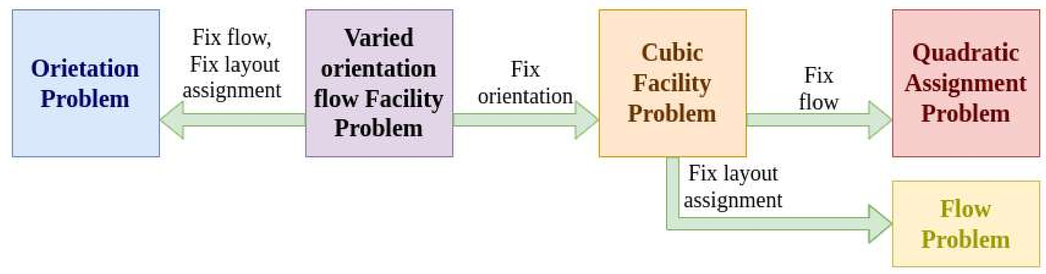

- **Quadratic Assignment Problem**: NP-hard, one of the most difficult problems to be solved in practice. ([1], [2], [3])
- **Cubic Facility Problem**: NP-hard, as the **Quadratic Assignment Problem** is NP-hard.
- **Varied orientation flow Facility Problem**: NP-hard, as the **Quadratic Assignment Problem** is NP-hard.
- **Flow Problem**: Easy problem.
- **Orientation Problem**: Unknown complexity; however, the Quadratic Unconstrained Binary Optimization, a related problem, is NP-hard.

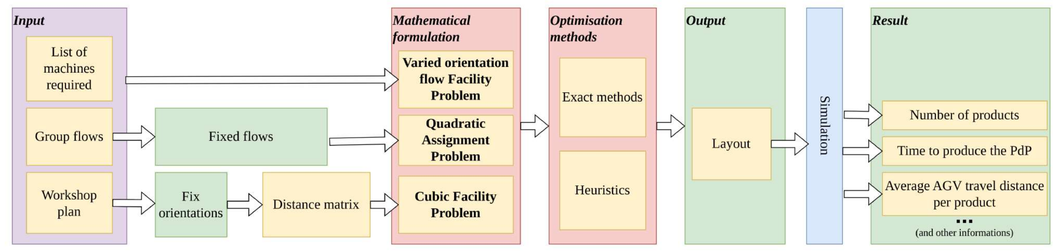

Methods

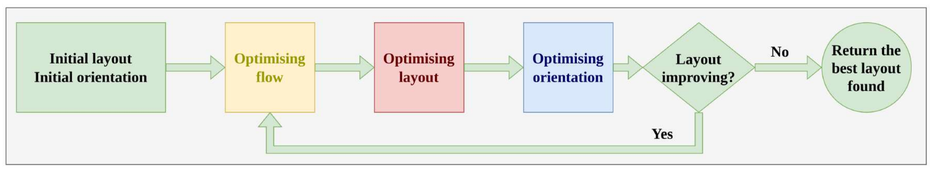

- **Optimising flow**: by solving a linear programming problem using CPLEX or Gurobi.
- **Optimising layout**: By solving a QAP, which is very difficult, we developed heuristics: *Local Search* and *Volume Algorithm* ([4], [5]).
- **Optimising orientation**: we developed two methods: *Local Search* and *MILP*.
- **Optimising both layout and flow** at the same time: By solving a Cubic Facility Layout Problem, we study Linearization methods.

Result and Conclusion

- Simulation results demonstrate that our methods can enhance production efficiency.
- The Michelin Ultra-Flexible Factory Layout Optimisation problem gives rise to numerous interesting and challenging mathematical problems.

References

[1] M. R. Garey and David S. Johnson.
Computers and in stractability: A guide to the theory of np-completeness. w. h freeman, san fran.
1979.

[2] Serigne Gueye and Philippe Michelon.
A linear formulation with $o(n^2)$ variables for quadratic assignment problems with manhattan distance matrices.
EURO Journal on Computational Optimization, 3:79–110, 2015.

[3] Matteo Fischetti, Michele Monaci, and Domenico Salvagnin.
Three ideas for the quadratic assignment problem.
Oper. Res., 60:954–964, 2012.

[4] Francisco Barahona and Ranga Anbil.
The volume algorithm: producing primal solutions with a subgradient method.
Mathematical Programming, 87:385–399, 2000.

[5] Francisco Barahona and Fabián A. Chudak.
Solving large scale uncapacitated facility location problems.
2000.

Acknowledgments

This thesis is one topic of Factolab, a collaboration between UCA and Michelin.

Contact Information

- Email: an.tran@doctorant.uca.fr

A Feynman-Kac Approach to Solving Complex Systems Applied to Solar Hydrogen Production

Idriss Adjaout, [a]Jean Francois Cornet, [a]Thomas Vourc'h,[a]Jeremy Dauchet, [b]Sophie Charton, [c]Nicolas Meynet
[a]Institut Pascal, [b]Cea Marcoule, [c]Engie Crigen

Problematic

Simulation of Photoelectrochemical Cells (device to use light to produce hydrogen) involves several tightly coupled physical phenomena, such as incident light interacting with matter, charge transport, and electrochemical reactions.
This requires a **multiphysics model** with some **non-hierarchical couplings**, where processes are interdependent and must be solved simultaneously.

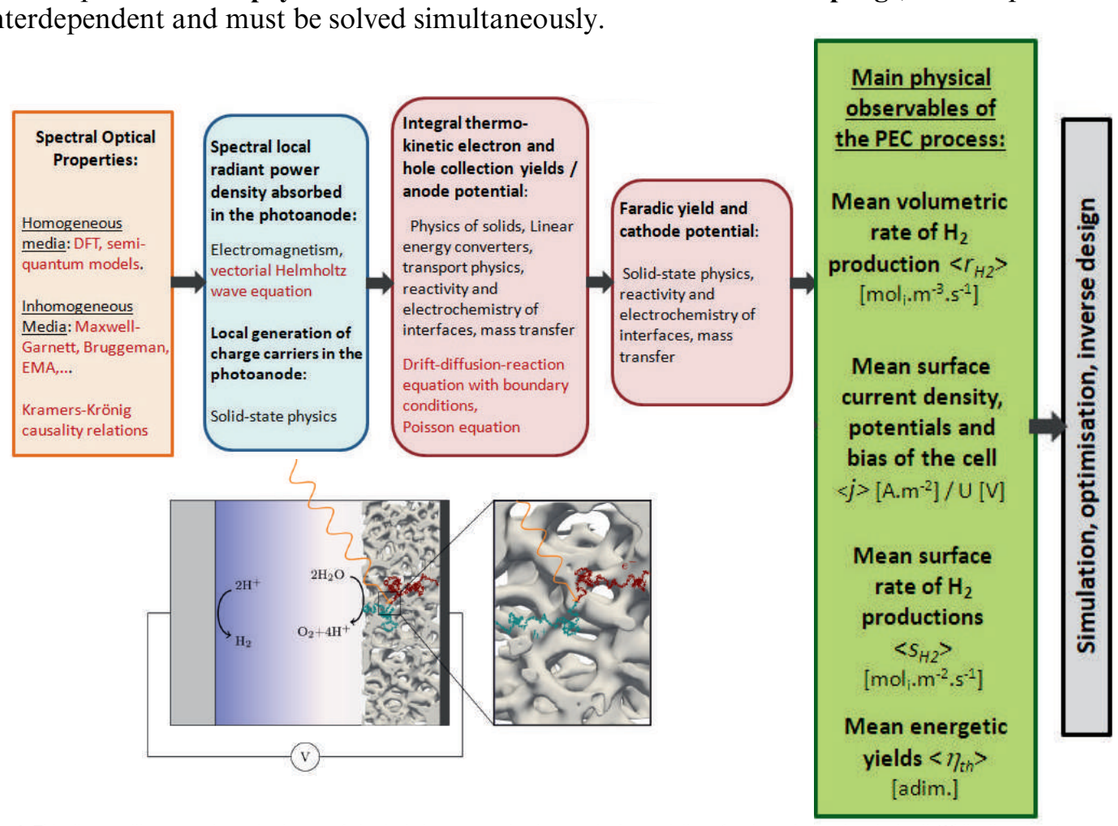

Fig. 1. This diagram illustrates the main classes of physical phenomena that interact in the modeling of a photoelectrochemical cell. While directional arrows suggest hierarchy some couplings are in fact bidirectional, representing strong feedback interactions (strong coupling). Resolving such systems without degrading the model is essential to fully capture all relevant physical effects and to enable inverse design approaches aimed at identifying optimal cell geometries. This makes the simulation of photoelectrochemical cells a challenging example of complex system modeling.

Numerical Modeling: Mesh vs. Mesh-Free

Numerical methods for solving such systems generally fall into two main categories:

- **Mesh-based methods**, such as the Finite Element Method (FEM) or Finite Volume Method (FVM), divide the simulation domain into small, discrete elements (a mesh). Physical equations are solved over these elements to approximate system behavior.

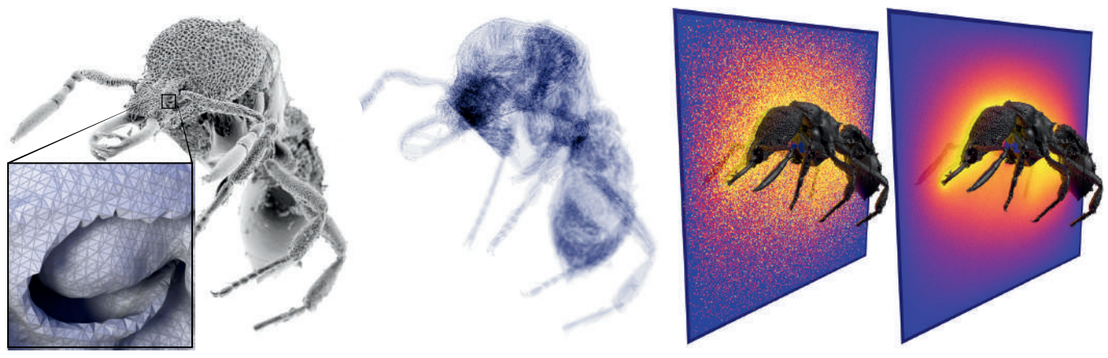

Fig. 2. Real-world geometry has not only rich surface detail (left) but also intricate internal structure (center). On such domains, FEM-based geometric algorithms struggle to mesh, setup, and solve PDEsDin this case taking more than 14 hours and 30GB of memory just for a basic Poisson equation. A Monte Carlo solver uses about 1GB of memory and takes less than a minute to provide a preview (center right) that can then be progressively refined (far right). [Boundary mesh of Fijian strumigenys FJ13 used courtesy of the Economo Lab at OIST.][2]

- **Mesh-free methods**, such as Monte Carlo compute solutions at arbitrary points without requiring a predefined mesh.

Mesh-free solvers offer several key advantages for modeling complex systems:

- They allow evaluation of quantities at a specific point in space and time without solving the entire field,
- They are insensitive to geometric complexity,
- They preserve physical accuracy without simplifying the model, which helps retain essential phenomena.

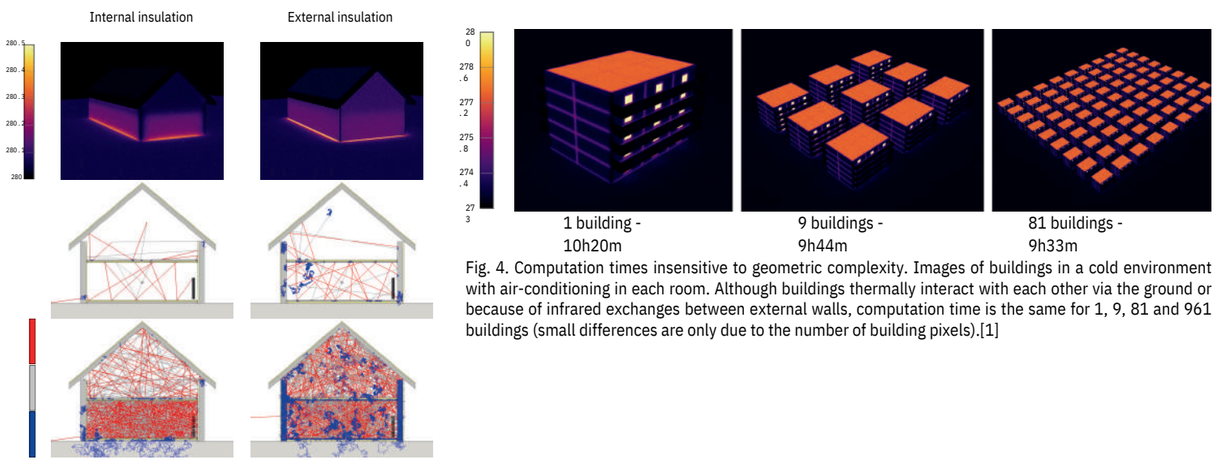

Fig. 4. Computation times insensitive to geometric complexity. Images of buildings in a cold environment with air-conditioning in each room. Although buildings thermally interact with each other via the ground or because of infrared exchanges between external walls, computation time is the same for 1, 9, 81 and 961 buildings (small differences are only due to the number of building pixels).[1]

Fig. 3. (top) Infrared renderings of a farm being insulated by (left) the interior or (right) the exterior. The boundary conditions are the heater at 300K inside the lower room, the ground at 286K at 3m depth, the surrounding air temperature at 280K and the incident radiance temperature at 280K for downward directions (coming from the upper atmosphere assuming a foggy environment i.e. equal to the air temperature). (below) Example paths: starting with convection from a probe inside the lower room, 3 paths in first picture, 60 in second picture. For each path, radiative subpaths are in red, conductive subpaths in blue and convective subpaths in gray. Conductive subpaths are successions of straight lines between δ-sphere centers (see Sec. 4.2). As internal air is perfectly mixed, there is no explicit heat migration within the fluid and convective subpaths are only sketched as straight lines from the surface location where convection is started to the surface location where it ends.[1]

Stochastic Process-Based Resolution Method

We will use mesh-free methods based on stochastic processes.

Historical approach: Roots in potential theory
The core idea is to evaluate the value of a physical field at a specific point in space and time by computing the **expectation of a stochastic process.**
Historically, these approaches originate from potential theory and are particularly well-suited to solving **Laplace or Poisson equations**. This technique is known as:
Walk on Spheres (WoS)

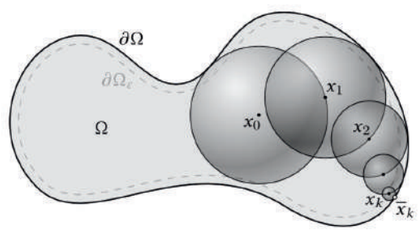

System:

$$\begin{cases} \Delta u = f, & x \in \Omega, \\ u = g, & x \in \partial\Omega. \end{cases}$$

Integral formulation:

$$u(x) = \frac{1}{|\partial B(x)|} \int_{\partial B(x)} u \, dS - \int_{B(x)} f(y)\, G(x,y)\, dy$$

Probabilistic formulation:

$$\hat{u}_f(x_k) = \begin{cases} g(x_k), & x_k \in \partial\Omega, \\ \hat{u}_f(x_{k+1}) - |B(x_k)| f(y_k) G(x_k, y_k), & \text{otherwise} \end{cases}$$

Generalization: Feynman–Kac Formula
A more general framework is provided by the **Feynman–Kac formula**, which extends the stochastic representation to drift–diffusion–reaction equations.

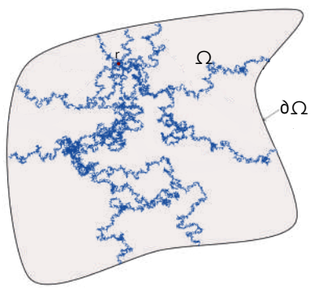

System:

$$\begin{cases} \partial_t u + \mu\, \partial_x u + \frac{1}{2}\sigma^2 \partial_{xx} u - Vu + f = 0, \\ u(x,T) = \psi(x). \end{cases}$$

Probabilistic formulation (Feynman–Kac formula):

$$\begin{aligned} u(x,t) &= \mathbb{E}\left[e^{-\int_t^T V\, ds}\, \psi(X_T) + \int_t^T e^{-\int_t^\tau V\, ds}\, f(X_\tau, \tau)\, d\tau \,\middle|\, X_t = x \right] \\ &= \mathbb{E}\left[\mathcal{F}(X_\tau, t-\tau) \mid X_t = x \right], \\ dX_s &= \mu\, ds + \sigma\, dW \end{aligned}$$

Hierarchical Coupling via Drift Velocity
It is possible to represent a system **coupled hierarchically**

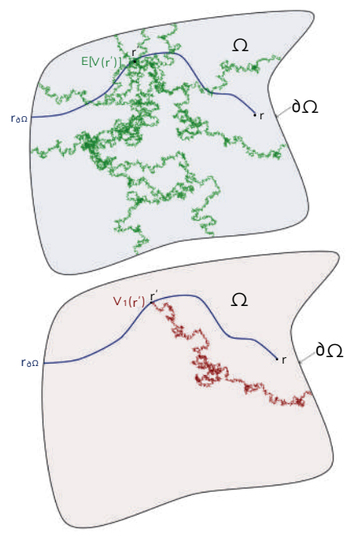

System:

$$\begin{cases} \partial_t u = -\nabla \cdot (-D\nabla u - \mu\, u\, \boldsymbol{E}), \\ \nabla \cdot \boldsymbol{E} = 0. \end{cases}$$

Probabilistic formulation:

$$\begin{aligned} u(\boldsymbol{r}, t) &= \mathbb{E}\left[\widetilde{\mathcal{F}}(\boldsymbol{\mathcal{R}}_\tau, t-\tau) \mid \boldsymbol{\mathcal{R}}_\circ = \boldsymbol{r} \right] \\ \mathrm{d}\boldsymbol{\mathcal{R}}_s &= -\mu \boldsymbol{\mathcal{E}}(\boldsymbol{\mathcal{R}}_s)\mathrm{d}s + \sqrt{2D}\mathrm{d}\mathfrak{W}_s \end{aligned}$$

Fig. 5. This introduces a significant difficulty: At each branching point or time step of the stochastic process, one must evaluate the velocity field to determine the path's evolution leading infinite branches. This issue creates a computational bottleneck

Fig.6 This numerical barrier has been addressed recently by Daniel Yaacoub, who proposed a reformulation of the Feynman–Kac representation for nonlinear drift problems. His approach enables the simulation to proceed by evaluating only one subpath at each step

Non-Hierarchical Coupling
Extending stochastic methods to **non-hierarchically coupled systems** is the natural next step to address complex systems such as strongly interacting multiphysics problems.
However, this would require the development of a probabilistic formulation that avoids an explosion in the number of sub-paths or branching evaluations, which would otherwise render the method computationally intractable.

System:

$$\begin{cases} \partial_t u = -\nabla \cdot (-D\nabla u - \mu\, u\, \boldsymbol{E}), \\ \nabla \cdot \boldsymbol{E} = -\dfrac{e\, u}{\varepsilon}. \end{cases}$$

References

[1] Mégane Bati, Stéphane Blanco, Christophe Coustet, Vincent Eymet, Vincent Forest, Richard Fournier, Jacques Gautrais, Nicolas Mellado, Mathias Paulin, and Benjamin Piaud. Coupling conduction, convection and radiative transfer in a single path-space: Application to infrared rendering. *ACM Transactions on Graphics (TOG)*, 42(4):1–15, 2023.

[2] Rohan Sawhney and Keenan Crane. Monte carlo geometry processing: A grid-free approach to pde-based methods on volumetric domains. *ACM Transactions on Graphics (TOG)*, 39(4):1–15, 2020.

[3] Rohan Sawhney, Bailey Miller, Ioannis Gkioulekas, and Keenan Crane. Walk on stars: A grid-free monte carlo method for pdes with neumann boundary conditions. *ACM Transactions on Graphics (TOG)*, 42(4):1–20, 2023.

[4] Daniel Yaacoub, Stéphane Blanco, Jean-François Cornet, Jérémi Dauchet, Richard Fournier, and Thomas Vourc'h. Branching stochastic processes for feynman-kac representations of drift-involving non-linearities. *arXiv preprint arXiv:2412.08215*, 2024.

The Use of Open Data in the Smart City: From Theory to Practice

Ecole doctorale Sciences Pour l'Ingénieur

Karidja Dominique Christelle ADJE ∗ †, Oussama HABACHI †, Gerard CHALHOUB †, Asma BEN LETAIFA ∗, and Majed HADDAD ‡

† University of Clermont Auvergne, ∗ SUP'COM/University of Carthage, ‡ Avignon University

Introduction

The objective of this thesis is to leverage user mobility data using Artificial Intelligence techniques, in order to improve the telecom infrastructure, specifically in terms of resource allocation optimization in Cell-Free Massive MIMO.

Massive increase in the number of users and Wireless services, with the integration of IoT into 5G cause serious challenges for traditional cellular networks (scalability, meeting growing demands for QoS and QoE—reduced latency, increased throughput, etc.)

- ✓ Cf-mMIMO operation and benefits
- ✓ One of the Cf-mMIMO challenges : the need to process or estimate the large number of channels across multiple users with low latency

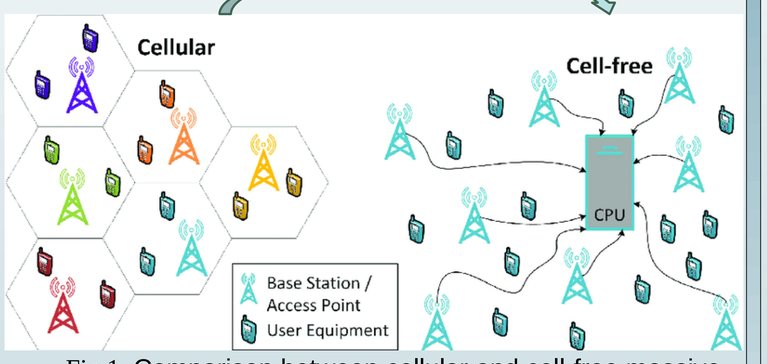

Fig.1: Comparison between cellular and cell-free massive MIMO systems (WSHMW Ahmad et *al.*)

To tackle this challenge, we propose a federated K-means clustering approach using user mobility data (channel variation) to distribute channel estimation between the CPU and APs, thus reducing processing delay.

Methods

FedEst Architecture

1. APs perform a K-means clustering :
   - group users based on their channel variation level (mobility data)
   - low/medium mobility: local clusters at APs level
   - high mobility : centralized clusters at CPU level to achieve global channel estimation

2. An aggregated QoS feedback is sent back to the APs to adjust their K-means at next time coherence interval

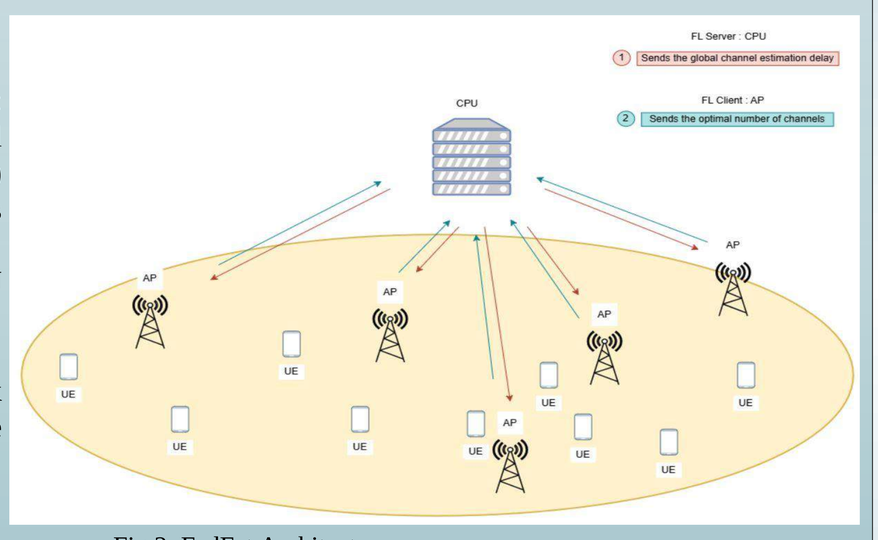

Fig.2: FedEst Architecture

System Model

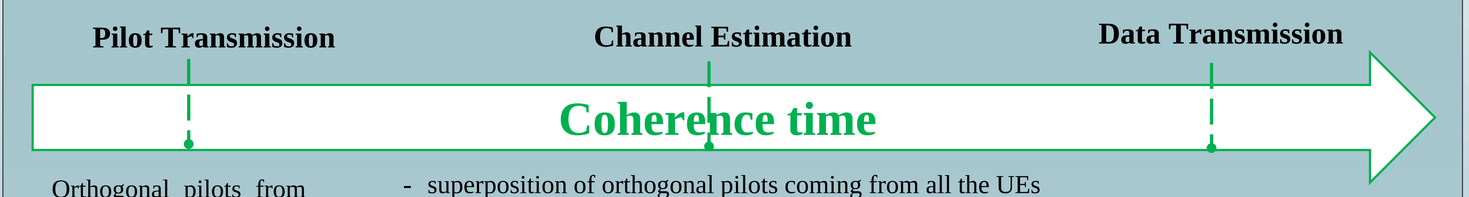

Orthogonal pilots from the UEs to an AP

- superposition of orthogonal pilots coming from all the UEs
- Apply appropriate estimator to estimate the channel for each UE

Note : the channel estimation process needs to be optimized to satisfy the coherence time interval, especially in dense scenarios.

FedEst Framework

01 — **Clustering phase**: capture the user mobility profiles (variation in pathloss between UEs and APs)

02 — **Offloading phase**: APs decide which UEs to offload for channel estimation to the CPU

- Local channel estimation at AP level: UEs with low mobility variation
- Channel estimation at CPU level: UEs with high mobility variation

03 — **Channels estimation phase**: CPU and APs estimate the channels for their respective users

04 — **Federation of APs:** adjust dynamically load between APs and CPU based on CPU's processing delay feedback

How can this dynamic adjustment of offloading be performed ?

⇨ By using a **delay gap** between AP and CPU

$$d_{\text{gap}} = \frac{s \cdot \left| d_{\text{a}}^{t-1} - d_{\text{CPU}}^{t-1} \right|}{\max(d_{\text{a}}^{t-1}, d_{\text{CPU}}^{t-1})}$$

1. Delay at AP **is greater than** the global CPU delay $(d_{\text{a}}^{t-1} > d_{\text{CPU}}^{t-1})$

⇨ **Increase fraction of UEs offloaded to CPU proportionally to the delay gap :**

- ✓ $C_a^t = \min\left(C_a^{t-1}\left(1 + d_{\text{gap}}\right), U_a\right)$ When the initial channel count C_a^{t-1} is large
- ✓ $C_a^t = \min\left(U_a - \left(U_a - C_a^{t-1}\right)\left(1 - d_{\text{gap}}\right), U_a\right)$ When C_a^{t-1} is small

2. Delay at AP **is less than** the global CPU delay $(d_{\text{a}}^{t-1} < d_{\text{CPU}}^{t-1})$

⇨ **Decrease fraction of UEs offloaded to CPU proportionally to the delay gap :**

- ✓ $C_a^t = \max\left(C_a^{t-1}\left(1 - d_{\text{gap}}\right), 0\right)$ When C_a^{t-1} is large
- ✓ $C_a^t = \max\left(U_a - \left(U_a - C_a^{t-1}\right)\left(1 + d_{\text{gap}}\right), 0\right)$ When C_a^{t-1} is small

Simulation Results

- ➢ Python-based simulation
- ➢ One CPU, 10 APs, and a set of users, each of whom is covered by several APs simultaneously
- ➢ TDD mode : ensures channel reciprocity between the uplink and downlink within a given coherence time interval
- ➢ Channel between UE and AP follows a complex Gaussian distribution of Rayleigh (channel gain combines Path Loss and the long-term fading coefficients, this study is derived from the WINNER report)
- ➢ User mobility model: random walk model
- ➢ UEs are grouped into 10 speed classes : speed varies progressively by ±5% around their initial velocity, capturing realistic mobility dynamics
- ➢ Users select their set of serving APs based on the received signal strength
- ➢ Each AP must estimate the channels between itself and the connected users to effectively allocate resources and meet the users' QoS requirements.
- ➢ High mobility profile : in which the channel estimation must fit within a 1 ms coherence interval
- ➢ Moderate /low mobility profile: in which the coherence interval is 2 ms

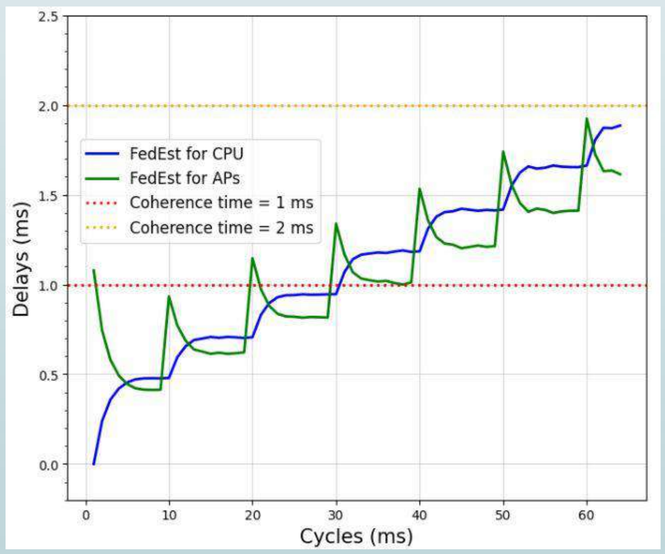

Fig.3: Channel estimation delay for CPU and APs in homogeneous scenario

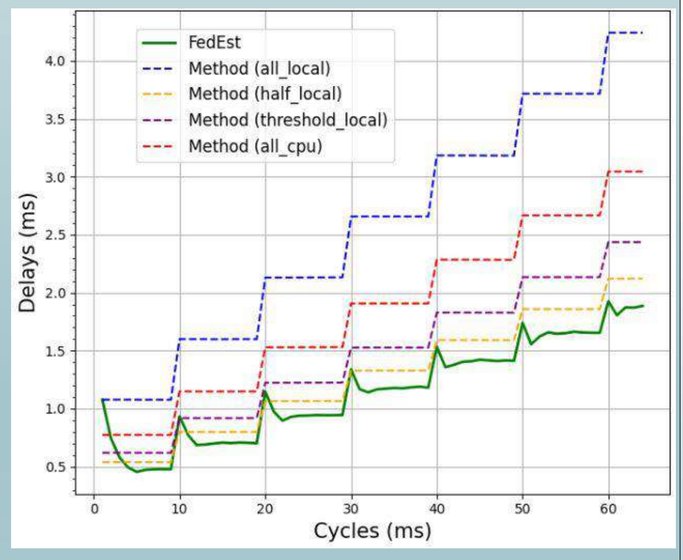

Fig.4: Real channel estimation delay in homogeneous scenario: FedEst vs benchmark

1. Homogeneous scenario

- 10 APs, each equipped with 64 antennas and capable of processing 561 channels/ms
- A CPU providing a total capacity of 7816 channels/ms
- Start with 10 users, increasing by 5 every 10 ms
- Time coherence interval: 70 cycles

2. Heteregeneous scenario

- 4 low-capacity Aps (32 antennas)
- 4 medium-capacity APs (64 antennas)
- 2 high-capacity APs (128 antennas)
- Start with 10 users, increasing by 10 every 50 ms for 150 cycles

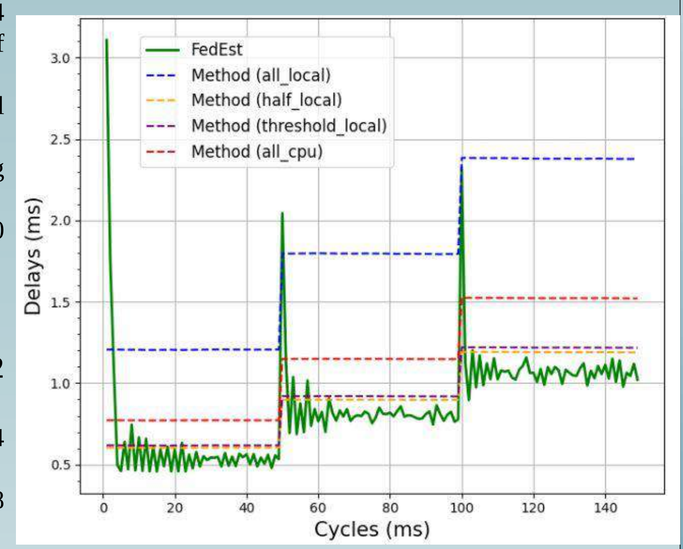

Fig.5: Real channel estimation delay in heterogeneous scenario: FedEst vs benchmark

Conclusion

- ✓ One of the main challenges in CF-mMIMO networks: the channel estimation load balancing between APs and the CPU.
- ✓ Proposition: a distributed approach that balances the channel estimation load between the CPU and the APs.
- ✓ The proposed FedEst framework leverages a Federated K-means approach to minimize overall estimation delay by classifying users based on their mobility profiles.
- ✓ Our approach significantly reduces channel estimation delays while supporting a larger number of users compared to other techniques, for both homogeneous and heterogeneous network topologies.
- ✓ Future work: we will implement this proposition at large scale by integrating CPUs at multiple layers of the distributed computing architecture, and we will tackle the challenge of optimizing the selection of subset of APs that serve each UE.

Etude comportement thermomécanique d'un plancher mixte Acier CLT

UNIVERSITÉ Clermont Auvergne

Ecole doctorale Sciences Pour l'Ingénieur

(1)ALI Ahmed, (1) DURIF Sébastien, (2)AUDEBERT Maxime,
(1) OULDBOUKHETINE Salaheddine, (1) BOUCHAIR Hamid

INP Sigma Clermont

POLYTECH CLERMONT-FERRAND

Introduction

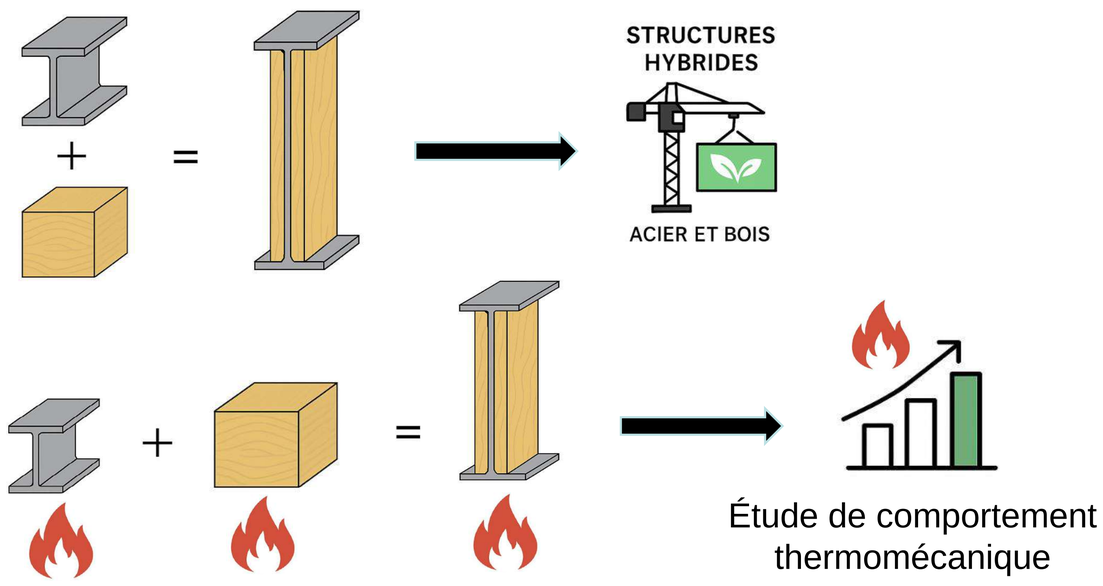

Étude de comportement thermomécanique

Méthodes

1. Modélisation thermique

- Simulation numérique en 2D/3D sous Abaqus.
- Définition précise des propriétés thermo-dépendantes des matériaux (acier, CLT).
- Prise en compte des flux convectifs et radiatifs et de la conductance à l'interface acier/bois.

2. Modélisation thermomécanique

- Étude du comportement global de la section mixte soumise à un chargement thermique et mécanique simultané.
- Analyse des déformations, contraintes, instabilités (flambement, décollement…).

3. Essais expérimentaux

- À petite échelle (thermique) :
- À grande échelle (thermomécanique) :

4. Validation croisée

- Comparaison des résultats expérimentaux avec les simulations numériques.
- Ajustement des modèles : maillage, conditions aux limites, contacts thermiques.

Résultats

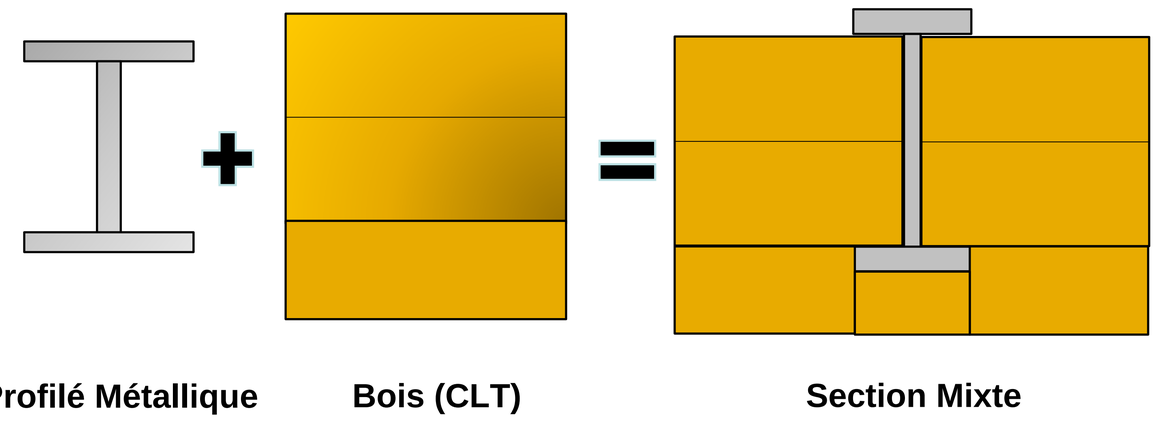

Profilé Métallique Bois (CLT) Section Mixte

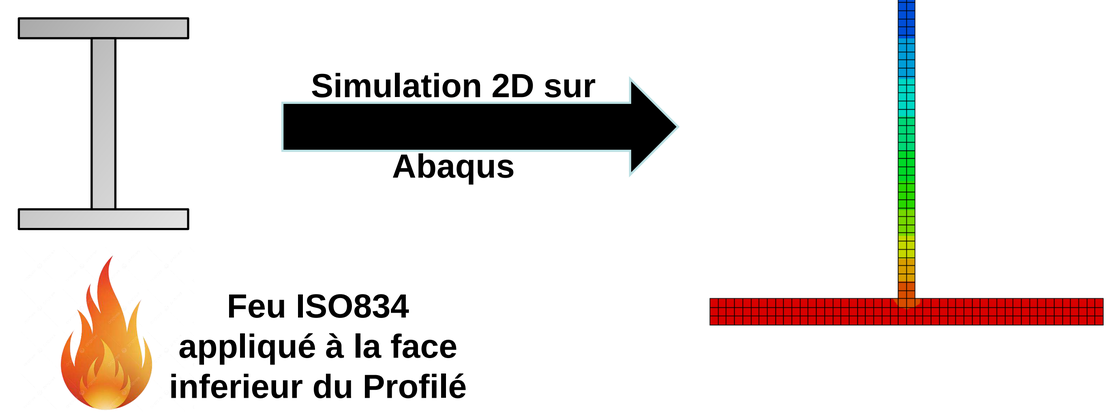

Feu ISO834 appliqué à la face inferieur du Profilé

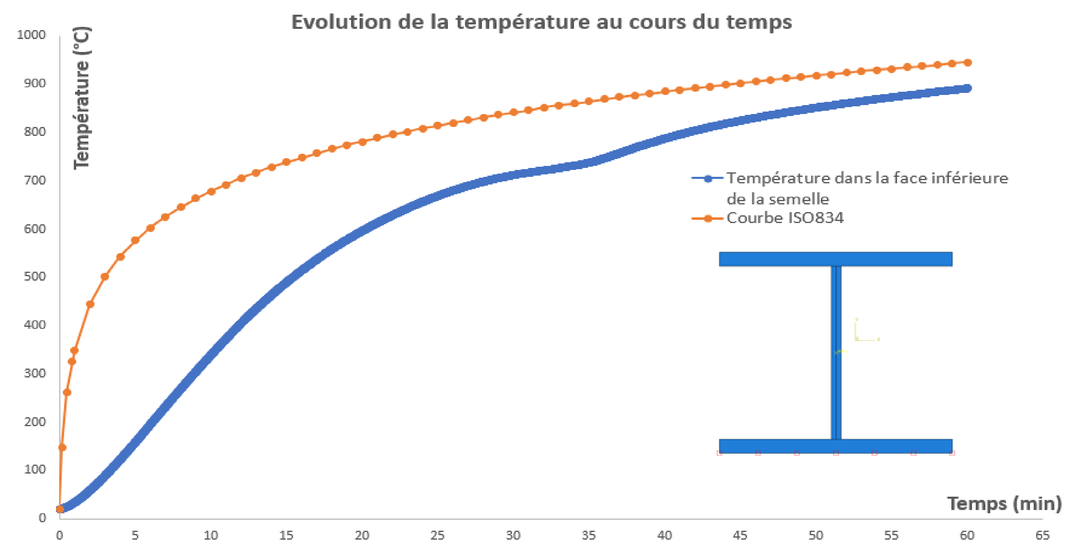

Conclusion

- Mieux comprendre comment les structures mixtes acier–bois réagissent face au feu, tant sur le plan thermique que mécanique.
- Confronter la modélisation numérique à la réalité, grâce à des essais à petite et grande échelle.
- Fournir des outils et des repères pratiques pour concevoir des structures plus sûres et plus performantes en cas d'incendie.
- Contribuer à une construction plus durable, en valorisant des solutions hybrides associant performance structurelle et respect de l'environnement.

Security of Privacy-Respecting Storage Mechanisms of Sensitive Data

Osama Allabwani[1,3], Olivier Blazy[2], Pascal Lafourcade[1], Olivier Raynaud[1]

1 - Université Clermont Auvergne, LIMOS, CNRS, Clermont-Ferrand, France
2 - École Polytechnique, Palaiseau, France
3 - BeYs

Context

During the last few decades multiple public and private organizations did a digital transformation of their administrative procedures which lead to users having to send digital copies of their official documents online. This leads to many risks such as mass theft of documents and non-consensual data analysis and online tracking.

In this thesis we aim to develop new cryptographic protocols that would help us minimize the amount of data shared. For example, an organization that wants just to verify the majority of a person shouldn't need to ask him for his identity card which contains much more information. One of the tools that we can use are Zero-Knowledge Proofs.

Zero-Knowledge Proofs

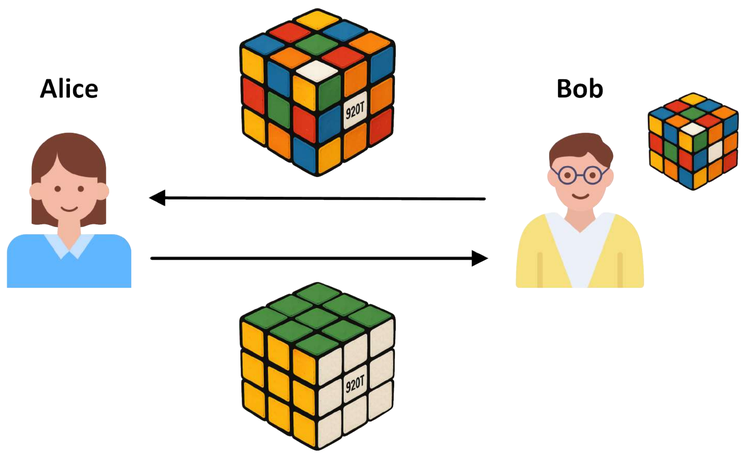

ZKPs are cryptographic protocols that allow a prover to prove to a third-party that a declaration is correct without revealing any information about the declaration other than its veracity.

Intuitive Example: Alice wants to prove to Bob that she knows how to solve a Rubik's cube without revealing the method of resolution. Bob gives Alice a Rubik's cube, then Alice turns here back to him to solve it and return the cube to him. Bob writes a password on the cube before handing it over to Alice to make sure that Alice doesn't just return to him a pre-solved cube that she got from her bag.

Real-Life Use Cases

A law called **SREN** was voted in France in 2024 which requires adult websites to implement strong age-verification mechanism because the current mechanism of just asking a user to affirm his age in a pop-up is not enough. The law requires solutions which maintain the anonymity of the user and the visited site. ZKPs can be implemented to comply to this law.

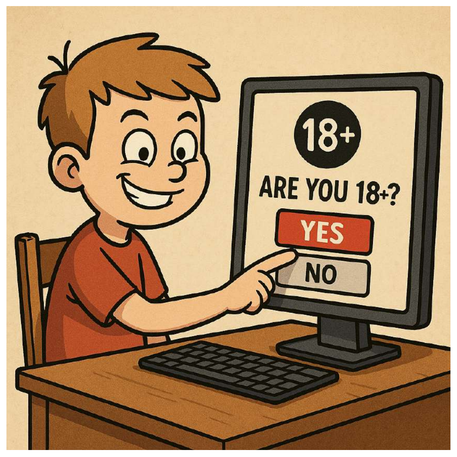

eIDAS is an EU regulation that establishes a framework for digital identity and authentication. It has proposed many standards for which we can develop protocols during the thesis.

First Year Results

k-Sanitizer Sanitizable Signatures with Personalized Admissibility Policies

Osama Allabwani, Olivier Blazy, Pascal Lafourcade, Charles Olivier-Anclin, Olivier Raynaud

Sanitizable signatures are a type of digital signature that allows a semi-trusted third party to modify some parts of the signed message without invalidating the signature. This is useful in scenarios where a third party needs to add/delete/correct information in a document while maintaining the integrity of the original signature. The modifiable parts are called admissible. Most existing works consider having one sanitizer and the ones that consider multiple sanitizers are limited by allowing all sanitizers to modify the same parts. There are many scenarios where we want to have different admissible parts for different sanitizers. Thus, we proposed a new scheme called *k-Sanitizer Sanitizable Signatures* (*k*-SAN).

Introducing *k*-sanitizers with different admissible parts required reworking the security model of traditional sanitizable signatures. We did this and proposed a new security property called full-sanitization verifiability which requires that a signature is valid if and only if all admissible parts are sanitized. This property is interesting for use cases where we don't trust the original signer to generate certain parts of the message. For example, let us say we have a product certificate where we want the original signer to provide the manufacturing details and we want an independent quality assurance company to fill the quality report. Here the manufacturer (signer) shouldn't be trusted to generate the quality report.

We also provided two constructions of *k*-SAN which are based on existing sanitizable signatures showing how we can transform existing constructions to support multiple sanitizers. This transformation does not work for all existing constructions as some of them lose security properties if we add multiple sanitizers. The proposed constructions support different security properties which makes them useful for different user cases.

Synthesis of Predictive Control Law Adaptation Mechanisms for Robot Mobility in Dynamic Natural Environments

Amir Amami[1], Frédéric Chausse[1], Roland Lenain[2] and Benoit Thuilot[1]

[1]Université Clermont Auvergne, Clermont Auvergne INP, CNRS, Institut Pascal, F-63000 Clermont-Ferrand, France

[2]Université Clermont Auvergne, INRAE, UR TSCF, F-63000 Clermont-Ferrand, France

Context & Motivations

- Agro-ecological farming requires frequent and precise operations that are difficult to perform manually due to labor constraints. Mobile robots offer a promising alternative, but their deployment remains limited, especially in heterogeneous and unstructured environments.
- Current control systems struggle to adapt to:
  - Varying surface types (e.g., mud, gravel, grass, tilled soil) and their impact on terrain adhesion
  - Tool changes affecting robot dynamics

Figure 1:Robot during autonomous cultivation

Existing Adaptive Control Architecture

Existing control strategies, previously developed in our lab, already incorporated the influence of ground-vehicle contact conditions, but primarily in the lateral direction.

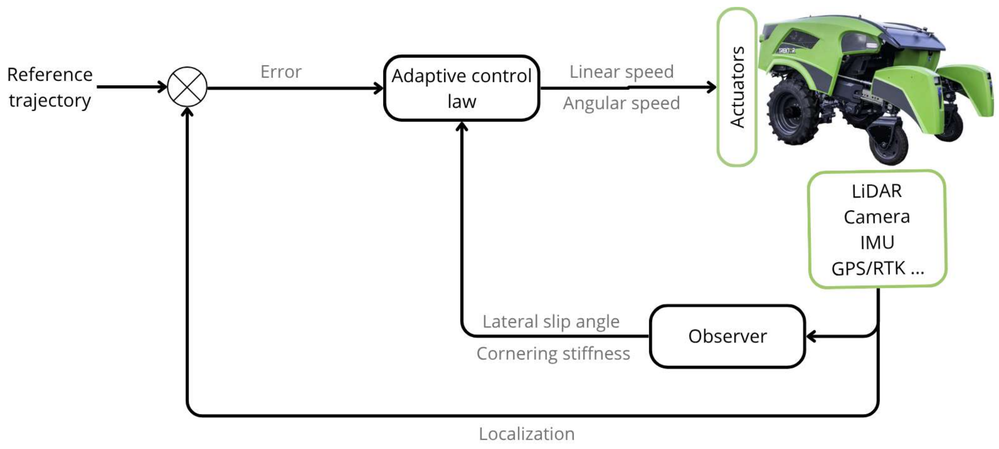

Figure 2:Adaptive Control Architecture

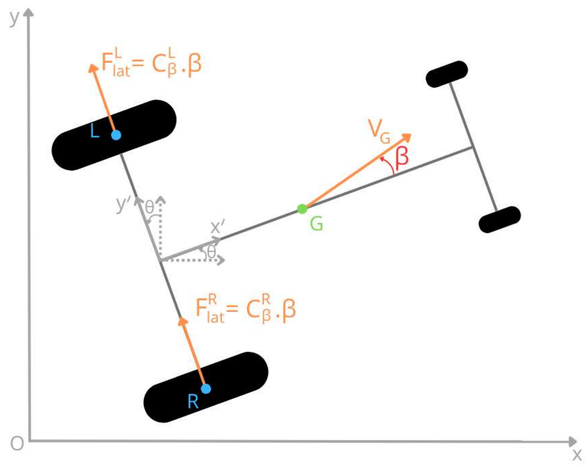

Figure 3:Modeling Lateral Dynamics

- Lateral forces $\boldsymbol{F_{Lat}}$ were modeled using Lateral slip $\boldsymbol{\beta}$ and cornering stiffness $\boldsymbol{C_\beta}$, capturing how the vehicle drifted sideways on different soils.
- Lateral slip $\boldsymbol{\beta}$ and cornering stiffness $\boldsymbol{C_\beta}$ were estimated in real time by observers and used by nonlinear adaptive control laws to adjust commands accordingly.

Limits of Reactive Control

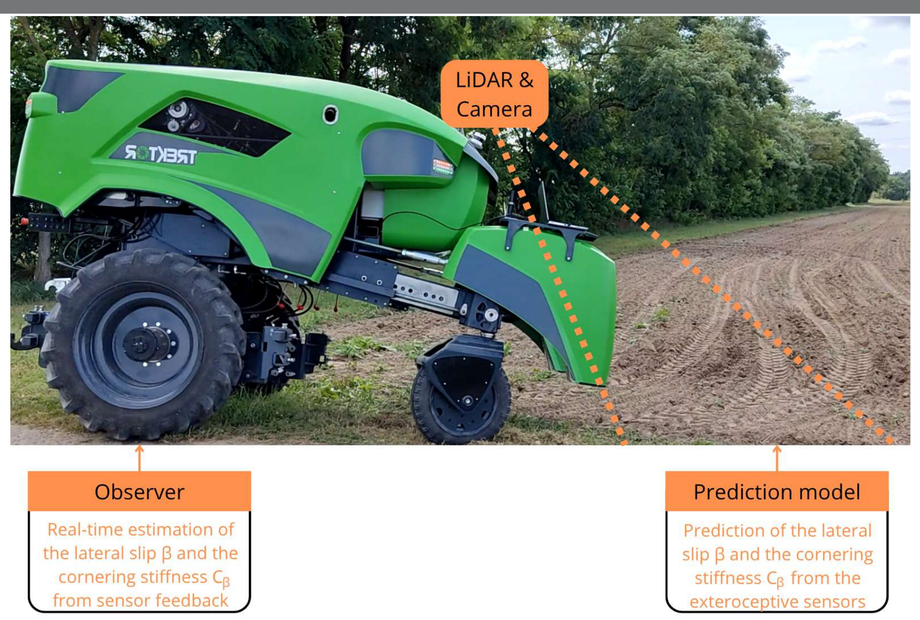

Figure 4:Lateral Dynamics: Observer vs. Prediction Model

- Observers are reactive, they detect terrain changes only after they affect the robot's behavior, leading to delayed adaptation and reduced precision.
- The ANR MUSCAA project aims to improve this by using exteroceptive sensors and enriched maps to anticipate changes and adjust control proactively.

Objectives

Longitudinal forces $\boldsymbol{F_{lon}}$ were modeled using longitudinal slip $\boldsymbol{g}$ and slip stiffness $\boldsymbol{C_g}$, capturing how wheel-ground interaction affects forward motion across varying soil conditions.

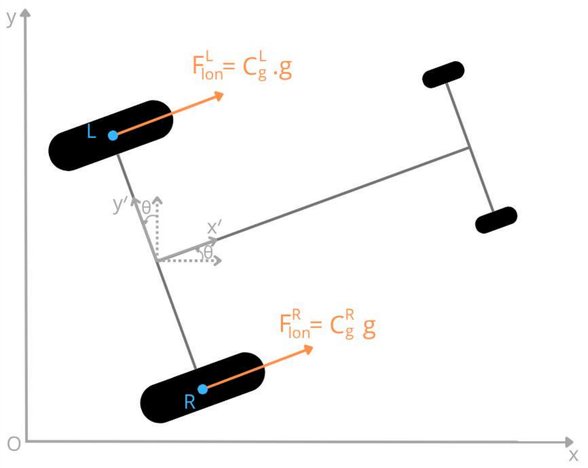

$$g = \frac{R_t\omega - V_x}{\max(|R_t\omega|, |V_x|)}$$

where:

- $\boldsymbol{R_t}$ is the dynamic radius of the wheel, which depends on tire deformation,
- $\boldsymbol{\omega}$ is the rotational speed of the wheel,
- $\boldsymbol{V_x}$ is the longitudinal speed of the wheel's center of rotation.

Figure 5:Modeling Longitudinal Dynamics

- **Grip observer** – Develop an observer to estimate longitudinal slip stiffness $\boldsymbol{C_g}$ from experiments, then share it with Georgia Tech to help train an AI-based adhesion predictor for future integration into our control stack.
- **Online control tuning** – Re-tune control law parameters in real time by leveraging existing lateral observers, complemented by incoming adhesion predictions and an enriched real-time map supplied by the partner lab.
- **Reinforcement-learning control-law selector** – Dynamically select the most effective control law, maximizing performance across varying surfaces.

Results

- Figure 6 displays the estimated slip stiffness values, capturing the evolution of grip across terrain transitions.

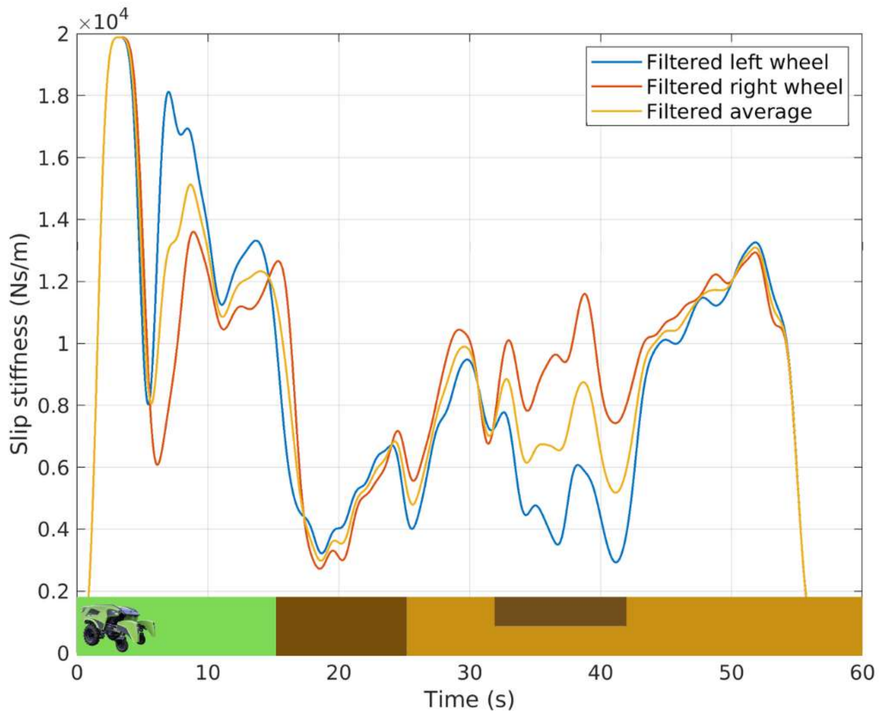

Figure 6:Estimated slip stiffness variation during terrain transitions

Conclusion and future work

- 69 field trials and simulation with a dynamic model confirmed the grip observer's robustness and convergence.
- The validated observer was shared with Georgia Tech to help develop a vision-based adhesion predictor for future integration into our control stack.
- Ongoing work focuses on integrating the predicted adhesion and existing lateral observers into the control loop, enabling real-time tuning of control laws based on terrain anticipation and real-time feedback.

amir.amami@doctorant.uca.fr

Numerical Assessment of Qualitative Levels in MCDM Process using Rasch Model: application to sustainable manufacturing process selection

Gezaei Abera A.[1,2], Severine Durieux (Prof.)[1,3], Romain Guillaume (PhD)[4], Emmanuel DUC (Prof.)[1], and Getasew Ashagrie T. (PhD)[2]

[1] *SIGMA Clermont, Institute Pascal, Clermont Auvergne INP, University of Clermont Auvergne, 20 Avenue Blaise Pascal, 63178 Aubière Cedex, France*

[2] *School of Mechanical and Industrial Engineering, Addis Ababa Institute of Technology, Addis Ababa University, Addis Ababa, Ethiopia*

[3] *IMT Mines Albi école de l'Institut Mines-Télécom, France*

[4] *Institut de Recherche en Informatique de Toulouse (IRIT), France*

June 26, 2025

Ecole doctorale Sciences Pour l'Ingénieur

Introduction and Problem Statement

The effective performance of manufacturing industries primarily depends on the effectiveness of the decisions made on policies, supply chain, product design, process design and selection, criteria prioritization, resources utilization, and other decision related cases. The multi-criteria consideration becomes the main challenge to evaluate the criteria accurately [Aruldoss et al., 2013]. This is due to the behavor of qualitative evaluation of all the criteria in the sustainability dimensions [P. Vonglao, 2017].

The main concern in this research is the difficulty of converting the qualitative evaluation levels into quantitative values in order to clearly analyse the decision process through quantified values.

Overall summary of the problem statement of this study is provided as follows:

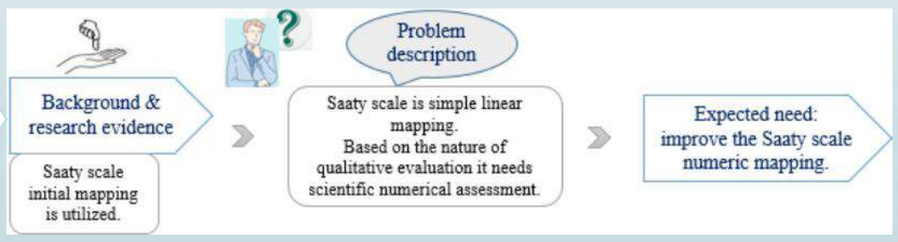

Governing principles on manufacturing sustainability overview:

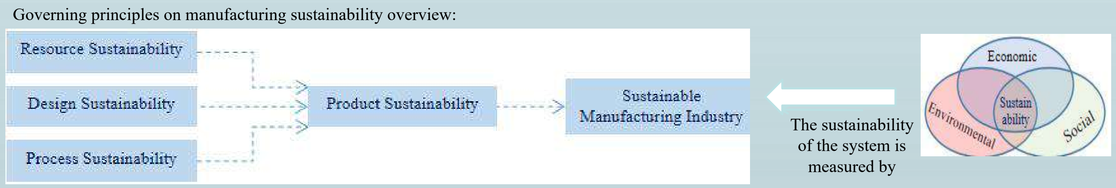

Objective

- To investigate the specific phenomenon on improving decision-making efficiency for manufacturing sustainability using qualitative multi-criteria evaluation in order to enhance the product and overall manufacturing industries performance.
- To convert the qualitative category levels into quantitative values.

In general, the objective of this research can be summarized in this research question, «How to quantify the qualitative evaluations of the alternatives with respect to the criteria to minimize uncertainty and make a sustainable decision?.

Objective summary:

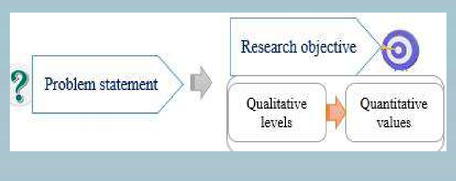

Methods

The multi-criteria decision making (MCDM) method considered as a general solving approach. Rasch model (mainly RSM) is used to estimate the triangular fuzzy number to substitute the qualitative levels *[Huang & Peng, 2012]*. The fuzzy AHP method have been applied to determine criteria weights in the qualitative-evaluation based MCDM analysis. In this study, the Rasch model based hybrid fuzzy AHP-TOPSIS method is used for case study to validate the research finding. *Figure (1)*, presented the summary of the overall research method.

Figure (1): Illustrates the detail methodology and important steps of this research work.

All the necessary steps of the research method have been incorporated in this figure (1) layout flowchart. Step-1 presents the identification and specification of criteria, and step-2 shows the basics steps and important equations of Rasch RSM used to find the step-parameter.

Results

A sample manufacturing process selection case study have been analyzed by considering the role of experts in evaluating the importance comparison and in giving the performance solution for the considered 13 KPIs. The consistency ratio has checked during the pairwise importance comparison in the AHP stage and all are optimized to be CR < 0.1. And, the weight for each KPI is calculated (*Table (a)*). The Rasch model helped us to determine the triangular fuzzy values. Finaly, by carrying out the fuzzy TOPSIS method and got the final preference ranking of the alternatives to make the final decision (see *Figure (2)*).

Table-(a): Presents the weight determined using fuzzy AHP process.

Level 3	Weight		
Buy To fly Ratio (KPI111)	0.375	0.666666667	1.125
Mass (KPI112)	0.208333333	0.333333333	0.625
Extraction and production of raw materials	0.497543627	0.642681527	0.839446678
Manufacture (KPI122)	0.143941176	0.208274867	0.299172134
Usage (KPI123)	0.070662829	0.101043911	0.146710737
End of Life Cycle (KPI124)	0.038126952	0.047999695	0.064173732
Functional Design (KPI211)	0.432900433	0.63334572	0.931264814
Supply Chain (KPI212)	0.168831169	0.260497956	0.410687352
Manufacture (KPI213)	0.077200577	0.106156324	0.157724628
Supply Chain (KPI221)	0.383295195	0.557892475	0.815587795
Preparation Tools & Consumables (KPI222)	0.172196796	0.263345111	0.407567463
Manufacture (KPI223)	0.080636316	0.121872613	0.188531742
Quality / Certification (KPI224)	0.042143402	0.056889801	0.081791858

Table (b): The quantitative values of the qualitative category levels determined using Rasch model (RSM) result:

		Calculated triangular fuzzy number		
Category level	Category	Lower	Middle	Upper
1	Very Low	0	0.117409269	0.234818538
2	Low	0.234818538	0.317227985	0.399637433
3	Medium	0.399637433	0.4972098	0.594782168
4	High	0.594782168	0.666981461	0.739180754
5	Very High	0.739180754	0.869590377	1

After substituting this fuzzy value to the performance evaluation matrix of the alternatives with respect to the KPIs, then multiply it with the weight gives;

Alt A			Alt B		
0.149864037	0.3314732	0.6691299	0.223043313	0.44465431	0.831578348
0.15399599	0.28986346	0.625	0.123912952	0.22232715	0.461987971
0.295930077	0.42865666	0.6205028	0.367774673	0.55886967	0.839446678
0	0.0244534	0.0702512	0.057524282	0.10355631	0.17794225
0.04202899	0.06739442	0.1084458	0.016592942	0.03205396	0.058631102
0.028182709	0.04174007	0.0641737	0.015236957	0.02386592	0.038169391
0.101653047	0.20091499	0.3721683	0	0.07436066	0.218678242
0.067471255	0.12952214	0.2442695	0.100417769	0.17374731	0.303572186
0.045917527	0.0708043	0.116587	0.018128127	0.03367576	0.063032666
0.153179108	0.27738961	0.4850971	0	0.06550175	0.191515133
0.127284558	0.22900237	0.4075675	0.127284558	0.22900237	0.407567463
0.04797728	0.08128677	0.139359	0	0.01430897	0.044270748
0	0.00667939	0.0192062	0.031151592	0.04947082	0.081791858

Figure (2): Shows the weighting of the alternatives in the fuzzy TOPSIS stage analysis and final decision.

Then calculating the relative closeness of the ideal solution for each alternative we found;

	Alt A	Alt B
Relative closeness	0.517158038	0.422667589
Rank	1	2
Decision	Alt A	

Discussion

As presented above, the target of this study is to find an approach that can convert the category levels into numerical values during qualitative assessment in manufacturing process selection.

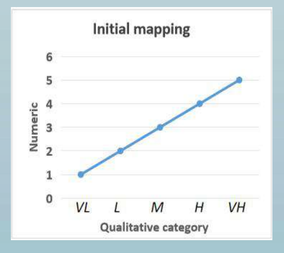

Saaty Scale traditional conversion approach

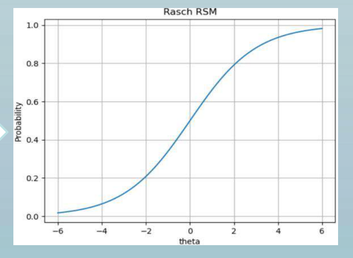

The effect of Rasch RSM in the qualitative to quantitative conversion process

The result shown in Figure (2) was intended to transorm the linear traditional conversion approach (by Saaty's scale) into an actual behaviour of the MCDM qualitative evaluation.

The step-parameter determined the value of the estimated fuzzy number.

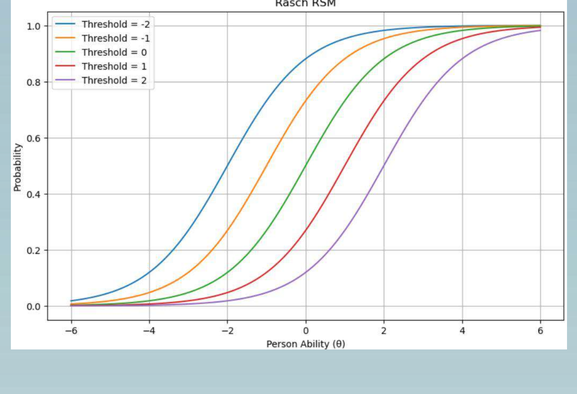

This figure shows how the graph changes with the Rasch parameters (especially the threshold value) and how affected to the Saaty's scale linear grapgh. Probability of responding an accurate answer to an item decreases with towards the higher categories. So, this highly affects the qualitative to quantitative conversion process in the Rasch RSM based process selection.

Therefore, the Rasch model or RSM could be a suitable quantifying method for the qualitative assessment in MCDM based manuafcturing process selection. And, it beables to make a sustainable decision in related cases of the manufacturing sector.

Conclusions

- This study has investigated an approach that can convert the qualitative category levels into quantitative values in the MCDM process.
- The Rasch RSM have been applied to convert the qualitative category levels into numerical values to apply in the sustainability of manufacturing process selection.
- It incorporates the effect of all factors in the decision-making process in order to improve the decision effectiveness.
- The determined triangular fuzzy number has substituted into the performance utility evaluation data of the alternatives assessed with respect to the criteria qualitatively.
- The hybrid fuzzy AHP-TOPSIS decision-making technique has utilized to crosscheck the validity of the numerical conversion method in sustainable manufacturing process selection. And this research output can be a vital imput in decision-making process.

Bibliography

(1) *Alonso, J. A., & Lamata, M. T. (2006). Consistency In The Analytic Hierarchy Process: A New Approach. International Journal of Uncertainty, Fuzziness and Knowledge-Based Systems, 14(04), 445–459. https://doi.org/10.1142/S0218488506004114*

(2) *Amrina, E. and S. M. Y. (2011). Key performance indicators for sustainable manufacturing evaluation in automotive companies, in 2011 IEEE international conference on industrial engineering and engineering management. IEEE, 093–1097. https://doi.org/10.1109/IEEM.2011.6118084*

(3) *Andrich, D. (1978). A rating formulation for ordered response categories. Psychometrika, 43(4), 561–573. https://doi.org/10.1007/BF02293814*

(4) *Andrich, D. (2011). Rating scales and Rasch measurement. Expert Review of Pharmacoeconomics & Outcomes Research, 11(5), 571–585. https://doi.org/10.1586/erp.11.59*

(5) *Chen, P. (2021). Effects of the entropy weight on TOPSIS. Expert Systems with Applications, 168, 114186. https://doi.org/https://doi.org/10.1016/j.eswa.2020.114186*

(6) *Huang, J.-H., & Peng, K.-H. (2012). Fuzzy Rasch model in TOPSIS: A new approach for generating fuzzy numbers to assess the competitiveness of the tourism industries in Asian countries. Tourism Management, 33(2), 456–465. https://doi.org/https://doi.org/10.1016/j.tourman.2011.05.006*

(7) *Jefmański, B., & Sagan, A. (2021). Item Response Theory Models for the Fuzzy TOPSIS in the Analysis of Survey Data. In Symmetry (Vol. 13, Issue 2). https://doi.org/10.3390/sym13020223*

(8) *Taddese, G., Durieux, S., & Duc, E. (2020). Sustainability performance indicators for additive manufacturing: a literature review based on product life cycle studies. International Journal of Advanced Manufacturing Technology, 107(7–8), 3109–3134. https://doi.org/10.1007/s00170-020-05249-2*

Contact address: *gezaei_abera.asmelash@doctorant.uca.fr*
severine.durieux@mines-albi.fr

Partners: Campus France · SIGMA Clermont INP · IMT Mines Albi · Addis Ababa University

Design and control of an operator-assistance system integrated into a cobot, for the manipulation of soft bodies

Alexis Babut, Chedli Bouzgarrou, Laurent Sabourin and Nicolas Bouton

Université Clermont Auvergne, Clermont Auvergne INP, CNRS, Institut Pascal
F-63000 Clermont-Ferrand, France

Interreg Sudoe — Co-funded by the European Union
ROBOTA-SUDOE

Context and Issues

- Many industrial sectors, particularly those involving the manipulation of deformable materials, remain largely unautomated.
- Human operators are exposed to significant physical strain: repetitive motions, awkward postures, fast pace...

Figure 1: Manual meat cutting.

Objectives

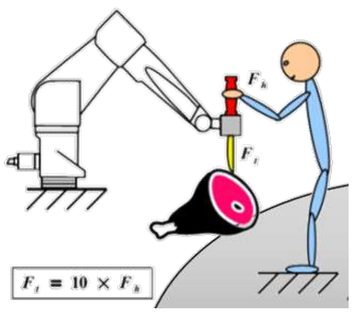

Figure 2: Schematic of robotic-assisted meat cutting.

1. Designing a collaborative robotic system (cobot) to assist the operator in handling soft bodies.
2. Optimising human-robot complementarity to improve the fluidity and safety of operations.
3. Developing control strategies that guarantee robust, latency-free interaction in real time.
4. Incorporate dynamic adaptation mechanisms to cope with variations in the environment and operators.

Architecture of the Robotic Cell

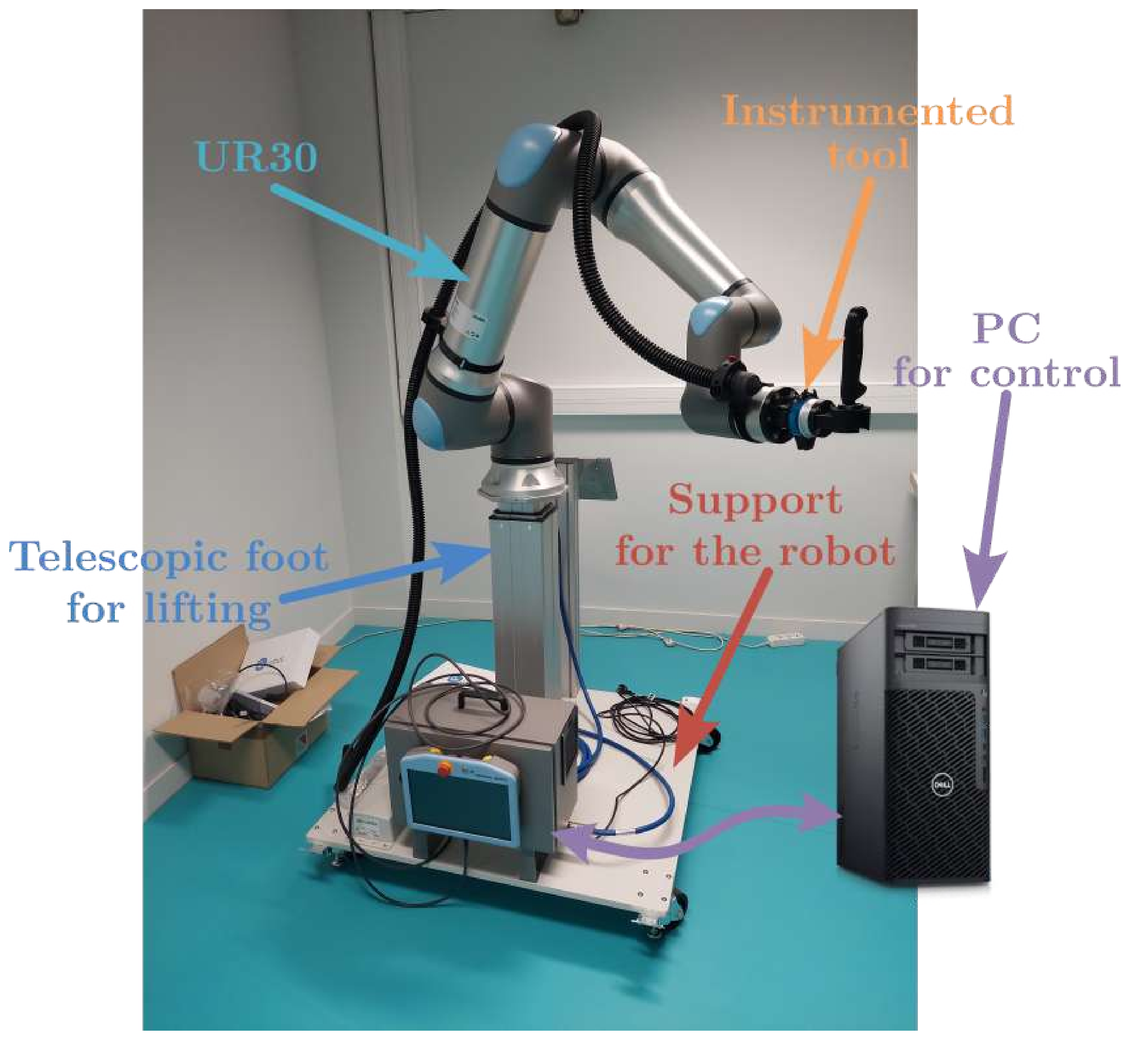

Figure 3: Main components of the robotic cell.

- **Communication:** The robot is operated from a Linux-based computer, connected through Ethernet ports.
- **Control:** Cartesian velocity commands are computed by a compliant controller running on the computer. Joint velocities are calculated on the same computer and sent to the robot thanks to ROS2 (Robot Operating System 2).
- **Instrumented tool:** A tool is mounted on the end-effector, equipped with sensors, a handle, and a blade.
- **Environment perception:** The system includes a 3D vision setup and a motion capture system.

Development of the Instrumented Knife

- For control, it is necessary to quantify the forces applied by the operator in order to amplify these forces and move the robot.

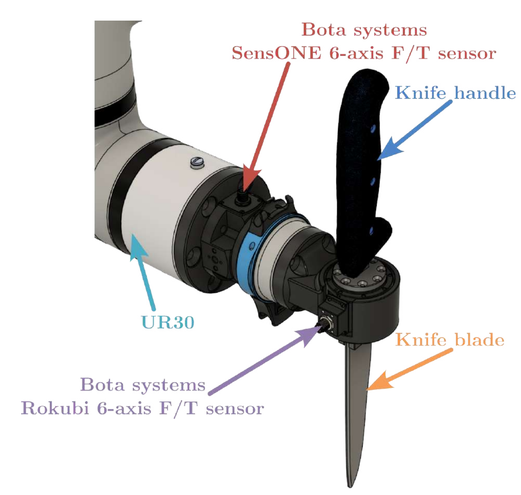

Figure 4: Prototype of an instrumented tool with 2 force/torque sensors.

- The **Rokubi sensor** at the handle captures the forces applied by the operator.
- The **SensONE sensor** is used to **estimate** the cutting forces through indirect measurement.

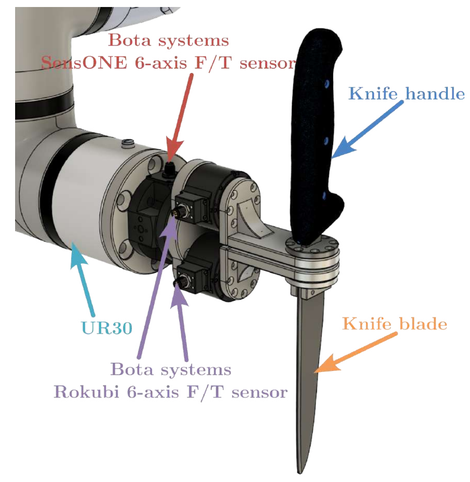

Figure 5: Prototype of an instrumented tool with 3 force/torque sensors.

- One **Rokubi sensor** still measures the user-applied forces.
- The addition of a second **Rokubi sensor** enables **direct measurement** of the cutting forces, providing redundancy and improved accuracy.

Compliant Motion Control

- The goal of admittance control is to compute the Cartesian speed of the robot end-effector $\dot{\mathbf{x}}_r$, resulting from the application of external forces $\mathbf{F}_{\text{ext}}$.
- The system is modelled as a mass-spring-damper system:

$$\mathbf{M}_{dx}(\ddot{\mathbf{x}}_r - \ddot{\mathbf{x}}_d) + \mathbf{D}_{dx}(\dot{\mathbf{x}}_r - \dot{\mathbf{x}}_d) + \mathbf{K}_{dx}(\mathbf{x}_r - \mathbf{x}_d) = \mathbf{F}_{\text{ext}}$$

- The reference acceleration $\ddot{\mathbf{x}}_r$ is computed as:

$$\ddot{\mathbf{x}}_r = \ddot{\mathbf{x}}_d + \mathbf{M}_{dx}^{-1}\left[\mathbf{F}_{\text{ext}} - \mathbf{D}_{dx}(\dot{\mathbf{x}}_r - \dot{\mathbf{x}}_d) - \mathbf{K}_{dx}(\mathbf{x}_r - \mathbf{x}_d)\right]$$

- Where:
  - $\mathbf{M}_{dx}$ is the desired inertia matrix,
  - $\mathbf{D}_{dx}$ is the desired damping matrix,
  - $\mathbf{K}_{dx}$ is the desired stiffness matrix.

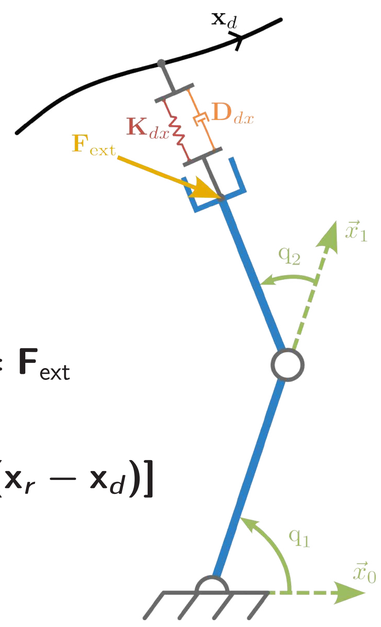

Figure 6: End-effector behaviour modelled.

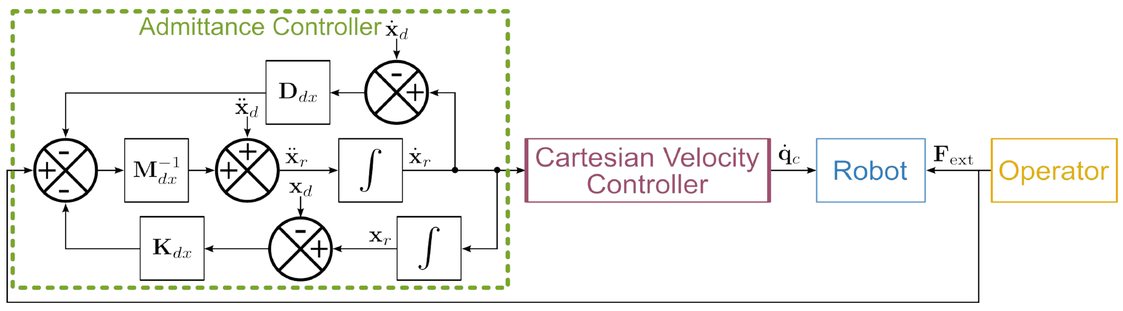

Figure 7: Block diagram of Cartesian admittance control.

References

[1] Mohammad Farajtabar and Marie Charbonneau.
The path towards contact-based physical human–robot interaction.
Robotics and Autonomous Systems, 182:104829, July 2024.

[2] Neville Hogan.
Impedance control: An approach to manipulation.
In *1984 American Control Conference*. IEEE, July 1984.

[3] Arvid QL Keemink, Herman van der Kooij, and Arno HA Stienen.
Admittance control for physical human–robot interaction.
The International Journal of Robotics Research, 37(11):1421–1444, April 2018.

alexis.babut@sigma-clermont.fr

Relations entre trajectoires de croissance et comportement mécanique des feuillus secondaires

Projet CONstruire en BOis avec les forêts de demain - CONBO

BAYLE Florian[1]

MORIN Xavier[2], SAUVAT Nicolas[1]

[1]Université Clermont Auvergne, CNRS, Clermont Auvergne INP, Institut Pascal, Clermont-Ferrand

[2]Université de Montpellier, CNRS, CEFE, Montpellier

florian.bayle@cnrs.fr

CONTEXTE

Ressources Forestières & Besoins en Bois d'Œuvre

La RE2020 impose des seuils d'indice carbone de plus en plus stricts pour le secteur de la construction, incitant à une augmentation significative de l'usage du bois.

En France, bien que les feuillus représentent 65 % du volume de bois sur pied, les prélèvements se concentrent sur les résineux, pour des raisons de transformation plus simple et de conformations plus régulières (IGN 2024). De plus, seulement 10% du volume de bois sur pied est destiné à être utilisé en bois d'œuvre de structure (FNB, 2023).

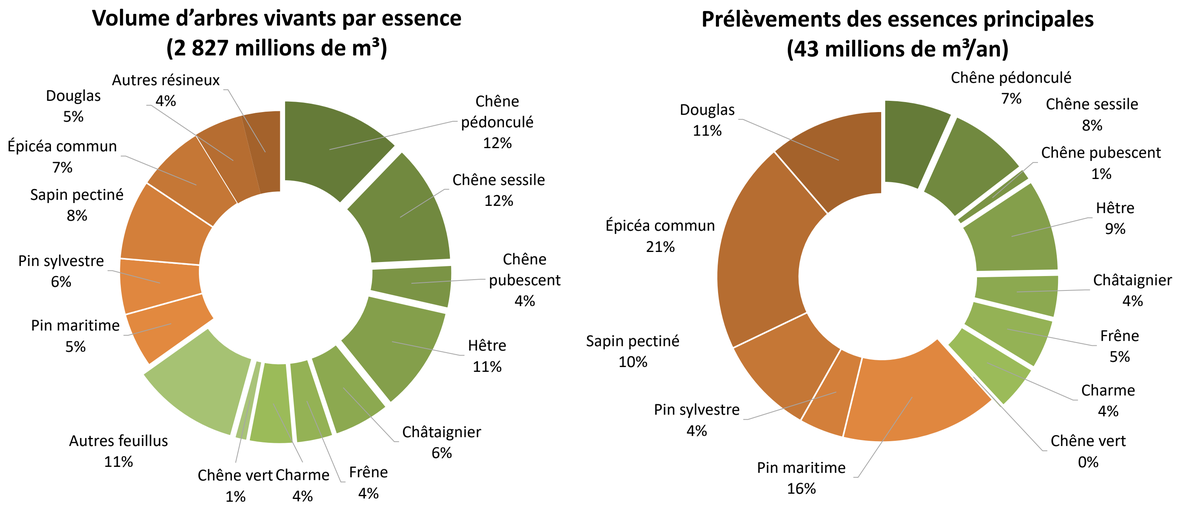

Volumes d'arbres vivants et de prélèvements des essences principales en France (données IGN 2024)

Feuillus : Intégration dans l'ingénierie de construction

Seules les essences majoritairement présentes sont aujourd'hui référencées dans les bois de construction (NF B 52-001) principalement des espèces résineuses ainsi que le chêne, le hêtre, le châtaignier et le peuplier de culture. Les essences secondaires peuvent toutefois constituer un réservoir de bois d'œuvre.

Etat sanitaire de la forêt française

Depuis 2018-2022, certaines crises (scolytes dans le Nord-Est, etc.) ont conduit à des taux de mortalité et de prélèvement, dans certains massifs, supérieurs à leur production biologique, ce qui compromet leur rôle de puits de carbone.

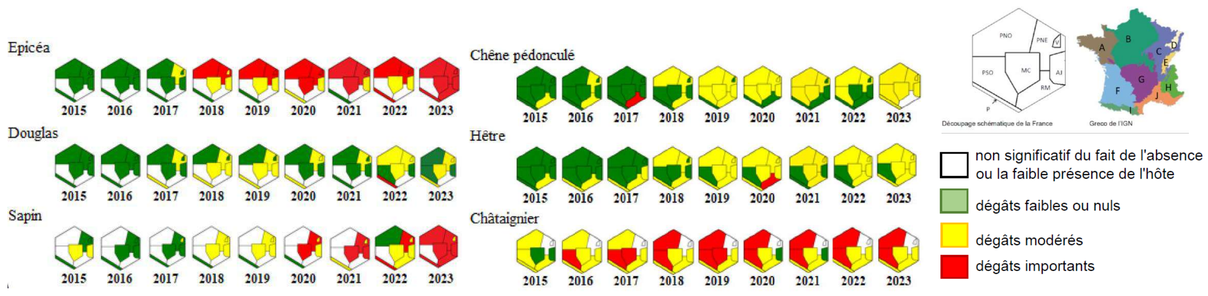

Répartition des volumes de bois sur pied et du volume de bois d'œuvre « structure » (FNB, 2023)

MÉTHODOLOGIE

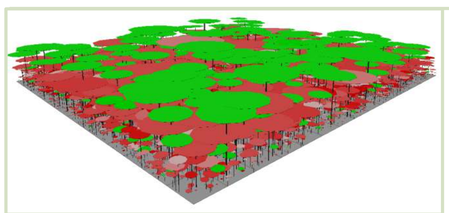

Visualisation 3D du modèle ForCEEPS, Morin, 2014

Modélisation de la forêt de demain → **Choix des espèces et sylvicultures prometteuses** → **Caractérisation des différentes espèces d'intérêt** → **Etablissement de groupes d'essences** → **Optimisation du dimensionnement des structures**

Pour chaque espèce étudiée (réalisation d'une méthodologie)

- *Modélisation des conditions de croissance*
- *Prélèvement sur le terrain*
- *Caractérisation physique et mécanique*
- *Modélisation des sciages in silico*
- *Identifications des grandeurs pilotes*

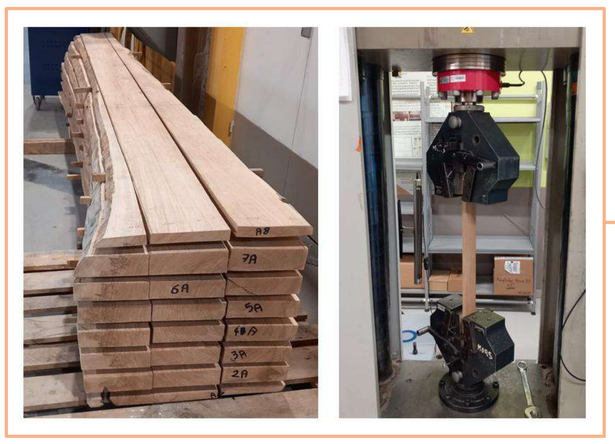

Campagne de caractérisation du chêne rouge d'Amérique

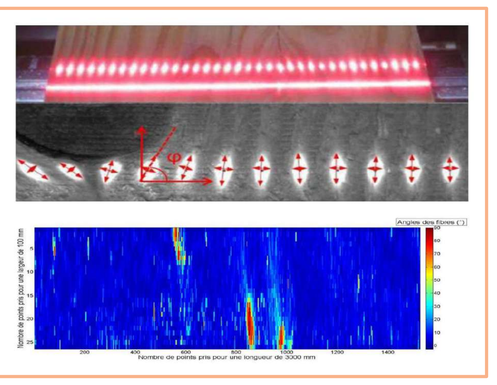

Utilisation de la pente de fil pour le classement mécanique du bois, Faydi et al.,2015

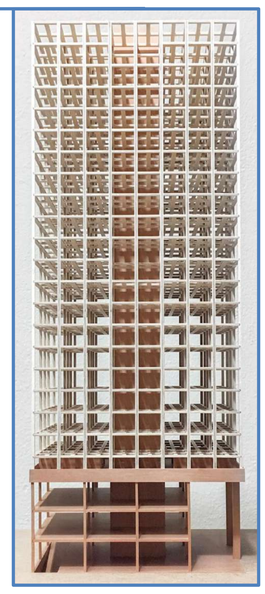

Tour de 75m de haut, poteaux en hêtre (feuillus), © Boltshauser Architekten

RÉSULTATS PRINCIPAUX ATTENDUS

Adapter les modèles de croissance existants aux feuillus dits secondaires intéressants pour la construction afin d'obtenir des informations sur la qualité du bois, en fonctions des trajectoires de croissance influencées par l'environnement (sécheresse, futaie régulière ou irrégulière, …).

Identifier des grandeurs mécaniques pilotes pour les feuillus secondaires, notamment en mettant en avant l'importance de la pente de fil comme paramètre influençant les propriétés mécaniques et permettant la caractérisation du matériau.

Justifier les écarts sur le dimensionnement des structures liés à une caractérisation mécanique plus fine des bois et des solutions constructives optimisant la diversité des essences.

REMERCIEMENTS

Ce projet a obtenu le soutien financier du CNRS à travers le programme 80|PRIME de la Mission pour les Initiatives Transverses et Interdisciplinaires.

RÉFÉRENCES

FCBA/BIPE (2019) Etude prospective : Evolution de la demande finale du bois dans la construction, la rénovation et l'aménagement des bâtiments – Fin. ADEME/France Bois Forêt/CODIFAB

FNB (2023) Etat des lieux des essences feuillus secondaires facilement mobilisables en France – Fin. France Bois Forêt

IGN (2024) Inventaire Forestier National

MASA/Département Santé des Forêt (2024) – Indicateurs de la santé des forêts 1989-2023

Masson et al. (2019) Comportements structurels des Essences de bois Feuillus français en vue de leur meilleure intégration aux EURocodes 5 Projet de Recherche Collaborative – Entreprise ANR-15-CE08-0027

Méthodologie d'amélioration conjointe du processus industriel et des infrastructures pour atteindre les objectifs nationaux bas carbone

Jean BEAKOU, Aurélie TALON, Anne-Lise HUYET, Jean-Luc PARIS

Université Clermont Auvergne, Clermont Auvergne INP, Institut Pascal, 63000 Clermont-Ferrand, France

Contexte

Objectif national du budget carbone : Secteur du bâtiment ↘ 45 % & Secteur industriel ↘ 29 %

À l'horizon 2029-2033

Manque de coordination de ces 2 secteurs

Interopérabilité des logiciels limités

Problématique

Comment évaluer puis comparer des solutions amélioratives co-conçues (infrastructures et process industriels) afin de minimiser leurs impacts environnementaux et maximiser leur efficacité opérationnelle ?

Méthodologie

Système initial
Infrastructures + Process industriel

Système modifié 1
Solution améliorative 1 : Infrastructures + Process industriel modifiés

Système modifié n
Solution améliorative n : Infrastructures + Process industriel modifiés

Evaluation

Méthodes

1 – Modélisation du processus industriel
Arena → caractérisation et quantification des performances du process industriel

2 – Modélisation des infrastructures
Revit → obtention du modèle numérique détaillé

3 – Analyse énergétique et environnementale
Climawin → évaluation des impacts énergétiques et environnementaux

Indicateurs

Energétiques et environnementaux
Confort d'été, énergétique, carbone

Conditions de travail
Pénibilité

Coûts
Construction, consommation électrique, immobilisation

Productivité
Quantité produite

Comparaison

Somme pondérée

Résultats

Classement des solutions amélioratives

Mise en œuvre

Système initial

Zone de vie (bureaux, magasin) à 18°C + Zone de production à 10°C

+

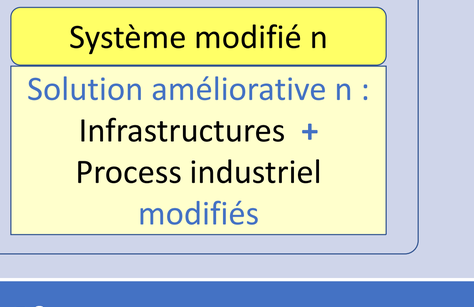

Chaîne de production à 8 stations

Systèmes modifiés

Modification des infrastructures :
- Ajout de cloisons
- Ajout d'isolation par l'extérieur

➔ *Amélioration des déperditions et réduction des volumes à refroidir*

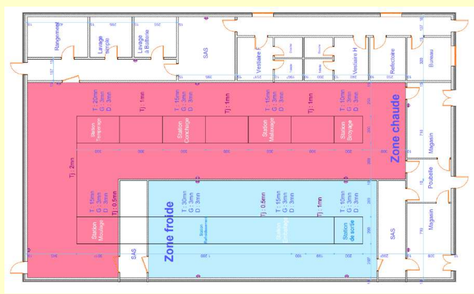

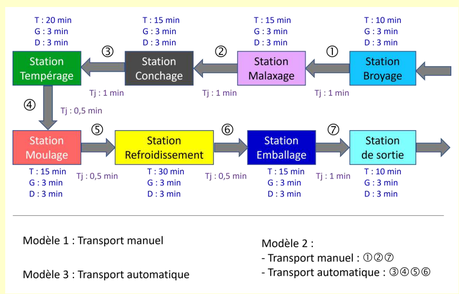

Modification du process industriel :
Modification du mode de transport entre les stations de travail

➔ *Amélioration des conditions de travail et de la productivité*

Combinaison de modifications

12 solutions améliorations

Après évaluation des critères pour chaque solution et classement par somme pondérée :

Solution la plus performance :

- Pas de travaux sur les infrastructures

L'amélioration énergétique et environnementale à cout terme n'est pas significative (en comparaison des 11 autres solutions) au regard des coûts des travaux d'infrastructures

- Transport automatique entre les stations

↗ *conditions de travail et productivité*

Conclusion

Proposition d'une méthodologie d'évaluation et de comparaison de solutions améliorations du système « infrastructures + process industriel » via des critères de conditions de travail, énergétiques et environnementaux, de coût et de productivité.

Perspectives

- Evaluation économique complète
- Analyse de la robustesse de la méthodologie
- Généralisation à d'autres industries

Bibliographie

- Bila Deroussy. (2015). "Optimisation des processus industriels et infrastructures." Revue de l'ingénierie industrielle.
- Giard, V., (2003). "Gestion de la production et des flux". Economica Paris.
- Nhat Phan. (2023). "Proposition d'une démarche générique pour la co-conception infrastructures et process industriels." Journal of Industrial Systems.
- Nathalie Gardes. (2022). "BIM et efficacité énergétique dans les bâtiments industriels." Editions Techniques de l'Ingénieur.
- ADEME. (2019). "Guide pratique de l'énergie durable." Publications ADEME.

Remerciements

Les auteurs remercient l'ensemble des participants de la journée scientifique pour votre temps et votre attention.

Occlusion-Aware and Risk-Adaptive: A Generic Framework for Autonomous Navigation in Resource-Constrained Settings

Mohamed Benrabah*, Roland Chapuis*, Romuald Aufrère*
*Université Clermont Auvergne, Institut Pascal

Objectives

- Develop a versatile architecture for multi-sensor perception and autonomous navigation, adaptable to diverse environments and capable of integrating heterogeneous data (sensors, maps, etc.).
- Address navigation under uncertainty by assessing collision risk (including occluded areas) and balancing safety with navigation efficiency.

Introduction

- **Context:** Autonomous vehicles (AVs) promise safer, efficient transportation, especially in information-dense urban settings.
- **Challenge:** Most current navigation systems rely on both centimeter-level map accuracy and high data density, making them brittle in dynamic settings, with outdated/missing maps, occluded areas, etc.
- **Problem formulation:** How to achieve safe, high-speed navigation under uncertainty, occlusions, and limited prior knowledge?

Perception & Obstacle Representation

- **Environment Modeling:** A 2D occupancy grid is built from LiDAR point clouds and robot pose estimates to capture visible obstacles.
- **Occlusions Reasoning:** We incorporate map priors from OpenStreetMap (OSM) to model hidden obstacles:
  - Hypothetical particles are sampled along OSM-derived lanes with assigned speeds $\|v_i\| \sim U([\underline{v_l}, \bar{v_l}])$ and lateral offset $\|v_i\| \sim U([\underline{b}, \bar{b}])$.
  - Converts occupied grid cells into static particles ($v_i = 0$).
- **Unified Obstacle Representation:** Both detected and hypothesized (occluded) objects are merged into a single particle set $\mathscr{P}$. This integration results in a unified representation for each particle:

$$X_i(t) = \begin{pmatrix} x_i(t) \\ y_i(t) \\ \theta_i(t) \\ v_i(t) \end{pmatrix} = g_i(X_{i_0}, t)$$

- **Collision Risk Evaluation** The fusion of sensor-based detections with map-based predictions enables informed collision risk assessment that covers both visible and occluded areas of the environment.

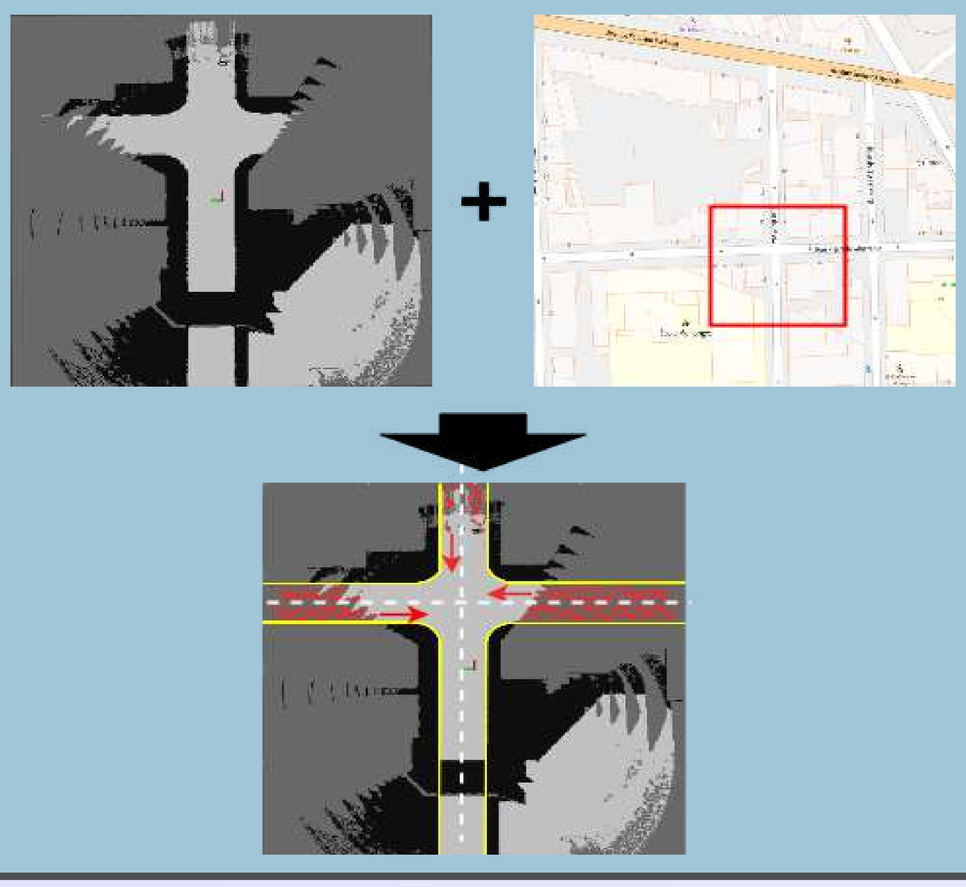

Tentacle-Based Planner

- **Planning and control:** We adopt a tentacle-based approach. A discrete set of trajectories (tentacles) is generated by sampling steering angles. For each:
  - Obstacles define a forbidden speed range $[v_{max}, v_{min}]$, depending on whether the vehicle must slow down to follow or accelerate to overtake, as well as it's acceleration and braking capabilities
  - The planner selects the highest admissible speed:

$$v_k = \max\left(\mathbb{J} \setminus \bigcup_i \mathbb{I}_i\right), \quad \text{avec } \mathbb{J} = [0, v_{\text{leg}}]$$

Some Results

- Simulations conducted on CARLA simulator.

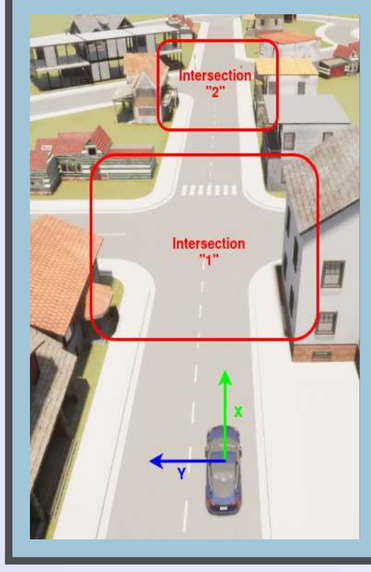

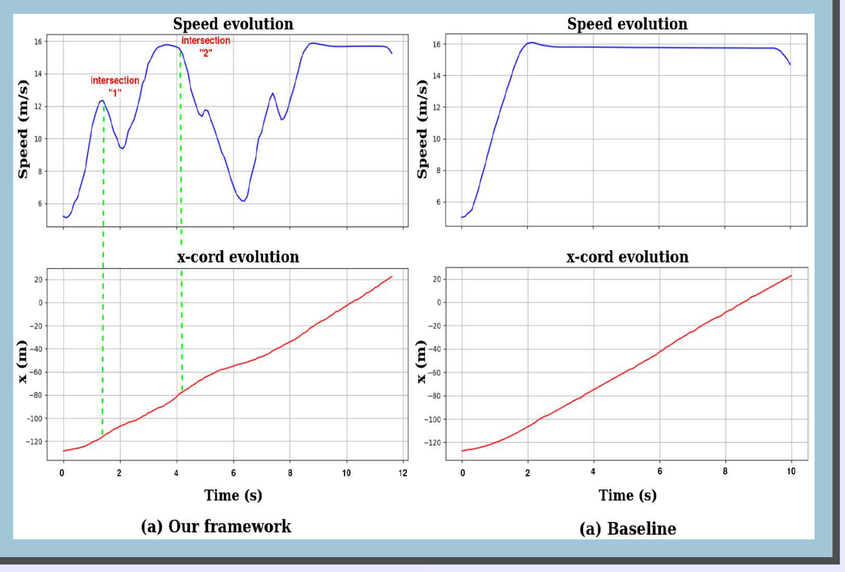

Contributions and Perspectives

- Proposed a framework fusing LiDAR and OpenStreetMap data for occlusion handling in autonomous navigation.
- Developed a novel path planning method tailored for resource-constrained systems.
- Demonstrated a balanced trade-off between safety and efficiency.
- Approach generalizable to other occlusion types; plans to integrate additional data (e.g., lane markings) for safer and more informed navigation.

References

[1] Benrabah, M., Randriamiarintsoa, E., Mousse, C. O., Morceaux, J., Aufrère, R., & Chapuis, R. (2023, June). Dual occupancy and knowledge maps management for optimal traversability risk analysis. In *2023 26th International Conference on Information Fusion (FUSION)* (pp. 1–6). IEEE.

[2] Benrabah, M., Orou Mousse, C., Randriamiarintsoa, E., Chapuis, R., & Aufrère, R. (2024). A review on traversability risk assessments for autonomous ground vehicles: Methods and metrics. *Sensors*, 24(6), 1909.

[3] Benrabah, M., Orou Mousse, C., Chapuis, R., & Aufrère, R. (2025). Efficient and risk-aware framework for autonomous navigation in resource-constrained configurations. *12th IFAC Symposium on Intelligent Autonomous Vehicles*, May 2025, Phoenix, Arizona, USA.

Acknowledgements

This work was supported by the International Research Center "Innovative Transportation and Production Systems" of the I-SITE CAP 20-25.

Contact

Email: mohamed.ben_rabah@uca.fr